

THE UNIVERSITY OF HULL

**Mathematical Modelling of Bone Remodelling at the Cellular
Level and the Interaction between Myeloma Cells and the
Bone Microenvironment**

Being a Dissertation submitted in partial fulfilment of
the requirements for the Degree of PhD in the University of Hull

By

Bingbing JI, BS and MS

July 2012

ABSTRACT

After an initial phase of growth and development, bone undergoes a continuous cycle of repair, renewal and optimization, by a process termed remodelling. Bone remodelling is the coordinated processes of resorption by osteoclasts and formation by osteoblasts, where old bone is replaced by new bone. Disorder of bone remodelling cycle can result in metabolic bone diseases, such as postmenopausal osteoporosis, hypothyroidism and primary hyperparathyroidism. Due to the large number of bone cell types, stages of differentiation, and the numerous growth factors and cell to cell interactions involved, our current understanding of bone remodelling and the coupling between osteoblasts and osteoclasts is still fragmentary.

In the first part of this research, a novel predator-prey based mathematical model is developed to simulate bone remodelling cycles in trabecular bone at the basic multicellular unit level, through integrating bone removal by osteoclasts and formation by osteoblasts. The model is able to replicate the curves of bone remodelling cycles obtained from standard bone histomorphometric analysis. The application of the model is firstly demonstrated by using experimental data recorded for normal (healthy) bone remodelling, to simulate the temporal variation in the number of osteoblasts and osteoclasts, and resultant effect on bone thickness. The reconstructed histomorphometric data and remodelling cycle characteristics compared well with the specified input data. Two sample pathological conditions, hypothyroidism and primary hyperparathyroidism, were then examined to demonstrate how the model could be applied more broadly. The model was validated by comparing model predictions (maximum populations of osteoclasts and osteoblasts) in the normal condition with experimental data. Further data is required to fully validate the model's predictive capability.

A second mathematical model is then developed to simulate how the interaction between multiple myeloma (MM) cells and the bone microenvironment leads to a 'vicious cycle' between tumour development and bone destruction. The model includes the roles of inhibited osteoblast activity and stimulated osteoclast activity, and is able to mimic the temporal variation of bone cell concentrations and resultant bone volume after invasion and then removal of the tumour cells. The model explains why MM-induced bone lesions rarely heal even after the complete removal of MM cells. The model's predictions agree with published experimental and clinical observations. The model is also used to simulate therapies for MM-

induced bone disease, including bisphosphonates, bortezomib and the inhibition of TGF- β . The simulation confirms that treatments with bisphosphonates and bortezomib can reduce the tumour burden and bone destruction, which is consistent with clinical observations. However, the inhibition of TGF- β does not appear to suppress bone destruction, although it does decrease the MM cell concentration.

ACKNOWLEDGEMENTS

The past three years is a so impressive and pleasant experience for me. In this final stage of my PhD study, I would like to thank a long list of people for their kindly, continual and strong help. Without this, it is impossible for me to overcome the difficulties and depressions experienced over this period.

I would like to give my deepest thanks to my supervisor Professor Michael Fagan for his excellent guidance, considerate help and sincere encouragement. I feel so lucky to have Michael as my supervisor. His great characters, such as politeness, responsibility, diligence and devotion to work, are worth me to learn throughout my lifetime.

I would like to give my warm and sincere thanks to Professor Ron Patton for his kindly help in the research.

I would like to give my profound appreciation to Dr Paul Genever for his strong support in the biological background of the research.

I would like to thank Dr Devi Putra for some early suggestions to the first part of this work and express my special appreciation to my colleague Dr Peter Watson for his excellent, careful editions on the first draft of the thesis, which does improve the thesis a lot.

I would like to express my appreciation to Dr Catherine Dobson and my colleagues in Medical and Biological Engineering Research Centre.

I would like to express my appreciation to China Scholarship Council and University of Hull for their financial support.

I would like to express my deepest, most profound and sincerest thanks and appreciation to Dan. The time with you is the most and most beautiful period for me.

I would like to send my endless love and appreciation to my family, parents and sisters. Your unselfish love and continual, generous and considerate help are the things I cannot lose in this world.

Thank you all!

TABLE OF CONTENTS

ABSTRACT	i
ACKNOWLEDGEMENTS	iii
TABLE OF CONTENTS	iv
GLOSSARY	vii
1. INTRODUCTION	1
2. LITERATURE REVIEW-BASIC BONE BIOLOGY	6
2.1 INTRODUCTION.....	6
2.2 BONE STRUCTURE AND COMPOSITION.....	6
2.3 BONE CELLS	9
2.4 BONE REMODELLING	14
2.4.1 HORMONAL REGULATION OF BONE REMODELLING.....	19
2.4.2 LOCAL REGULATION OF BONE REMODELLING.....	20
2.4.3 RELATIONSHIP BETWEEN LOCAL AND SYSTEMIC FACTORS	
21	
2.5 BONE DISEASES CAUSED BY DISORDERS OF BONE	
REMODELLING.....	22
2.6 DISCUSSION	25
3. LITERATURE REVIEW-MATHEMATICAL MODELLING OF BONE	
REMODELLING CYCLES AT THE CELLULAR LEVEL.....	27
3.1 INTRODUCTION.....	27
3.2 MATHEMATICAL MODELS OF BONE REMODELLING AT THE	
CELLULAR LEVEL	28
3.3 DISCUSSION	38
4. A PREDATOR-PREY BASED MATHEMATICAL MODEL OF THE BONE	
REMODELLING PROCESS.....	41
4.1 INTRODUCTION OF MATHEMATICAL MODELLING	41

4.2	PREDATOR-PREY MODELS	43
4.3	DEVELOPMENT OF THE MODEL OF THE BONE REMODELLING PROCESS	44
4.3.1	MODEL EQUATIONS.....	44
4.3.2	MODEL CALCULATION	48
4.3.3	SIMULATION RESULTS AND ANALYSIS	59
4.4	MODEL PARAMETERS AND BIOCHEMICAL FACTORS	81
4.4.1	RELATING THE MODEL PARAMETERS TO BIOCHEMICAL FACTORS.....	81
4.4.2	VALIDATION OF THE PROPOSED CONNECTIONS	83
4.5	DISCUSSION	86
5.	MATHEMATICAL MODELLING OF THE PATHOLOGY OF MULTIPLE MYELOMA INDUCED BONE DISEASE.....	89
5.1	INTRODUCTION.....	89
5.2	DEVELOPMENT OF THE MODEL OF THE NORMAL BONE ENVIRONMENT	91
5.2.1	BASIC STRUCTURE OF THE MODEL	91
5.2.2	MODEL EQUATIONS.....	93
5.2.3	SIMULATION RESULTS AND DISCUSSION	98
5.3	DEVELOPMENT OF THE MODEL OF MULTIPLE MYELOMA- INDUCED BONE DISEASE	106
5.3.1	BASIC STRUCTURE OF THE MODEL	106
5.3.2	MODEL EQUATIONS.....	109
5.3.3	SIMULATION RESULTS	115
5.3.4	SENSITIVITY STUDY	120
5.3.5	DISCUSSION	123
5.4	SIMULATION OF THERAPIES FOR MM-INDUCED BONE DISEASE 124	

5.4.1	BISPHOSPHONATE TREATMENT	124
5.4.2	BORTEZOMIB TREATMENT.....	129
5.4.3	TGF- β TREATMENT.....	134
5.5	CONCLUSION	138
6.	DISCUSSION	139
7.	CONCLUSIONS AND FUTURE WORK	143
	APPENDIX A	163

GLOSSARY

Bisphosphonates	They are also called diphosphonates, and are a class of drugs that prevent the loss of bone mass, used to treat osteoporosis and similar diseases.
BMPs (Bone morphogenetic proteins)	A group of growth factors also known as cytokines and as metabologens.
BMSCs (Bone marrow stromal cells)	Also known as mesenchymal stem cells. They are multipotent stem cells that can differentiate into a variety of cell types.
BMU (Basic multicellular unit)	A bone remodelling unit consisting of osteoclasts and osteoblasts.
Bone lining cells	Bone lining cells are derived from inactive osteoblasts and osteoblast precursors which cease activity or differentiated and flattened out on bone surfaces.
Bortezomib	It is the first therapeutic proteasome inhibitor to be tested in humans.
CAMs (Cell adhesion molecules)	Cell adhesion molecules are proteins located on the cell surface involved with the binding with other cells or with the extracellular matrix (ECM) in the process called cell adhesion.
Cancellous bone	Type of porous bone that consists of a network of thin bars or plates of bone, in a lattice type configuration (also known as trabecular bone), found inside the ends of long bones, and in the vertebrae.

Cortical bone	Dense bone that forms the surface of bones.
Cytokines	Any of the several cells that are released by the cells of the immune system and act as intercellular mediators in the generation of an immune response.
Deposition	The laying down of new bone.
Hill function	A mathematical formulation is used to represent to intercellular between ligands and receptors.
Histology	Study of the microscopic structure and arrangement of tissue.
Histomorphometry	Classification of structure at microscopic level.
Hypothyroidism	Hypothyroidism is the disease state in humans and in animals caused by insufficient production of thyroid hormone by the thyroid gland. Cretinism is a form of hypothyroidism found in infants.
IGF-1 (Insulin-like growth factor 1)	Insulin-like growth factor 1 also called somatomedin C is a protein in humans encoded by the IGF1 gene.
IL-6 (interleukin-6)	Interleukin-6 is a protein that in humans is encoded by the IL6 gene.
<i>In silico</i>	<i>In silico</i> means experiments “performed on computer or via computer simulation”.
<i>In vivo</i>	<i>In vivo</i> means experiments performed in living organisms.
<i>In vitro</i>	<i>In vitro</i> means experiments performed outside of living organisms.

Marrow	Soft fatty substance in the cavities of bones in which blood cells are produced.
M-CSF (Macrophage colony stimulating factor)	M-CSF is a secreted cytokine which influences hematopoietic stem cells to differentiate into macrophages or other related cell types.
MIP-1α (Macrophage inflammatory protein-1)	Macrophage inflammatory protein-1 belonging to the family of chemotactic cytokines is crucial for immune responses towards infection and inflammation.
Modelling	Theoretical representation simulating the behaviour or activity of systems (biological or otherwise).
Multiple Myeloma	A hematological malignancy that develops within the bone marrow microenvironment.
Multiple Myeloma-induced bone disease	Bone related disease resulting from multiple myeloma with symptoms of bone pain, bone fracture and bone destruction. These complications are devastating to patients.
OPG (osteoprotegerin)	OPG is a protein and belongs to tumor necrosis factor (TNF) receptor superfamily, acting as a cytokine receptor.
Osteoblasts precursors	Mesenchymal stem cells which commit to the osteoblastic lineage.

Osteoblasts	Osteoblasts are derived from mesenchymal progenitors and are responsible for building new bone by synthesizing and secreting unmineralized bone matrix, and also participate in the bone calcification
Osteoclast precursors	Hematopoietic precursors, which are capable of differentiating into osteoclasts.
Osteoclast	Osteoclasts are multinucleated giant cells which range in diameter from 20 to over 100 μm , with one osteoclast containing from 1 to more than 50 nuclei Osteoclasts are responsible for resorbing bone during the remodelling cycle.
Osteocytes	Osteocytes are defined by location, and they are the osteoblasts buried in the newly formed osteoid during bone formation.
Osteoporosis	A bone disease characterised by decreasing bone mass and connectivity.
Parathyroid hormone	A polypeptide with a molecular weight of 9500, which is the most important hormone regulating calcium homeostasis and bone remodelling.
Primary Hyperparathyroidism	Primary hyperparathyroidism causes hypercalcemia (elevated blood calcium levels) through the excessive secretion of parathyroid hormone (PTH). The classic bone disease in hyperparathyroidism is osteitis fibrosa cystica, which results in pain and sometimes pathological fractures. Other bone diseases associated with hyperparathyroidism are osteoporosis, osteomalacia, and arthritis.

Radiotherapy	Radiotherapy is the use of high energy x-rays and similar rays (such as electrons) to treat disease.
RANK (receptor activator of NFkB)	RANK is a type I membrane protein expressed on the surface of osteoclasts.
RANKL (the receptor activator of nuclear factor kappa-B ligand)	RANKL is a member of the tumor necrosis factor (TNF) cytokine family and primarily expressed by osteoblast precursors acting as a key factor for osteoclast differentiation.
Remodelling	Process of renewal of bone by resorption and formation, conducted by osteoclasts and osteoblasts.
SLRPs (Small leucine-rich proteoglycans)	SLRPs are a family of proteins that are present in extracellular matrix.
TGF-β (Transforming growth factor beta)	TGF-β is a protein that controls proliferation, cellular differentiation, and other functions in most cells.
Thyroid Hormone	The thyroid hormones are tyrosine-based hormones produced by the thyroid gland primarily responsible for regulation of metabolism.
Trabecular	Thin bar or plate of bone found in cancellous (or trabecular) bone.
Uncommitted progenitors	Mesenchymal stem cells which are able to differentiate into different cell types, including osteoblastic cells, myocytes and adipocytes.
VCAM-1 (vascular cell adhesion molecule-1)	VCAM-1 is a protein in humans which is encoded by the VCAM1 gene, with the function of cell adhesion molecule.
VEGF (vascular endothelial growth factor)	Vascular endothelial growth factor is a signal protein produced by cells that stimulates vasculogenesis and angiogenesis.

**VLA-4 ($\alpha 4\beta 1$ integrin
presents on the surface of
multiple myeloma cells)
Wnt signalling pathway**

VLA-4 is a member of the integrin family of adhesion receptors and involves both cell-extracellular matrix and cell-cell adhesion.

Wnt signalling pathway is a network of proteins that pass signals from receptors on the surface of the cell to DNA expression in the nucleus, which controls cell-cell communication in the embryo and adult.

1. INTRODUCTION

Bone is a remarkable dynamic tissue which continuously repairs, renews and adapts in response to localized environmental changes, maintaining its function to provide structural support and a mineral reservoir (Parfitt, 1994; Sommerfeldt and Rubin, 2001). This dynamic behaviour is achieved through the remodelling process, which occurs at the basic multicellular unit (BMU) (Frost, 1986). Bone remodelling is a coupled process of bone resorption, carried out by osteoclasts, and bone formation, carried out by osteoblasts. The balance between the volume of resorbed and newly formed bone, and the activation frequency (remodelling rate) of the BMU, determines the integrity of the bone structure and strength throughout its life (Christiansen, 2001; Seeman and Delmas, 2006).

Positive balance and rapid remodelling cycles in healthy young individuals result in increasing bone mass and density, and therefore strengthen the bone. As juvenile growth ceases with epiphyseal closure, the remodelling rate decreases and the balance gradually shifts towards zero (Parfitt, 2000). The balance in healthy adult bone is approximately zero and the mean activation frequency is about 0.33 per year for trabecular bone (Agerbaek et al., 1991; Eriksen et al., 1985, 1986b), where Eriksen et al. (1985) defines activation frequency as the formation rate of a new remodelling cycle at a particular point. Thus, remodelling of a point will occur every three years or so. The remodelling balance becomes negative throughout the ageing process and disuse (Zaidi, 2007), with bone loss beginning between the ages of 18 and 30 years old, although the process is slow because the activation frequency is so low (Gilsanz et al., 1988). Pathologies such as hyperthyroidism, oestrogen deficiency, thyrotoxicosis and hypogonadism, can speed up the bone loss process (high-turnover osteoporosis) and cause structural damage, decreased bone strength and increased fracture risk (Eriksen et al., 1985; Seeman and Delmas, 2006; Zaidi, 2007). However, there are also some pathological conditions, such as hypothyroidism, which can induce a positive remodelling balance (Eriksen et al., 1986a). In this case, the positive balance is due to the significant reduction of bone resorption compared to healthy bone, whilst bone formation remains unchanged.

The BMU cycle suggests that osteoporosis and other bone-loss diseases can be treated by the repeated use of selected agents that affect different parts of the remodelling process, and therefore create an overall incremental gain in bone mass

(Frost, 1979). For example, the use of therapeutic agents to increase BMU activations, in conjunction with reducing osteoclast activity while maintaining osteoblast activity, will lead to an accumulation of new bone, in a similar way to that of hypothyroidism. This has led to the development of anti-resorptive therapies for post-menopausal bone loss, which includes oestrogens, the selective oestrogen receptor modulator tamoxifen and raloxifene, bisphosphonates and calcitonin (Rodan and Martin, 2000; Zaidi, 2007). These developments suggest that a comprehensive understanding of the remodelling process at the BMU level, could lead to better methods for manipulating the remodelling cycle in treating bone loss diseases.

Recent reviews of the bone remodelling process have revealed a growing number of factors that are involved in its regulation (Allori et al., 2008; Zaidi, 2007). These include autocrine and paracrine signalling molecules, systemic hormones and extracellular matrix components that affect cell-to-cell communication, migration, adhesion, proliferation and differentiation. Most of these findings are obtained from isolated observations of either *in vitro* studies or *in vivo* experiments using genetically manipulated animals. These findings have shown that osteoblasts are able to regulate the activity of osteoclasts, for example, expression of receptor activator of NFB ligand (RANKL) by osteoblasts directly interacts with RANK on osteoclast progenitors to drive osteoclastogenesis. This process also depends on the level of osteoprotegerin (OPG) that can act as a soluble decoy receptor for RANKL, thereby inhibiting RANK-mediated osteoclastogenesis (for a review see Boyce and Xing (2008)). However, bone remodelling is a very complex and integrated process, and these localized findings only give limited information about the overall effects of these factors on the bone remodelling process. This highlights the need for tools which can integrate these partial observations to a set of rules that define the behaviour of this complex system. Mathematical modelling has been proven to be a powerful tool in modelling and understanding biological processes.

Bone can resist the invasion of the majority of arriving cancerous cells due to its special properties. Diseases such as multiple myeloma (MM), breast cancer and prostate cancer can develop and survive within the bone microenvironment, due to phenotypic properties which influence the bone microenvironment to facilitate their growth and survival (Smith and Martin, 2011). MM is the second most frequent hematological malignancy, and MM-induced bone disease is a major cause of morbidity (Fowler et al., 2011). MM cells enhance bone resorption and suppress

bone formation, which consequently leads to a negative bone balance and results in osteolytic lesions that rarely heal (Matsumoto and Abe, 2011; Roodman, 2011). Histomorphometric studies reveal that the increased bone resorption arises due to the remodelling sites developing increased resorption surfaces and depth (Taube et al., 1992; Wittrant et al., 2004). In addition, the coupling between bone resorption and formation is also disturbed in MM patients (Calvani et al., 2004).

The interaction between MM cells and the bone microenvironment (MM-bone interaction) plays an important role in the development of MM bone disease, as it promotes tumour growth and survival, as well as the consequent bone destruction (Fowler et al., 2011). Cytokines with osteoclast activating functions, such as the receptor activator of nuclear factor kappa-B ligand (RANKL), macrophage colony stimulating factor (M-CSF), interleukin-6 (IL-6), IL-11 and IL-1 β (Terpos and Dimopoulos, 2005) are produced or stimulated by MM-bone interaction and further stimulate osteoclast activation and proliferation, therefore lead to increased bone resorption. In turn, growth factors released from bone resorption stimulate the growth of myeloma cells (Wittrant et al., 2004), including transforming growth factor-beta (TGF- β), bone morphogenetic proteins (BMP), heparin-binding fibroblast growth factors and insulin-like growth factor I (Blum et al., 2004; Guise and Chirgwin, 2003). Such reciprocal interaction produces a 'vicious cycle' between MM cells and the bone microenvironment, stimulating both tumour development and bone destruction (Fowler et al., 2011; Wittrant et al., 2004).

The research in this thesis consists of two major parts. Firstly, a novel predator-prey based mathematical model has been developed to describe the temporal dynamic interaction between osteoclasts and osteoblasts at a single BMU, with their corresponding bone resorption and formation activities. The model was developed to mimic the reconstructed remodelling cycles (curves) in both normal and pathological conditions, which are obtained from histomorphometric analysis (Agerbaek et al., 1991; Eriksen et al., 1984b; Eriksen et al., 1985, 1986a), and to replicate the observed dynamic interaction between osteoclasts and osteoblasts during the remodelling process. To our knowledge, this is the first attempt to develop mathematical models which are able to replicate such reconstructed remodelling curves quantitatively. The model has the potential to be used in modelling of pathological conditions and in the analysis of the underlying mechanisms of their treatment. Secondly, a mathematical model was developed to simulate the pathology

of MM-induced bone disease. It was developed in parallel with the recently published model of Wang et al. (2011), and similarly based on the earlier work of Pivonka et al. (2008, 2010), but importantly also included the underlying mechanisms involved in the inhibition of osteoblasts and their role in the development of MM bone disease. Wang et al. (2011) did not include this half of the bone remodelling process. The model can simulate the development of MM cells and the induced bone destruction, and explains why MM induced bone lesions rarely heal even after the complete removal of MM cells. The model reconstructs the variation of cell concentrations and the resultant bone destruction after the invasion and then the removal of the tumor cells, which matches published experimental observations. The model could also be used to test and evaluate proposed therapeutic interventions for MM bone disease (e.g. bisphosphonate, Bortezomib and inhibition of TGF- β) and even propose new treatments.

This thesis consists of seven chapters, plus a glossary to define key biological and technical terms and one appendix. The appendix contains a summary of publications associated with this study. A brief description of the contents of each chapter follows.

Chapter 2 briefly discusses some basic background knowledge of bone biology, including bone structure, bone composition, the underlying biological mechanisms of bone remodelling cycles and the biochemical factors regulating the bone remodelling process.

Chapter 3 reviews a group of recently developed mathematical models of the bone remodelling process at the cellular level. They demonstrate great potential in developing our understanding of the bone remodelling process.

Chapter 4 introduces a proposed predator-prey based mathematical model of bone remodelling at the cellular level in trabecular bone. The relevant literature regarding mathematical modelling is firstly introduced, including definition of the mathematical modelling and the process to build a mathematical model. Secondly, the development of the predator-prey based mathematical model is discussed, including model equations, model calculations, and simulation results and analysis.

Chapter 5 describes the development of a mathematical model which demonstrates how the interaction between MM cells and the bone microenvironment, drives the development of MM and consequent bone destruction. Initially, a model based on the work of Pivonka et al. (2008) was developed to simulate the bone

microenvironment under normal condition. This model was then extended to mimic the pathology of MM-induced bone disease, by including the invasion of the tumour cells. The equations used to construct these two models are discussed in detail, along with the simulation results and subsequent analysis. The model was validated by comparing model predictions with published experimental observations.

Chapter 6 gives a summary of the key results of the previous chapters and discusses how they fit into the current literature regarding the relevant bone biology and the mathematical models of the bone remodelling process.

Chapter 7 outlines the main conclusions from the current research and suggest the direction of future work.

Hence, the main contributions of this work are summarised as follow:

1. To develop a mathematical model to simulate the bone remodelling cycles for trabecular bone based on a predator-prey model;
2. To understand the roles of biochemical factors, including RANKL, OPG, TGF- β and systemic hormones (such as PTH) in the bone remodelling process;
3. To model the pathologies of bone related diseases, such as hypothyroidism and primary hyperparathyroidism;
4. To develop a mathematical model to simulate the pathology of MM-induced bone disease;
5. To investigate the role of the interaction between MM cells and the bone microenvironment, in the development of the tumour cells and the subsequent bone destruction;
6. To simulate current therapies and evaluate the efficacy of potential therapies of MM-induced bone disease.

2. LITERATURE REVIEW-BASIC BONE BIOLOGY

2.1 INTRODUCTION

This chapter reviews basic bone biology and provides the underpinning knowledge of bone structures and cellular activity required for this project. Bone structures, composition and cells are introduced first, followed by principles and regulatory factors of bone remodelling, together with bone metabolic diseases resulting from disorders of bone remodelling cycles.

2.2 BONE STRUCTURE AND COMPOSITION

The skeletal system plays both a biomechanical and metabolic role in the human body, and consists of a series of individual bones which are connected by soft tissue structures (Jee, 2001). Bone is the main constituent of the skeletal system and differs from connective tissue in terms of rigidity and hardness, enabling the skeleton system to maintain the shape of the body, protect the internal organs, supply the framework for the bone marrow and transmit the forces induced by muscular contractions during movement.

The skeleton is divided into axial and appendicular subdivisions according to its different compositions and functions as shown in Table 2.1.

Feature	Axial	Appendicular
Main bone tissue	Cancellous	Cortical
Adjacent soft tissue	Viscera	Muscle
Cortices	Thin	Thick
Marrow	Hematopoietic	Fatty
Turnover	High	Low
Cortical	Mechanical	Mechanical
Cancellous	Metabolic	Mechanical

Table 2.1: Compositions and functions of axial and appendicular subdivisions of the skeleton. Reproduced from Bronner and Worrell (1999).

The long bones such as humerus, femur and tibia are usually used as the classical model to introduce the macroscopic structure of bone (Jee, 2001). A typical adult long bone comprises of a diaphysis in the middle, which is enclosed by two more wider and rounded epiphyses. The diaphysis is connected with each epiphysis by a conical region named the metaphysis. The main composition of the diaphysis is cortical bone (or compact bone), while the epiphysis is primarily constructed from trabecular (or cancellous) bone which is encapsulated by cortical bone (Figure 2.1). Cortical bone is a dense, solid mass with only microscopic channels. It accounts for approximately 80% of the skeletal mass in the adult human skeleton, forms the outer wall of all bones and is responsible for the support and protection of the skeleton. Trabecular bone accounts for the remaining 20% and is located in the internal structure of bones. Cortical bones differ from trabecular bone in terms of their development, architecture, function, proximity to bone marrow, blood supply, rapidity of turnover time and magnitude of age-dependent changes and fractures (Jee, 2001).

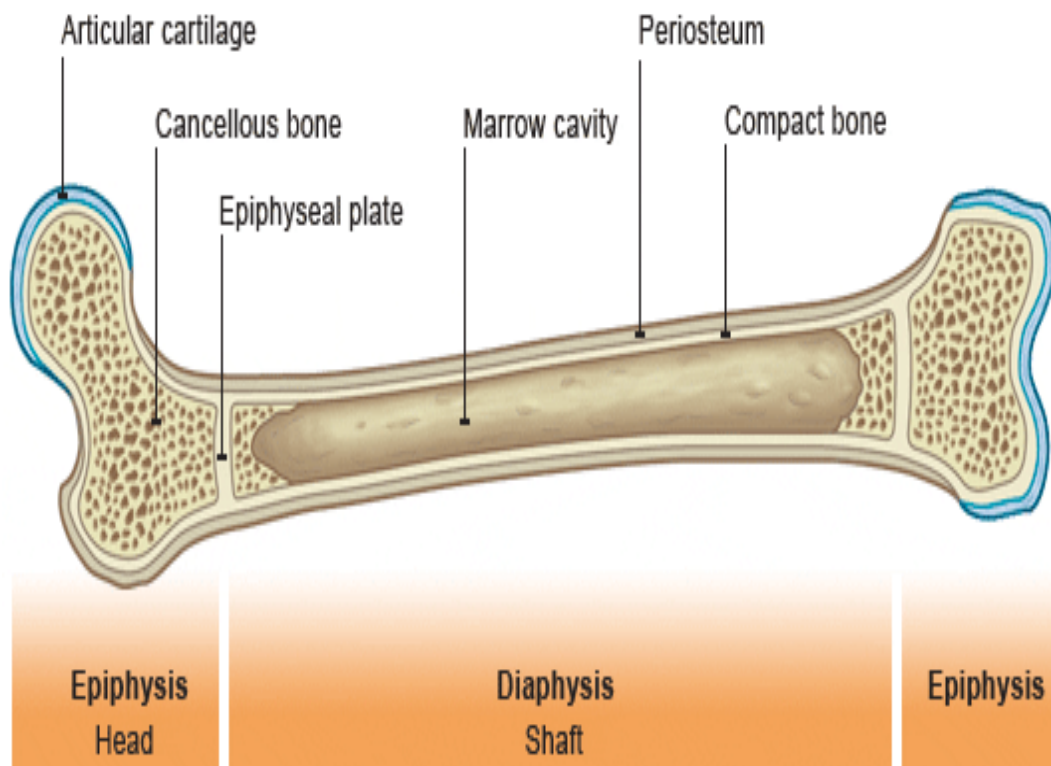


Figure 2.1: Schematic diagram of the macroscopic structure of a long bone. Reproduced from Physical Education: The skeleton bones and joints [Online], http://www.bbc.co.uk/schools/gcsebitesize/pe/appliedanatomy/2_anatomy_skeleton_rev4.shtml [Accessed 25, May 2011].

The main structural unit of cortical bone is different from that of trabecular bone. It is the osteon (Haversian system), which is a cylinder about 200 to 500 μm (micrometre) in diameter, and accounts for two thirds of the volume; whilst the remaining one third is interstitial bone, which is composed of the remnants of past generations of osteons and circumferential lamellae. In comparison, the trabecular packet (hemiosteon) serves as the structural unit of trabecular bone and is a shallow crescent-shaped hemiosteon which has a 600 μm radius, 50 μm thick and 1 mm length. Table 2.2 shows details of BMUs of cortical and trabecular bone as below.

Parameter	Cortical (Osteonal)	Cancellous (Trabecular Packet)
Length (mm)	2.5	1.0
Circumference (mm)	0.6	0.6
Wall thickness (mm)	0.075	0.040
Number/mm ³ bone volume	15	40
Total number in skeleton	21×10^6	14×10^6
Duration of resorption (days)	24	21
Duration of formation (days)	124	91
Remodelling period (days)	148	112
Bone turnover rate (%/year)	43	26

Table 2.2: Comparison of adult cortical and cancellous bone multicellular units. Modified from Recker (1983).

The composition of bone includes minerals, organic matrix, cells and water. Minerals account for 65% of bone and can be found within collagen fibres in the form of small crystals in the shape of needles, plates and rods. The mineral is largely impure hydroxyapatite ($\text{Ca}_{10}(\text{PO}_4)_6(\text{OH})_2$), which contains carbonate, citrate, magnesium, fluoride and strontium. These constituents are incorporated into the crystal lattice or absorbed onto the crystal surface (Gehron and Boskey, 1996; Lian et al., 1999). The organic matrix accounts for the remaining 35% of bone and is made up of 90% collagen and about 10% of various non-collagenous proteins, and has a

wide variety of functioned roles and determines the structural, mechanical and biochemical properties of the tissue (Gehron and Boskey, 1996; Gorski, 1998; Lian et al., 1999).

2.3 BONE CELLS

Bone cells include osteoblasts, osteoclasts, the immune regulatory system that supplies the precursor cells and regulates bone growth and maintenance, osteocytes, bone lining cells and cells of the marrow compartment (Jee, 2001). Only osteoclasts, osteoblasts, bone lining cells and osteocytes are discussed in this chapter, as these are the most relevant cells to this study.

OSTEOCLASTS

Osteoclasts are multinucleated giant cells which range in diameter from 20 to over 100 μm , with one osteoclast containing from 1 to more than 50 nuclei (Figure 2.2) (Jee, 2001). Osteoclasts are responsible for resorbing bone during the remodelling cycle. The surface of an osteoclast adjacent to the bone surface has a striated appearance and a ruffled border, and secretes products which lead to bone resorption.



Figure 2.2: Light micrograph of an osteoclast. Reproduced from Hill M, Musculoskeletal System – Bone Development [Online]. Available:[http://php.med.unsw.edu.au/embryology/index.php?title=Musculoskeletal System - Bone Development#Introduction](http://php.med.unsw.edu.au/embryology/index.php?title=Musculoskeletal%20System%20-%20Bone%20Development#Introduction) [Accessed 30, March 2011].

The differentiation of osteoclasts from their early precursors involves several stages as summarized in Figure 2.3 (Roodman, 2006). Osteoclasts are derived from cells in the mononuclear/phagocytic lineage of the hematopoietic marrow. The granulocyte-macrophage colony-forming unit (CFU-GM) is capable of differentiating into granulocytes, monocytes and osteoclasts, and is identified as the earliest osteoclastic precursor. CFU-GM-derived cells first differentiate into osteoclastic precursors, which later fuse to form multinucleated osteoclasts (Roodman, 2006). Active osteoclasts are usually observed in cavities on the surface of trabecular bone or internally in cortical bone in Howship's lacunae. The life span of osteoclasts *in vivo* is reported to be up to 7 weeks, after which they undergo apoptosis (Majeska, 2001).

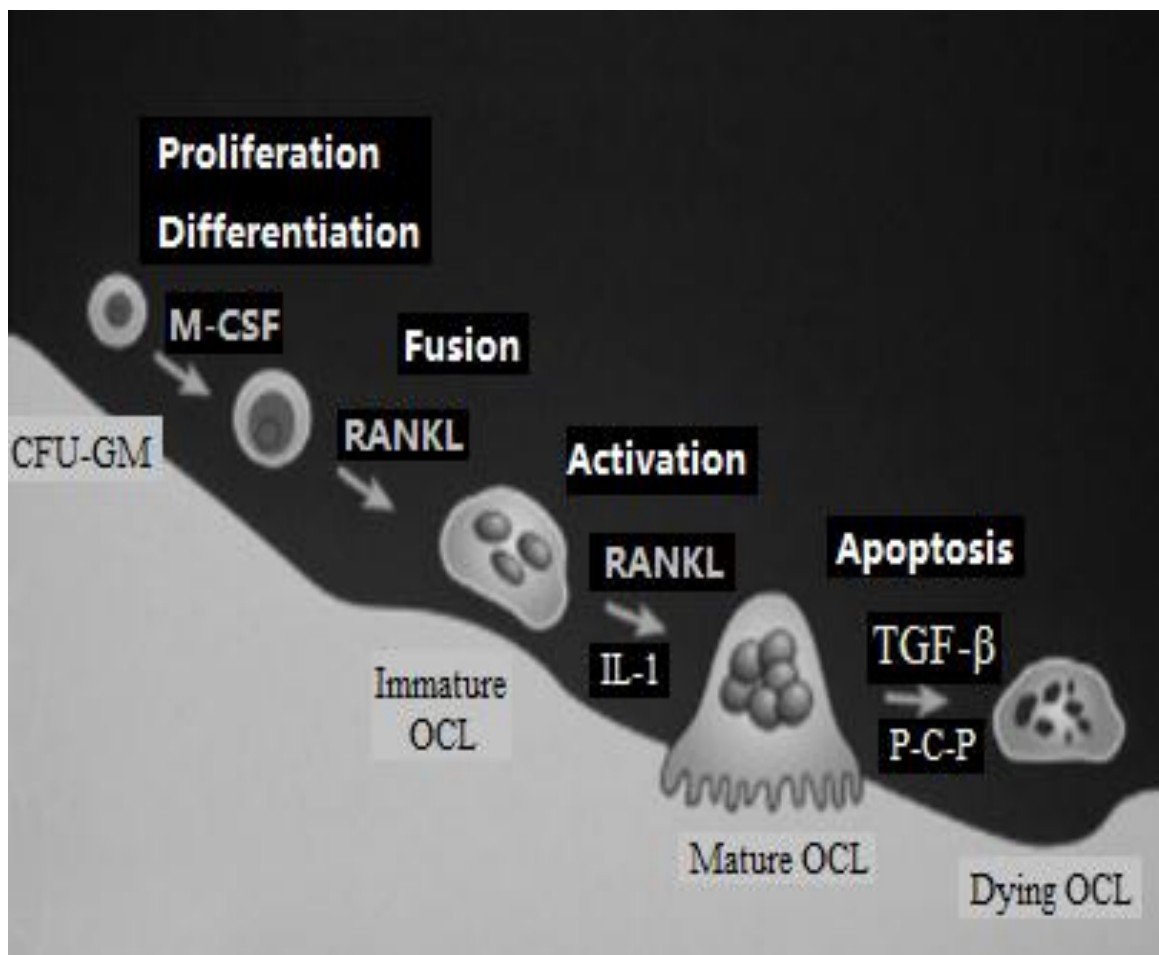


Figure 2.3: The osteoclast life cycle from proliferation and differentiation to apoptosis. Reproduced from Roodman (2006).

OSTEOBLASTS

Osteoblasts are responsible for building new bone by synthesizing and secreting unmineralized bone matrix, and also participate in the bone calcification (Jee, 2001). They control the flow of calcium and phosphate in and out of bone and regulate bone resorption indirectly by interacting with osteoclastic cells. Active osteoblasts are cuboidal in shape, and are typically 15 to 30 μm thick (Figure 2.4) (Jee, 2001).

Osteoblasts are derived from mesenchymal progenitors and their life consists of the several differentiation steps illustrated in Figure 2.5 (Eijken, 2007). Firstly, mesenchymal stem cells commit to the osteoblastic lineage, which then proliferates and differentiates into pre-osteoblasts. These pre-osteoblasts are able to produce extracellular matrix, and differentiate into mature osteoblasts that are capable of synthesizing extracellular matrix and initiating its mineralization. Several mature osteoblasts are eventually deposited within the newly formed bone matrix as osteocytes. The remaining mature osteoblasts undergo apoptosis or become bone lining cells (Eijken, 2007).

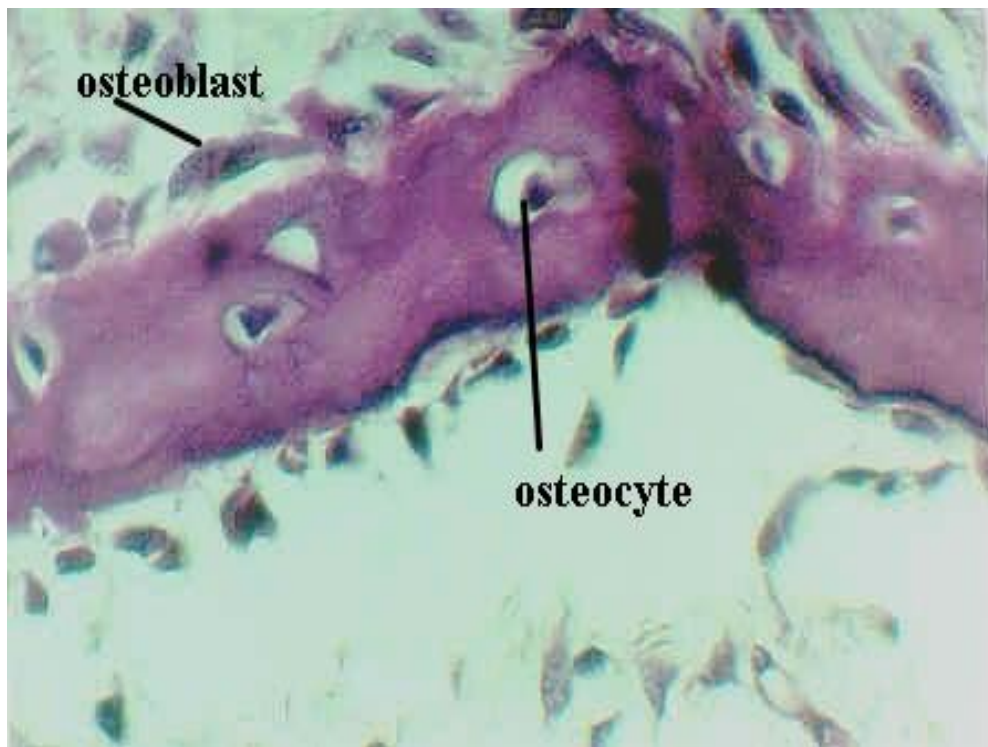


Figure 2.4: Light micrograph of an osteoblast and osteocyte. Reproduced from Laboratory Exercises: intramembranous Bone Development [Online]. Available: http://microanatomy.net/bone/devbone2_lab.htm [Accessed 30, March 2011].

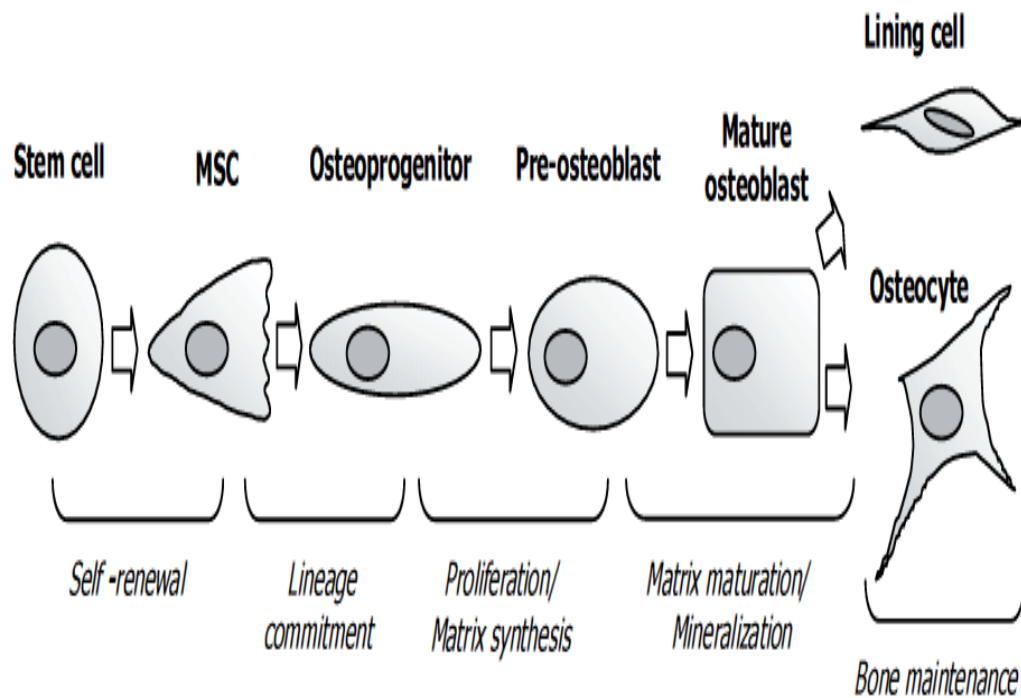


Figure 2.5: The differentiation stages of the osteoblast from stem cells. Reproduced from Eijken (2007).

BONE LINING CELLS

Bone lining cells are situated on the quiescent bone surface. They are a distinct morphological phenotype with a thin, flat nuclear profile with attenuated (1 μm thick and up to 12 μm long) cytoplasm (Jee, 2001). Gap junctions exist between adjacent bone lining cells, and between bone lining cells and osteocytes (Jee, 2001). Bone lining cells are derived from inactive osteoblasts and osteoblast precursors, which have ceased activity or differentiation (Jee, 2001).

Bone lining cells build three-dimensional networks with osteocytes. It is believed that these three-dimensional networks, in which the cells communicate with each other, are able to sense the stress and strain experienced within a bone, and subsequently transmit signals to the bone surface to initiate the remodelling process (Baron, 1999; Burr, 1997; Parfitt, 1983; Roodman, 1996).

OSTEOCYTES

Osteocytes are the most abundant cell type in mature bone, with about ten times more osteocytes than osteoblasts in healthy human bone. Osteocytes are formed from

the osteoblasts deposited in the newly formed osteoid during bone formation (see Figure 2.6) (Bonewald, 2004; Jee, 2001).

The location of osteocytes makes them capable of sensing the magnitude and distribution of strains, and translate these signals into biochemical signals (Bonewald, 2004; Jee, 2001). Their functions can be summarized in two ways: (1) they stabilize bone mineral by maintaining an appropriate level of local ionic milieu, and control the efflux of calcium ions in collaboration with bone lining cells (Holtrop and Weinger, 1972; Miller et al., 1980; Miller and Jee, 1987; Talmage, 1969); (2) they detect micro-damage of bone (Bentolila et al., 1998; Lanyon, 1996; Lanyon et al., 1993; Mori and Burr, 1993) and respond to mechanical strain induced within bone tissue through cell-cell interaction (Lanyon et al., 1993).

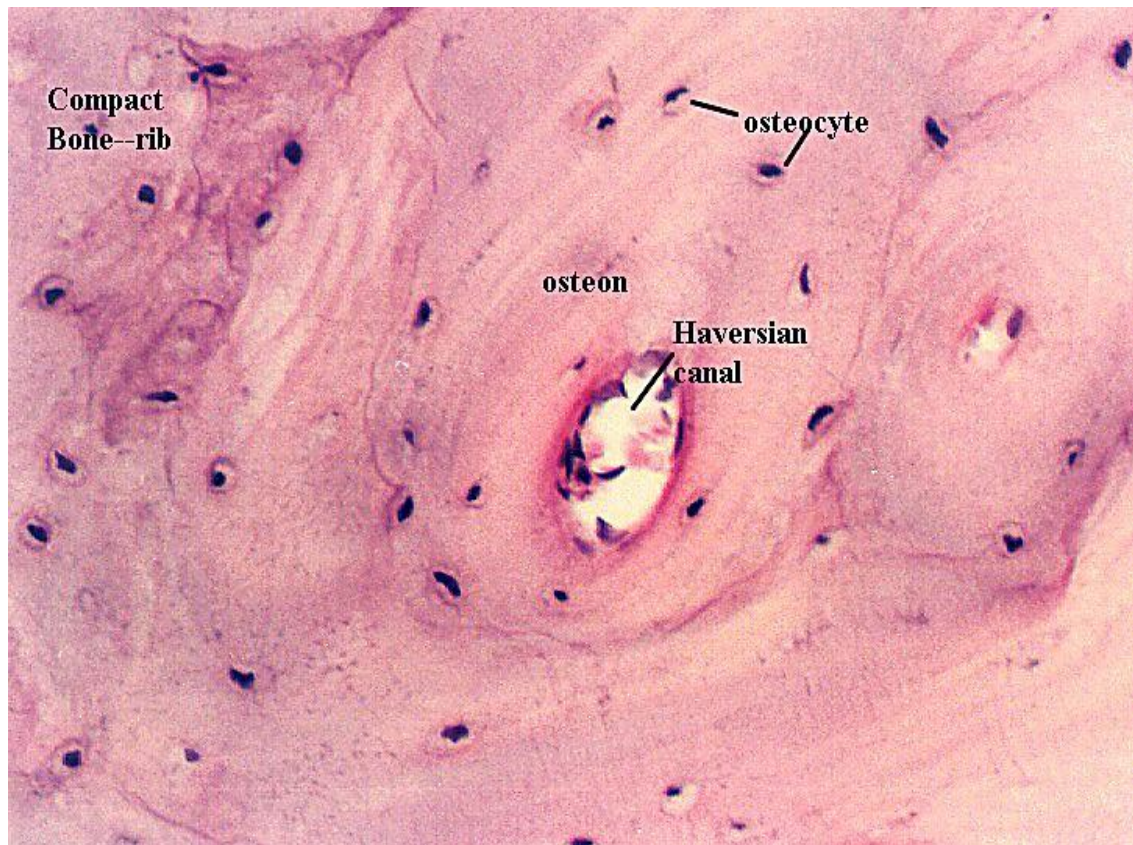


Figure 2.6: Microphotograph of several layers of osteocytes in the lacunae of Harversian canal. Reproduced from Compact Bone Histology [Online]. Available: http://www.cytochemistry.net/microanatomy/bone/compact_bone_histology.htm [Accessed 30, March 2011].

2.4 BONE REMODELLING

Bone formation begins *in utero* and continues throughout adolescence by “modelling” until skeletal maturity is reached (Einhorn, 1996). Bone is a metabolically active organ that is able to adapt its structural and material properties to the mechanical demands placed upon it, via a localized process termed “bone remodelling” (Raisz, 1999). The bone remodelling cycle consists of a series of highly regulated sequential steps involving the interactions of osteoclastic and osteoblastic lineages, the mesenchymal osteoblastic lineage and the hematopoietic osteoclastic lineage (Raisz, 1999). In addition, bone remodelling processes are able to maintain mineral homeostasis and the biomechanical integrity of the skeleton via repairing fatigue damage (Mundy and Boyce, 1996).

Bone remodelling is a continuous process of bone resorption performed by osteoclasts, followed by bone formation performed by osteoblasts, and occurs in the skeleton of vertebrates throughout their lifetime (Mundy, 1999). It occurs asynchronously at multiple spatially and temporally discrete sites of the skeleton in order to repair damaged portions or replace older bone with new bone (Pivonka et al., 2008).

An ideal condition consists of the amount of newly formed bone equalling the amount of the resorbed bone, thereby preserving bone mass (Glowacki, 1996; Kessenich and Rosen, 1996). This balance is maintained by the tight coupling between osteoclastic and osteoblastic cells, *i.e.* the activation of an osteoclast cannot usually occur in the absence of osteoblasts. In fact, the bone remodelling cycle is initiated by osteoblastic cell signalling to generate osteoclast-active cytokines, and this mechanism ensures that bone remodelling begins and ends with osteoblast activity (Kessenich and Rosen, 1996). Osteoblasts indirectly regulate the bone resorption performed by osteoclasts via the RANKL-RANK-OPG pathway (Bell, 2003; Boyce and Xing, 2008).

AIMS OF BONE REMODELLING

Bone remodelling is carried out to achieve three main aims (Burr, 2002): (1) to regulate the balance of essential minerals in the body by changing their concentration in serum; (2) to enable the skeleton to adapt to its mechanical environment, which reduces the risk of fracture; (3) to provide a mechanism for repairing bone damage.

The first aim can be carried out by site-independent bone remodelling, as the location of bone remodelling is not important, providing bone integrity is not challenged and the mineral balance is maintained (Burr, 2002). However, the other two aims require site-dependent remodelling, since it is unnecessary for the remodelling system to increase its turnover rate throughout the whole skeletal when only a single location is damaged (Burr, 2002).

THE BONE MULTICELLULAR UNIT

A BMU is a temporal association of a group of cells that accomplish one quantum of bone turnover, *i.e.* removal and replacement of existing bone with a new structural unit (Hernandez et al., 2000). The BMU originates within the bone and progresses across the trabecular bone surface (or through the Haversian canal in cortical bone) during its lifespan (Figure 2.7).

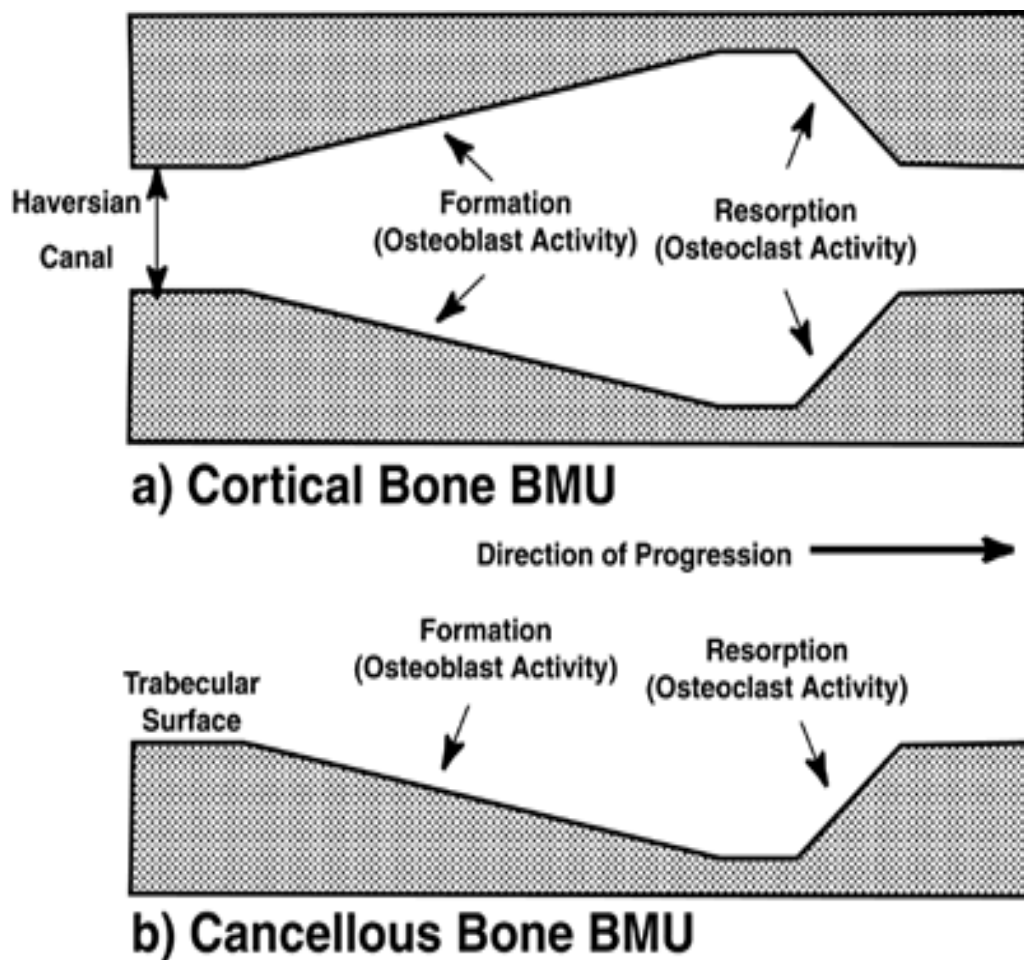


Figure 2.7: The basic multicellular unit (BMU) in cortical and cancellous bone. Reproduced from Hernandez et al. (2000).

As shown in Figure 2.8, the life cycle of a BMU consists of six stages: resting, activation, resorption, reversal (coupling), formation, mineralization and back to resting (Jee, 2001).

Resting

In the resting phase the bone surfaces are inactive with respect to bone remodelling. Almost 80% of trabecular and cortical bone surfaces in large adult animals, including humans, are in the resting phase at any given time (Jee, 2001). The resting bone surfaces are covered by bone lining cells that may function as osteogenic precursor cells and an endosteal membrane.

Activation

The activation of bone remodelling refers to the conversion of a bone surface from a state of resting into a period of resorption. It is still not completely clear which factor initiates this activation, although local structural and biomechanical requirements are believed to be involved (Jee, 2001).

Resorption

The resorption phase begins when osteoclasts arrive and make contact with the bone surface. Osteoclasts resorb bone and form Howship's lacunae in trabecular bone, and Haversian canals in cortical bone (Jee, 2001). The mean resorption depths in trabecular and cortical bone are 60 μm in radius and 100 μm in diameter, respectively (Jaworski et al., 1975).

Reversal (Coupling)

After the maximum resorption depth has been achieved by the osteoclasts, the reversal phase begins. There is a 1 to 2 weeks duration between the completion of bone resorption and the commencement of bone formation. From a histology perspective, the reversal phase is a period when there are no osteoclasts in the Howship's lacunae and Haversian canals (Jee and Ma, 1997). During the reversal phase osteoclasts undergo apoptosis, while macrophage-like cells appear on the bone surface. These latter cells may release factors that are able to suppress osteoclast activity and stimulate osteoblast activity.

Formation and Mineralization

Bone formation involves bone matrix synthesis followed by extracellular mineralization. Osteoblasts begin to build a layer of matrix called the osteoid seam. The osteoid seam achieves about 70% of its final mineralization after 5 to 10 days, with complete mineralization taking about 3 to 6 months in both cortical and cancellous bone (Ericksen et al., 1994; Frost, 1995; Jee, 1988; Parfitt et al., 1987; Recker, 1983).

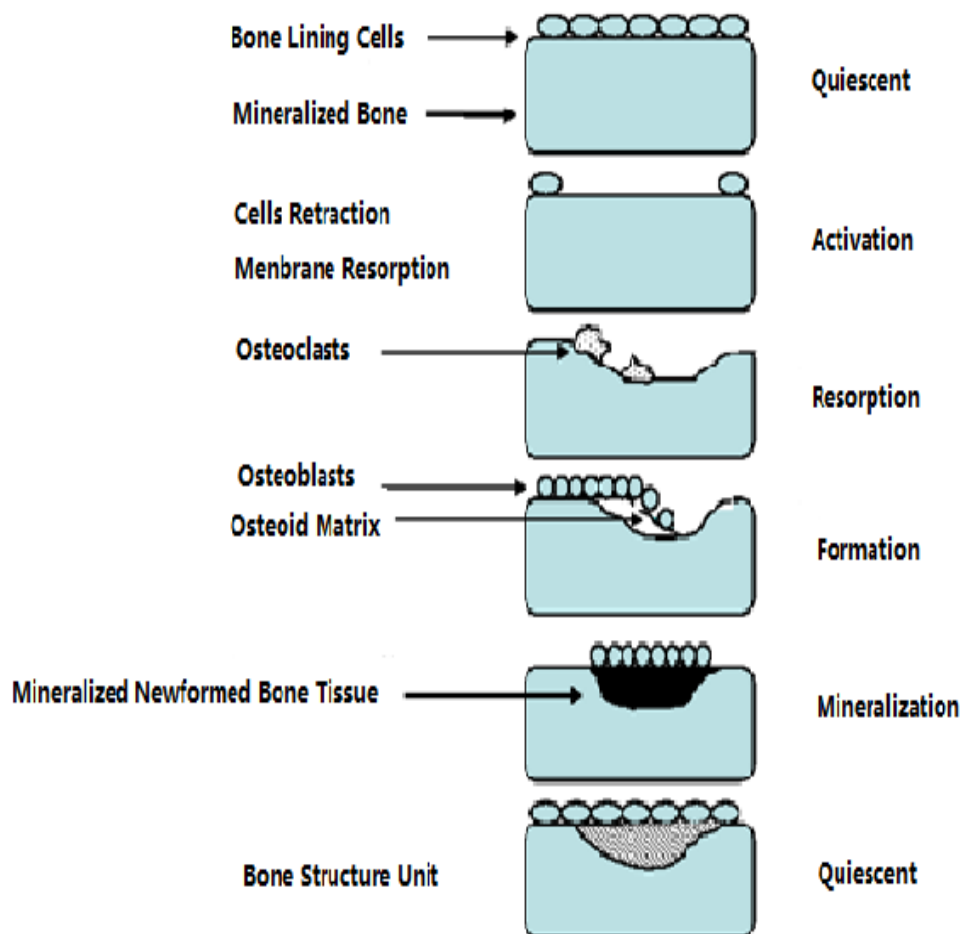


Figure 2.8: The different phases of the bone remodelling cycle. Reproduced from Medicina Oral, Patología Oral y Cirugía Bucal [Online]. Available: http://scielo.isciii.es/scielo.php?pid=S1698-69462006000200012&script=sci_arttext&tlng=en [Accessed 30, March 2011].

REGULATORY FACTORS OF BONE REMODELLING

Many factors can regulate bone remodelling and thereby influence the peak bone mass and the remodelling rate, including environmental factors (such as diet, calcium intake and level of exercise), local factors in the bone microenvironment and

systemic hormones. Bone remodelling is regulated by local factors, such as cytokines (both paracrine and autocrine), growth factors, cell to cell communications (Bland, 2000; Mundy and Boyce, 1996) and systemic factors (*e.g.* systemic hormones). Systemic factors regulate bone remodelling indirectly via local factors or directly by binding to their own receptors (Figure 2.9) (Lemaire et al., 2004). Systemic and local factors affect osteoblastic and osteoclastic cells by regulating the replication of undifferentiated cells, the recruitment of cells and the differentiated function of cells (Canalis, 1993).

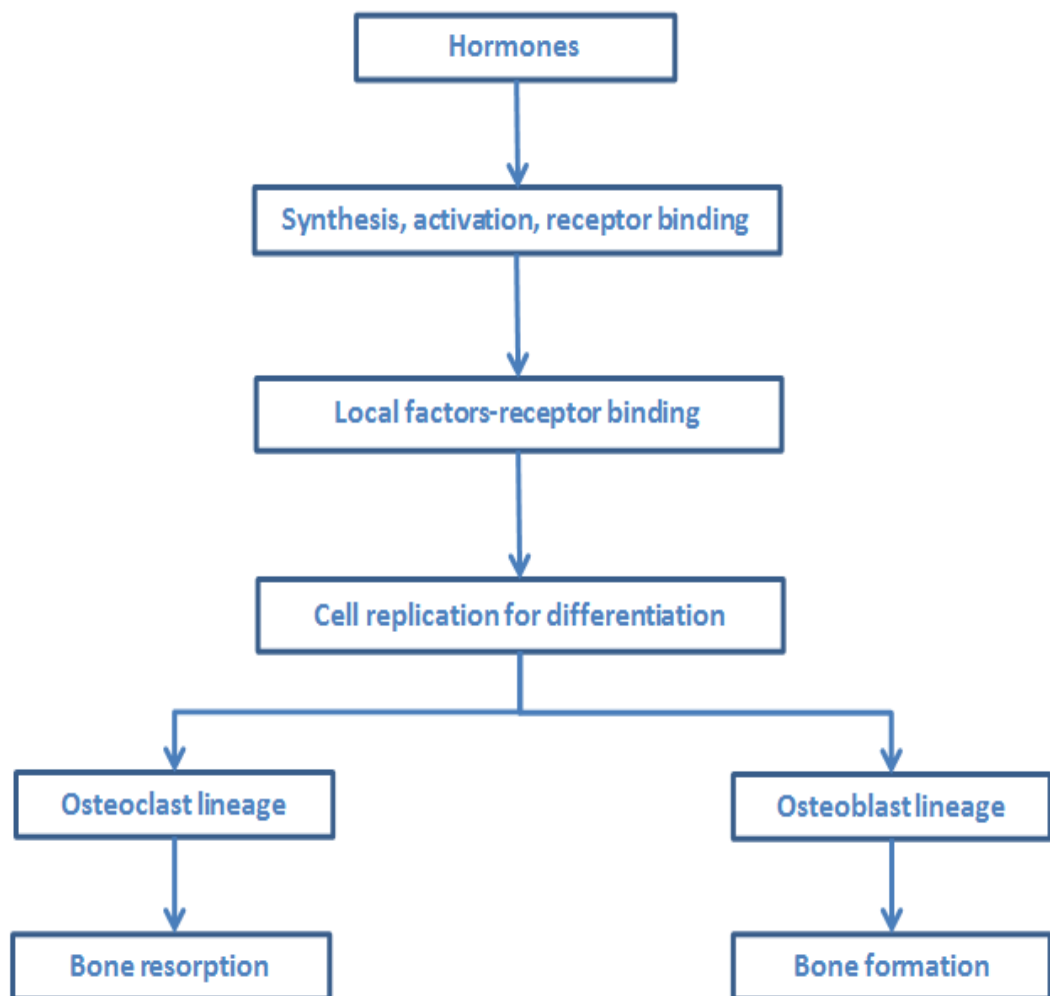


Figure 2.9: Schematic representation of the regulation of bone remodelling by hormones and local factors. Reproduced from Canalis (1993).

2.4.1 HORMONAL REGULATION OF BONE REMODELLING

Bone remodelling is regulated by a variety of systemic hormones, such as parathyroid hormone, calcitonin, insulin, growth hormone and steroids (e.g. vitamin D, glucocorticoids, sex steroids and thyroid hormone) (Canalis, 1993). The effect of parathyroid and thyroid hormone on bone remodelling is discussed here.

Parathyroid Hormone

Parathyroid hormone (PTH) is a polypeptide with a molecular weight of 9500, and is regarded as the most important hormone regulating calcium homeostasis and bone remodelling (Parfitt, 1976). It has been used in numerous clinical trials as an anabolic agent for the treatment of osteoporosis. Interestingly, PTH has a dual effect on bone: catabolic when released into plasma quasi-continuously or continuously; and anabolic when injected intermittently (Dempster et al., 1993; Meng et al., 1996; Watson et al., 1999).

Osteoclasts do not have PTH receptors, although they are expressed on the osteoblast surface, and PTH can stimulate bone resorption by osteoclasts indirectly via osteoblasts (Goltzman, 1999; Teitelbaum, 2000). For example, quasi-steady state levels of plasma PTH stimulate the production of RANKL by osteoblasts, however it inhibits the production of OPG by osteoblasts, therefore causing an increase in population of active osteoclasts (Aubin and Bonnelye, 2000; Halladay et al., 2001; Ma et al., 2001; Teitelbaum, 2000). Thus, the observed catabolic effect of PTH requires the presence of osteoblasts or osteoblast-derived factors. Continuous treatment with PTH suppresses bone formation *in vitro* as it directly inhibits bone collagen synthesis. In contrast, intermittent treatment with PTH results in a stimulation of bone collagen synthesis and bone formation (Canalis et al., 1989).

Thyroid Hormone

Thyroid hormones are potent stimulators of osteoclasts and osteoblasts (Melsen and Mosekilde, 1977; Mosekilde and Melsen, 1978a, b; Mundy et al., 1976) and play an important role in the skeletal growth and development in children (Altabas et al., 2007). Thyroid hormone deficiency in childhood causes retardation of skeletal development and growth arrest. In comparison, excessive production of thyroid hormones results in accelerated growth and can even prematurely close the growth plates and cranial sutures. In adult thyrotoxicosis, accelerated bone remodelling paralleling an imbalance between bone resorption and bone formation, leads to net

bone loss and increased risk of bone fracture (Bassett and Williams, 2003). Therefore, thyroid hormones are important in skeletal development and metabolism.

Excessive levels of thyroid hormones increase the activity of both osteoblasts and osteoclasts, which can result in accelerated bone remodelling (Altabas et al., 2007). Thyroid hormone deficiency causes reduced bone remodelling rates and elevated bone mineral density in adults. However, the exact molecular mechanisms of thyroid hormone acting on bone are not completely understood (Altabas et al., 2007).

2.4.2 LOCAL REGULATION OF BONE REMODELLING

In addition to systemic regulatory factors, bone remodelling is also under the control of local factors, since bone remodelling is a local phenomenon happening in the bone microenvironment (Lemaire et al., 2004; Mundy and Boyce, 1996). Most of the local factors are produced by skeletal cells, however some are derived from cells of the immune or hematological system that are present in the bone microenvironment (Canalis, 1993).

Early attempts to understand the structural adaptation of the skeleton theorised that bone remodelling must be regulated by local factors (McLeod et al., 1998), although it remained unknown which factors were involved. One of the first to be identified was cytokines (Raisz, 1999). These “osteoclast-activating factors”, which can be produced by inflammatory cells (such as macrophages), are involved in the local bone loss associated with periodontal disease and inflammatory arthritis (Lorenzo, 1991). At about the same time, prostaglandins (particularly prostaglandin E₂) were demonstrated to stimulate bone resorption (Kawaguchi et al., 1995). To date a large number of cytokines and growth factors which are capable of affecting bone cell functions have been identified (Horwood et al., 1998b; Mizuno et al., 1998; Raisz, 1999; Yasuda et al., 1998).

Communication between osteoclastic cells and osteoblastic cells plays an important role in bone remodelling. For many years it has been hypothesized that osteoclast development and activity are under the control of osteoblasts or stromal cells (Rodan and Martin, 2000). However, details of the molecular and physiological mechanisms were not identified until the end 1990s, when some of the proteins responsible for the interaction between cells of osteoclastic and osteoblastic lineages were discovered. The mechanism by which such proteins pass messages between

osteoclastic and osteoblastic cells is called the RANK-RANKL-OPG signalling pathway (Hofbauer and Schoppet, 2004; Martin, 2004; Robling et al., 2006).

The RANK-RANKL-OPG Pathway

The RANK-RANKL-OPG pathway involves three components: (1) receptor activator of nuclear factor κ beta (NF-κ) ligand (RANKL), a protein primarily produced by osteoblastic precursors as a soluble form; (2) receptor activator of nuclear factor κ beta (NF-κ) (RANK) expressed on the surface of hematopoietic precursor cells (referred to as osteoclastic precursor cells); (3) osteoprotegrin (OPG), a “decoy receptor” primarily released by mature osteoblasts (Martin, 2004; Pivonka et al., 2008; Simonet et al., 1997). RANKL interacts with its receptor (RANK) and thereby promotes osteoclast formation (as well as maintaining their viability and activity) (Martin, 2004; Pivonka et al., 2008). OPG can suppress the interaction of RANKL/RANK by binding to RANKL as a soluble decoy receptor (Pivonka et al., 2008). Its signalling pathway is called the RANK–RANKL–OPG pathway and plays an important role in the coupling between bone resorption by osteoclasts, and bone formation by osteoblasts.

Bone contains many growth factors, such as TGF-β (transforming growth factor beta), whose content in dried bone powder is approximately 1000-fold greater than the levels required for osteoblastic stimulation (Hauschka, 1989). These growth factors released during bone resorption can influence the osteoblastic cells. The effect of TGF-β on the osteoblastic lineage is bi-directional and dependent upon the state of osteoblasts (Hauschka, 1989; Simmons and Grynopas, 1990). On one hand, TGF-β has the potential to stimulate osteoblast recruitment, migration and proliferation of osteoblast precursors (Bonewald and Dallas, 1994b; Eriksen and Kassem, 1992; Mundy and Boyce, 1996). On the other hand, TGF-β suppresses the differentiation of osteoblastic precursors into active osteoblasts (Alliston et al., 2001). Therefore, TGF-β inhibits the population of active osteoblasts until it is removed or becomes inactive (Mundy, 1999).

2.4.3 RELATIONSHIP BETWEEN LOCAL AND SYSTEMIC FACTORS

The RANK-RANKL-OPG pathway, together with the dual action of TGF-β on osteoblasts, builds a control network through which systemic factors can regulate bone remodelling (Lemaire et al., 2004; Manolagas, 2000). Many factors regulate

bone resorption such as parathyroid hormones (PTH), prostaglandins, interleukins, vitamin D₃ and corticosteroids, and exert an indirect effect. They signal to the osteoblast/stromal cells, and these signals are then translated into different levels of RANKL and OPG expression, which in turn regulate osteoclast formation (Bell, 2003; Martin, 2004). For example, the receptors of PTH are expressed on the surface of osteoblasts (Goltzman, 1999; Teitelbaum, 2000). Quasi-steady state levels of PTH increase the production of RANKL and inhibit the production of OPG by osteoblasts (Aubin and Bonnellye, 2000; Halladay et al., 2001; Ma et al., 2001; Teitelbaum, 2000), which as a result increases the population of active osteoclasts. The RANK-RANKL-OPG pathway is described as the ‘convergence hypothesis’, because of its importance as the control mechanism (Hofbauer et al., 2000). Many bone diseases are caused by disorders of the RANKL/OPG ratio, such as osteoporosis, Paget's disease, tumor metastasis, humoral hypercalcemia of malignancy, and multiple myeloma (Boyle et al., 2003; Hofbauer et al., 2000; Hofbauer et al., 2004; Rodan and Martin, 2000).

2.5 BONE DISEASES CAUSED BY DISORDERS OF BONE REMODELLING

Bone remodelling is a highly integrated process of bone resorption by osteoclasts and successive bone formation by osteoblasts, thus it maintains skeletal mass with renewal of the mineralized matrix. Disorders of bone remodelling can result in metabolic bone diseases, and some key examples are given below.

Osteoporosis

Osteoporosis is an age-related bone disease, which often leads to spine, wrist and hip fracture, and is charactered by low bone mass and microarchitectural deterioration of bone tissue (Ismael, 1997). Bone loss is an inevitable age-related condition and is determined by the remodelling rate and the negative bone balance between bone resorption and formation (Seeman, 2003). It appears to begin between the ages of 18 to 30 years, onseting after the rapid increase during adolescence, however this process is slow because the remodelling rate is low (Gilsanz et al., 1988; Ji et al., in press). Osteoporosis refers to a condition when bone mass decreases to a critical level, below which fracture risk is substantially high (Riggs and Melton, 1992). Osteoporosis is a worldwide health problem and affects millions of people, including

postmenopausal women and the majority of the elderly (Christiansen, 1999), and can complicate a variety of sporadic behavioural, nutritional and environmental factors (Riggs, 1991).

Osteoporosis can be classified into primary osteoporosis and secondary osteoporosis, depending on whether or not an identifiable aetiological mechanism is recognized (Kassem et al., 1996; Kleerekoper and Avioli, 1990). In addition, osteoporosis can also be classified into juvenile osteoporosis and ‘involutional osteoporosis’, which includes postmenopausal osteoporosis and senile osteoporosis (Kassem et al., 1996). In 1982, Riggs characterized two distinct syndromes of involutional osteoporosis: high turnover and low turnover osteoporosis. High turnover osteoporosis occurs in postmenopausal women between the ages of 50 and 65 years old, and is pathogenetically related to oestrogen deficiency. Low turnover osteoporosis occurs in both men and women aged predominantly over 75, and affects both trabecular and cortical bone. It is caused by an age-related decline in osteoblast function and can lead to hip and vertebral fractures (Kanis, 1996). Such a classification of osteoporosis is straightforward, however it may be too simple to cover all cases. Under some conditions, the mechanisms of bone loss involve abnormalities of both bone resorption and formation (Kanis, 1996).

Paget’s Disease

Paget’s disease is characterized by excessive and abnormal bone remodelling, and is caused by increased osteoclastic resorption located in one region of the skeleton, such as the skull, pelvis or the ends of long bones. In tissues affected by Paget’s disease, osteoclasts are abundant and may contain up to 100 nuclei per cell. However, the factors which cause this increase in population and activity of osteoclasts have not been identified (Glowacki, 1996). The consequences of Paget’s disease include susceptibility to bone deformity, pain, degenerative arthritis and secondary neurological abnormalities (Glowacki, 1996).

Primary Hyperparathyroidism

Primary hyperparathyroidism is characterized by hypercalcemia resulting from overproduction of parathyroid hormones by the parathyroid gland (Bilezikian, 1993). Primary hyperparathyroidism is a relatively common disease, with estimates of incidence as high as 0.1% to 0.2% (Bilezikian, 1990). The condition can occur in

people of all ages, however it happens more frequently in those aged over 60 and in women (by a ratio of 3:2 compared to men) (Bilezikian, 1993).

Two major organs affected by primary hyperparathyroidism are bones and the kidneys (Bilezikian, 1993). Within patients suffering from primary hyperparathyroidism, the total amount of work performed by osteoclasts and osteoblasts reduces, producing a near zero balance between bone resorption and formation at the end of bone remodelling cycle. However, the bone remodelling rate at a given point on the trabecular surface in patients with primary hyperparathyroidism is increased compared to a healthy individual (Eriksen et al., 1986b). The kidneys may also suffer renal stones (nephrolithiasis) or diffuse calcium-phosphate complexes in the parenchyma (nephrocalcinosis) of patients with primary hyperparathyroidism (Bilezikian, 1993).

Hypothyroidism and Hyperthyroidism

Thyroid hormones are stimulators of osteoclasts and osteoblasts (Mosekilde and Melsen, 1978a, b; Mundy et al., 1976), and can promote bone resorption directly and indirectly via osteoblasts (Ishikawa et al., 1998; Zaidi et al., 2009). Hypothyroidism is caused by the deficiency of thyroid hormones in humans and other vertebrates, and can be associated with an abnormality in the thyroid gland, or less commonly, the pituitary or hypothalamus. Hyperthyroidism is the opposite of hypothyroidism and is caused by the excessive production of thyroid hormones (Torre et al., 2008).

During the bone remodelling cycle in patients with hypothyroidism, the bone resorption rate decreases, while the bone resorption period is prolonged compared to a normal condition. The bone resorption depth, which is dependent on both the bone resorption rate and period, decreases in comparison to normal controls as the rate of change in the bone resorption decrease is larger than that of the bone resorption period increase (Eriksen et al., 1986a). For patients with hypothyroidism, the bone formation rate decreases, while the bone formation period increases. The bone formation depth, which is determined by both the bone formation period and rate, increases in comparison to normal controls as the rate of change in the formation period increase is larger than that of the formation rate decrease. Thus, a positive balance is created at the end of a bone remodelling cycle. However, the obvious increase in bone mass cannot be observed during a relatively a short period, since the bone turnover rate decreases compared to the normal condition.

For patients with hyperthyroidism, both bone resorption and formation rates increase, while resorption, formation and quiescent periods all decrease in comparison to the normal condition (Eriksen et al., 1985, 1986a). The amount of resorbed bone is relatively similar with that in healthy condition. However, the amount of deposited bone decreases due to a reduction in the formation period, which leads to a negative balance at the end of a bone remodelling cycle (Eriksen et al., 1985, 1986a).

Multiple Myeloma

Bone can prevent the invasion of most cancer cells due to its special properties (Smith and Martin, 2011). However, MM cells are able to survive and develop within the bone microenvironment and can alter its characteristics to facilitate their growth and survival (Smith and Martin, 2011). MM is the second most frequent hematological malignancy and is associated with high morbidity rates and short lifespan after diagnosis (Fowler et al., 2011). The American Cancer Society estimates that there are approximately 20000 new cases of MM diagnosed and 10800 deaths associated with MM each year in the United States alone (Jemal et al., 2004). MM-induced bone disease is a major cause of morbidity for patients suffering from MM, with up to 60% experiencing bone fractures (Fowler et al., 2011). MM can induce a negative bone balance and osteolytic lesions via increasing bone resorption, while suppressing bone formation (Matsumoto and Abe, 2011; Roodman, 2011).

2.6 DISCUSSION

Bone remodelling is a vital process that enables the continuous renewal of bone throughout its life. The purpose, stages and regulatory factors involved in bone remodelling are introduced in this chapter, together with the details of several metabolic bone diseases resulting from disorders of bone remodelling.

It should be recognized that some issues discussed in this chapter are still not completely understood. While it is known that PTH has an important effect on bone resorption as well as bone formation, the mechanisms by which PTH regulates bone remodelling are still not fully understood, and further research is still required.

Inevitably, this chapter does not cover all aspects of bone biology. For instance, in addition to PTH and thyroid hormones discussed in this chapter, other hormones, such as insulin, growth hormone, glucocorticoids and sex steroids, also

influence bone remodelling. Mechanical stress or strain on bone is also a driver of bone remodelling. The relationship between mechanical stress and bone remodelling is not discussed in this chapter, since it only focuses on local biochemical factors and systemic hormones.

This chapter has reviewed the basic biological knowledge relevant to this study. Chapter 3 follows with another review to discuss several previously developed mathematical models of the bone remodelling cycle, in order to provide a general overview of the developments in mathematical modelling.

3. LITERATURE REVIEW-MATHEMATICAL MODELLING OF BONE REMODELLING CYCLES AT THE CELLULAR LEVEL

3.1 INTRODUCTION

Understanding the bone remodelling process at the BMU level could lead to improved methods for manipulating the remodelling cycle for the treatment of bone diseases. For example, the use of therapeutic agents to increase BMU activations, in conjunction with a reduction in osteoclast activity while maintaining osteoblast activity, will lead to an accumulation of new bone, in a similar way to the process of hypothyroidism (Rodan and Martin, 2000; Zaidi, 2007). Indeed, this approach has already led to the development of anti-resorptive therapies for post-menopausal bone loss, including oestrogens, raloxifene, bisphosphonates and calcitonin.

Recent reviews have revealed a growing number of factors involved in the regulation of bone remodelling (Allori et al., 2008; Zaidi, 2007). These include autocrine and paracrine signalling molecules, systemic hormones and extracellular matrix components, all of which affect cell-to-cell communication, migration, adhesion, proliferation and differentiation. Most of these findings were obtained from isolated observations of either *in vitro* studies, or *in vivo* experiments using genetically manipulated animals. These findings have shown that osteoblasts are able to regulate the activity of osteoclasts; for example expression of RANKL by osteoblasts, directly interacts with RANK on osteoclast progenitors to drive osteoclastogenesis. This process also depends on the level of OPG that can act as a soluble decoy receptor for RANKL (for a review, see Boyce and Xing (2008)). However, these findings only give limited information about the overall effects of these factors. This highlights the need for tools which can integrate these partial observations into a set of rules that define the behaviour of this complex system.

In contrast to *in vivo* and *in vitro*, which refer to biological experiments performed inside and outside of living organisms, experiments performed via computer simulation are termed *in silico* (Miramontes, 1992). *In silico* experiments are being increasingly used to understand and predict the quantitative behaviour of biological systems, since computer simulations have several advantages over biological experiments (Di Ventura et al., 2006). In particular, *in vivo* and *in vitro*

experiments can be time consuming and expensive. For example, one single cycle of bone remodelling in a healthy individual takes over 200 days (Eriksen et al., 1984b; Eriksen et al., 1984a), and there is also around a 900 day quiescent period before the next remodelling cycle occurs (Eriksen et al., 1986a). *In silico* simulations are able to model this process much quicker and at a reduced cost. Additionally, ethical considerations often prevent the performance of certain experiments on humans, as they can pose health risks.

In recent years a number of mathematical models of the bone remodelling process at the cellular level have been developed, and have helped develop the understanding of the process, solve disputed issues and propose potential therapies for prevalent bone related diseases. These models have demonstrated a great potential in furthering our understanding of this complex biological process, and are reviewed in this chapter.

3.2 MATHEMATICAL MODELS OF BONE REMODELLING AT THE CELLULAR LEVEL

The mechanostat theory developed by Frost in 1987 has led to the development of a series of mathematical models explaining the biomechanical properties of bone (Frost, 1987; Martin, 1995; Turner, 1999). However limited attempts have been performed to mimic bone remodelling cycles at the cellular level. The details of existing mathematical models of the bone remodelling process that have been developed are summarized below.

Kroll and Rattanakul's Models

As discussed in Chapter 2, parathyroid hormones (PTH) results in net bone loss when administered in a continuous way; however it causes net bone formation when administered intermittently. In order to explain such paradoxical behaviour, Kroll (2000) developed a mathematical model to simulate the dynamic interaction of pre-osteoblasts, osteoblasts and osteoclasts in response to PTH. This model aimed to provide a basis for PTH-based therapies treating bone related disease.

The model developed by Kroll (2000) proposed that PTH regulates osteoclasts indirectly via osteoblastic cells, because osteoclastic cells do not have the receptors for PTH (in contrast to preosteoblastic precursors and preosteoblasts). PTH stimulates the differentiation of preosteoblastic precursors into preosteoblasts, but

inhibits the differentiation of preosteoblasts into osteoblasts, via binding to the receptors (Kroll, 2000).

Kroll's model consisted of four ordinary differential equations which describe the temporal variation in concentrations of preosteoblasts, osteoblasts, osteoclasts and PTH. The ratio of osteoblasts to osteoclasts was used to indicate the net effect of PTH on bone resorption and bone formation. The simulation results demonstrated that intermittent PTH administration increases bone formation, however constant PTH administration increases bone loss. These are consistent with the mechanism of osteoporosis proposed by Samuels et al. (1993) and confirms biological experimental observations.

Assumptions were made to facilitate the construction of this model. The delay time for the differentiation of preosteoblastic precursors into preosteoblasts, and the differentiation of preosteoblasts into osteoblasts, were set at 1 and 2 hours, respectively. Additionally, the proliferative effect of PTH on both osteoblast and osteoclast cell populations was dependent on temporal aspects. However, the model of Kroll (2000) assumed that PTH exerts a constant, progressive effect on the development of osteoclasts.

Rattanakul et al. (2003) extended Kroll's model by including the effect of oestrogen stimulation on the dynamics of osteoblast and osteoclast populations, and observed the underlying mechanisms of PTH mediating the bone remodelling process. Rattanakul's model was made up of three ordinary differential equations, which describe the dynamic of PTH level and the concentrations of osteoclast and osteoblast. This model was biologically based on clinical observations reported within literature (Burgess et al., 1999; Dempster et al., 1993; Hock and Gera, 1992; Kong et al., 1999; Momsen and Schwarz, 1997; Takahashi et al., 1999).

It assumed that a nonlinear system to simulate the temporal effect of PTH as well as the action of oestrogen replacement therapy, while assuming that the removal rate of PTH from the system is proportional to its current level. The model demonstrated that limit cycle behaviour could develop into chaotic dynamics for certain ranges of the system's parametric values (Rattanakul et al., 2003).

Komarova's Model

Interactions between osteoclastic and osteoblastic cells are clearly critical in the regulation of bone remodelling. Komarova et al. (2003) constructed a mathematical model to replicate autocrine and paracrine interactions among osteoclastic and osteoblastic lineages, based on the assumption that local effectors secreted by osteoclasts and osteoblasts can regulate their formation rates. The model consisted of three ordinary differential equations, which describe the variation in the concentrations of osteoclasts, osteoblasts and bone volume with time. This was the first model to mimic the temporal dynamics of bone remodelling cycles at a single BMU.

Komarova et al. (2003) proposed a simplified interaction between osteoclasts and osteoblasts, where mature cells and their precursors are not distinguished and considered as one variable (as shown schematically in Figure 3.1). The rates of overall production of each cell population represented the net effect of the recruitment of precursors and the formation of mature cells. The rates of cell removal reflected cell death, as well as the differentiation of osteoblasts into osteocytes and bone lining cells. Finally, it was assumed that cells were able to interact with each other via effectors, which are released or activated by bone cells and act in an autocrine or paracrine manner.

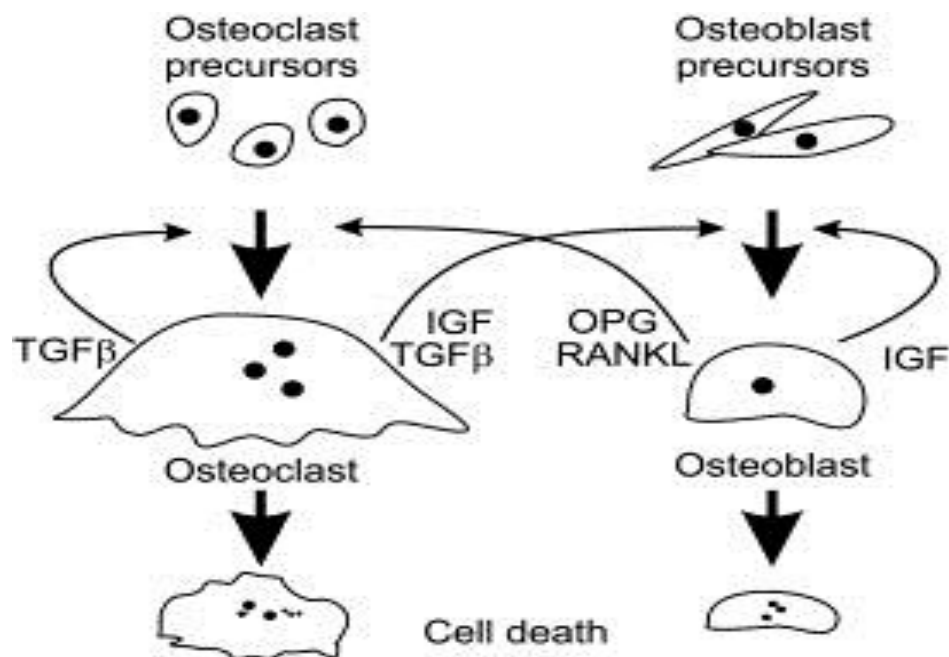


Figure 3.1: Schematic representation of the interaction between osteoclast lineage and osteoblast lineage included in the model of Komarova et al. (2003). Reproduced from Komarova et al. (2003).

The model was capable of simulating the temporal variation in cell populations and bone mass during a cycle of bone remodelling at a discrete site. The model simulation indicated that the system exists in two stable modes, (1) a remodelling cycle in response to an external stimulus and (2) a series of internally initiated cycles of bone remodelling, which correspond to targeted and random bone remodelling, respectively. Additionally, the system also exists in an unstable mode, characterized by unstable oscillatory changes in cell numbers and bone mass with increasing amplitude. The behaviour of this unstable mode is very similar to bone remodelling in individuals with Paget's disease. The model also showed that the dynamic behaviour of the system was dependent on the parameters representing autocrine regulation of osteoclasts.

Inevitably, there are some limitations in Komarova's model: (1) only two cell types were considered; (2) paracrine and autocrine factors were assumed to regulate only the formation of osteoblasts and osteoclasts, while cellular activity and death were assumed to be proportional to cell population; and (3) parameters describing the effectiveness of autocrine and paracrine regulation included the actions of multiple factors.

Moroz's Model

The model of Komarova et al. (2003) reconstructed the variation in populations of osteoclasts and osteoblasts, and bone mass during a remodelling cycle at a single site, and predicted the existence of variable modes of dynamic behaviour of the BMU in remodelling cycles. However, the paracrine and autocrine regulation loops were defined through a range of parameters which exceed biological capabilities. In addition, osteocytes were not included in this model, despite their importance in the regulation of bone remodelling (Bonewald, 2004; Noble, 2003; Taylor et al., 2003).

Moroz et al. (2006) further developed the model of Komarova et al. (2003) by defining autocrine and paracrine parameters within biological capabilities, and including the role of osteocyte apoptosis in the bone remodelling process. The model structure is shown in Figure 3.2. It consisted of four ordinary differential equations, which represented the temporal variation in populations of osteoclasts, osteoblasts and osteocytes, as well as bone volume.

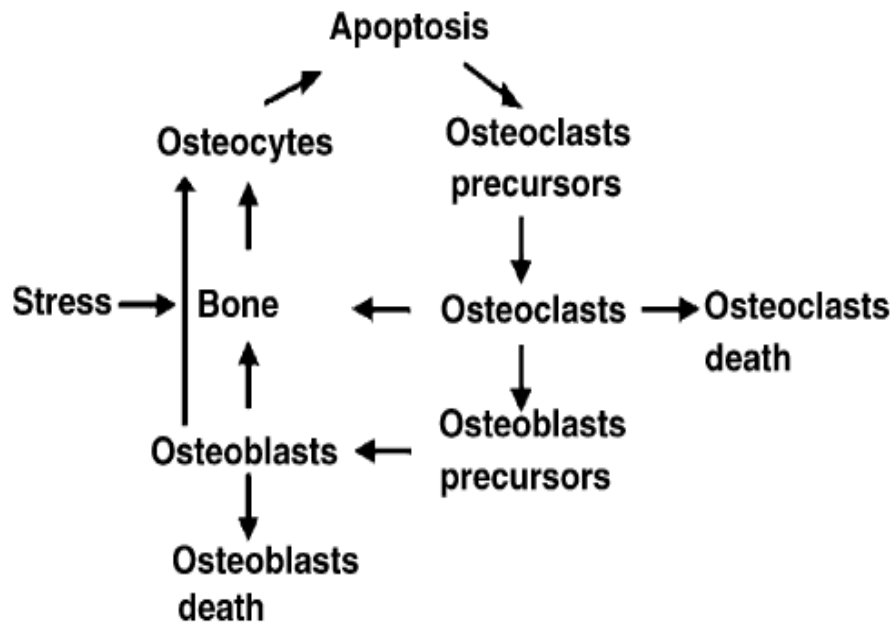


Figure 3.2: Schematic representation of the interaction between osteoclastic and osteoblastic lineages included in the model of Moroz et al. (2006). Reproduced from Moroz et al. (2006).

Moroz's model demonstrated the existence of a basic steady state, with the existence of a surface in a four dimensional 'osteoclast - osteoblast - osteocyte – bone' space indicating that there is a first integral for this dynamic system, which can be explained as a conservative value. The model also demonstrated the existence of the recovering potential, which is directed against both mechanical and biomechanical damage to the bone. This model was validated by comparison to the normal bone remodelling process; however more work is needed to study a broader range of constants.

Lemaire's Model

The RANK-RANKL-OPG pathway is an important factor in the interaction between osteoclasts and osteoblasts, and serves as a control network for regulating the bone remodelling process (Lemaire et al., 2004; Manolagas, 2000; Simonet et al., 1997). The model of Lemaire et al. (2004) was the first attempt to incorporate the RANK-RANKL-OPG pathway into mathematical modelling, and was based on the idea that the relative proportions of immature and mature osteoblasts control the degree of osteoclastic activity; while osteoclasts regulate osteoblasts depending on their stage of differentiation.

Unlike the simulation of bone remodelling cycles at discrete sites performed by Komarova et al. (2003), Lemaire's model analysed the stable state of many BMUs

over a finite volume of bone, since observable states in biological systems usually correspond to stable states of the system. It also distinguished between the different stages of osteoclastic and osteoblastic lineages. Four stages of osteoblastic lineage (uncommitted progenitors, osteoblast precursors, active osteoblasts and osteocytes, bone lining cells and apoptotic osteoblasts) and three stages of osteoclastic lineage (osteoclast precursors, active osteoclasts and apoptotic osteoclasts) were considered. The structure of this model is shown in Figure 3.3.

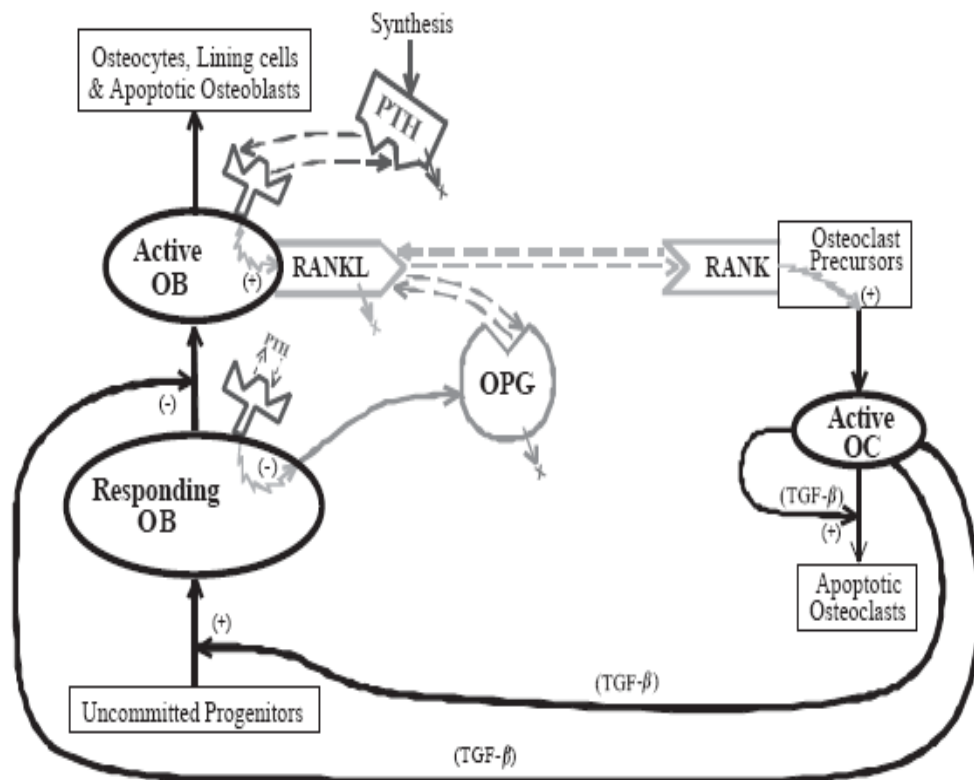


Figure 3.3: Schematic representation of the basic structure of the model of Lemaire et al. (2004). Reproduced from Lemaire et al. (2004).

The model consisted of three ordinary differential equations which describe the variation in concentrations of osteoblast precursors, osteoblasts and osteoclasts. It simulated the tight coupling between osteoclasts and osteoblasts, the catabolic effect induced by continuous administration of PTH and the catabolic action of RANKL (as well as its reversal by soluble antagonist OPG). In addition, the model also simulated several skeletal diseases by inserting dysfunctional connections in the coupling network, explored different diseases hypotheses and investigated potential therapeutic interventions.

The work of Lemaire not only switched researcher focus from a bone remodelling cycle to the spatial average of many BMUs, but also incorporated more

biological factors into mathematical modelling. However, in the model it was presented that OPG was secreted by osteoblastic precursors, while RANKL was secreted by active (mature) osteoblasts. This is an obvious mistake since it is generally accepted that RANKL is primarily produced by osteoblastic precursors, while OPG is primarily produced by active (mature) osteoblasts (Pivonka et al., 2008). Further discussion of this point is included below.

Pivonka's Model

RANKL and OPG are primarily expressed in osteoblastic precursor cells and active (mature) osteoblasts, respectively (Aubin and Bonnellye, 2000; Collin-Osdoby et al., 2001; Hofbauer et al., 2000; Pivonka et al., 2008). However, the functional utility of this particular ligand-decoy-receptor expression profile was not reported before the work of Pivonka et al. (2008). In order to understand the functional implications of this particular RANKL/OPG expression profile on bone volume, Pivonka et al. (2008) developed the work of Lemaire et al. (2004) and proposed an extended bone-cell dynamics model, which described the functional behaviour of BMUs.

The model of Pivonka et al. (2008) consisted of four ordinary differential equations, which described the temporal variation in concentrations of osteoblast precursors, osteoblasts and osteoclasts, and bone volume. The model incorporated the following significant modifications to the model of Lemaire et al. (2004): (1) one differential equation was added to describe temporal changes in bone volume; (2) one differential equation was added to describe the role of TGF- β released from the bone matrix during bone resorption; and (3) OPG and RANKL were expressed on both osteoblastic cell lines, and the activator/repressor functions were modified. The biological mechanisms of the model are presented in Figure 3.4.

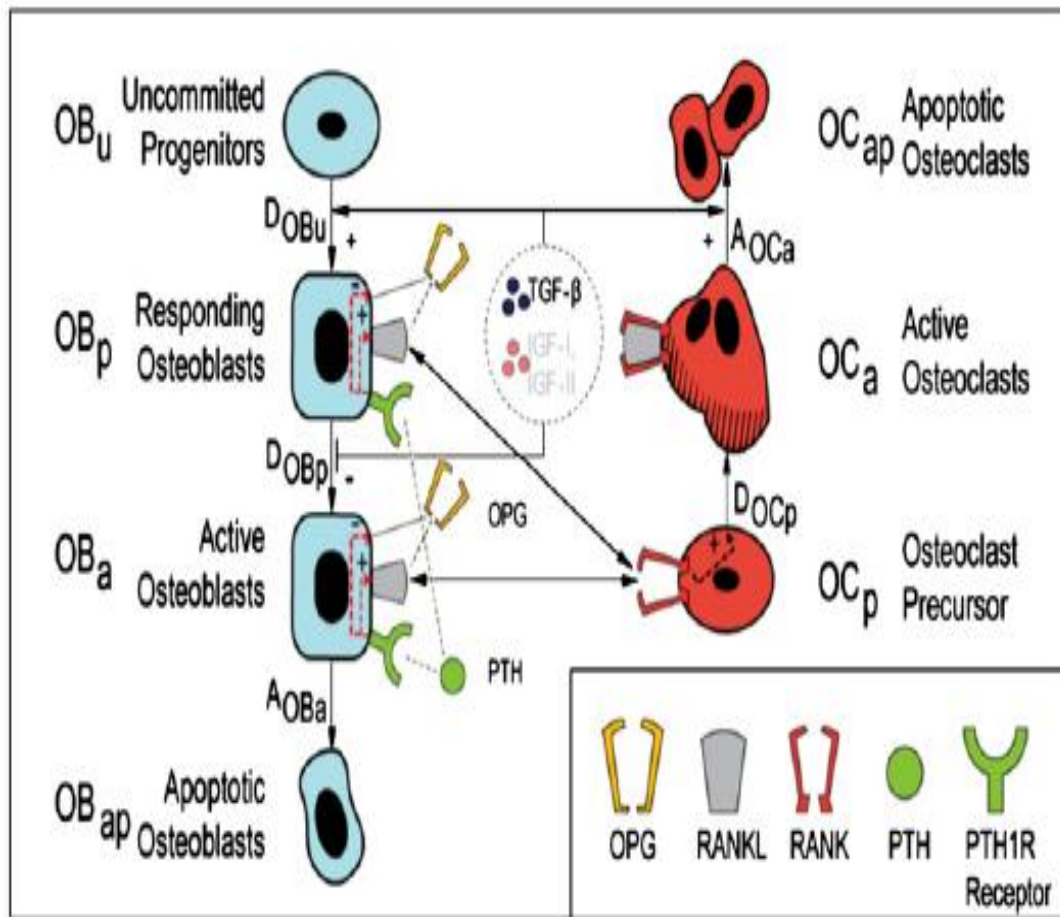


Figure 3.4: Schematic representation of the basic structure of the model of Pivonka et al. (2008). Reproduced from Pivonka et al. (2008).

Bone volume was selected as the criterion to identify the functional utility of the ligand expression on particular cell types. The simulation results indicated that the ligand expression profile (RANKL expressed on osteoblastic precursors, while OPG expressed on mature osteoblasts) permitted BMUs to be at their most functionally responsive. This implied that BMUs produce the greatest change in bone volume in response to changes in differentiation rates. The authors also identified a small number of parameter combinations corresponding to physiological responses (two of which were related to TGF- β), which provided a partial explanation for the physiological action of TGF- β on bone.

Pivonka et al. (2010) developed their work further by building another mathematical model to investigate the effect of the RANK-RANKL-OPG signalling pathway on the bone remodelling process. The simulation results indicated that bone diseases resulting from the disorder in the RANK-RANKL-OPG pathway, are more effective in producing bone resorption than bone formation. This agrees with

Hofbauer's "convergence hypothesis", which theorised that catabolic bone diseases act most effectively through the RANK-RANKL-OPG system. Additionally, the model results demonstrated that the severity of catabolic bone diseases is positively proportional to the number of affected components of this pathway. Several successful virtual therapies for different diseases states, using both single and dual therapies, were identified through optimization algorithms and the theoretical model (Pivonka et al., 2010).

Ryser's Model

The bone remodelling process is influenced by the spatial organization of BMUs. In order to study the spatial properties of BMUs, Ryser et al. (2007) developed a spatio-temporal model to simulate the dynamics of bone cell populations, as well as RANKL and OPG for a trabecular BMU at the cellular level.

Several assumptions were made in this model: (1) the cell populations were assumed as a continuum, therefore cell densities rather than individual cells were modelled; (2) only three types of bone cells (osteoclasts, osteoblasts and osteocytes) were considered; and (3) the mechanical factors responsible for the BMU steering (microscopic strains and damages) were modelled implicitly in the form of appreciate RANKL distribution in the initial field (Ryser et al., 2007).

The model was made up of five nonlinear partial differential equations. This enabled it to simulate the spatial and temporal features of the cutting cone and the movement of BMU. The model also identified the relationship between biochemical factors and the known population dynamics of bone cells, evaluated biological experimental findings and proposed new therapies. The model has been demonstrated to successfully reconstruct the dynamics of a BMU and the distinct features of the cutting cone.

Buenzli's Model

Following the spatio-temporal model of Ryser et al. (2007) for trabecular bone, Buenzli et al. (2011) extended the purely temporal model of Pivonka et al. (2008), and proposed another spatio-temporal model to investigate the cell distribution and regulatory factors in cortical bone. This model integrated some of the most important interaction pathways existing between osteoclastic and osteoblastic cells, and was constructed through a number of additional material-balance equations.

The structure of BMUs (shown in Figure 3.5) is well understood at the descriptive level (Martin et al., 1998; Parfitt, 1994), however, no work had been performed to identify the link between the structure of BMUs and the underlying cellular interaction mechanisms. Buenzli et al. (2011) built such links and tested their ability to reconstruct the spatio-temporal dynamics of individual BMUs. The experimentally observed cell distribution of cortical BMUs was retrieved under particular conditions. In addition to cell distribution, the spatial distribution of regulatory factors could also be calculated, providing new insights into how different regulatory factors exert their action on bone cells.

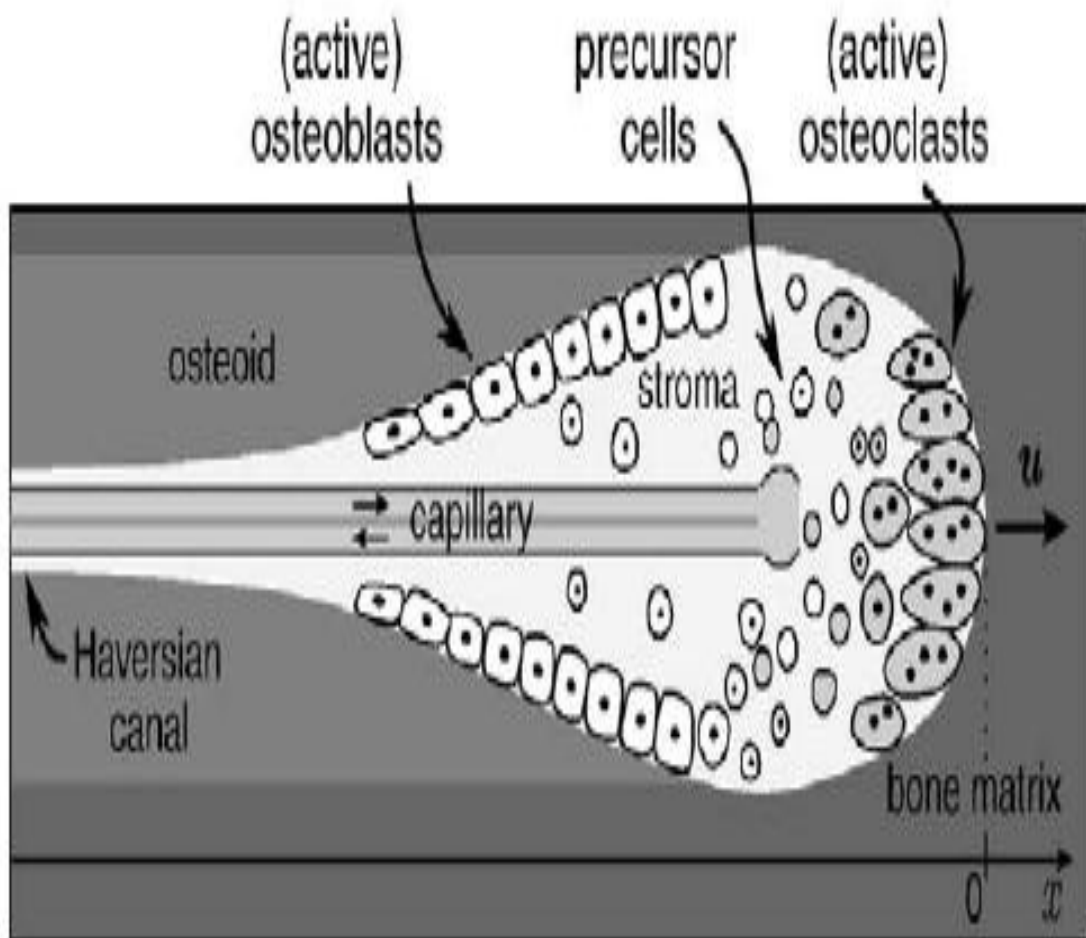


Figure 3.5: Schematic figure of the internal organisation of cortical BMU.

Reproduced from Buenzli et al. (2011).

Osteoclasts resorb the bone matrix at the front while osteoblasts lay down osteoid towards the back to refill the cavity. The central capillary provides a supply of precursor cells, as well as various nutrients.

Zumsande's Model

Bone remodelling cycles should reside in a stable state, where under physiological conditions and in the absence of external stimuli, populations of osteoclasts and osteoblasts remain approximately the same over time. Such a stable state is dynamical and has to be robust against variations in model parameters. Zumsande et al. (2011) declared that the physiological state of the bone remodelling system is possibly characterized by parameter values close to a bifurcation point (the critical threshold is where the stability to perturbations is lost), as this is when the system exhibits the strongest response of steady states to parameter changes.

Zumsande and colleagues applied a generalized modelling method to analyse a large number of models with respect to their bifurcation properties. The simulation results demonstrated that the stability of the steady state in a two-dimensional model requires OPG to dominate over RANKL. It is known that several bone related diseases (such as postmenopausal osteoporosis, Paget's disease, osteopetrosis and osteopenia) are results of dysfunctions in bone remodelling. They suggested that such diseases are caused by the transition of a steady state due to an instability in a Hopf bifurcation, although this theory is yet to be substantiated. Any future confirmation would imply the importance of this bifurcation theory in the analysis of such diseases.

3.3 DISCUSSION

Mathematical models are a natural extension of conceptual models and are able to provide dynamic, qualitative or quantitative descriptions of biological systems (Defranoux et al., 2005). Mathematical models create the ability to simulate the natural behaviour of a system, as well as its modulation by therapeutic or dietetic interventions.

In this chapter, a series of mathematical models of bone modelling at the cellular level have been reviewed in order to give a general view of the development in this area. The schematic diagram shown in Figure 3.6 displays the relationship between these mathematical models. There are four subgroups. The first two (the models of Kroll (2000) and Rattanakul et al. (2003)), focus on explaining the paradoxical effect of PTH on bone remodelling. Models of the third subgroup, originating from the model of Komarova et al. (2003), simulate the tight interaction between osteoblastic and osteoclastic cells, and replicate the variation in cell

populations and bone mass during bone remodelling cycles. The final subgroup consists of four models originated from the model of Lemaire et al. (2004), which incorporates the RANK-RANKL-OPG signalling pathway when rebuilding bone remodelling cycles. Zumsande et al. (2011) reviewed previously proposed mathematical models and developed a large class of models using a generalized modelling method, without employing specific function forms.

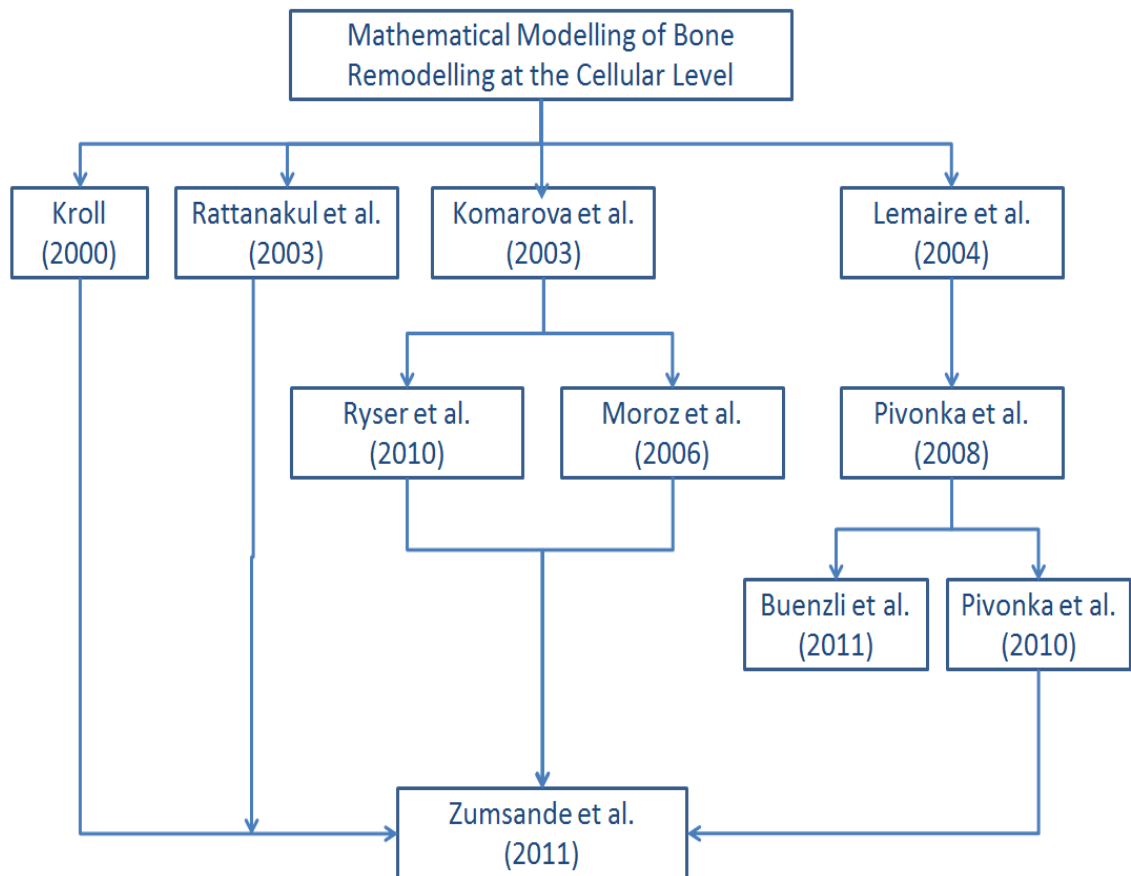


Figure 3.6: Schematic diagram of the development of mathematical models of bone remodelling at the cellular level.

The mathematical models discussed in this chapter all consist of a set of differential equations, which describe the rate of change of different cell types involved the bone remodelling cycle. In order to simulate the complicated bone remodelling process via a group of differential equations, simplifications are inevitably required to facilitate the construction of models. Therefore, all the models covered in this chapter have their own limitations. However, the encouraging results obtained from them have demonstrated the great potential of mathematical modelling

in developing the understanding of bone remodelling, combining the fragmentary experimental results, and evaluating and proposing prospective therapies.

The differential equations describing the models in this chapter were developed based on biological knowledge and model parameters were related to biochemical factors or signalling pathways. However, these mathematical models have not yet reconstructed the bone remodelling process in a quantitative way. They are only qualitative and as a result, it is impossible to make a quantitative comparison between these model simulations and experimental observations.

This chapter has demonstrated the need to develop a quantitative model of the bone remodelling process, and subsequent validation through comparisons between theoretical predictions and experimental observations. This produces a practical method of investigating the bone remodelling process and therapeutic interventions. The details of such a mathematical model are discussed in Chapter 4.

4. A PREDATOR-PREY BASED MATHEMATICAL MODEL OF THE BONE REMODELLING PROCESS

The simulation results of the mathematical models reviewed in Chapter 3 generally agree with published experimental results, which demonstrate the potential application of mathematical modelling in furthering understanding of the bone remodelling process. However, so far these models were built on a qualitative analysis of the bone remodelling process.

This thesis proposes a novel predator-prey based mathematical model to quantitatively reconstruct bone remodelling cycles at the cellular level. The model describes the temporal dynamic interaction between osteoclasts and osteoblasts at a single BMU (basic multicellular unit), and their corresponding bone resorption and formation activities. The model mimics the variation in bone thickness at a particular point during the bone remodelling process in both normal and pathological conditions, which were obtained from histomorphometric analysis (Agerbaek et al., 1991; Eriksen et al., 1984b; Eriksen et al., 1985, 1986a), and replicates the observed dynamic interaction between osteoclasts and osteoblasts.

There are three novelties of the proposed model: (1) the adoption of a predator-prey model to replicate the sequential dynamic interaction of osteoclasts and osteoblasts at a BMU; (2) the bone remodelling cycles are reconstructed quantitatively for the first time; and (3) a feedback mechanism is used to maintain the balance of bone thickness during a remodelling cycle.

4.1 INTRODUCTION OF MATHEMATICAL MODELLING

Before discussing the development of the predator-prey based mathematical model, it is necessary to introduce the basic knowledge of mathematical modelling (*i.e.* the definition of mathematical modelling and the general rules which govern their construction).

Nagle et al. (2008) defined mathematical modelling as mimicking reality by mathematical language. Mathematical modelling can assist us to comprehend nature and find solutions to practical problems. Figure 4.1 illustrates several steps that are required to build a mathematical model (Nagle et al., 2008). The initial step, termed

‘formulate the problem’, entails translating the realistic problem into mathematical language. Secondly, ‘develop the model’ requires the definition of assumptions and the fixation of relationships between the modelled problem and mathematical equations. Such problems are often complicated, and involve many factors and interrelated processes. It is impossible for a single model to include all of these factors and processes, and a compromise is usually required between model simplicity and the complexity of realistic problems. It is necessary to distinguish between critical and uncritical factors, as only critical factors are considered in mathematical modelling. The relationship between the modelled problem and mathematical equations consists of a single or a series of mathematical equations. In most cases, the chosen mathematical equations need to be modified several times in order to build a successful model. Finally, ‘test the model’ is used to check whether or not the model meets the expected requirements and provides an acceptable accuracy. This is usually achieved by comparing the model predictions with experimental results.

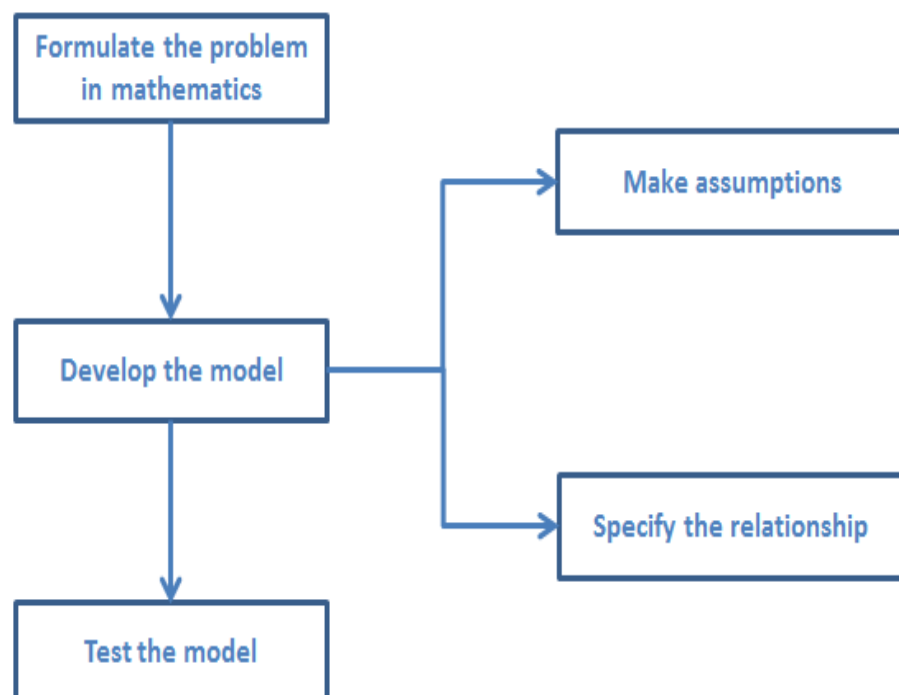


Figure 4.1: General steps of mathematical modelling of practical problems. Modified from Nagle et al. (2008).

4.2 PREDATOR-PREY MODELS

The proposed mathematical model of the bone remodelling process is based on a predator-prey relationship. A predator-prey model consists of two first order, non-linear differential equations, to represent the interaction between predators and preys in biological systems, such as foxes and rabbits, and rabbits and grasses (Brauer and Castillo-Chávez, 2001; Hoppensteadt, 2006). A class of Gause-type predator-prey model can be represented in the following form (Gause et al., 1936; Kuang, 1990):

$$\dot{x}(t) = x(t)(\alpha - \beta y(t)) \quad (4-1)$$

$$\dot{y}(t) = -y(t)(\gamma - \delta y(t)) \quad (4-2)$$

where,

- $x(t)$ and $y(t)$ represent the populations of the prey and predator, respectively;
- $\dot{x}(t)$ and $\dot{y}(t)$ represent the variations in the populations of the prey and predator with time; and
- α , β , γ and δ are model parameters defining the interaction between the prey and predator.

The predator-prey model contains several assumptions (Hiorns et al., 1981): (1) the prey has a unlimited food supply, while the food of the predator is completely dependent on the prey's population; (2) the variation in the populations of prey and predator with time is assumed to be proportional to their population size; and (3) the environment keeps constant (in favourable conditions for both species) and the effect of genetic adaptation is ignored.

An example of the predator-prey theory is shown in Figure 4.2, which demonstrates the interaction between baboons (prey) and cheetahs (predator) (Hiorns et al., 1981). The initial values of baboons and cheetahs are assumed to be 80 and 40, respectively.

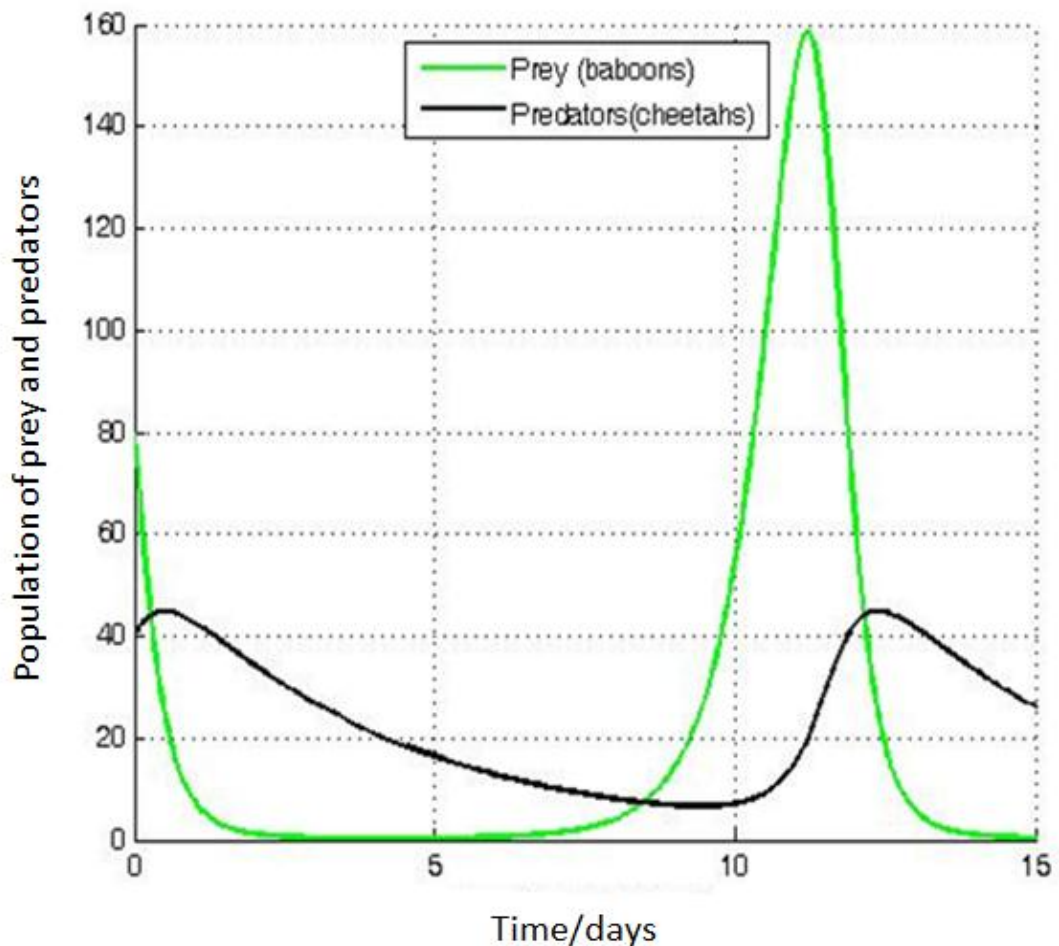


Figure 4.2: The interaction between baboons and cheetahs in a predator-prey relationship. Reproduced from Lotka-Volterra equation [online]. Available at: http://en.wikipedia.org/wiki/Lotka%E2%80%93Volterra_equation [Accessed on 02 August 2011].

4.3 DEVELOPMENT OF THE MODEL OF THE BONE REMODELLING PROCESS

4.3.1 MODEL EQUATIONS

The proposed mathematical model simulates the dynamic interaction between osteoclasts and osteoblasts and their corresponding resorption and formation activities at a BMU (basic multicellular unit) during the bone remodelling process, where the interaction is based on the competition model of a predator-prey system (Gause et al., 1936; Kuang, 1990). The motivation to adopt the predator-prey model was based on its key characteristic of competitive cyclic growth between the prey and predator populations, and the fact that their populations cannot decrease to negative values. These properties are similar to the growth of osteoclasts, which is

tightly coupled to the growth of osteoblasts during the remodelling process at a BMU (Parfitt, 2000; Udagawa et al., 2006).

Differentiation into the osteoclastic and osteoblastic lineages involves several intermediate stages. For example, the osteoclast lineage develops from hematopoietic precursor cells through monocyte differentiation and fusion to osteoclast formation (Roodman, 1999; Teitelbaum, 2000), while the osteoblast lineage arises from mesenchymal stem cells through to preosteoblasts, mature bone-forming osteoblasts, osteocytes and bone lining cells (Aubin, 1998). In this current model, the terms ‘osteoclast’ and ‘osteoblast’ include both precursor and mature cells. Therefore, the rate of change in cell populations includes the production of precursors, the formation of mature cells and their eventual removal or transformation.

Based on this definition the model proposed that the osteoclast-osteoblast interaction was defined through the following set of differential equations:

$$\dot{x}_{oc}(t) = (a - b\sqrt{x_{ob}(t)})x_{oc}(t) \quad (4-3)$$

$$\dot{x}_{ob}(t) = (c \frac{x_{oc}^2(t)}{K_{oc} + x_{oc}^2(t)} - d)x_{ob}(t) \quad (4-4)$$

where,

- $x_{oc}(t)$ and $x_{ob}(t)$ are the osteoclast and osteoblast populations, respectively;
- $\dot{x}_{oc}(t) = dx_{oc}(t)/dt$ and $\dot{x}_{ob}(t) = dx_{ob}(t)/dt$ represent the variations of $x_{oc}(t)$ and $x_{ob}(t)$ with time; and
- a, b, c, d and K_{oc} are unknown scalar parameters.

The model defined by Eqs. (4-3) and (4-4) is based on an idea first proposed by Putra et al. (2009). It belongs to the class of Gause-type predator-prey models (Gause et al., 1936). The global stability of such Gause-type predator-prey systems has been discussed in the work of Kuang (1988, 1990). Its selection was not based on any specific underlying biological mechanisms, except the requirement to replicate the dynamics between osteoblasts and osteoclasts. For example, the terms of $\sqrt{x_{ob}(t)}$ and $x_{oc}^2(t)$ in Eqs. (4-3) and (4-4) respectively are selected in order to keep the effects of $x_{oc}(t)$ and $x_{ob}(t)$ in a similar degree, because the maximum population of $x_{ob}(t)$ is typically two orders of magnitude greater than the maximum population of osteoclasts.

However, following a detailed investigation of the results and a parameter sensitivity study, relationships between the parameters and some biological factors did become evident, as discussed later. It can be shown that all solutions for $x_{oc}(t)$ and $x_{ob}(t)$ result in periodic orbits (Kuang, 1990). This property guarantees the periodicity of remodelling cycles and the coupling between osteoclast and osteoblast population growth. However, the factors activating the bone remodelling cycle (such as biological and mechanobiological signals) were not included and the periodicity of the model did not correspond to one single bone remodelling cycle, but rather reflects the average of many bone remodelling cycles.

The model for the bone resorption and formation activities was proposed as:

$$\dot{D}(t) = F_{form}(t) \times F_{feedback}(t) - F_{res}(t) \quad (4-5)$$

where,

- $D(t)$ represents the instantaneous cavity depth created by a BMU during one single bone remodelling cycle. The initial value of $D(t)$ is zero and then becomes negative during the resorption phase, before returning to zero or finishing with a negative or positive value, depending whether there is net bone resorption or formation;
- $\dot{D}(t) = dD(t)/dt$ represents the variation of that cavity depth with time;
- $F_{form}(t)$ and $F_{res}(t)$ are the bone formation and resorption rates, respectively; and
- $F_{feedback}(t)$ represents a feedback mechanism to co-regulate bone formation during the bone remodelling cycle.

The bone resorption and formation rates are dependent on the resorptive and formative activities of osteoclasts and osteoblasts and population of cells (Lemaire et al., 2004), and it is assumed that each cell type has the same and constant level of activity during one bone remodelling cycle (Lemaire et al., 2004; Rodan and Martin, 2000). Based on these assumptions, the bone resorption and formation rates were solely related to the population of osteoclasts and osteoblasts. The functions to define these relationships were proposed as follows:

$$F_{form}(t) = e \frac{x_{ob}(t)}{K_{ob} + x_{ob}(t)} \quad (4-6)$$

$$F_{res}(t) = f x_{oc}^2(t) \quad (4-7)$$

where e , f and K_{ob} are also unknown scalar parameters. The equation describing the feedback mechanism was defined as:

$$F_{feedback}(t) = \exp((\bar{D} - D(t))/D_M) \quad (4-8)$$

where,

- \bar{D} is defined as the reference value of $D(t)$ and equals the balance between the cavity depth resorbed by osteoclasts, and the depth refilled by osteoblasts during one BMU remodelling cycle ($\bar{D} = \text{maximum formation height} - \text{maximum resorption depth}$); and
- The term $(\bar{D} - D(t))$ represents the cavity depth needed to be refilled and is normalized by its maximal value D_M (D_M actually equals the maximum cavity depth resorbed by osteoclasts during one BMU remodelling cycle).

The feedback mechanism is designed to sense the remaining cavity depth refilled by osteoblasts during one BMU remodelling cycle, and then regulate the bone formation rate. The proposed equations of the feedback mechanism satisfied this requirement completely: *i.e.* at the beginning of bone formation period, the term $(\bar{D} - D(t))$ reaches its maximal value since the cavity has not been refilled at all, and the feedback mechanism outputs its maximum; as the bone formation proceeds, the value of the term $(\bar{D} - D(t))$ decreases as well as $F_{feedback}(t)$, since more of the cavity is being refilled. The exponent function $\exp((\bar{D} - D(t))/D_M)$ in Eq. (4-8) is chosen in order to keep the value of $F_{feedback}(t)$ positive all the time.

The feedback mechanism ensured that the rate of bone matrix formation was related to the current cavity depth. This allowed the model to exhibit the observed phenomenon that the apposition rates are large at the start of the formation period, and decrease gradually towards zero at the end (Eriksen et al., 1984b; Eriksen et al., 1985, 1986b).

Using Eqs. (4-6) to (4-8), Eq. (4-5) can be reformulated as:

$$\dot{D}(t) = e \frac{x_{ob}(t)}{K_{ob} + x_{ob}(t)} \exp((\bar{D} - D(t))/D_M) - f x_{oc}^2(t) \quad (4-9)$$

Thus the model for bone remodelling was based on Eqs. (4-3), (4-4) and (4-9), which were solved using the Matlab computational software package (v7.7.0, Mathworks, Natick, USA; with the Runge-Kutta integration method ode45 and a specified tolerance of 10^{-10}).

4.3.2 MODEL CALCULATION

The model equations contain eight parameters (a to f , K_{ob} and K_{oc}), all of which directly affect the resulting solutions. Different parameter combinations correspond to various biochemical conditions such as healthy condition, hypothyroidism (HT) and primary hyperparathyroidism (PHPT). In order to determine the parameters corresponding to these conditions, a genetic algorithm approach was used to search for the parameter values in the parameter space. Detailed information regarding the calculation of the model parameters and the solution of model equations is provided in the following sections.

4.3.2.1 CALCULATION OF MODEL PARAMETERS

Genetic algorithms are capable of searching for global solutions to both constrained and unconstrained problems in the form of $\min_x F(X)$, by mimicking the principles of biological evolution based on rules modelled on gene combinations in reproduction (MathWorks, 2011). Genetic algorithms repeatedly modify a population of individual solutions and apply the principle of survival of the fittest in searching potential solutions to the problem. At each step, a new generation is produced in a similar way in natural adaptation by selecting individuals in the fixed domain according to their fitting level and then breeding them together operators learned from natural genetics (MathWorks, 2011). Genetic algorithms usually provide a group of potential solutions to a problem, and then the best one could be chosen by users. Especially for the problems with multiple solutions, they can be found simultaneously. Genetic algorithms works in the following steps: creating a random initial population, producing a new sequence of new populations and stopping when the set criterion is met.

Due to its random nature, the genetic algorithm approach improves the chance of finding a global solution and obtains several advantages compared to traditional search and optimization methods as follows (MathWorks, 2011):

- The genetic algorithm searches a population of points in parallel rather than a single point, and the best point in the population approach an optimal solution;
- The genetic algorithm does not require derivative information, and only objective function and corresponding fitness levels are required;

- The genetic algorithm can solve the problems whose objective functions are discontinuous, nondifferentiable, stochastic or highly nonlinear;
- The genetic algorithm choose the next generation randomly rather than selecting next point in the sequence by a deterministic computation; and
- The genetic algorithm uses an encoding of the parameter set rather than the parameter set itself except when real-valued individuals are used.

A genetic algorithm was employed in this study to search for the values of model parameters corresponding to various biochemical conditions in the parameter space. Several steps are required to calculate the values of parameters for each condition by the genetic algorithm method. Figure 4.3 demonstrates the procedure required to calculate model parameters in the normal (healthy) condition.

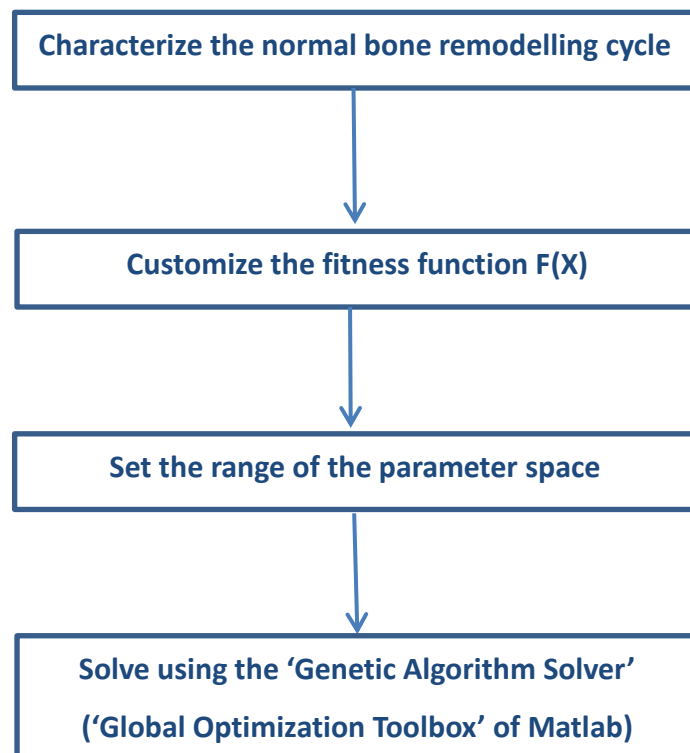


Figure 4.3: Steps used to calculate model parameters in the healthy condition based on a genetic algorithm.

Up to nine phenomena were used to characterize the normal bone remodelling cycle and they were defined in Table 4.1.

Phenomena	Definition
Resorption period	$t_{res} - t_{initial}$
Maximum resorption depth	$D(t_{initial}) - D(t_{res})$
Formation period	$t_{form} - t_{res}$
Maximum formation height	$D(t_{form}) - D(t_{res})$
Quiescent period	$t_{end} - t_{form}$
Maximum resorption rate	$Max(F_{res}(t)), t \in [t_{initial}, t_{res}]$
Maximum formation rate	$Max(F_{form}(t) \times F_{feedback}(t)), t \in [t_{res}, t_{form}]$
Maximum osteoclast population	$Max(x_{oc}(t))$
Maximum osteoblast population	$Max(x_{ob}(t))$

Table 4.1: Definition of nine phenomena which were used to characterize the normal bone remodelling cycle.

where,

- $t_{initial}$ and t_{res} represent the times when the bone resorption phase begins and ends;
- t_{form} and t_{end} are the times when the bone formation phase and quiescent phase end;
- $D(t_{initial})$, $D(t_{res})$ and $D(t_{form})$ are the cavity depth corresponding to times, $t_{initial}$, t_{res} and t_{form} ; and
- $F_{res}(t)$ and $F_{form}(t) \times F_{feedback}(t)$ represent the rates of bone resorption and formation.

The published experimental data is incomplete for PHPT and HT; in particular, the osteoclast and osteoblast populations are not reported. Considering that it is not necessary to use all quantities in Table 4.1 to calculate model parameters

based on genetic algorithm, in the simulation only the first seven quantities in Table 4.1 were used to optimize the values of model parameters for the normal, HT and PHPT conditions. However, the osteoclast and osteoblast populations predicted by the model for the normal condition can be used to confirm the validity of the approach, which provides a significant advantage.

After characterization of normal bone remodelling by seven phenomena, the definition of a customizable fitness function was required. Based on the fitness function, the genetic algorithm searches the solution space to minimise the difference between the model predictions and published experimental data. The fitness function was defined as follows:

$$F(X) = \sum_{i=1}^7 \text{abs}((P(X)_i - E_i)) \quad (4-10)$$

$$X = [a, \dots, f, K_{ob}, K_{oc}]$$

where,

- $X = [a, \dots, f, K_{ob}, K_{oc}]$ is a row vector consisting of eight parameters in the model equations and represents one point in the parameter space; and
- $P(X)_i$ and E_i ($i=1, \dots, 7$) represent the model outputs corresponding to each point in the parameter space, and the experimental values of the first seven phenomena in Tables 4.1.

For a random point in the parameter space we can obtain one group of data, $P(X)_i$ ($i=1, \dots, 7$), and then calculate the difference between $P(X)_i$ ($i=1, \dots, 7$) and E_i ($i=1, \dots, 7$). The genetic algorithm was able to find a group of parameters that minimises the difference between the model predictions $P(X)_i$ ($i=1, \dots, 7$) and experimental data E_i ($i=1, \dots, 7$) (for more specific details on this aspect see: <http://www.mathworks.com/help/toolbox/gads/f6010dfi3.html>). Once the genetic algorithm identified the optimum parameter values, Eqs. (4-3), (4-4) and (4-9) were subsequently used to calculate the detailed variations of $x_{oc}(t)$, $x_{ob}(t)$ and $D(t)$ with time.

4.3.2.2 THE SOLUTION OF MODEL EQUATIONS

There are two forms of solutions to an ordinary differential equation: the analytical and numerical solution (Cox, 1996; Gray et al., 1997). An analytical solution of an ordinary differential equation is a differentiable function in terms of explicit or implicit elementary functions, such as a finite combination of powers, radicals, exponentials, logarithmic, trigonometric and inverse trigonometric functions (Cox, 1996; Gray et al., 1997). The analytical solution is an accurate solution and is able to explain exactly how the model will behave under any circumstance (MyPhysicsLab, 2011).

However, not all ordinary differential equations can be solved in an analytical manner, and the Peano existence theorem is used to specify when an analytical solution exists (Cox, 1996). Although an analytical solution to a differential equation can exist, in some cases the complexity of the solution renders it unpractical to use. Consequently, numerical solutions are often used as an alternative method to analyse model behaviour, as they provide approximations to analytical solutions (Cox, 1996; Gray et al., 1997).

The proposed mathematical model consists of a set of first order, nonlinear, ordinary differential equations. The initial conditions of these ordinary differential equations were defined as $x_{oc}(t) = x_{ob}(t) = 0.1$ and $D(t) = 0$. The model equations belong to a first-order initial value problem. The solutions to the model equations represent the variation in the population of osteoclasts and osteoblasts, and the cavity depth over time. The numerical method was used to approximate the solution of such a first-order initial value problem. However, it should be noted that numerical solutions have some disadvantages (ODE Laboratories, 2011). For example, in comparison to an analytical solution which is a whole continuum of values, a numerical solution is made up of a finite group of values, and it naturally misses a lot of values. There are several numerical methods available to approximate the solution to ordinary differential equations, including Euler's method, Heun's method and Runge-Kutta's method (Gray et al., 1997).

Euler's method

Consider a first-order initial value problem is defined as follows (Gray et al., 1997):

$$\dot{y} = f(t, y), \text{ for } a \leq t \leq b \quad (4-11)$$

$$y(a) = Y_0$$

Firstly, divide the interval $a \leq t \leq b$ into a set of equal subintervals:

$$a = t_0 < t_1 < \dots < t_N = b$$

where, $h = t_{n+1} - t_n$ represents ‘step size’ of the solution, and is a positive small scalar less than 1. In order to deduce the formula of Euler’s method it is assumed that Eq. (4-11) has the analytical solution $y(t)$. According to Taylor series, $y(t)$ can be expanded as follows:

$$\begin{aligned} y(t_1) &= y(t_0) + (t_1 - t_0) \cdot \dot{y}(t_0) + \dots + \frac{(t_1 - t_0)^N}{N!} y^{(n)}(t_0) \\ &= y(t_0) + h \cdot \dot{y}(t_0) + \dots + \frac{h^N}{N!} y^{(n)}(t_0) \end{aligned} \quad (4-12)$$

Since h is a relatively small number less than unit, h^2, \dots, h^N , should be even smaller. Therefore, it is reasonable that the terms including h^2, \dots, h^N can be eliminated to make the equation simpler. Therefore, Eq. (4-12) can be reformatted to the following:

$$\begin{aligned} y(t_1) &\approx y(t_0) + h \cdot \dot{y}(t_0) \\ &= y(t_0) + h \cdot f(t_0, Y_0) \end{aligned} \quad (4-13)$$

If the initial condition of the equation is defined as $y(t_0) = Y_0$, and the left-hand term of Eq. (4-13) is defined as Y_1 , then Eq. (4-13) becomes:

$$Y_1 = Y_0 + h \cdot f(t_0, Y_0) \quad (4-14)$$

where, Y_1 is a numerical approximation of $y(t_1)$. Likewise, an approximation of $y(t_n)$ can be obtained, producing the following general approximate equality:

$$Y_{n+1} = Y_n + h \cdot f(t_n, Y_n), \quad 0 \leq n \leq N - 1 \quad (4-15)$$

Eq. (4-15) is called Euler’s method. It was the first numerical method to solve ordinary different equations approximately, and serves as a foundation for more complicated numerical methods (such as the Runge-Kutta method). However, solutions of Euler’s method are not particularly accurate and some improvements are required to increase their accuracy (Gray et al., 1997).

Heun’s method

Euler’s method is rarely used in the solution of ordinary differential equations due to its inaccuracy (Zill, 2005). The underlying foundation of Euler’s method is to use the

tangent line to the actual solution curve at the left end-point (its coordinates have already been established) of the interval (also called step size), as an estimation of the coordinates of the right end-point of the interval (Gray et al., 1997; ODE Laboratories, 2011). Thus, for the concave-up curve in Figure 4.4, the tangent line at the left end-point of the interval underestimates the vertical coordinate of the next point at the right end-point of the interval. A similar effect is observed with a concave-down curve, but the next point is overestimated. In reality it is difficult to know whether or not the estimation of the next point is overestimated or underestimated.

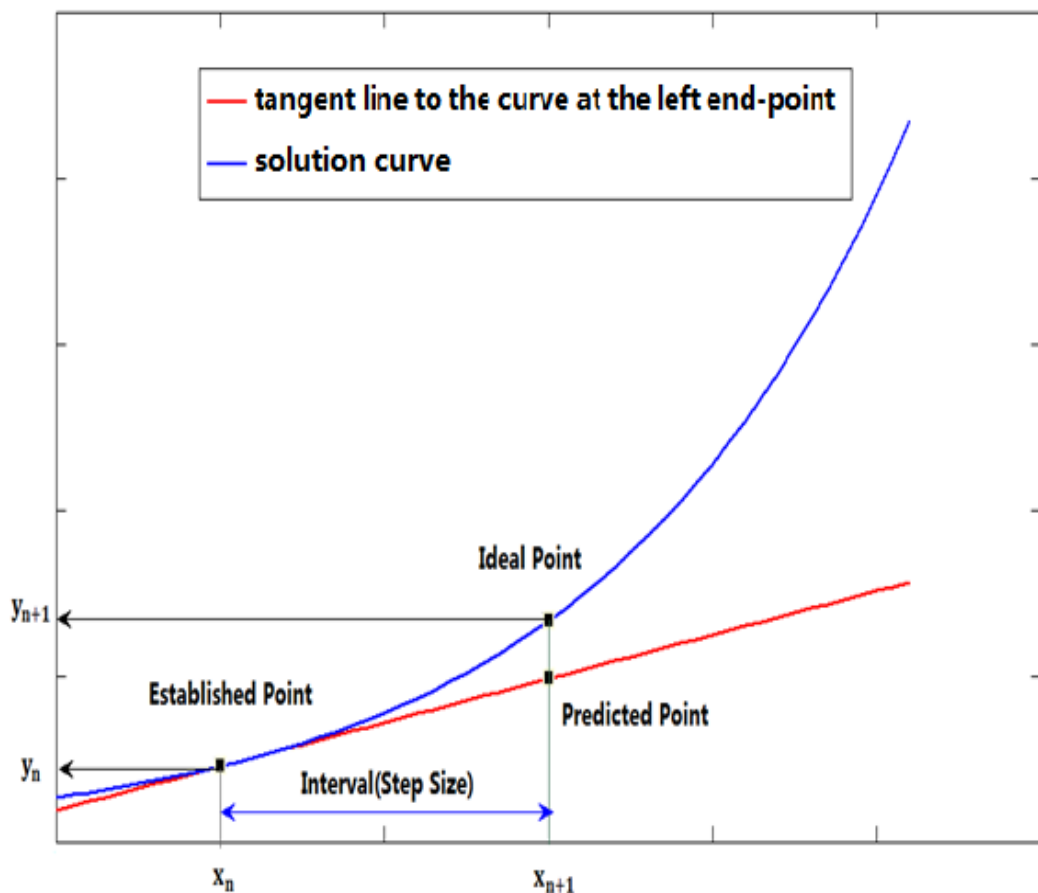


Figure 4.4: Prediction of coordinates of the next point based on the tangent line to the solution curve. Modified from ODE Laboratories [online]. Available at: <http://calculuslab.deltacollege.edu/ODE/7-C-2/7-C-2-h.html> [Accessed on 18 August 2011].

In order to fix the problem of underestimation or overestimation, the tangent line to the curve at the next iteration point is considered. At this stage, the coordinates of the right end-point of the interval are unknown; therefore a prediction of their positioning is made. However, it is assumed that the coordinates are initially

known and the solution to this problem is discussed later (Gray et al., 1997; ODE Laboratories, 2011). Through taking the slope of the tangent line to the curve at the right end-point of the interval, a line can be created passing through the left end-point of the interval to predict the vertical coordinate of the next point. This is termed the predicted line based on the right tangent. As illustrated in Figure 4.5, ‘Predicted Point 2’ is produced by the predicted line based on the right tangent, and is higher than the ‘Ideal Point’ on the solution curve which is concave up. In addition, ‘Predicted Point 1’ is produced by the tangent line to the curve at the left end-point.

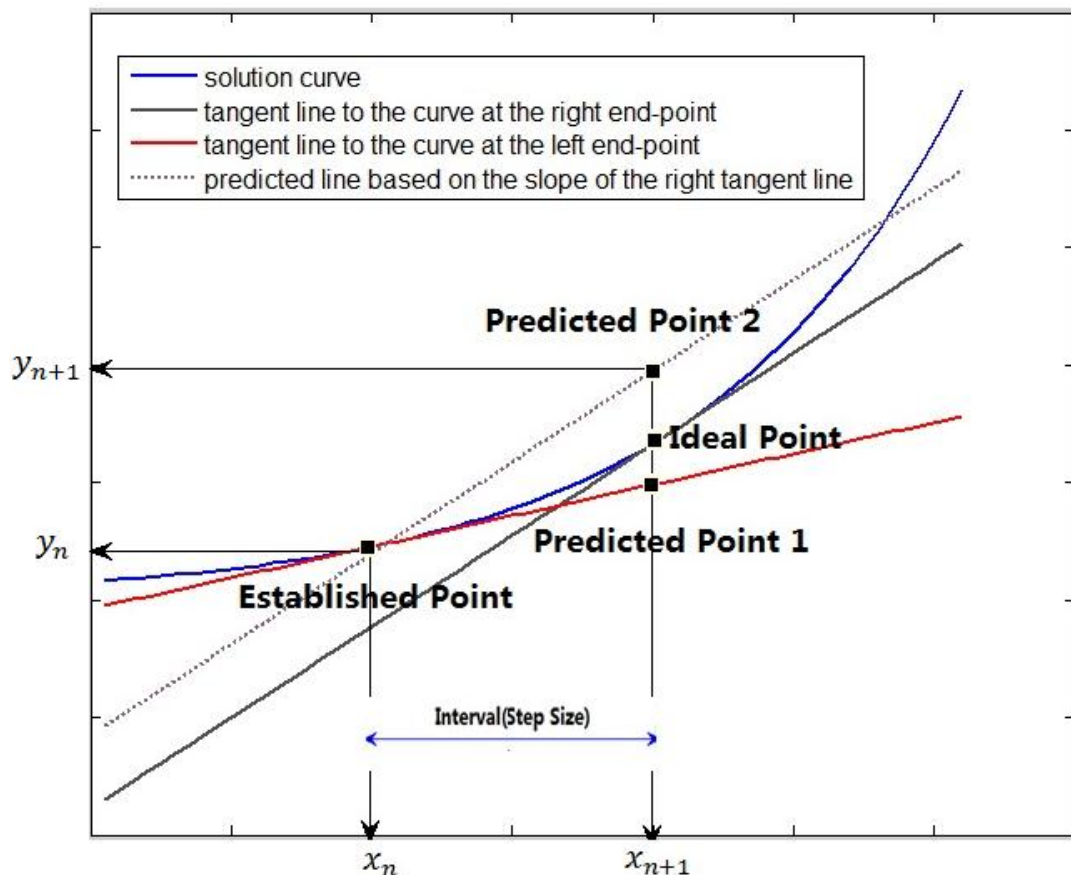


Figure 4.5: Prediction of coordinates of the next point based on the slope of the tangent line to the solution curve at the right end-point of the interval. Modified from ODE Laboratories [online]. Available at: <http://calculuslab.deltacollege.edu/ODE/7-C-2/7-C-2-h.html> [Accessed on 18 August 2011].

Figure 4.5 shows that ‘Predicted Point 1’ and ‘Predicted Point 2’ result in an underestimation and overestimation for the concave-up solution curve, respectively (the situation is reversed for the concave-down curve). Heun’s method takes the average of the slopes of the left and right tangent lines and produces a line crossing an ‘Established Point’ (Gray et al., 1997; ODE Laboratories, 2011). As displayed in

Figure 4.6, ‘Predicted Point 3’ is produced by this line, and lies between ‘Predicted Point 1’ and ‘Predicted Point 2’, which are respectively underestimated and overestimated compared to the ‘Ideal Point’. Therefore, ‘Predicted Point 3’ should be closer to the ‘Ideal Point’.

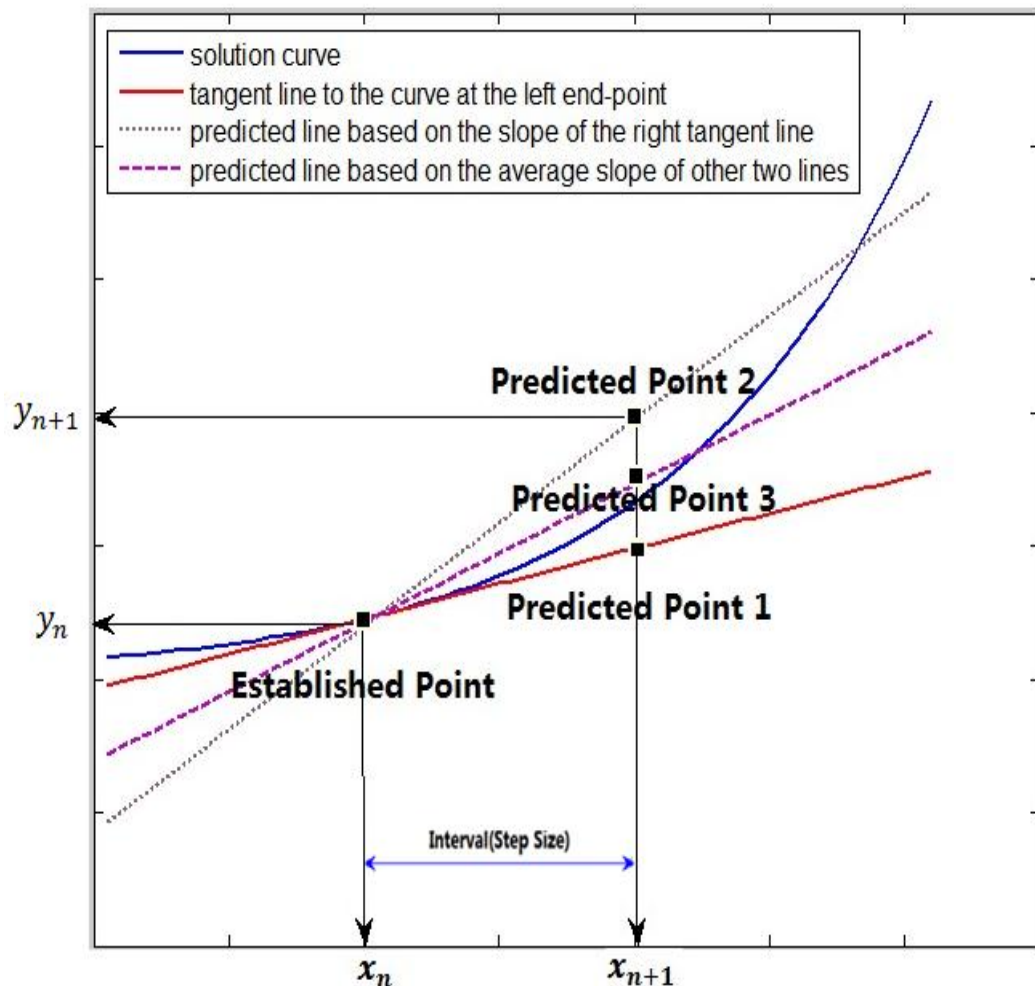


Figure 4.6: Prediction of coordinates of the next point based on the average of slopes of the tangent line to the solution curve at the left and right end-point of the interval.

Modified from ODE Laboratories [online]. Available at:

<http://calculuslab.deltacollege.edu/ODE/7-C-2/7-C-2-h.html> [Accessed on 18 August 2011].

Heun’s method uses the slope of the tangent line at the right end-point of the interval to predict the vertical coordinate of the right end-point (Gray et al., 1997; ODE Laboratories, 2011). This appears contradictory since it is impossible to determine the tangent line at the right end-point before the position of the right end-point is known. Euler’s method is used to roughly estimate the coordinates of the right end-point. Euler’s method is usually referred to as a predictor algorithm,

whereas Heun's method is referred to as a predictor-corrector algorithm. Based on the discussion above, the iteration formulas for Henu's method is as follows:

$$h = t_{n+1} - t_n \quad (4-16)$$

$$Y_{n+1} = Y_n + \left(\frac{h}{2}\right) \cdot (f(t_n, Y_n) + f(t_n+h, Y_n + hf(t_n, Y_n))), 0 \leq n \leq N - 1 \quad (4-17)$$

Runge-Kutta's method

Runge-Kutta's method is actually a general class of algorithm and includes different Runge-Kutta's methods of various orders (Gray et al., 1997; ODE Laboratories, 2011). The formal derivation of Runge-Kutta's method is not introduced since it is a rather complicated procedure. The general formula of Runge-Kutta's method is as follows (Gray et al., 1997; ODE Laboratories, 2011):

$$h = t_{n+1} - t_n \quad (4-18)$$

$$Y_{n+1} = Y_n + h(w_1k_1 + w_2k_2 + \dots + w_mk_m) \quad (4-19)$$

where,

- w_i ($i = 1, 2, \dots, m$) are a set of constants representing weighted coefficients, and satisfy the equation $w_1 + w_2 + \dots + w_m = 1$; and
- k_i ($i = 1, 2, \dots, m$) represents the estimated values of the solution curve evaluated at a series of selected points between the interval $[t_n, t_{n+1}]$.

The part ' $w_1k_1 + w_2k_2 + \dots + w_mk_m$ ' in Eq. (4-19) is a weighted average of estimations of a group of points in the solution curve located in the interval $[t_n, t_{n+1}]$, and are devised based on a Taylor polynomial of degree m . The order of Runge-Kutta's method is represented by ' m ' in Eq. (4-19). The fourth-order Runge-Kutta method is widely applied, and thus is taken as an example here. The values of w_i ($i = 1, 2, \dots, m$) and k_i ($i = 1, 2, \dots, m$) are as follows:

$$w_1 = \frac{1}{6}; w_2 = \frac{2}{6}; w_3 = \frac{2}{6}; w_4 = \frac{1}{6}$$

$$k_1 = f(t_n, Y_n)$$

$$k_2 = f\left(t_n + \frac{h}{2}, Y_n + \frac{k_1}{2}\right)$$

$$k_3 = f\left(t_n + \frac{h}{2}, Y_n + \frac{k_2}{2}\right)$$

$$k_4 = f(t_n + h, Y_n + k_3)$$

where,

- $f(t_n, Y_n)$ denotes the derivative of the solution curve $y(t)$ at the point (t_n, Y_n) ;
- k_1 is the estimating slope of the tangent line to the solution curve at moment t_n obtained from Euler's method;
- k_2 and k_3 estimate the slope of the tangent line to the solution curve at the point $t_n + \frac{h}{2}$, and the calculation of k_3 is dependent on k_2 ; and
- k_4 is the estimation of the slope of the tangent line to the solution curve at the moment $t_n + h$, based on k_3 .

when 'm' equals 1, Eq.(4-19) is altered to:

$$Y_{n+1} = Y_n + hf(t_n, Y_n) \quad (4-20)$$

Eq. (4-20) is the same as the formula for Euler's method, which means that Euler's method is actually the first-order Runge-Kutta method.

Adaptive methods

Time steps are very important for the accuracy of numerical methods. A large time step is used for low frequency curves, while a small time step is used for high frequency curves [\[http://www.mathworks.com/support/tech-notes/1500/1510.html#fixed\]](http://www.mathworks.com/support/tech-notes/1500/1510.html#fixed), but it is possible that the frequency of a curve (function) may vary in that case. If the time step is too large, it possibly misses some points and the overall accuracy of the solution is affected; conversely, if the time step is too small, the associated computation time increases.

These issues can be solved by adaptive methods, which are numerical solutions with a variable time step. One way of achieving adaptive methods is to combine two Runge-Kutta methods of different orders, such as the Runge-Kutta (2nd and 3rd order) integration method and the Runge-Kutta (4th and 5th order) integration methods, with corresponding solvers (ode23 and ode45) in Matlab (Mathews and Fink, 2004). Two different approximations of the solution are produced at each step. A close comparison between the two results provides confidence in the suitability of the applied time step. However, if the difference between the two results exceeds a specified accuracy limit, the time step is deemed too large and re-calculation is required with a reduced time step. The process of reducing the time step should be repeated until the resultant approximations are in close agreement.

The Runge-Kutta (4 and 5th order) integration method, whose corresponding Matlab solver is ode45, was selected to solve the equations in the proposed mathematical model based on the following: (1) Runge-Kutta's method is considered to be one of the most accurate numerical procedures in approximating solutions of a first-order initial-value problem (Zill, 2005). (2) Runge-Kutta's method includes a class of numerical solutions with different orders (*i.e.* fourth and fifth order). (3) Ode45 belongs to an adaptive method and uses a variable time step to solve nonstiff model equations. Ode45 is cited as an ideal choice when solving equations using the adaptive method (<http://www.mathworks.com/help/techdoc/ref/ode113.html>) (accessed on 23th August 2011).

A numerical method is stable when small changes in the initial condition only produce small variations in the computation results; otherwise it is unstable. It is necessary to analyse the stability of a numerical method, since each step after the first step of the numerical calculation produces another initial-value problem. The round-off error and error in the initial value will result in a deviation from the true value if numerical solution is not stable (Zill, 2005).

To determine if a numerical solution is stable, the equations should be solved in two different time steps. If the error increases with smaller step sizes, the numerical method is deemed unstable (although such errors cannot be measured in most cases because the accurate solution is not known). Alternatively, the effect of adding a slight perturbation to the initial value can be simulated.

4.3.3 SIMULATION RESULTS AND ANALYSIS

Based on the proposed mathematical model, a normal bone remodelling cycle was reconstructed and the sensitivity of the results to the model parameters was investigated. Two pathological conditions, PHPT and HT, were subsequently examined to demonstrate how the model can be used to simulate other abnormal conditions.

4.3.3.1 THE NORMAL BONE REMODELLING CYCLE

Table 4.2 presents published experimental data for the normal trabecular bone remodelling cycle. Using the parameter values shown in Table 4.3 theoretical values of the histomorphometric measures were calculated using a genetic algorithm approach (see Table 4.2). The model predictions produced a close match with the

experimental data (with the exception of the maximum formation rate). Although a close match in the first seven quantities is to be expected, the predicted maximum osteoclast and osteoblast populations also agreed well with the experimental data, despite their exclusion from the solution process. However, it should be noted that the cell populations quoted in Table 4.2 were estimated from experimental measurements of Haversian remodelling (Jaworski et al., 1981; Jaworski and Hooper, 1980; Parfitt, 1994). Based on examination of 86 remodelling sites, it was observed that the number of osteoclasts varied between 4 and 16. Thus assuming that the trench-shaped remodelling volume in trabecular bone is approximately half of that of the tunnel-shaped remodelling volume in cortical bone, the number of osteoclasts in trabecular bone remodelling was estimated to be approximately 8.

Phenomena	Experimental (mean) values	Source	Model predictions
Resorption depth	62 μm	[1]	62.2 μm
Resorption period	48 days	[1]	50.8 days
Maximum resorption rate	3.9 $\mu\text{m/day}$	[1]	3.8 $\mu\text{m/day}$
Formation height	62 μm	[2]	62.2 μm
Formation period	145 days	[2]	145 days
Maximum formation rate	2.1 $\mu\text{m/day}$	[2]	1.4 $\mu\text{m/day}$
Quiescent period	902 days	[3]	901.4 days
Maximum osteoclast population	8 cells	[4,5]	9.0 cells
Maximum osteoblast population	2000 cells	[4,5]	1930.7 cells

Table 4.2: Histomorphometric data for normal trabecular bone remodelling as reported in literature and predicted by the proposed mathematical model.

[1] Eriksen et al., 1984a; [2] Eriksen et al., 1984b; [3] Eriksen et al., 1986;

[4] Parfitt, 1994; [5] Jaworski et al., 1981].

Parameter	Value
a	0.0558 day^{-1}
b	$0.0065 \text{ cells}^{-1/2} \text{ day}^{-1}$
c	$1.82 \times 10^9 \text{ day}^{-1}$
d	0.0099 day^{-1}
e	$17.2 \mu\text{m}^{-1}$
f	$0.0461 \text{ cells}^{-2} \mu\text{m}^{-1}$
k_{oc}	$2.44 \times 10^{11} \text{ cells}^2$
k_{ob}	$4.32 \times 10^4 \text{ cells}$

Table 4.3: Parameter values derived by the mathematical model for the normal remodelling cycle.

The simulations set the initial conditions to $x_{oc}(0) = x_{ob}(0) = 0.1$ so that the osteoclast and osteoblast populations were approximately zero at the start of the resorption period. Sensitivity studies (in section 4.3.3.2) revealed that the simulations were only marginally affected by the initial choice of these parameters. Experimental observations and BMU theory suggest that there should not be any osteoclasts and osteoblasts active during the quiescent period (Parfitt, 1994). Therefore, due to the requirement of the simulations to define $x_{oc}(t)$ and $x_{ob}(t)$ (equations (4-3) and (4-4)) as real (rather than integer) terms, any values below 0.5 were regarded as zero (*i.e.* no active osteoclast or osteoblast). The end of the resorption period (and start of the formation period) was defined when the number of osteoclasts fell below 0.5. However, because the maximum number of osteoblasts is typically two orders of magnitude greater than the maximum number of osteoclasts, the end of the formation period (and the start of the quiescent period) was defined as the moment when the formed cavity depth $D(t)$ reached 99.5% of its maximal value (as shown in Figure 4.8) (rather than the time when the osteoblast population fell below 0.5).

Examination of the osteoblast population in Figure 4.7 suggested that there were still a significant number of non-active osteoblasts present when 99.5% of the cavity was refilled, which takes significantly longer to decay. The reason for this inconsistency lies in the underlying predator-prey equations, in which the preys (osteoclasts) thrive again as soon as the predators (osteoblasts) have decreased (and vice versa), and not after a period where neither population is present. Maintenance of so many inactive osteoblasts is physiologically unlikely, which highlights a limitation of the predator-prey approach.

The corresponding cyclic variations in the osteoblast and osteoclast populations, along with bone thickness, predicted by the model are presented in Figure 4.7 and Figure 4.8, respectively. The dynamic interaction between the osteoclasts and osteoblasts is shown in Figure 4.9. The latter illustrates how the remodelling cycle commences with the growth of the osteoclast population in the absence of osteoblasts. As the osteoclast population continues to grow, the osteoblast population also starts to increase; then, as the osteoblast growth increases further, the osteoclast numbers start to decline. While the osteoclast population is decreasing, the osteoblast population grows faster but starts to decrease again as the osteoclasts completely disappear. As the osteoblast population diminishes the BMU enters the quiescent period, with small values of the osteoblast population then being interpreted as quiescent-osteoblasts. It should be noted that Figure 4.9 does not reflect the difference in the rates at which these populations change, or the much shorter period of osteoclast activity compared to that of osteoblasts. However, this can be observed in Figure 4.7, which shows the rapid decline of the osteoclast population as the number of osteoblasts increase.

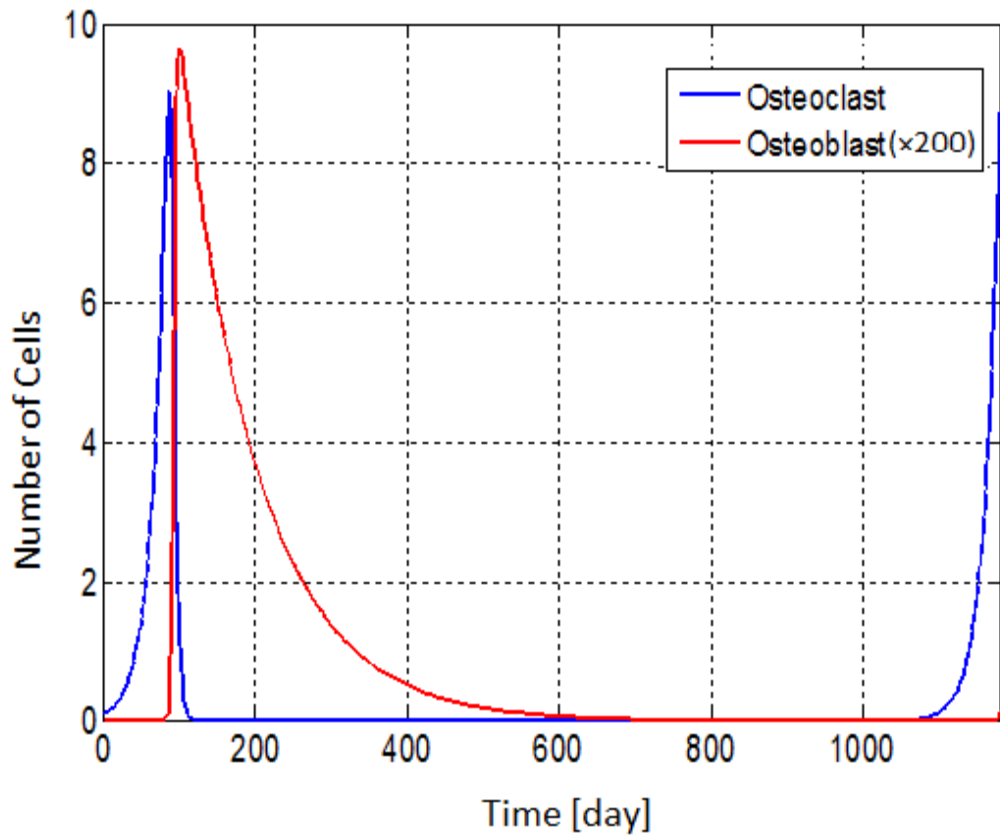


Figure 4.7: Model predictions of the variation in osteoclast and osteoblast populations during the normal bone remodelling cycle; (note the osteoblast scaling factor).

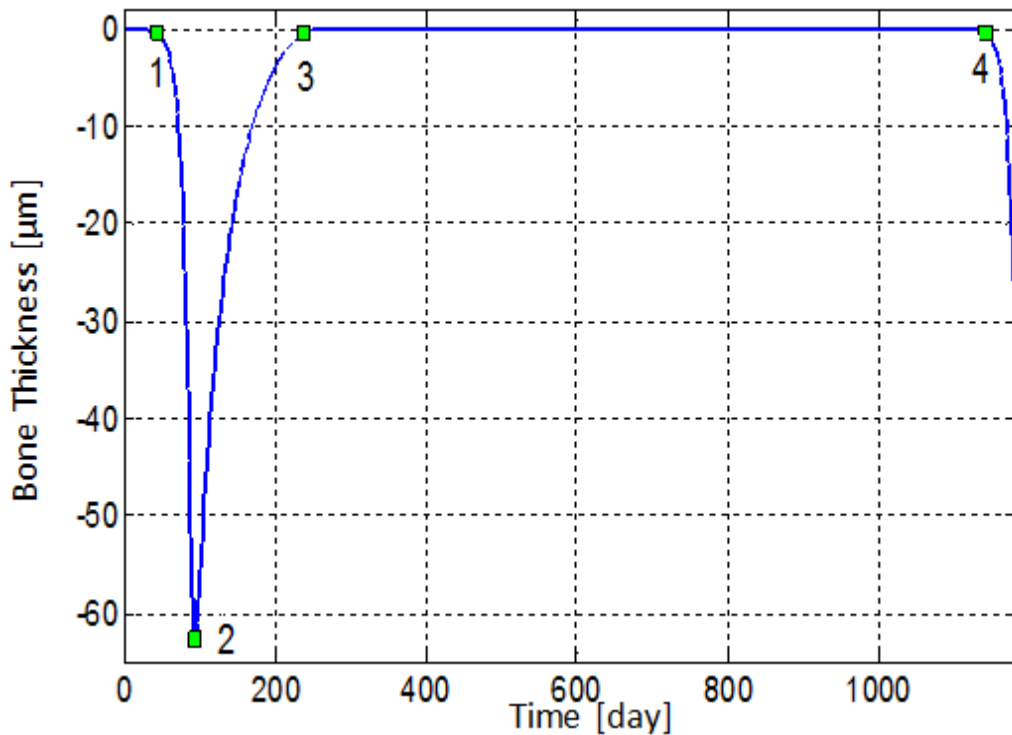


Figure 4.8: Model predictions of the variation in bone thickness during the normal bone remodelling cycle (note the osteoblast scaling factor)(1: $(t_{initial}, D_{initial})$, 2: (t_{res}, D_{res}) , 3: (t_{form}, D_{form}) , 4: (t_{end}, D_{end})).

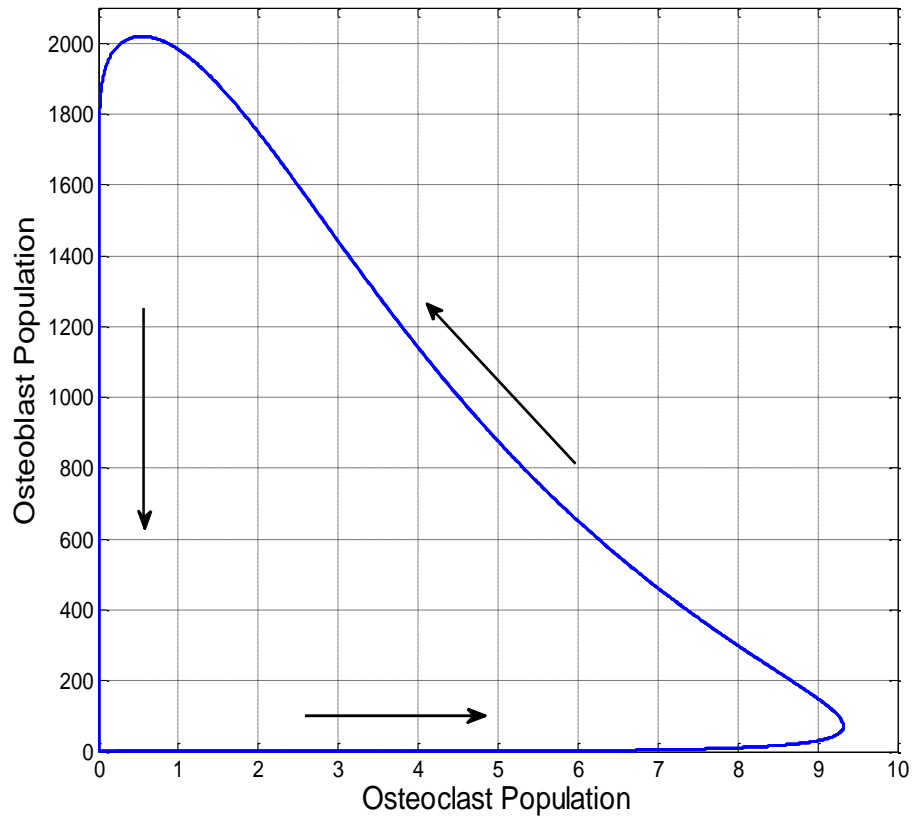


Figure 4.9: The periodic orbit of the osteoclast-osteoblast interaction during the normal bone remodelling cycle, which proceeds in an anti-clockwise direction.

4.3.3.2 SENSITIVITY OF THE MODEL TO PARAMETER VARIATIONS

The sensitivity of the simulations to variations in parameters a , b and K_{oc} in Eqs. (4-3) and (4-4), is shown in Figure 4.10. The deviation in the maximum number of osteoclasts and osteoblasts is presented when the parameters were varied between 0.5 and 1.5 of the ‘normal’ value. This sensitivity analysis shows that: parameter a affects the growth of both osteoclasts and osteoblasts; parameter b affects mainly the growth of osteoblasts; while parameter K_{oc} affects only the growth of osteoclasts. Parameter d (not shown) influences the apoptosis or elimination rate of osteoblasts and an increase in its value accelerates their removal. The parameter K_{ob} in Eq. (4-9) is responsible for controlling the maximum formation rate. The values of parameters c , e and f were assumed to be constant in all simulations, because c and e are respectively dependent on K_{oc} and K_{ob} , and f is a scaling coefficient for the bone resorption. A summary of the sensitivity results is provided in Table 4.4.

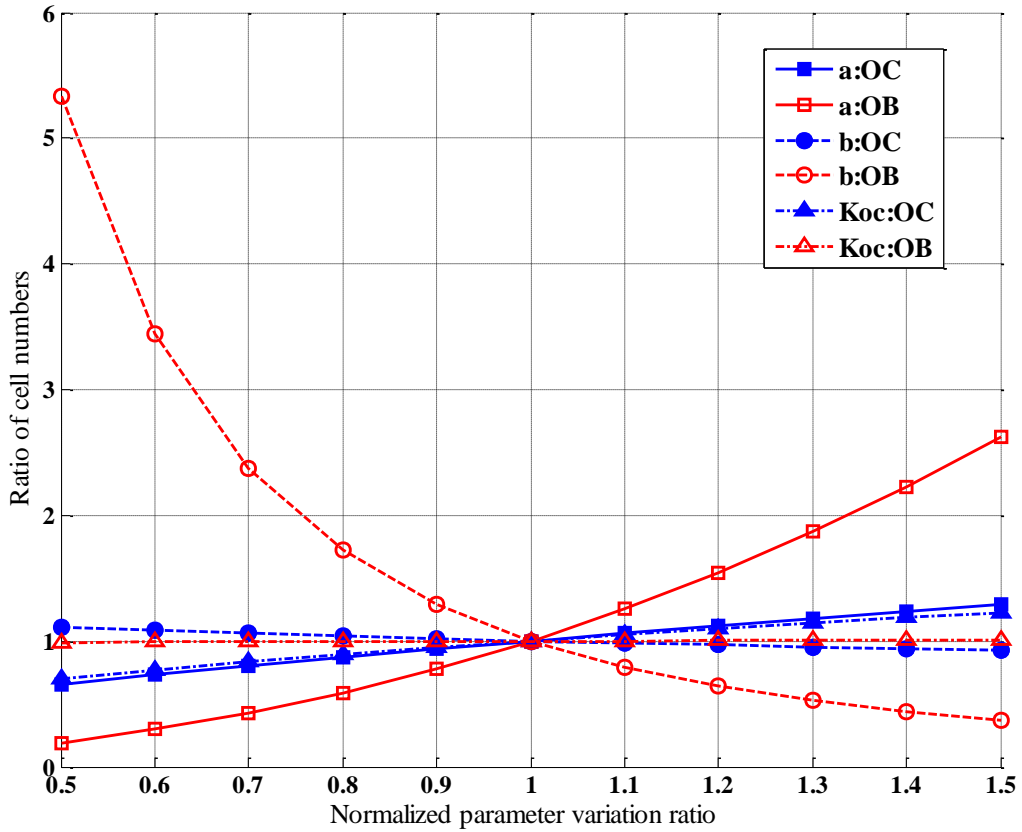


Figure 4.10: The effects of independently varying each model parameter on the osteoblast and osteoclast populations. Parameter variance was normalized to the values of the base case (as defined in Tables 1 and 2), for example, the lines a:OB and a:OC demonstrate the variation in osteoblast and osteoclast populations as parameter a is varied between 0.5 and 1.5 times its base value.

Parameters	Observations
$a \uparrow$	osteoclasts \uparrow osteoblasts \uparrow
$b \downarrow$	osteoclasts $-$ osteoblasts $\uparrow\uparrow$
$d \uparrow$	osteoclasts $-$ osteoblasts $-$ period \downarrow
$K_{oc} \uparrow$	osteoclasts \uparrow osteoblasts $-$
$K_{ob} \uparrow$	formation rate \downarrow

Table 4.4: Summary of the relationship between the model parameters and remodelling activity (Symbols: \downarrow = decrease, \uparrow = increase, $\uparrow\uparrow$ = significant increase, $-$ = little or no effect).

4.3.3.3 SIMULATIONS OF THE REMODELLING CYCLES IN PATHOLOGICAL CONDITIONS

Once the basic equations describing the remodelling cycle are established, modifications can be made to simulate pathological conditions, with the potential of examining the effectiveness of different therapies. Histomorphometric analyses of trabecular bone samples from 19 primary PHPT patients (6 male and 13 females) and 18 HT female patients have been reported (Eriksen et al., 1986a, 1986b). The key data is displayed in Table 4.5.

The controlling parameters for these two pathologies was calculated using the procedures outlined above, and then compared to those of the normal remodelling cycle in Table 4.6. The resulting remodelling cycles for PHPT and HT conditions are shown in Figure 4.11 to Figure 4.14. The basic shapes of the curves were similar to those for normal remodelling (see Figure 4.7 and Figure 4.8) in both cases, although the maximum number and ratio of osteoclasts to osteoblasts are different in each case, as is the period of the remodelling cycle. A comparison between the histomorphometric data and the calculated theoretical values is provided in Table 4.5. The experimental and theoretical data generally produced a close comparison, although there are differences in the resorption and formation rates, along with an 18% difference in the PHPT resorption period. The model was also able to predict the osteoclast and osteoblast populations for each condition, which are not previously reported in the literature. The predicted osteoblast and osteoclast cell populations in the PHPT condition were nearly double those of the HT condition, with the number of PHPT osteoclasts and osteoblasts 26% and 29% higher than the 'normal' case, respectively (see Table 4.2). As a result, the osteoblast to osteoclast ratio for these two conditions was 219.8 and 233.2 respectively, while the ratio for normal remodelling was 214.5.

Phenomena	PHPT		HT	
	Experimental (mean) values	Model predictions	Experimental (mean) values	Model predictions
Resorption depth	45.2 μm	45.2 μm	42.1 μm	42.1 μm
Resorption period	31 days	25.4 days	76 days	75.9 days
Maximum resorption rate	5.7 $\mu\text{m/day}$	5.9 $\mu\text{m/day}$	2.9 $\mu\text{m/day}$	1.4 $\mu\text{m/day}$
Formation height	45.2 μm	45.2 μm	59.0 μm	59.0 μm
Formation period	172 days	172 days	620 days	625.9 days
Maximum formation rate	2.2 $\mu\text{m/day}$	1.1 $\mu\text{m/day}$	0.74 $\mu\text{m/day}$	0.3 $\mu\text{m/day}$
Quiescent period	390 days	393 days	2098 days	2068.6 days
Maximum osteoclast population	–	11.3 cells	–	5.5 cells
Maximum osteoblast population	–	2483.8 cells	–	1280.1 cells

Table 4.5: Comparison of the experimental and predicted remodelling cycles in PHPT and HT with experimental data from Eriksen et al. (1986a, b).

Parameters	HT	Normal	PHPT
a	0.0327 day ⁻¹	0.0558 day ⁻¹	0.1231 day ⁻¹
b	0.0044 cells ^{-1/2} day ⁻¹	0.0065 cells ^{-1/2} day ⁻¹	0.0129 cells ^{-1/2} day ⁻¹
c^*		1.82 × 10 ⁹ day ⁻¹	
d	0.0025 day ⁻¹	0.0099 day ⁻¹	0.0150 day ⁻¹
e^*		17.2 μm ⁻¹	
f^*	0.0461 cells ⁻² μm ⁻¹		
k_{oc}	1.81 × 10 ¹¹ cells ²	2.44 × 10 ¹¹ cells ²	1.74 × 10 ¹¹ cells ²
k_{ob}	9.64 × 10 ⁴ cells	4.32 × 10 ⁴ cells	6.42 × 10 ⁴ cells

Table 4.6: Comparison of parameter values derived by the model for normal and disease conditions (* parameters c , e and f are assumed to be constant).

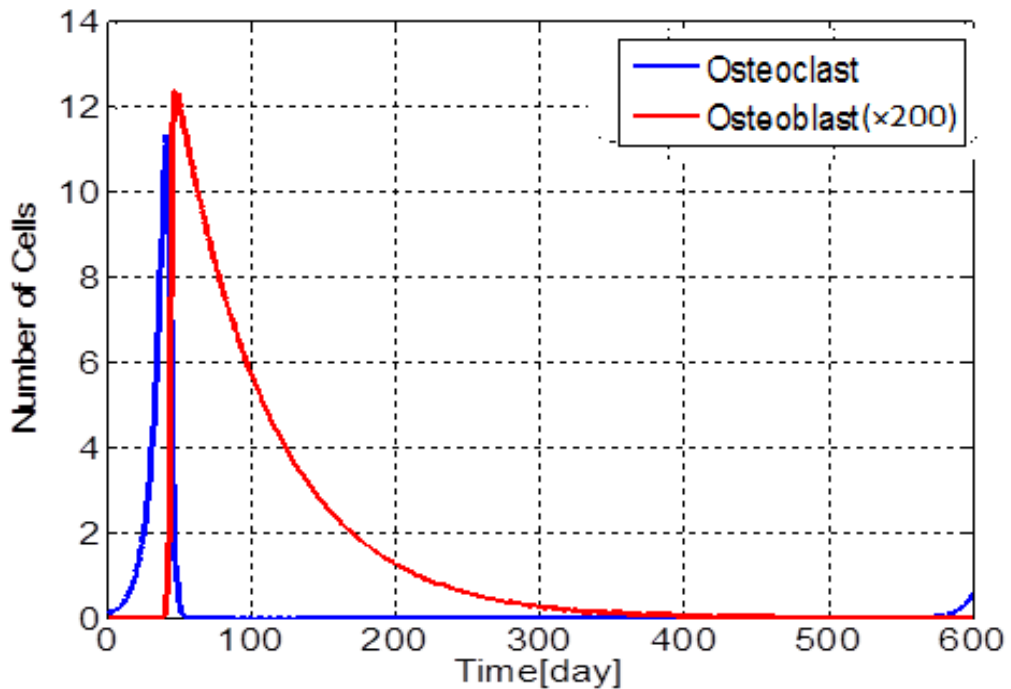


Figure 4.11: Model predictions of the variation in osteoclast and osteoblast populations during the remodelling cycle with PHPT (note the osteoblast scaling factor).

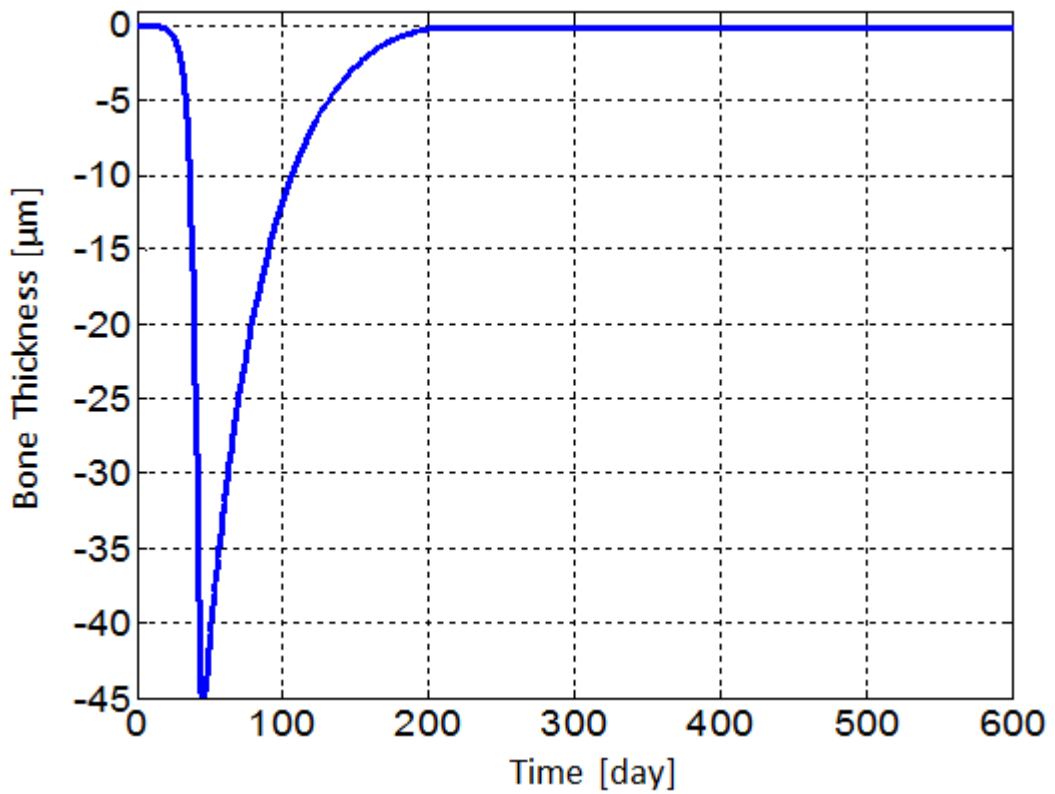


Figure 4.12: Model predictions of the bone thickness during the remodelling cycle with PHPT.

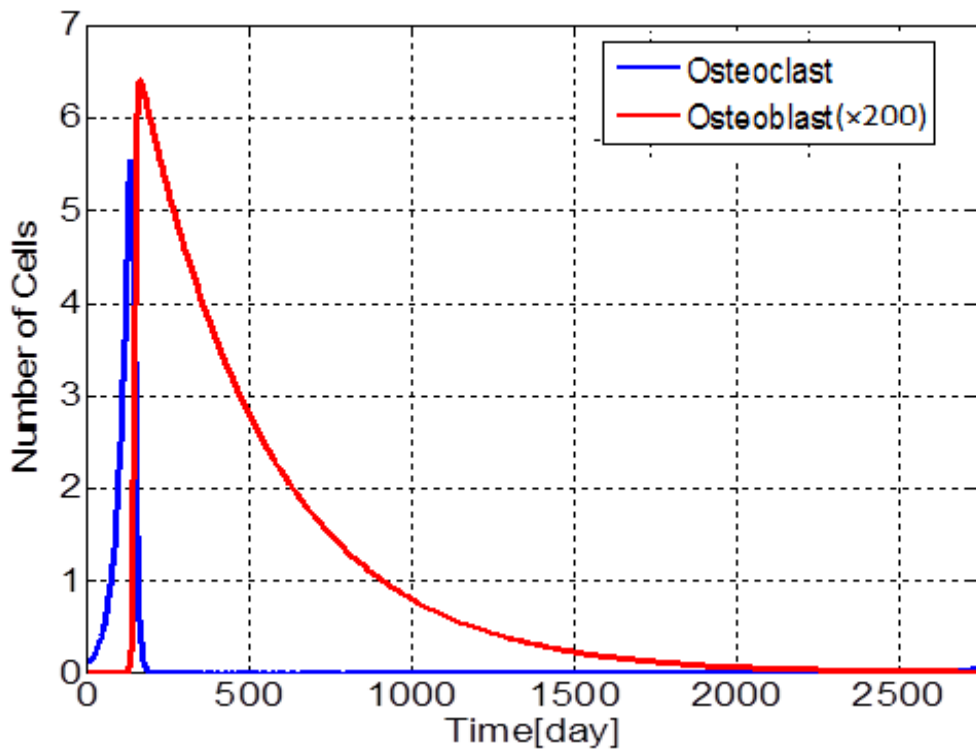


Figure 4.13: Model predictions of the variation in osteoclast and osteoblast populations during the remodelling cycle with HT.
(note: the osteoblast scaling factor).

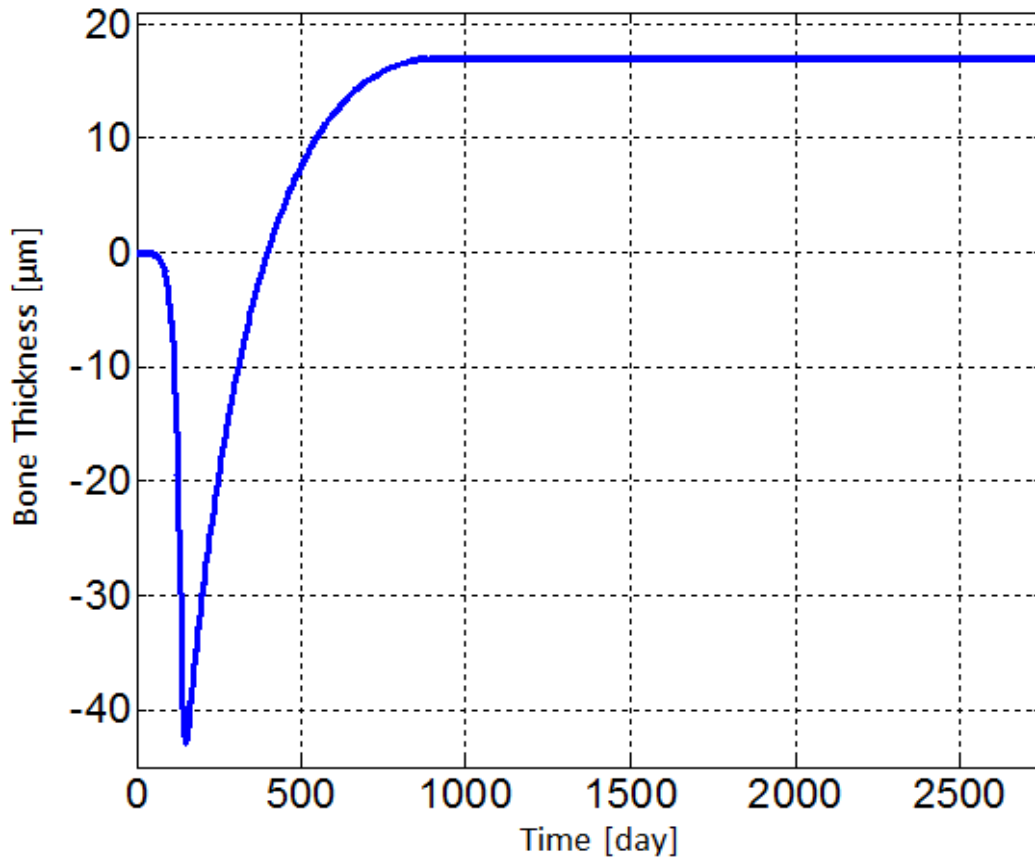


Figure 4.14: Model predictions of the variation in bone thickness during the remodelling cycle with HT.

4.3.3.4 STABILITY ANALYSIS OF THE SOLUTIONS

As discussed in section 4.3.4, it is necessary to check the stability of the numerical solution to an initial-value problem of ordinary differential equation. The method adopted to check the stability of the numerical solution by observing the effect of adding a disturbance to the initial condition. The model simulated the variation in the population of osteoblasts and osteoclasts, and the resultant bone mass, with the initial conditions of $x_{oc}(0)=x_{ob}(0)=0.1$ and $\bar{D} = 0$. A slight perturbation was subsequently added to the initial condition so that $x_{oc}(0) = x_{ob}(0) = 0.11$ and $\bar{D} = 0.01$. The simulation was repeated with the perturbed initial condition and the simulation results were correspondingly compared to those obtained through the original initial condition.

Figure 4.15 to Figure 4.17 demonstrate that the perturbation in the initial condition resulted in maximal changes of the osteoclast and osteoblast populations, and bone mass during normal bone remodelling cycles of 15%, 21.4% and 6.5%, respectively (where maximal change was defined as the maximal change caused by

the perturbation divided by maximal quantity under the unperturbed initial condition). The maximal changes of the osteoclast and osteoblast populations, and bone mass during the remodelling cycle with PHPT were 9.7%, 10.6% and 8.4%, respectively (see Figure 4.18 to Figure 4.20). During the remodelling cycle with HT, the maximal changes of osteoclast and osteoblast populations, and bone mass were 11%, 12.4% and 10.6%, respectively (see Figure 4.21 to Figure 4.23).

Considering that the initial conditions of the osteoclast and osteoblast populations were both varied by 10% (note the percentage variation in the initial condition of bone mass could not be calculated since the original initial value of bone mass equals zero), the resultant changes were not significant and the trends of the solution curves remained consistent. Therefore, it was concluded that the numerical solutions used in the proposed model were stable under normal and two pathological conditions.

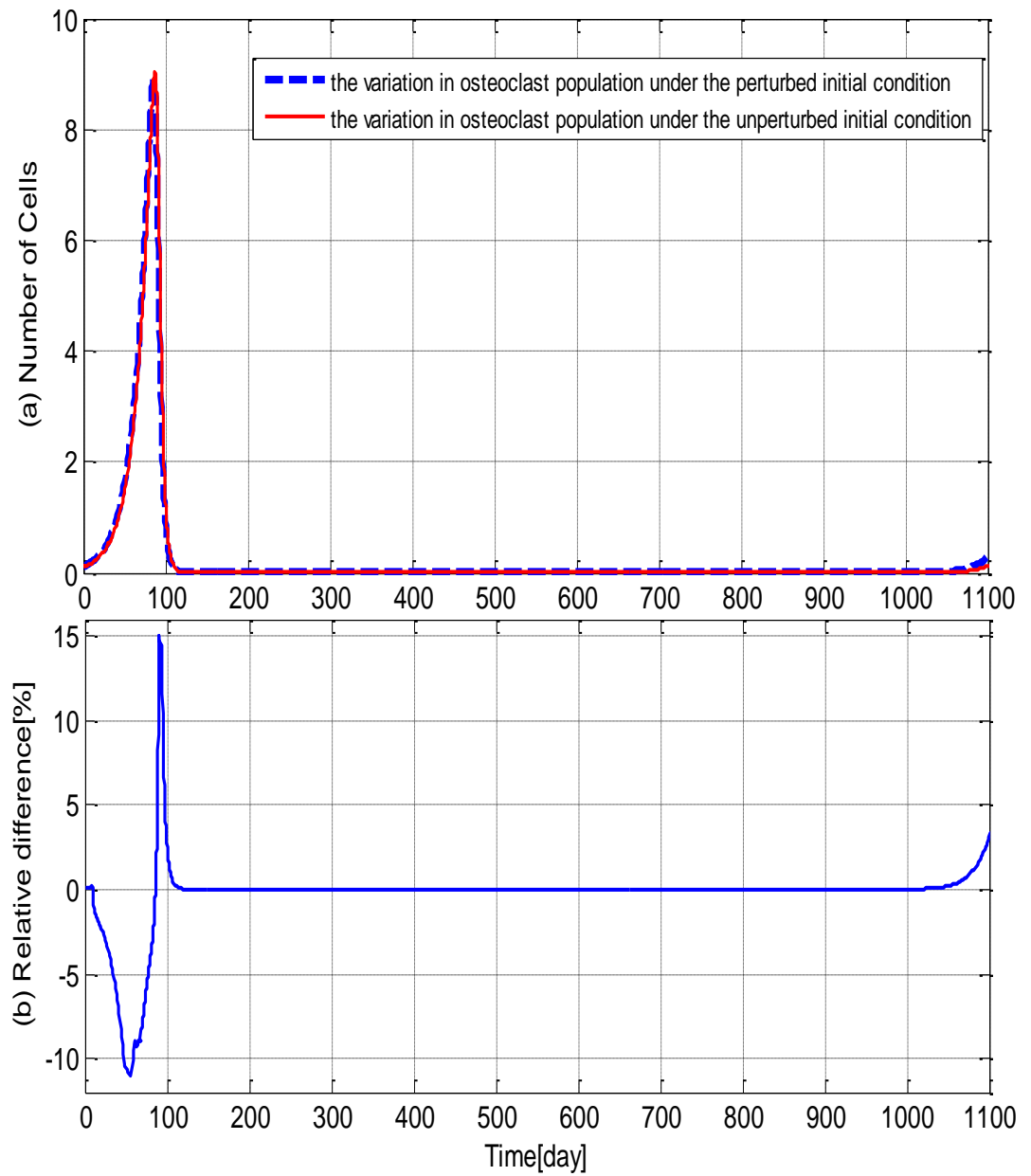


Figure 4.15: (a) Model predictions of the variations in osteoclast population under the unperturbed and perturbed initial conditions, during the normal bone remodelling cycle; (b) Difference between the variations in osteoclast population produced by the unperturbed and perturbed initial conditions, during the normal bone remodelling cycle.

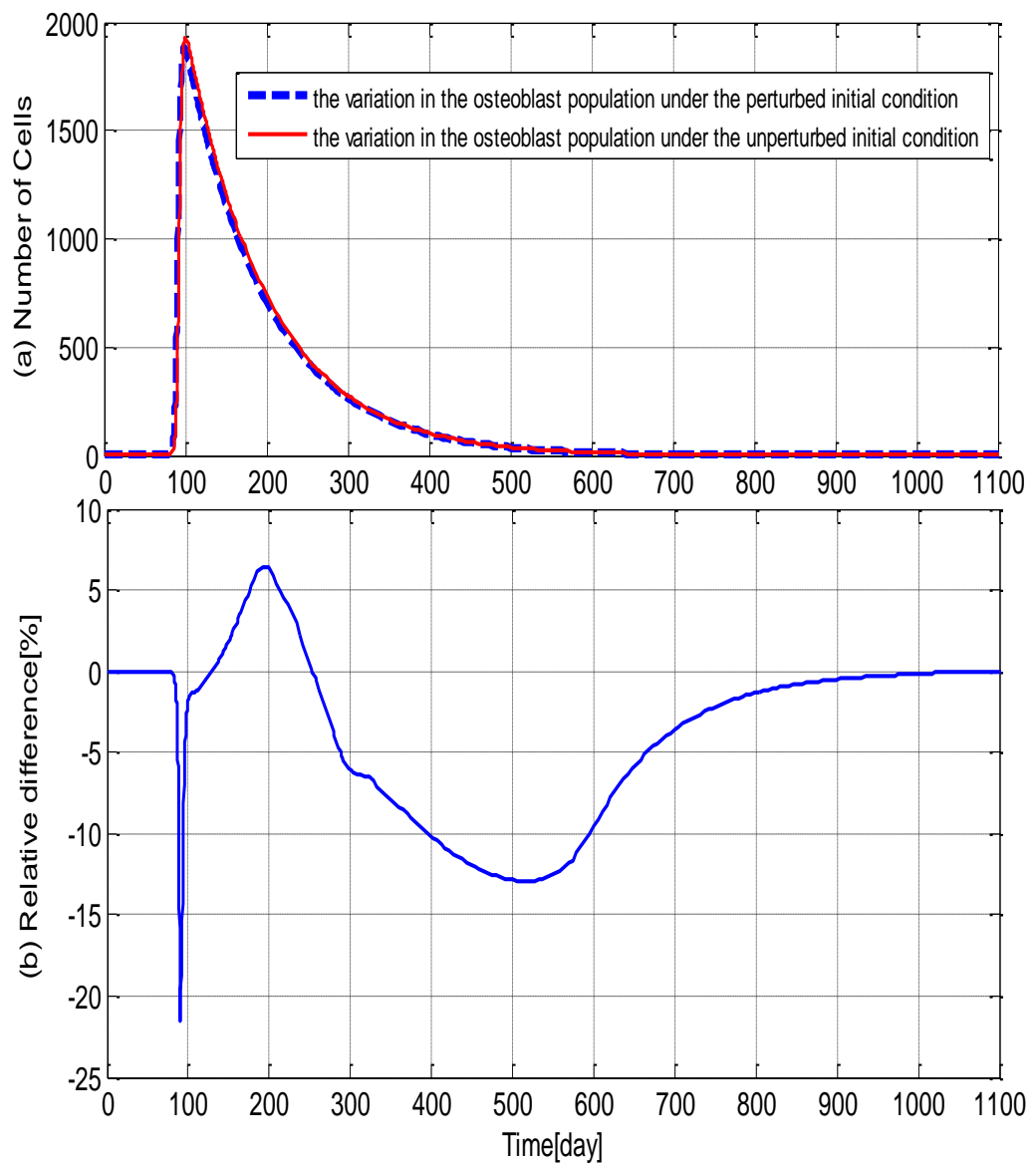


Figure 4.16: (a) Model predictions of the variations in osteoblast population under the unperturbed and perturbed initial conditions, during the normal bone remodelling cycle; (b) Difference between the variations in the osteoblast population produced by the unperturbed and perturbed initial conditions, during the normal bone remodelling cycle.

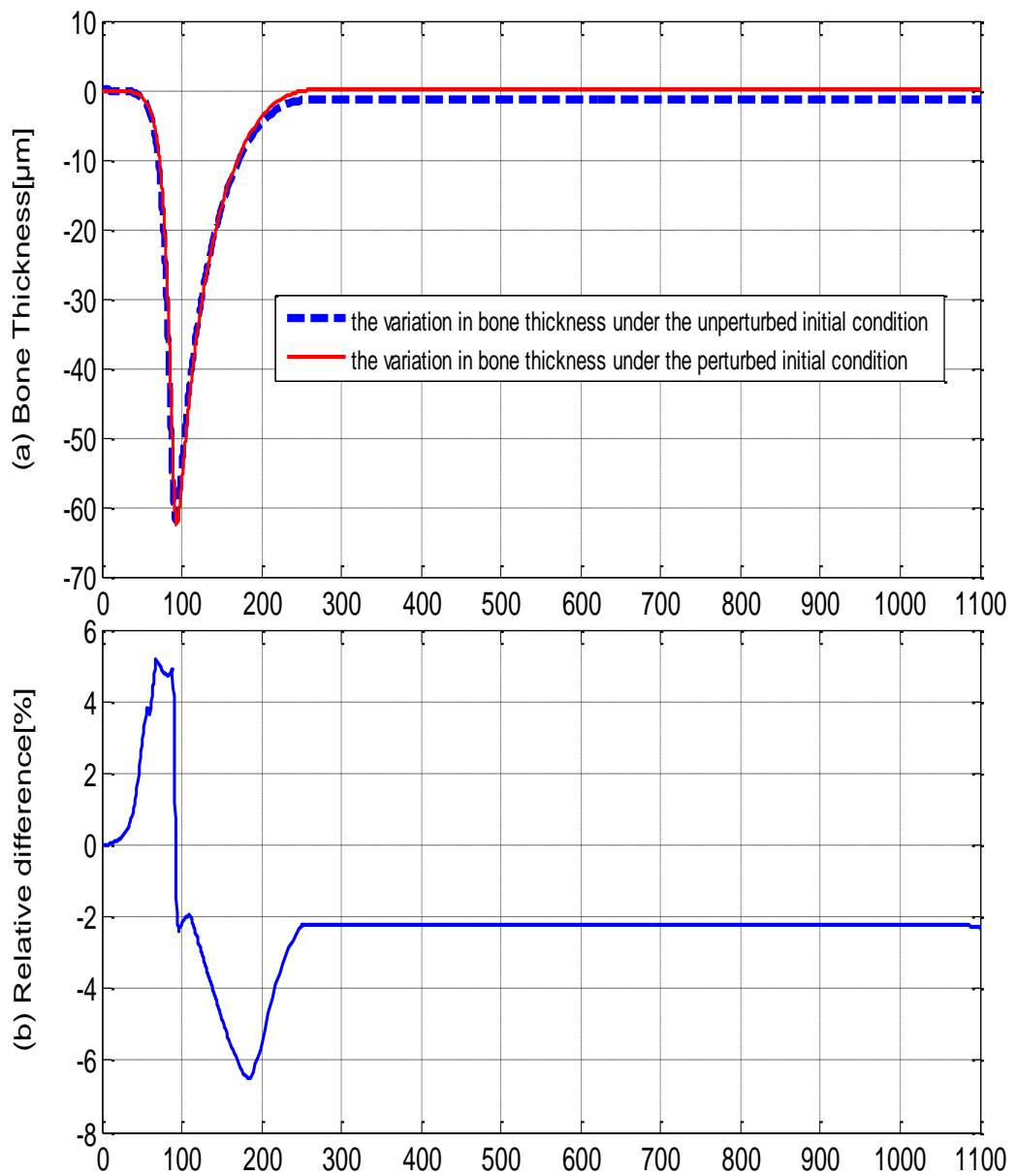


Figure 4.17: (a) Model predictions of the variations in bone thickness under the unperturbed and perturbed initial conditions, during the normal bone remodelling cycle; (b) Difference between the variations in bone thickness produced by the unperturbed and perturbed initial conditions, during the normal bone remodelling cycle.

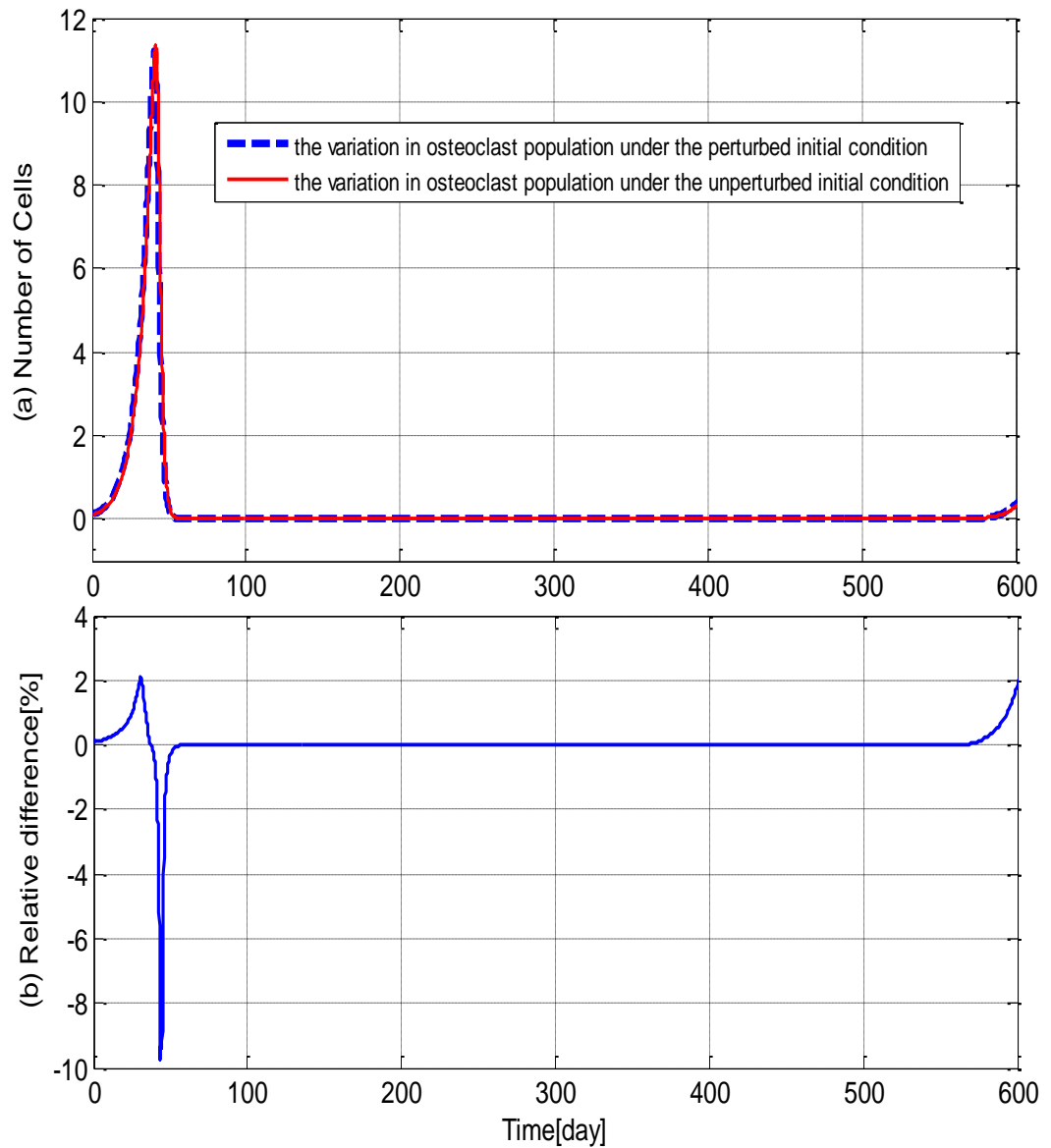


Figure 4.18: (a) Model predictions of the variations in osteoclast population under the unperturbed and perturbed initial conditions, during the remodelling cycle with PHPT; (b) Difference in the variations in the osteoclast population produced by the unperturbed and perturbed initial conditions, during the remodelling cycle with PHPT.

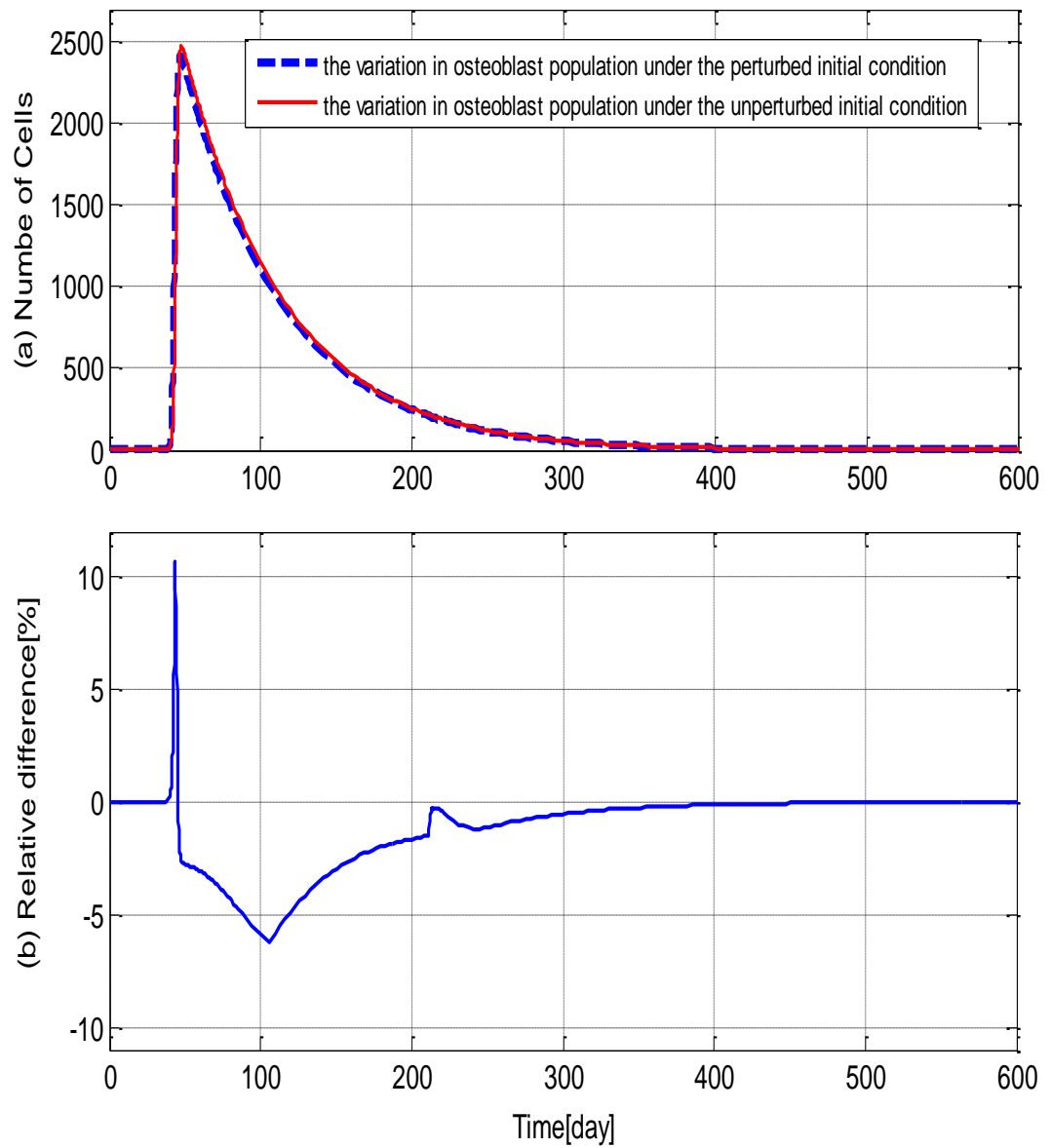


Figure 4.19: (a) Model predictions of the variations in osteoblast population under the unperturbed and perturbed initial conditions, during the remodelling cycle with PHPT; (b) Difference between the variations in osteoblast population produced by the unperturbed and perturbed initial conditions, during the remodelling cycle with PHPT.

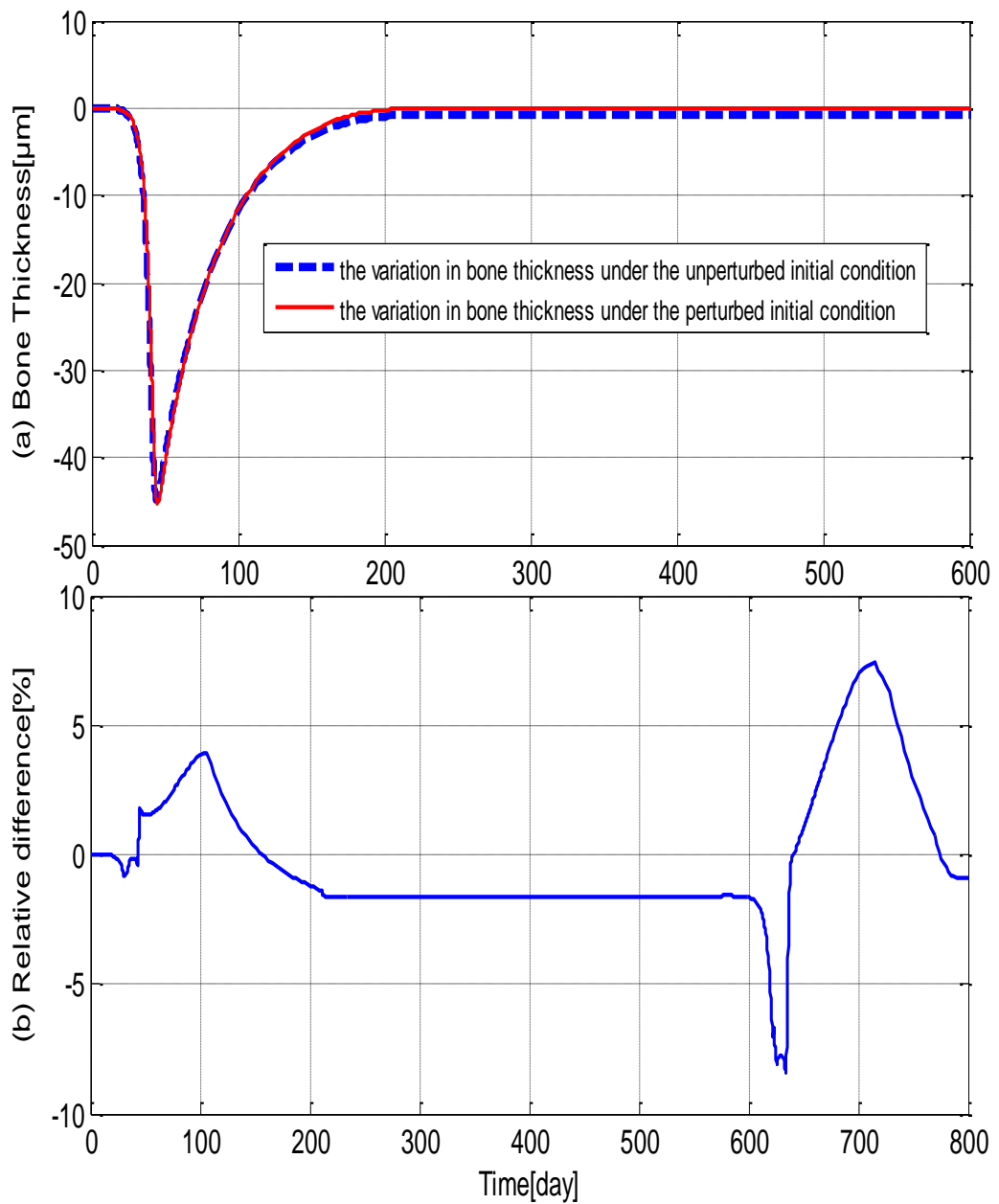


Figure 4.20: (a) Model predictions of the variations in bone thickness under the unperturbed and perturbed initial conditions, during the remodelling cycle with PHPT. (b) Difference between the variations in bone thickness produced by the unperturbed and perturbed initial conditions, during the remodelling cycle with PHPT.

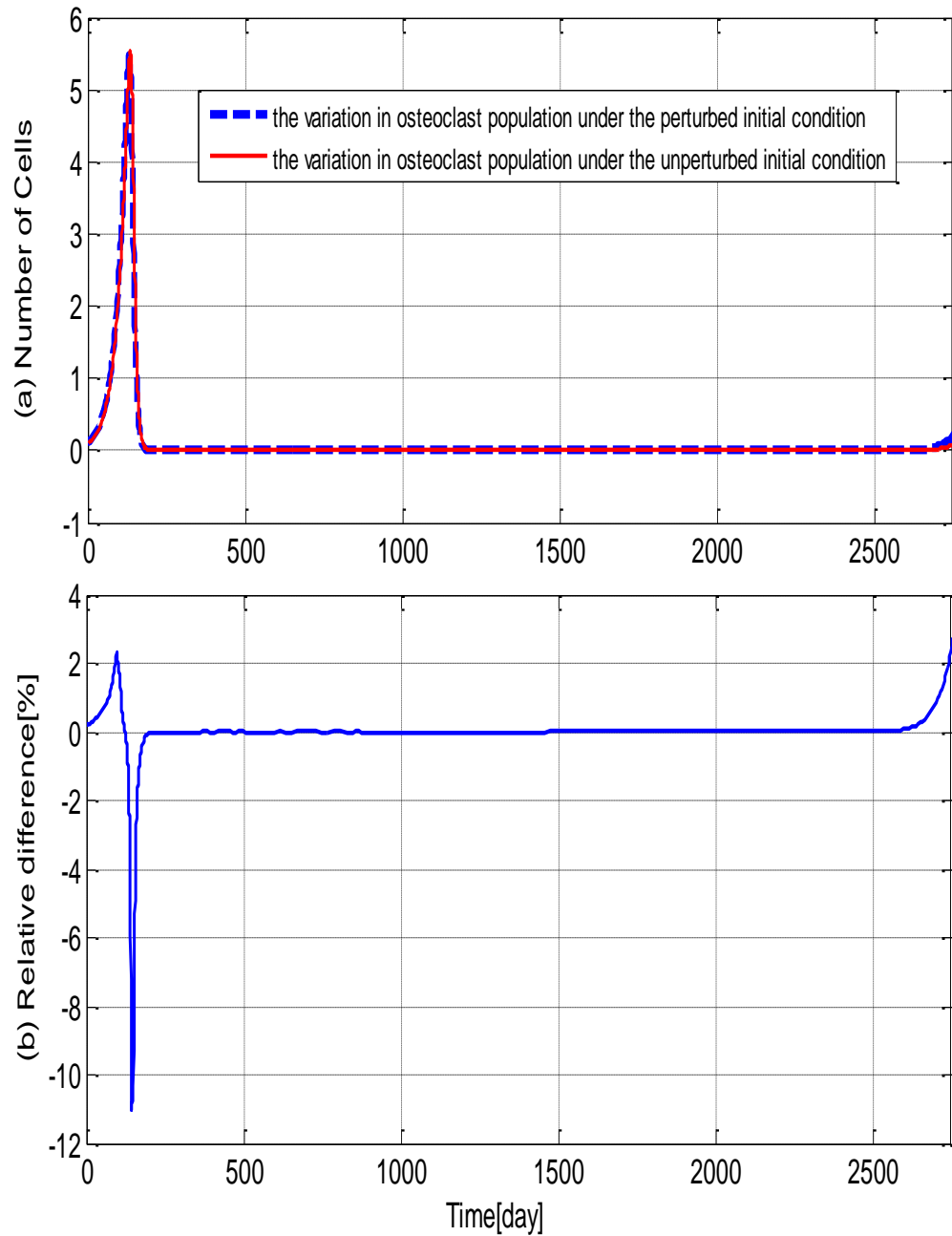


Figure 4.21: (a) Model predictions of the variations in osteoclast population under the unperturbed and perturbed initial conditions, during the remodelling cycle with HT. (b) Difference between the variations in osteoclast population produced by the unperturbed and perturbed initial conditions, during the remodelling cycle with HT.

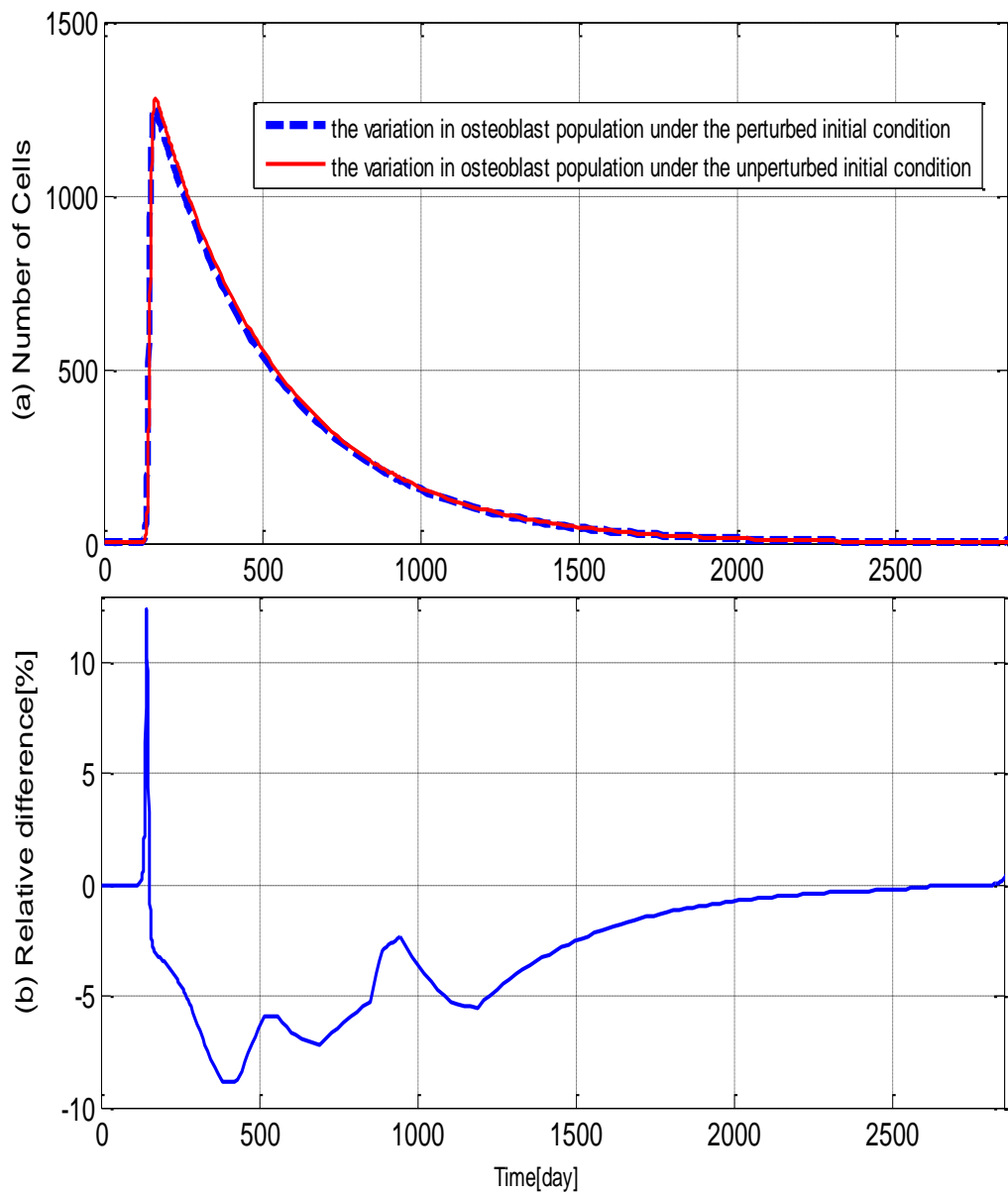


Figure 4.22: (a) Model predictions of the variations in osteoblast population under the unperturbed and perturbed initial conditions, during the remodelling cycle with HT. (b) Difference between the variations in osteoblast population produced by the unperturbed and perturbed initial conditions, during the remodelling cycle with HT.

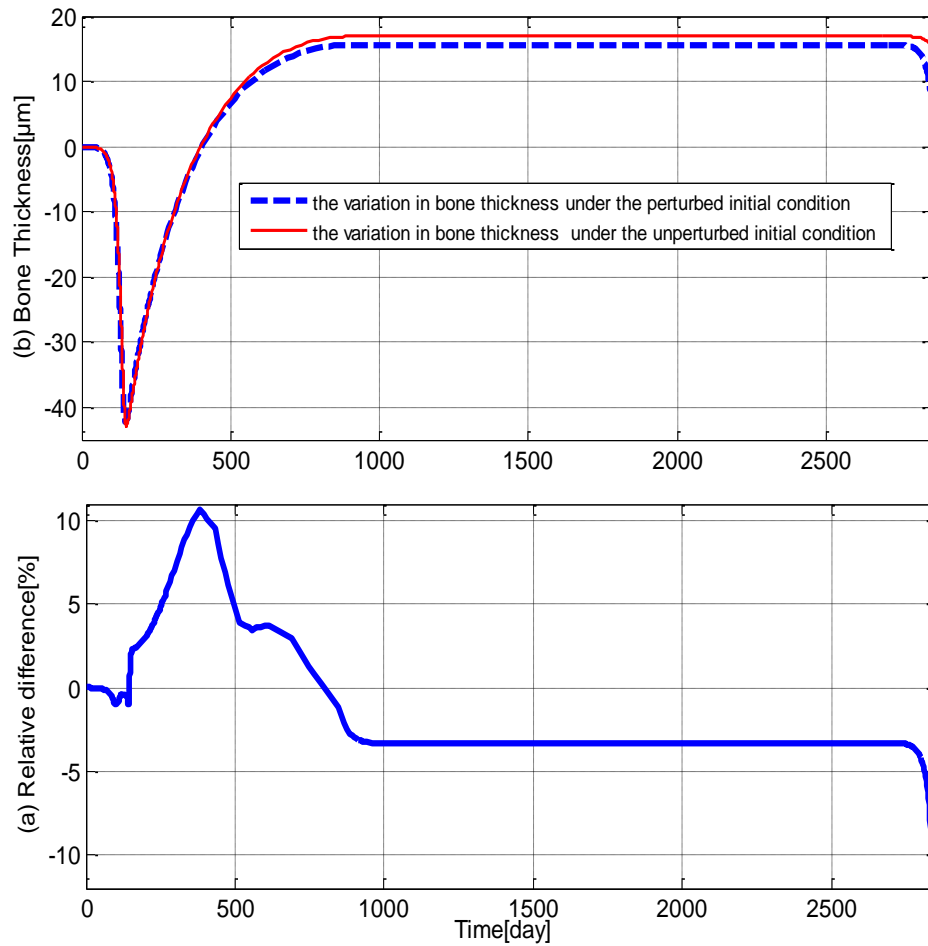


Figure 4.23: (a) Model predictions of the variations in bone thickness under the unperturbed and perturbed initial conditions, during the remodelling cycle with HT; (b) Difference between the variations in bone thickness produced by the unperturbed and perturbed initial conditions, during the remodelling cycle with HT.

4.4 MODEL PARAMETERS AND BIOCHEMICAL FACTORS

4.4.1 RELATING THE MODEL PARAMETERS TO BIOCHEMICAL FACTORS

The predator-prey based mathematical model shows significant potential to simulate the interaction between bone cells, and predict the resulting change of bone mass for the normal condition and two pathological conditions. The reconstructed bone remodelling cycles and the resultant bone volume were consistent with experimental data. The model was partially validated through comparing the model predictions for the osteoclast and osteoclast populations in a single BMU of normal bone remodelling, with experimental data. However, further data is required to validate the model predictions for the osteoclast and osteoblast populations in the cases of PHPT and HT. In order to understand the underlying mechanism of these two pathological conditions, and simulate potential therapies based on the proposed predator-prey based mathematical model, it is necessary to construct a connection between the model parameters and biochemical factors.

The RANK-RANKL-OPG pathway, together with the action of growth factors, constructs a basic control network of bone remodelling (Canalis, 1993; Manolagas, 2000). Disturbance of the RANKL:OPG ratio caused by local or systemic dysfunctions (Manolagas, 2000) may result in various bone diseases, including osteoporosis, Paget's disease, tumor metastasis, humoral hypercalcemia of malignancy and multiple myeloma (Boyle et al., 2003; Hofbauer et al., 2004; Hofbauer et al., 2001; Hofbauer and Schoppet, 2004; Rodan and Martin, 2000).

The sensitivity analysis of the model demonstrated that parameter ' a ' stimulates the differentiation of osteoclasts, which is similar to the behaviour of RANKL, while parameter ' b ' inhibits the differentiation of osteoclasts, which is similar to the behaviour of OPG. Based on these observations, it is assumed that model parameters ' a ' and ' b ' are related to RANKL and OPG respectively, with the $a:b$ ratio representing the RANKL: OPG ratio. It should be noted that the effects of RANKL and OPG are dependent on each other since OPG acts through the inhibition of the production of RANKL. However, they were represented as two independent parameters in the proposed mathematical model for simplicity, which highlights a limitation of the model.

In a normal bone remodelling cycle the equivalent amount of bone resorbed by osteoclasts is formed by osteoblasts. A coupling mechanism between osteoblasts and osteoclasts is responsible for this ideally zero bone balance in the normal bone remodelling cycle (Matsuo and Irie, 2008). Osteoclasts are able to liberate, secrete or produce coupling factors which act on osteoblast precursors to stimulate bone formation, and maintain the bone balance in remodelling cycles (Martin and Sims, 2005; Matsuo and Irie, 2008). For example, liberated coupling factors include TGF- β , bone morphogenetic proteins (BMPs) and insulin-like growth factor (IGF)-II, all of which are released by bone resorption from the bone matrix (Matsuo and Irie, 2008; Pfeilschifter and Mundy, 1987; Wozney et al., 1988). The defined variation of osteoblasts in Eq. (4-4) demonstrates that model parameters ' K_{oc} ' and ' d ' are both related with the coupling interaction between osteoclasts and osteoblasts. Therefore, the complex term ' $\frac{1}{K_{oc} \cdot d}$ ' is used here to represent the coefficient of the coupling mechanism. An increase in ' $\frac{1}{K_{oc} \cdot d}$ ' will represent an enhancement in the coupling between osteoblasts and osteoclasts, while a decrease will result in an impairment in the coupling.

Similarly, the bone formation rate defined in Eq. (4-6) includes the parameter ' K_{ob} ' which is negatively related to the bone formation rate. Thus, ' $\frac{1}{K_{ob}}$ ' is used to represent the osteoblastic activity, and an increase or decrease in this term indicates the promotion or suppression of osteoblastic activity, respectively.

The remaining model parameters (c, e and f) were defined as constants (the reasoning for this is discussed in section 4.3.3.2) to reduce the number of parameters required to be related with biochemical factors. As a result, the proposed connections between the model parameters and biochemical factors are summarized in Table 4.7.

Parameters	Biochemical Factors
a	RANKL
b	OPG
a/b	ratio of RANKL to OPG
$\frac{1}{K_{oc} \cdot d}$	coupling coefficient between osteoclasts and osteoblasts; represent the ratio of osteoblast to osteoclast
$\frac{1}{K_{ob}}$	osteoblast activity
c, e, f	constants

Table 4.7: Possible connections between the model parameters and biochemical factors involved in the bone remodelling process.

4.4.2 VALIDATION OF THE PROPOSED CONNECTIONS

To validate the proposed connections between the model parameters and biochemical factors, the values of the parameters listed in Table 4.7 were calculated under the normal condition, PHPT and HT (see Table 4.8). Since these parameters are connected with the biochemical factors (as shown in Table 4.7), the analysis of the values in Table 4.8 can determine the variation of these biochemical factors in the normal and pathological conditions. The proposed connections between model parameters and biochemical factors then can be validated by comparing model predictions with published observations involving biochemical factors.

As observed in Table 4.8, parameters ' a ' and ' b ' for HT were lower than those related to the normal condition, which indicates that the levels of RANKL and OPG are reduced (see Table 4.7). This partially agrees within the findings of Kanatani et al. (2004), who reported a decline in OPG in the case of HT, although no change in RANKL was observed. However, Miura et al. (2002) indicated that the RANKL level can decrease under this condition. As shown in Table 4.8, the model

predicted an increase in the levels of RANKL and OPG in PHPT compared to the normal condition. The prediction is confirmed in part by literature that has observed increased RANKL levels in patients with PHPT (Horwood et al., 1998a; Itoh et al., 2000; Lee and Lorenzo, 1999; Nakchbandi et al., 2008). Validation of the prediction of OPG levels requires further investigation, since the effect of PTH on the production of OPG remains controversial. Several *in vitro* studies indicated that OPG secretion is suppressed by PTH (Itoh et al., 2000; Lee and Lorenzo, 1999; Onyia et al., 2000), while *in vivo* experiments provided conflicting results (Nakchbandi et al., 2008; Stilgren et al., 2003).

The a:b ratio for HT was lower than that for the normal condition (7.43 compared to 8.58) (see Table 4.8), suggesting a decrease in the RANKL:OPG ratio and a resultant decline in osteoclast population, since RANKL simulates the differentiation and activation of osteoclasts (Aubin and Bonnellye, 2000; Burgess et al., 1999; Hofbauer et al., 2000), while OPG inhibits the differentiation and activation of osteoclasts (Filvaroff and Derynck, 1998; Greenfield et al., 1999; Gunther and Schinke, 2000). A tight coupling exists between osteoclasts and osteoblasts as the differentiation of osteoblast precursors is stimulated by osteoclasts (Matsuo and Irie, 2008), thus a decrease in osteoclast population will lead to the decline in osteoblast population. The model prediction that the populations of osteoclasts and osteoblasts decrease is confirmed by the work of Eriksen et al. (1986a). Eriksen et al. (1986a) reported that the decreased level of thyroid hormone in HT led to a decline in the populations of osteoclasts and osteoblasts, since thyroid hormone is a potent stimulator of osteoclasts and osteoblasts.

In addition, the a:b ratio for PHPT was higher than that for the normal condition (9.54 compared to 8.58) (see Table 4.8). Likewise, the increased a:b ratio leads to the increase in the populations of osteoclasts and osteoblasts, which is confirmed by observations that osteoclast and osteoblast populations increase in patients with PHPT (Chappard et al., 1996; Schulz et al., 1976; Singer and Eyre, 2008; Vera et al., 2011).

Table 4.8 indicates that ' $\frac{1}{K_{oc \cdot d}}$ ' in HT equated to 2.21×10^{-9} , which was higher than the value associated with the normal condition (4.14×10^{-10}). This suggests that the coupling coefficient between osteoblasts and osteoclasts for HT is more intensive compared to normal condition, causing the ratio of $OB_a:OC_a$ in HT to be higher. This agrees with the model predictions as the $OB_a:OC_a$ ratio is larger in HT compared to

the normal condition (232.7 and 217.4, respectively). As a result, the increased ratio of $OB_a:OC_a$ in HT will lead to a positive bone balance at the end of bone remodelling cycles, which is confirmed by the experimental observations of higher amount of bone formation compared to resorption within individuals with this condition (as shown in Table 4.5). In addition, ' $\frac{1}{K_{oc-d}}$ ' in PHPT was similar to that associated with the normal condition (3.83×10^{10} and 4.14×10^{10} , respectively) indicating that the coupling coefficient between osteoblasts and osteoclasts should be similar in both cases. Again, this is consistent with the predicted $OB_a:OC_a$ ratios for PHPT and the normal condition (219.8 and 217.4, respectively).

Finally, the term ' $\frac{1}{K_{ob}}$ ' is related to osteoblastic activity and its value in HT was lower than that corresponding to the normal condition (respective values of 1.03×10^{-5} and 2.31×10^{-5} are shown in Table 4.8), which indicates a decrease in osteoblastic activity in individuals with HT. This is consistent with experimental observations of the mean bone formation rate in HT (59 $\mu\text{m}/620$ day) being lower than that under normal condition (45.2 $\mu\text{m}/172$ day) (Ji et al., 2012). In addition, ' $\frac{1}{K_{ob}}$ ' in PHPT equalled to 1.56×10^{-5} , which was lower than that under the normal condition (2.31×10^{-5}), indicating a decrease in osteoclastic activity in PHPT compared to the normal condition. This was also confirmed by decreasing mean bone formation rate in PHPT (45.2 $\mu\text{m}/172$ day) compared to the normal condition (62 $\mu\text{m}/145$ day) (Ji et al., in press).

Parameters	HT	Normal	PHPT
a	0.0327 day ⁻¹	0.0558 day ⁻¹	0.1231 day ⁻¹
b	0.0044 cells ^{-1/2} day ⁻¹	0.0065 cells ^{-1/2} day ⁻¹	0.0129 cells ^{-1/2} day ⁻¹
a/b	7.43	8.58	9.54
K_{oc}	1.81 × 10 ¹¹ cells ²	2.44 × 10 ¹¹ cells ²	1.74 × 10 ¹¹ cells ²
d	0.0025 day ⁻¹	0.0099 day ⁻¹	0.0150 day ⁻¹
$\frac{1}{K_{oc} \cdot d}$	2.21 × 10 ⁻⁹	4.14 × 10 ⁻¹⁰	3.83 × 10 ⁻¹⁰
K_{ob}	9.64 × 10 ⁴ cells	4.32 × 10 ⁴ cells	6.42 × 10 ⁴ cells
$\frac{1}{K_{ob}}$	1.03 × 10 ⁻⁵	2.31 × 10 ⁻⁵	1.56 × 10 ⁻⁵

Table 4.8: Calculations of parameter values for normal and two pathological conditions, HT and PHPT.

4.5 DISCUSSION

Bone remodelling is most commonly considered at BMU level, which integrates the osteoclastic removal and osteoblastic formation processes. The sequence of activities that take place during remodelling occur over an extended timeframe, for example typically 200 days for normal remodelling (Eriksen et al., 1984b; Eriksen et al., 1984a) followed by a quiescent period of possibly 900 days (Eriksen et al., 1986b). In the ideal situation, the volume of bone removed and deposited should be the same, but whether this occurs in reality depends on many complex factors. In the simplest terms, it relies on the number of cells involved and the period and rate of the cellular resorption and formation processes. A change in any of these will lead to a variation in the remodelling outcome and a net loss or gain in bone volume.

The aim of the proposed mathematical model was to simulate the activity and interactions between the cells and thereby predict the resultant effect on the bone. A predator-prey based mathematical relationship was used to define the basic associations, although the gaps between bouts of activity are much longer than would normally be expected in predator-prey situations. In this first application of the model, the model parameters were initially established for normal (healthy) remodelling, with the resultant governing equations then used to confirm that the predicted cellular activity matched the primary histomorphometry data (as would be expected); but in addition, the pattern of the whole remodelling cycles are predicted. However, it should be noted that this primary data is limited and was collated from a number of different sources, therefore the values of the model parameters require cautious consideration. Also, there will be some inevitable statistical variation in the experimental data, the effect of which requires further investigation. In the future this variability could be included automatically in the solution phase of the model, to provide an envelope of bone remodelling behaviour.

The potential of the model to investigate the bone remodelling cycle and the effects of different pathological conditions was demonstrated by considering PHPT and HT. The natural histories of these two conditions are quite different (as shown in Table 4.5) (Eriksen et al., 1986a, 1986b), although the model enables reconstruction of the remodelling cycles, along with prediction of the complex temporal interaction between the osteoblasts and osteoclasts, and the resultant effect on bone thickness. In contrast to the 'normal' case, the number of cells involved in BMU remodelling in these two conditions is not reported within literature, but they can be predicted by simulation. Despite the fact that the two conditions are very different (for example, the formation periods and the predicted numbers of cells vary), it is interesting to note that the $OB_a:OC_a$ ratios were similar. Unfortunately, at the present time, there is no published data available to confirm these predictions.

The bone remodelling activity is initiated and regulated by molecular reactions and processes. In an attempt to examine the sensitivity of the simulation results to the model parameters and thereby identify possible relationships with biochemical factors, the effects of parameter variations on the remodelling process and results were examined (see Table 4.4).

Based on sensitivity studies and model equations, relationships were built between the model parameters and regulatory biochemical factors of bone

remodelling cycles. The predictions based on suggested connections between model parameters and biochemical factors were consistent with published experimental observations, thus validating the proposed connections.

Further work is required to validate the proposed model, but the predicted histomorphometric measures and remodelling cycles compare well with the sample input data. It was concluded that this shows that the model has merit and predictive potential, especially in the future modelling of pathological conditions and in the optimisation of their treatment.

In this chapter a predator-prey based model of the bone remodelling cycle has been described. However, the model does not consider the complex cellular interactions which are involved in the bone remodelling process. In the following Chapter 5, a second mathematical model is developed which includes these cellular interactions in both normal and chronic pathological (multiple myeloma) conditions.

5. MATHEMATICAL MODELLING OF THE PATHOLOGY OF MULTIPLE MYELOMA INDUCED BONE DISEASE

5.1 INTRODUCTION

Bone can prevent the invasion of the majority of cancer cells due to its special properties (Smith and Martin, 2011). However, multiple myeloma (MM) as well as breast and prostate cancers can develop and survive within the bone microenvironment, as their phenotypic properties are capable of changing the bone microenvironment in ways that favour growth and survival of the tumour cells. MM is the second most frequent haematological malignancy (Fowler et al., 2011) and can induce a destructive bone disease, which leads to bone removal, bone pain and pathological fractures. It is reported that 60% to 70% of individuals with MM experience either bone pain or fracture at the time of diagnosis, while 90% of patients develop bone lesions during the course of the disease (Heider et al., 2005; Nau and Lewis, 2008; Roodman, 2004). MM-induced bone disease is a major cause of morbidity for patients with MM. The American Cancer Society estimated there were approximately 20,000 patients diagnosed with MM within the United States in 2004, with 10,800 associated deaths (Jemal et al., 2004).

MM induces an increase in bone resorption and suppresses bone formation, resulting in a negative bone balance and osteolytic lesions that rarely heal (Matsumoto and Abe, 2011; Roodman, 2011). Histomorphometric studies have revealed that the increased resorption arises from enlarged resorption surfaces and deeper resorption depths at individual bone remodelling sites (Taube et al., 1992; Wittrant et al., 2004). In parallel, uncoupling between bone resorption and bone formation is also observed in MM patients (Calvani et al., 2004).

The interaction between MM cells and the bone microenvironment (MM-bone interaction) plays an important role in the development of MM-induced bone disease. It promotes tumour growth and survival, as well as the consequent bone destruction (Fowler et al., 2011). Recently, many biochemical factors have been implicated in the development of MM-induced bone disease, such as cytokines with osteoclast activating function (e.g. the receptor activator of nuclear factor kappa-B ligand) (Gittoes and Franklyn), macrophage colony stimulating factor (M-CSF),

interleukin-6 (IL-6) and IL-11, IL-1 β (Terpos and Dimopoulos, 2005)), which are produced or stimulated by MM-bone interaction and further stimulate osteoclast activation and proliferation. In turn, the growth of myeloma cells are stimulated by growth factors released from bone resorption (Wittrant et al., 2004), which include transforming growth factor-beta (TGF- β), bone morphogenetic proteins (BMP), heparin-binding fibroblast growth factors and insulin-like growth factor (Blum et al., 2004; Guise and Chirgwin, 2003). Such reciprocal interaction produces a 'vicious cycle' between MM cells and the bone microenvironment, stimulating both tumour development and bone destruction (Fowler et al., 2011; Wittrant et al., 2004).

Only two models have been developed previously to analyse the role of MM-bone interaction in the development of MM disease. Ayati et al. (2010) proposed a model to simulate the dynamics of normal bone remodelling and MM disease. However, this model did not include the specific molecular mechanisms involved in the development of MM-induced bone disease, and the model parameters were not based on biological evidence. Wang et al. (2011) constructed another model to mimic MM-bone interaction and identify the signalling mechanisms which are believed to drive the progression of MM disease. This model included IL-6 and signalling pathways involved in MM and bone marrow stromal cell (BMSC) adhesion. However, Wang et al. (2011) did not consider the MM induced inhibition of osteoblastic activity, despite the fact that the suppression of osteoblast activity and the enhancement of osteoclast activity play an equally important role in bone destruction and development of tumour cells in MM patients (Matsumoto and Abe, 2011; Terpos and Dimopoulos, 2005).

Suppression of osteoblast activity is caused by soluble factors produced by MM cells and MM-bone interaction, which prevent their precursors from differentiating into mature osteoblasts (Roodman, 2011). Reduction in osteoblast activity not only increases the ratio of RANKL to OPG, enhancing osteoclastogenesis and bone resorption, but also stimulates anti-apoptotic and growth factors for MM cells, which forms a positive feedback between osteoblast suppression and the growth of MM cells (Fowler et al., 2011; Roodman, 2011). Importantly, several treatments of MM disease target suppression of osteoblastic activity, such as Bortezomib related therapy (Roodman, 2011) and inhibition of TGF- β (Matsumoto and Abe, 2011).

A mathematical model is described in this chapter that simulates the development of tumour cells and MM-induced bone disease. It was developed in parallel with the recently published model of Wang et al. (2011), which in turn was based on the earlier work of Pivonka et al. (2008). However, unlike the model of Wang et al. (2011), this model includes the underlying mechanisms of osteoblast inhibition and its role in the development of MM-induced bone disease. The model can simulate the development of MM and the induced bone destruction, and explain why MM induced bone lesions rarely heal after the complete removal of MM cells, as well as simulate the effects of different treatment therapies.

5.2 DEVELOPMENT OF THE MODEL OF THE NORMAL BONE ENVIRONMENT

A basic mathematical model is discussed initially which simulates the variation of bone cell concentrations in the bone microenvironment, and the resultant change of bone volume with time under normal conditions. It is based on the work of Pivonka et al. (2008). The model also simulates how variations in OPG, RANKL and PTH level influence cell concentrations, bone volume and of $OB_a:OC_a$ ratio. This model is then extended to simulate the pathology of MM-induced bone disease, through the incorporation of the interaction between MM cells and the bone microenvironment.

5.2.1 BASIC STRUCTURE OF THE MODEL

The bone microenvironment consists of many different components including multiple cell types, matrix proteins and endothelial cells. This study only focuses on osteoclastic and osteoblastic lineages, since they are responsible for the resorption and formation of bone, respectively, and play an important role in bone remodelling cycles. The osteoblastic lineage communicates with the osteoclastic lineage within the basic multiple unit (BMU) by at least three ways: cell-to-cell contact, diffusible paracrine factors and cell-to-bone matrix interaction (Matsuo and Irie, 2008). Cell-to-cell contact comprises of intercellular interaction between membrane-bound ligands and receptors, and transportation of small water-soluble molecules through gap junctions between two cell types. Osteoclast-to-osteoblast communication through diffusible paracrine factors means that diffusible paracrine factors (such as growth factor, cytokines and other small molecules) secreted by one cell type act on the other via diffusion. Cell-to-bone matrix interaction represents the interaction between

growth factors released by osteoclasts during bone resorption, and cells in osteoclastic and osteoblastic lineages (Pfeilschifter and Mundy, 1987).

Bone remodelling cycles can be categorised into three stages of initiation, transition and termination of remodelling (Matsuo and Irie, 2008). The initiation phase is defined as the period when osteoblast precursors are recruited, osteoclasts are differentiated and activated, and bone resorption commences. During the transition phase, bone resorption is inhibited, osteoclasts undergo apoptosis, osteoblasts are recruited and differentiated, and bone resorption is reversed into bone formation. The termination of remodelling marks the formation of new bone and the start of the quiescent period.

Many cytokines, biochemical mechanisms and signalling pathways are involved in the remodelling cycle, however not all these factors were considered in this study for simplicity. The basic structure of the model under normal remodelling conditions is presented in Figure 3.4. Differentiation into active osteoclasts and osteoblasts from their progenitors involves several intermediate stages. A total of seven stages have been identified in the differentiation of osteoblasts from mesenchymal stem cells to osteocytes and bone lining cells (Aubin, 1998), while the osteoclast lineage develops from hematopoietic precursor cells through monocyte differentiation and fusion to osteoclast formation (Roodman, 1999; Teitelbaum, 2000). This study only considers four stages of osteoblastic differentiation (uncommitted progenitors; osteoblast precursors; active osteoblasts; and osteocytes, bone lining cells or apoptotic osteoblasts) and three stages of osteoclastic differentiation (osteoclast precursors; active osteoclasts; and apoptotic osteoclasts), similar to that of Pivonka et al. (2008).

During the initiation phase shown in Figure 3.4, RANKL secreted by osteoblast precursors is able to induce osteoclast differentiation through binding to RANK expressed on osteoclast precursors, while OPG is produced by active osteoblasts to inhibit the differentiation of osteoclasts via binding to RANKL (Boyce and Xing, 2008). Bone is a major reservoir of growth factors such as TGF- β and IGFs (Cohen, 1997; Roodman, 1999). Growth factors are released to the bone microenvironment by osteoclasts during bone resorption. The effect of TGF- β on the osteoblastic lineage is dependent on the stages of cell maturation (Erlebacher et al., 1998). TGF- β is able to promote differentiation from uncommitted progenitors (OBU) into osteoblast precursors (OBp), while suppressing osteoblast precursor

differentiation into active osteoblasts (OB_a) (Janssens et al., 2005). In addition, TGF- β influences the osteoclast lineage, and has been reported to promote the apoptosis of active osteoclasts (Fuller et al., 2000).

5.2.2 MODEL EQUATIONS

Based on the underlying mechanisms illustrated in Figure 3.4, three ordinary differential equations were proposed to represent the communication between osteoclastic and osteoblastic lineages. Although differentiation of progenitors into active osteoclasts and osteoblasts contains several intermediate stages, the model only considered four osteoblastic lineages and three osteoclastic lineages, contained three state variables: osteoblast precursors, active osteoblasts, and active osteoclasts. Again, based on the ideas of Pivonka et al. (2008), Eqs. (5-1) to (5-3) were defined to describe the temporal variation in osteoblastic precursors, active osteoblasts and active osteoclasts, respectively.

$$\frac{dOB_p}{dt} = D_{OB_u} \cdot \pi_{act,OB_u}^{TGF\beta} \cdot OB_u - D_{OB_p} \cdot \pi_{rep,OB_p}^{TGF\beta} \cdot OB_p \quad (5-1)$$

$$\frac{dOB_a}{dt} = D_{OB_p} \cdot \pi_{rep,OB_p}^{TGF\beta} \cdot OB_p - A_{OB_a} \cdot OB_a \quad (5-2)$$

$$\frac{dOC_a}{dt} = D_{OC_p} \cdot \pi_{act,OC_p}^{RANKL} \cdot OC_p - \pi_{act,OC_a}^{TGF\beta} \cdot A_{OC_a} \cdot OC_a \quad (5-3)$$

where,

- OB_p , OB_a and OC_a represent concentrations of osteoblast precursors, active osteoblasts, and active osteoclasts, respectively;
- $\frac{dOB_p}{dt}$, $\frac{dOB_a}{dt}$ and $\frac{dOC_a}{dt}$ denote the variations of OB_p , OB_a and OC_a , respectively;
- OB_u and OC_p are concentrations of uncommitted osteoblastic progenitors and osteoclastic precursors, respectively, with their values set as constants in the model due to their relatively large populations;
- D_{OB_u} , D_{OB_p} and D_{OC_p} represent the differentiation rates of uncommitted osteoblast progenitors, osteoblast precursors and osteoclast precursors, respectively;
- A_{OB_a} and A_{OC_a} are apoptosis rates of active osteoblasts and active osteoclasts, respectively; and
- π functions denote the stimulating or inhibiting functions of ligand to receptor binding.

As demonstrated in Figure 3.4, the communications between osteoclastic and osteoblastic lineages are performed through cell-to-cell contact and cell-to-bone matrix interaction, which are all related to various receptor-ligand interactions. These can promote or inhibit cell responses such as differentiation, proliferation, apoptosis and production of molecules. ‘Hill functions’ are used to represent the cellular interaction via the single ligand to receptor binding denoted by π functions (Pivonka et al., 2008), with Eqs. (5-4) and (5-5) describing the stimulating and inhibiting functions of the binding of the ligand-receptor. ‘L’ represents the concentration of the ligand; ‘ β ’ represents maximal expression level of the promoter and is assumed to equal 1 in the model following the work of Pivonka et al. (2008); ‘n’ is the coefficient which regulates the steepness of the function ‘ π ’ and is also assumed to equal 1 following the work of Pivonka et al. (2008); ‘ k_1 ’ and ‘ k_2 ’ represent the dissociation constant, respectively.

$$f(x) = \beta\pi_{act} = \frac{\beta(L)^n}{k_1+(L)^n} \quad (5-4)$$

$$f(x) = \beta\pi_{rep} = \frac{\beta}{1+(\frac{L}{k_2})^n} \quad (5-5)$$

The RANK-RANKL-OPG pathway plays an important role in the regulation of osteoclast activity, as osteoclastogenesis is stimulated by RANKL (via binding to RANK on the osteoclast progenitors) and inhibited by OPG (a soluble decoy receptor for RANKL) (Boyce and Xing, 2008). Growth factors (such as TGF- β) released during bone resorption can stimulate osteoblast recruitment, and migration and proliferation of osteoblast precursors (Bonewald and Dallas, 1994; Eriksen and Kassem, 1992; Mundy et al., 1996), while inhibiting the production of mature osteoblasts. Again similar to the modelling of Pivonka et al. (2008), $\pi_{act,OB_u}^{TGF\beta}$, $\pi_{rep,OB_p}^{TGF\beta}$, $\pi_{act,OC_a}^{TGF\beta}$ and π_{act,OC_p}^{RANKL} in Eqs. (5-1) to (5-3) represent the effect of TGF- β and RANKL on osteoclastic and osteoblastic lineages, respectively, where,

- $\pi_{act,OB_u}^{TGF\beta}$ represents the stimulation of uncommitted osteoblastic progenitors into osteoblastic precursors;
- $\pi_{rep,OB_p}^{TGF\beta}$ represents the inhibition of the differentiation of osteoblastic precursors into active osteoblasts;
- $\pi_{act,OC_a}^{TGF\beta}$ denotes that TGF- β is able to promote the apoptosis of active osteoclasts; and

- π_{act,OC_p}^{RANKL} denotes that RANKL produced by osteoblastic precursors stimulates the differentiation of osteoclastic precursors into active osteoclasts. This also includes OPG secreted by active osteoblasts inhibiting the differentiation osteoclastic precursors, by binding to RANK expressed on osteoclastic precursors.

According to the proposed forms of ‘Hill function’ in Eqs. (5-4) and (5-5), π functions involving TGF- β and RANKL were defined as follows:

$$\pi_{act,OB_u}^{TGF\beta} = \frac{TGF\beta}{K_{D1,TGF\beta} + TGF\beta} \quad (5-6)$$

$$\pi_{rep,OB_p}^{TGF\beta} = \frac{1}{1 + (TGF\beta / K_{D2,TGF\beta})} \quad (5-7)$$

$$\pi_{act,OC_a}^{TGF\beta} = \frac{TGF\beta}{K_{D3,TGF\beta} + TGF\beta} \quad (5-8)$$

$$\pi_{act,OC_p}^{RANKL} = \frac{RANKL}{K_{D,RANKL} + RANKL} \quad (5-9)$$

where,

- TGF β and RANKL represent the concentrations of TGF- β and RANKL, respectively; and
- The definitions and values of $K_{D1,TGF\beta}$, $K_{D2,TGF\beta}$, $K_{D3,TGF\beta}$ and $K_{D,RANKL}$ are included in Table 5.1.

In the model, parameters without corresponding experimental data, which are usually related with experimental data (*e.g.* D_{OB_u} and D_{OB_p} involve the experimental data of the population of OB_p), are estimated or calculated via the genetic algorithm as shown in Table 5.1. The estimation of values of model parameters is achieved through trying different values in a domain and then picking up the most fitting one with corresponding experimental data. Based on the estimated values, the remaining unknown model parameters are calculated according to relevant experimental data through the genetic algorithm following the same procedure discussed in Chapter 4. Although all the unknown model parameters could be calculated via the genetic algorithm, it would greatly increases the complexity and consuming time.

Parameters	Value	Description
D_{OB_u}	3.24e+2 /day (estimated)	Differentiation rate of osteoblast progenitors
D_{OB_p}	3.67e-1 /day (estimated)	Differentiation rate of osteoblast precursors
A_{OB_a}	3.00e-1 /day (Pivonka et al., 2008)	Rate of elimination of active osteoblasts
D_{OC_p}	1.73e-1 /day (estimated)	Differentiation rate of osteoclast precursors
A_{OC_a}	1.20 /day (estimated)	Rate of elimination of active osteoclasts
$K_{D1,TGF\beta}$	4.28e-4 pM (Pivonka et al., 2008)	Activation coefficient related to growth factors binding on OB_u
$K_{D2,TGF\beta}$	2.19e-4 pM (Pivonka et al., 2008)	Repression coefficient related to growth factors binding on OB_p
$K_{D3,TGF\beta}$	4.28e-4 pM (Pivonka et al., 2008)	Activation coefficient related to growth factors binding on OC_a
$K_{D1,PTH}$	2.09e+1 pM (calculation by GA)	Activation coefficient for RANKL production related to PTH binding
$K_{D2,PTH}$	2.21e-1 pM (calculation by GA)	Repression coefficient for OPG production related to PTH binding
$K_{D,RANKL}$	4.12e+1 pM (estimated)	Activation coefficient related to RANKL binding to RANK
α	1.00 pM/% (Pivonka et al., 2008)	TGF- β content stored in bone matrix
$\tilde{D}_{TGF\beta}$	2.00e+2 /day (Wakefield et al., 1990)	Rate of degradation of $TGF\beta$

Table 5.1: Definitions and values of model parameters used in the model
(GA = genetic algorithm).

β_{PTH}	9.74e+2 pM/day (Schmitt et al., 1998)	Rate of synthesis of systemic PTH
\tilde{D}_{PTH}	3.84e+2 /day (Schmitt et al., 1998)	Rate of degradation of PTH
β_{OPG}	5.02e+6 /day (estimated)	Minimum rate of production of OPG per active osteoblast
\tilde{D}_{OPG}	4.16 /day (Hideshima et al., 2007)	Rate of degradation of OPG
OPG_{max}	7.98e+2 pM (Terpos et al., 2003)	Maximum possible OPG concentration
β_{RANKL}	8.25e+5 /day (estimated)	Production rate of RANKL per cell
\tilde{D}_{RANKL}	4.16 /day (Fan et al., 2004)	Rate of degradation of RANKL
R^{RANKL}	3.00e+6 (Pivonka et al., 2008)	Maximum number of RANKL on the surface of each osteoblastic precursor
$K_{A,RANK}$	7.19e-2 /pM (Cheng et al., 2004)	Association rate constant for RANKL binding to RANK.
K_{res}	2.00e+2% /(pM*day) (Kuehl and Bergsagel, 2002)	Relative rate of bone resorption (normalized with respect to normal bone resorption)
K_{form}	3.32e+1% /(pM*day) (calculation by GA)	Relative rate of bone formation (normalized with respect to normal bone resorption)

Table 5.1(cont): Definitions and values of model parameters used in the model (GA = genetic algorithm).

In the work of Pivonka et al. (2008), the concentration of TGF- β is proposed as:

$$TGF\beta = \frac{\alpha \cdot K_{res} \cdot OC_a + S_{TGF\beta}}{\tilde{D}_{TGF\beta}} \quad (5-10)$$

where, the definitions and values of α , K_{res} , $S_{TGF\beta}$ and $\tilde{D}_{TGF\beta}$ in Eq. (5-10) are also included in Table 5.1.

Since the concentration of RANKL is regulated by OPG, the concentration of OPG is introduced first. Also, the production of OPG is down-regulated by PTH, and the concentration was therefore defined as:

$$OPG = \frac{P_{OPG,d} + \beta_{OPG} \cdot OB_a \cdot \pi_{rep,OB_a}^{PTH}}{\frac{\beta_{OPG} \cdot OB_a \cdot \pi_{rep,OB_a}^{PTH}}{OPG_{max}} + D_{OPG}} \quad (5-11)$$

where, π_{rep,OB_a}^{PTH} represents the repression of the differentiation of OB_a by PTH. The definitions and values of $P_{OPG,d}$, β_{OPG} , OPG_{max} and D_{OPG} in Eq. (5-11) are included in Table 5.1. The concentration of PTH and π_{rep,OB_a}^{PTH} used in Eq. (5-11) are defined as:

$$PTH = \frac{\beta_{PTH} + P_{PTH,d}(t)}{\tilde{D}_{PTH}} \quad (5-12)$$

$$\pi_{rep,OB_a}^{PTH} = \frac{1}{1 + PTH/K_{D3,PTH}} \quad (5-13)$$

where, the definitions and values of β_{PTH} , $P_{PTH,d}(t)$, \tilde{D}_{PTH} and $K_{D3,PTH}$ in Eqs.(5-12) and (5-13) are included in Table 5.1. The concentration of RANKL is proposed as:

$$RANKL = \frac{P_{RANKL,d} + \beta_{RANKL} \cdot OB_p}{(1 + K_{A,OPG} \cdot OPG + K_{A,RANK} \cdot RANK) \cdot \left(\frac{\beta_{RANKL}}{RANKL \cdot \pi_{act,RANKL}^{PTH}} + D_{RANKL} \right)} \quad (5-14)$$

where, $\pi_{act,RANKL}^{PTH}$ represents the PTH stimulation of the production of RANKL and its definition is given by:

$$\pi_{act,RANKL}^{PTH} = \frac{PTH}{K_{D1,PTH} + PTH} \quad (5-15)$$

The definitions and values of $P_{RANKL,d}$, β_{RANKL} , $K_{A,OPG}$, $K_{A,RANK}$, R^{RANKL} , D_{RANKL} and $K_{D1,PTH}$ in Eqs.(5-14) and (5-15) are included in Table 5.1.

The model is also able to describe the temporal variation of bone volume during bone remodelling cycles, through the following equation:

$$\frac{dBV}{dt} = -K_{res} \cdot OC_a + K_{form} \cdot OB_a \quad (5-16)$$

where, BV represents the normalized bone volume and the definitions and values of K_{res} and K_{form} in Eq. (5-16) are included in Table 5.1.

5.2.3 SIMULATION RESULTS AND DISCUSSION

The model of the normal bone microenvironment is able to reconstruct the concentrations of osteoblastic precursors, active osteoblasts and active osteoclasts, and also analyse how variations in OPG, RANKL and PTH influence cell concentrations, bone volume and the $OB_a:OC_a$ ratio.

Figure 5.1 presents the temporal variation in concentrations of OB_p , OB_a and OC_a in the normal bone microenvironment, and confirms that they remain constant with time. Figure 5.2 displays that bone volume also stays constant with time in the normal condition. These results agree with the conclusion that the bone microenvironment always remains in a dynamic steady-state, as do other biological

systems under physiological conditions without external stimuli (Lemaire et al., 2004; Zumsande et al., 2011).

Figures 5.3 to 5.5 reveal how the cell concentrations, bone volume and $OB_a:OC_a$ ratio vary when injecting 10 or 20 pM/day of OPG into the system. As demonstrated in Figure 5.3, an increase in the level of OPG leads to a rapid decline in OC_a and OB_p , followed by a relatively smaller decrease in OB_a , which agrees with the experimental observation that OPG suppresses the differentiation of OC_a and promotes the apoptosis of OC_a (Hofbauer et al., 2001). The injection of OPG at 10 or 20 pM/day causes the $OB_a:OC_a$ ratio to initially increase by 1.2% or 2.4%, but drops down to 0.4% or 0.7% (shown in Figure 5.5), which results in an increase of 1.7% or 3.7% in bone volume (shown in Figure 5.4). The rising level of OPG results in the increase in bone volume, which is confirmed by the observation of Simonet et al. (1997). The simulation results also indicate that the influence of the OPG injection on cell concentrations, bone volume and $OB_a:OC_a$ ratio is positively related to the injection rate (e.g. the rapid injection rate, 20pM/day, results in a larger drop in cell concentrations, and increase in bone volume and $OB_a:OC_a$ ratio, compared to that of 10pM/day).

Figures 5.6 to 5.8 demonstrate the effect of an external injection of RANKL at 5 or 10 pM/day on cell concentrations, bone volume and the $OB_a:OC_a$ ratio, respectively. The rising RANKL level causes an increase in OC_a and OB_p followed by a less pronounced increase in OB_a and the quicker injection rate produces a larger increase in cell concentrations (shown in Figure 5.6). The $OB_a:OC_a$ ratio undergoes an initial 0.4% or 0.7% decrease and then returns to a stable level, 99.7% or 99.9% of its initial value, due to the injection of RANKL at 5 or 10 pM/day (shown in Figure 5.8), resulting in an 0.6% or 1.4% decrease in bone volume (shown in Figure 5.7). These simulation results are consistent with the experimental findings (Filvaroff and Derynck, 1998; Manolagas, 2000).

Figures 5.9 and 5.11 show that how an increase in PTH level of 500 or 1000 pM/day induces variations in cell concentrations, bone volume and $OB_a:OC_a$ ratio, respectively. As shown in Figure 5.9, the increasing level of PTH induces an increase in concentrations of OB_p , OB_a and OC_a , and the rate of 1000 pM/day results in a bigger increase in cell concentrations compared to that of 500 pM/day. The $OB_a:OC_a$ ratio declines after the injection of PTH (shown in Figure 5.11), which results in a decrease in bone volume (shown in Figure 5.10). The proportionate decreases in

$OB_a:OC_a$ ratio and bone volume are both positively related to the injection rate. These simulation results agree with the experimental and clinical observations that PTH can induce an increase in the concentrations of OB_p , OB_a and OC_a , and a decrease in bone volume (Tam et al., 1982; Watson et al., 1999). It should be noted that Figure 5.3 to Figure 5.11 also demonstrate that the bone microenvironment is dynamically stable against small perturbations and is able to return to the stable state again after small perturbations, although there is a net change to the bone volume.

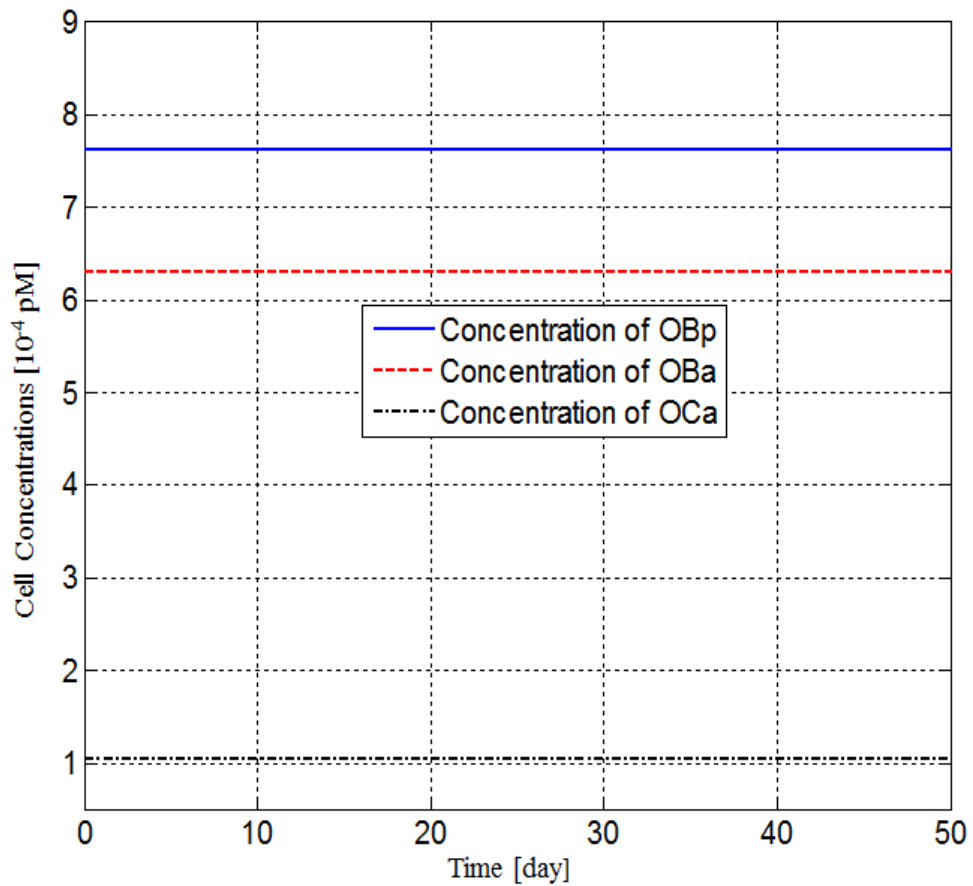


Figure 5.1: Model simulations of the variation in the concentrations of osteoblast precursors, active osteoblasts and active osteoclasts in the normal (healthy) condition.

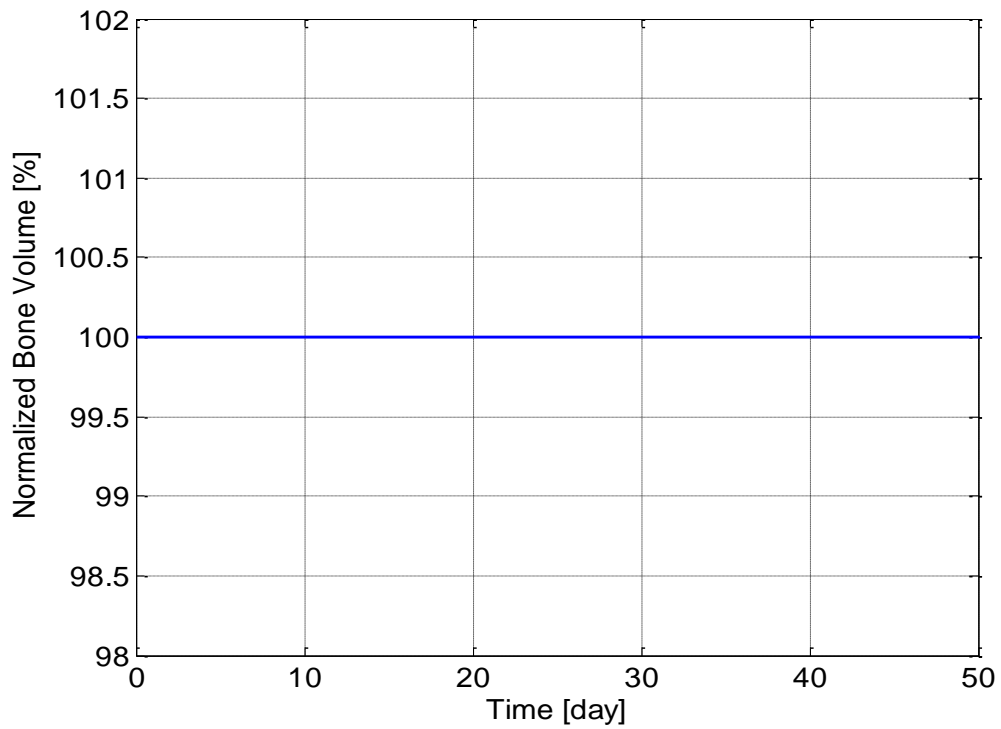


Figure 5.2: Model simulations of the variation in bone volume in the normal (healthy) condition.

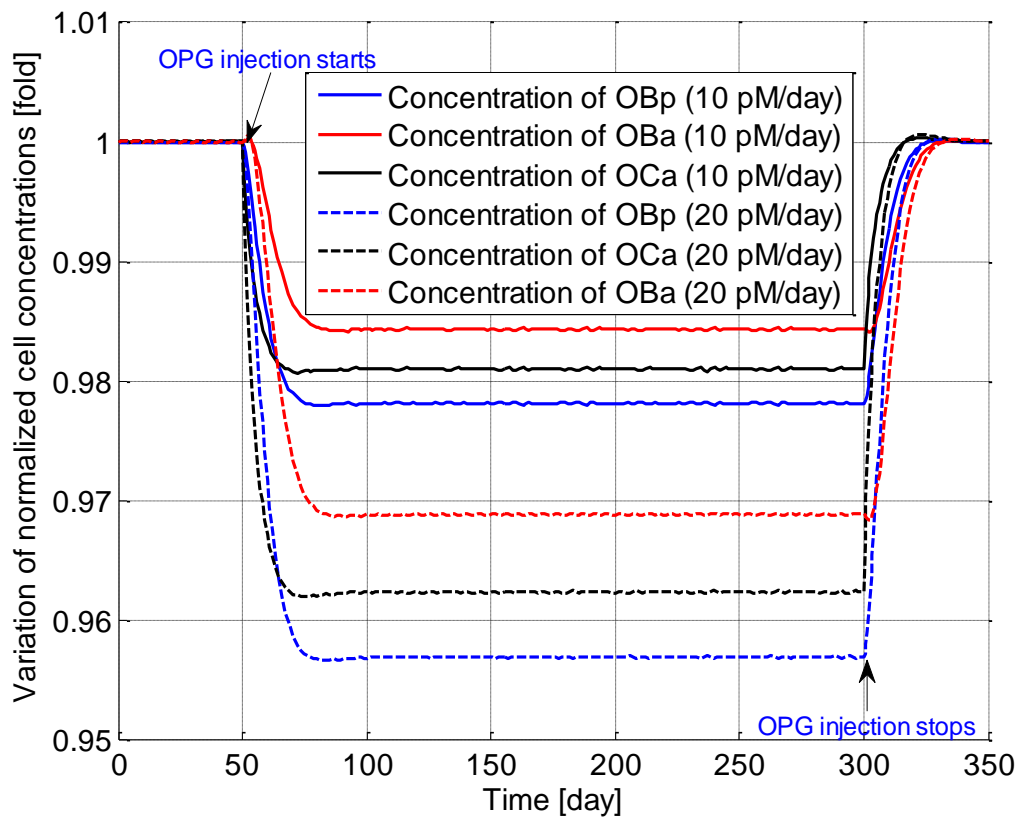


Figure 5.3: Model simulations of the variation in normalized cell concentrations with respect to its initial value after injection of OPG at the rate of 10 or 20 pM /day from day 50 to day 300.

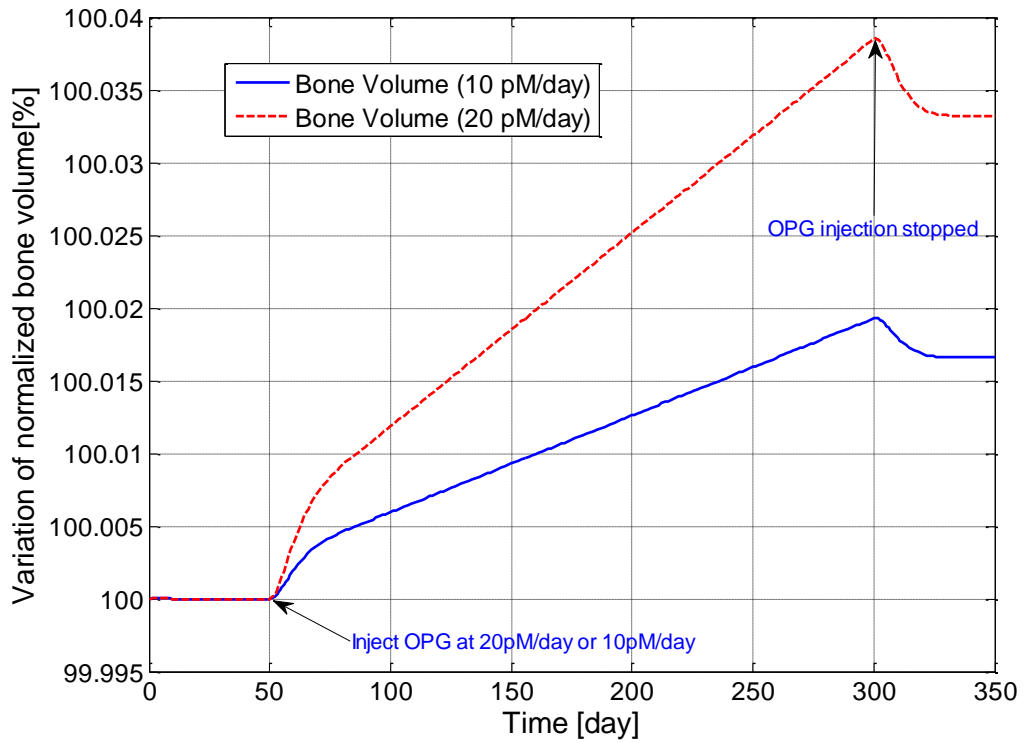


Figure 5.4: Model simulations of the variation in normalized bone volume with respect to its initial value after injection of OPG at the rate of 10 or 20 pM /day from day 50 to day 300.

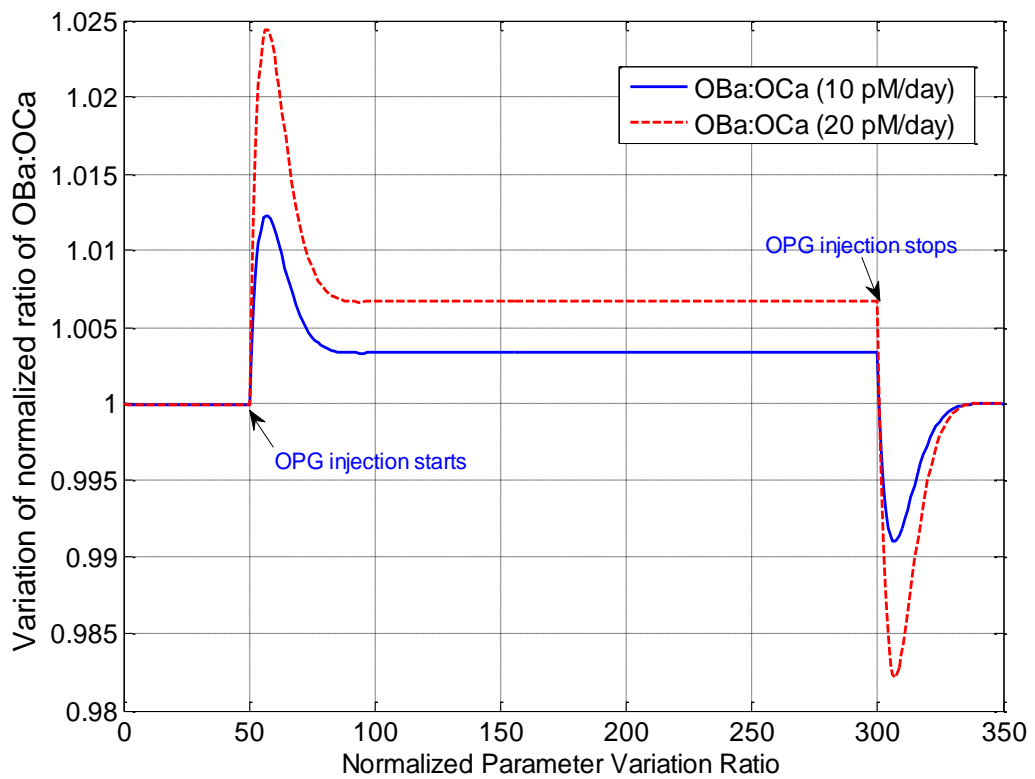


Figure 5.5: Model simulations of the variation in the normalized ratio of $OB_a:OC_a$ with respect to its initial value after injection of OPG at the rate of 10 or 20 pM /day from day 50 to day 300.

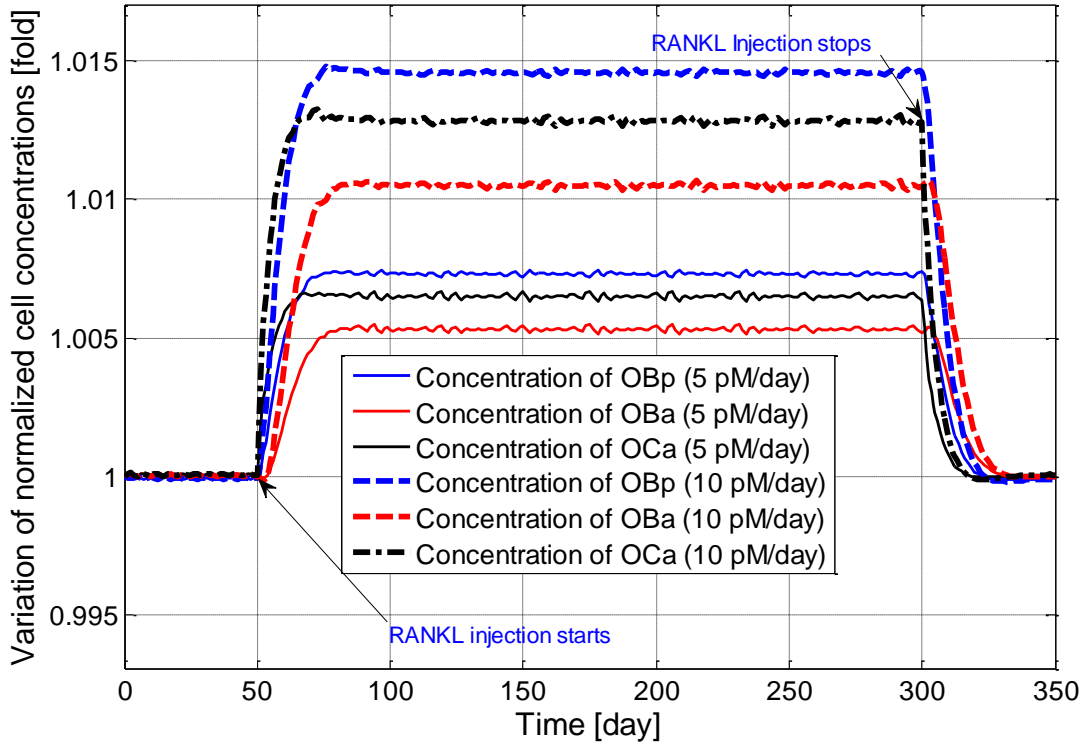


Figure 5.6: Model simulations of the variation in normalized cell concentration with respect to its initial value after injection of RANKL at the rate of 5 or 10 pM/day from day 50 to day 300.

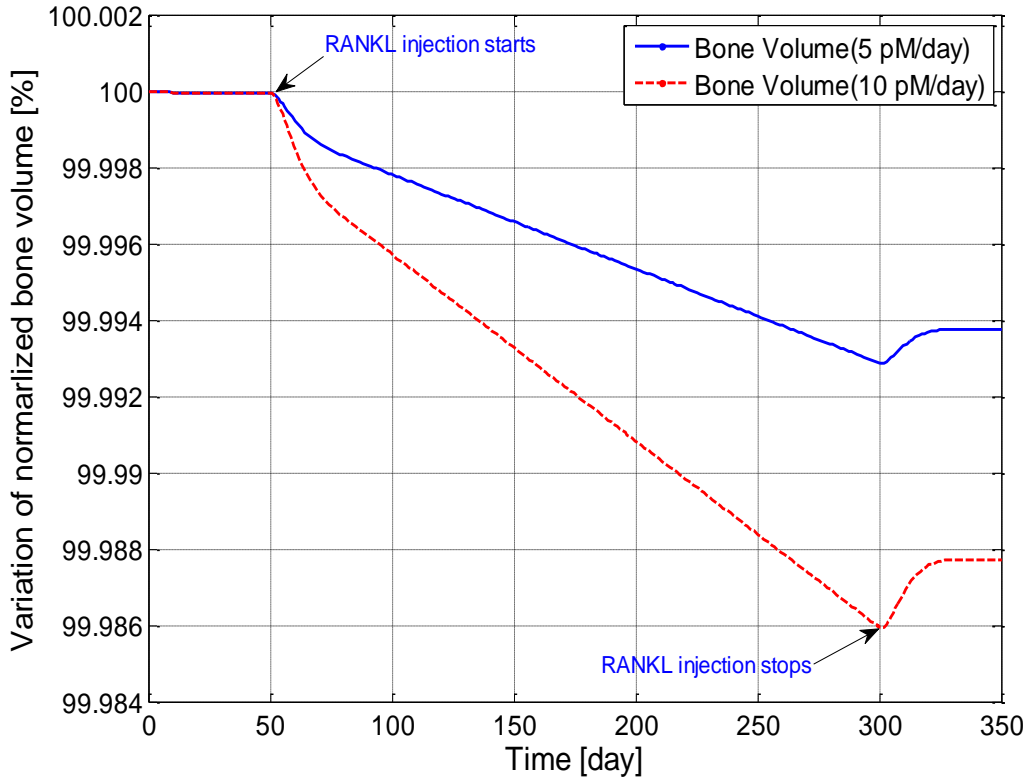


Figure 5.7: Model simulations of the variation in normalized bone volume with respect to its initial value after injection of RANKL at the rate of 5 or 10 pM/day from day 50 to day 300.

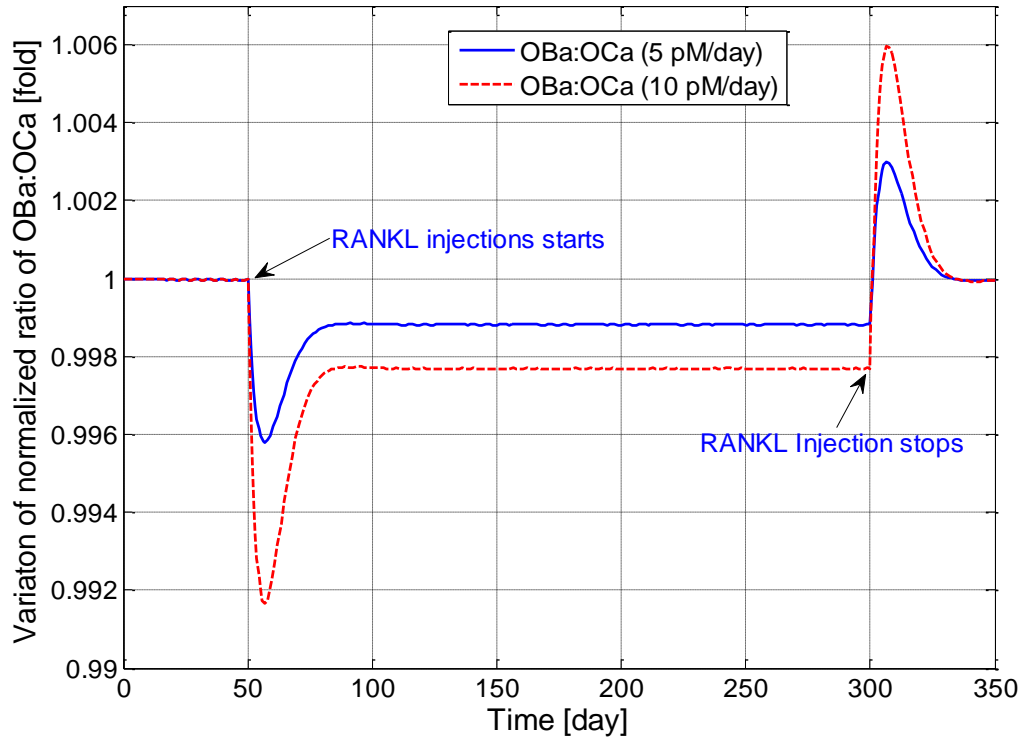


Figure 5.8: Model simulations of the variation in the normalized ratio of $OB_a:OC_a$ with respect to its initial value after injection of RANKL at the rate of 5 or 10 pM/day from day 50 to day 300.

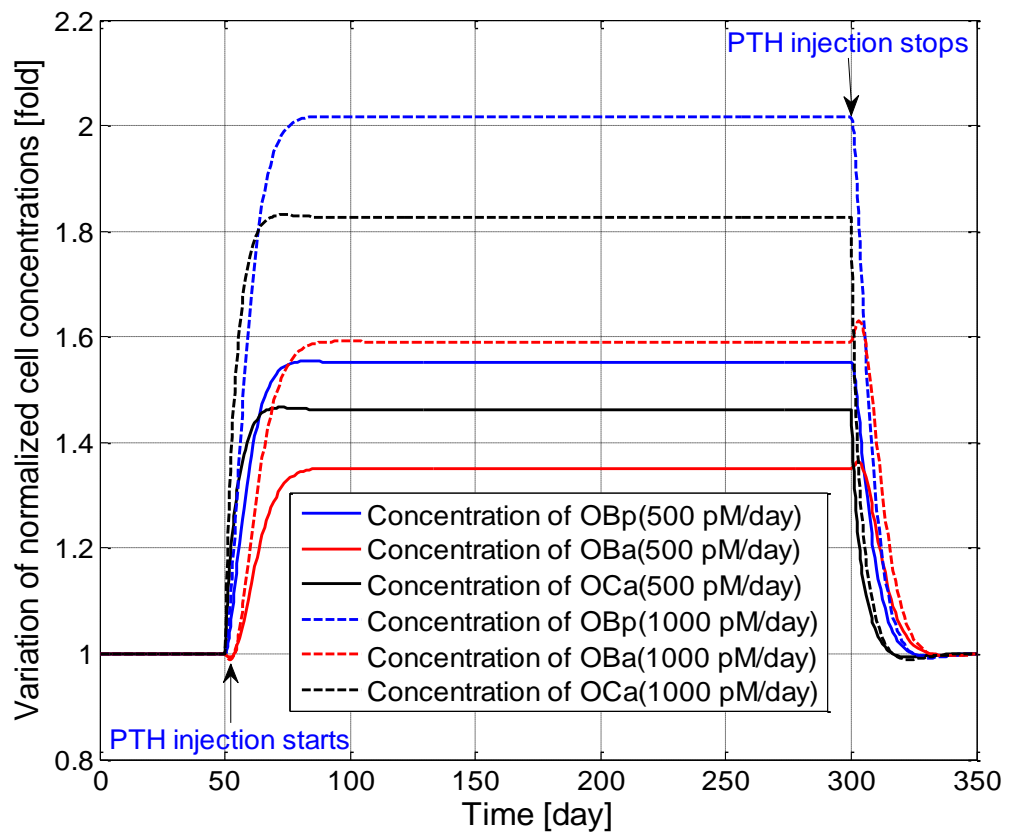


Figure 5.9: Model simulations of the variation in normalized cell concentrations with respect to its initial value after injection of PTH at the rate of 500 or 1000 pM/day from day 50 to day 300.

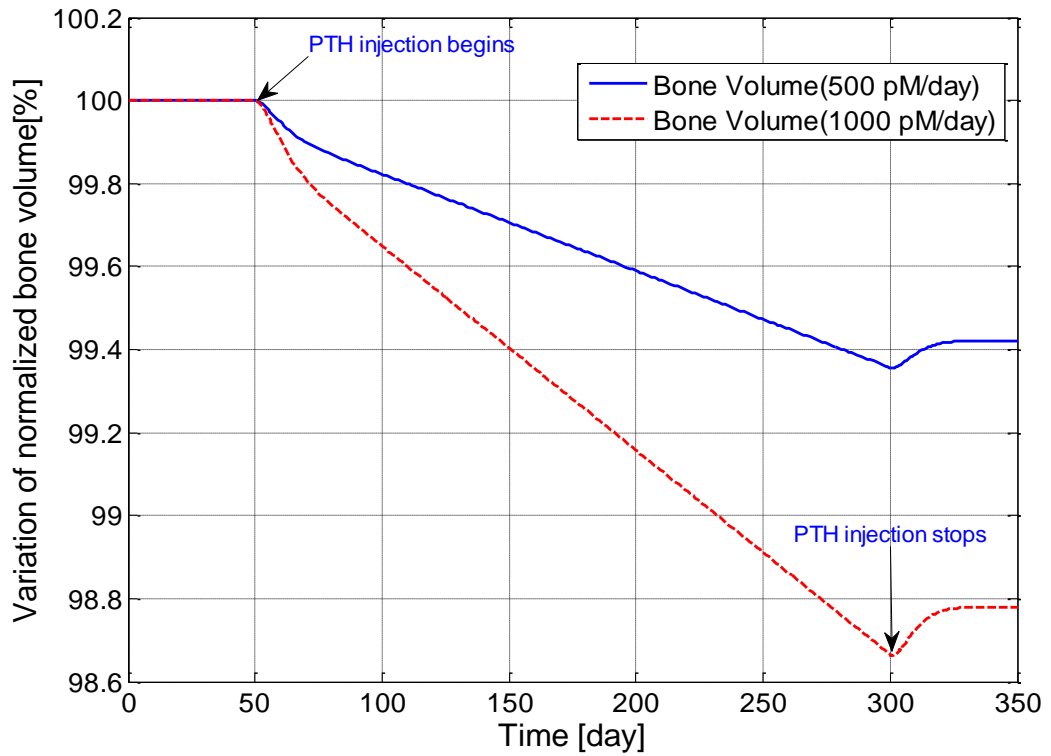


Figure 5.10: Model simulations of the variation in normalized bone volume with respect to its initial value after injection of PTH at the rate of 500 or 1000 pM/day from day 50 to day 300.

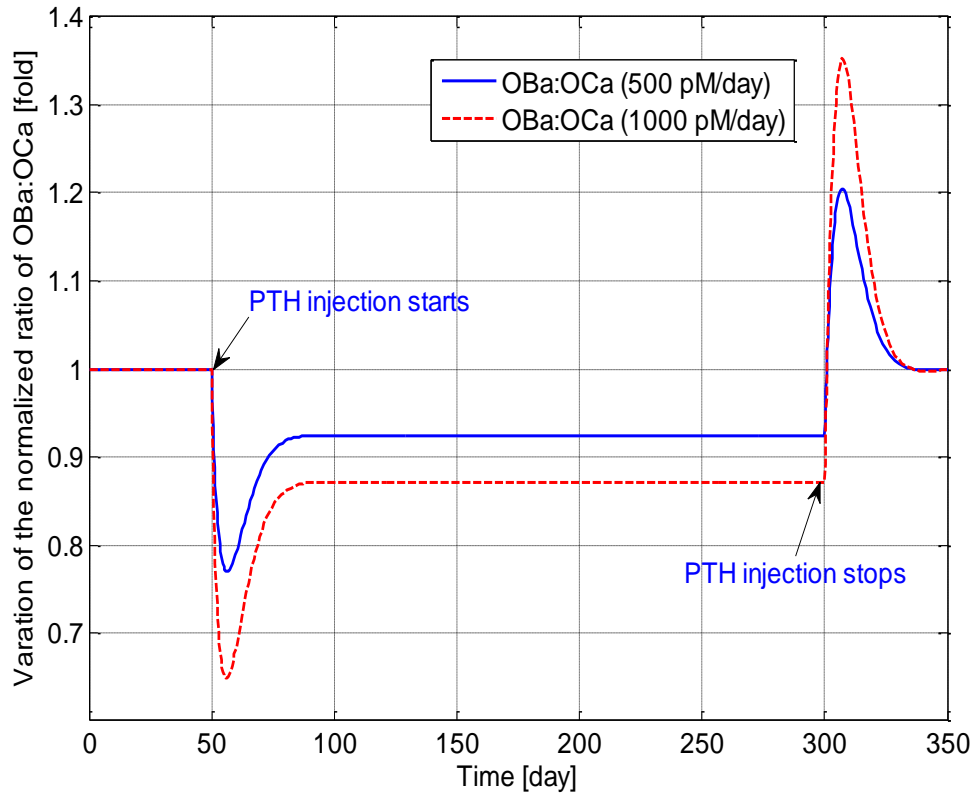


Figure 5.11: Model simulations of the variation in the normalized ratio of $OB_a:OC_a$ with respect to its initial value after injection of PTH at the rate of 500 or 1000 pM/day from day 50 to day 300.

5.3 DEVELOPMENT OF THE MODEL OF MULTIPLE MYELOMA-INDUCED BONE DISEASE

The model introduced in the previous section has been shown to simulate the normal state of the bone microenvironment by describing the variations in cell concentrations and bone volume with time. The following section now describes how the model was extended to simulate the development of MM cells and MM-induced bone disease.

5.3.1 BASIC STRUCTURE OF THE MODEL

The bone microenvironment consists of many different components including multiple cell types, matrix proteins and endothelial cells. The contribution of each of these components to the progress and survival of tumour cells is still not completely clear (Fowler et al., 2011; Roodman, 2011). However, it is certain that the suppression of osteoblast activity and enhancement of osteoclast activity, are both key factors in development of tumour cells and the bone destruction (Matsumoto and Abe, 2011; Terpos and Dimopoulos, 2005).

The basic structure of the model of MM-induced bone disease is shown in Figure 5.12. It demonstrates the ‘vicious cycle’ associated with MM disease, with the appearance of MM cells changing the bone microenvironment, resulting in osteolysis, which in turn promotes the proliferation of further MM cells (Wittrant et al., 2004). The model structure consists of two parts: part A (in blue) is associated with osteoclasts and the bone resorption aspects of the disease, while part B (in red) deals with osteoblasts and bone formation activities.

Part A describes how MM cells increase bone resorption, which in turn stimulates the further proliferation of MM cells. Two positive feedback cycles exist in part A. Firstly, IL-6 secreted by bone marrow stromal cell (BMSC) stimulates the production of RANKL (Kwan Tat et al., 2004), while MM cells suppress the production of OPG (Terpos and Dimopoulos, 2005). Consequently, the increased RANKL-OPG ratio promotes bone resorption (Terpos and Dimopoulos, 2005). In turn, TGF- β released from the bone resorption stimulates the secretion of IL-6 by BMSC (Hideshima et al., 2007; Teoh and Anderson, 1997), where the production of IL-6 can also be enhanced by the BMSC-MM cell adhesion (Urashima et al., 1996). Secondly, IL-6 and BMSC-MM cell adhesion promotes the proliferation of MM

cells, which in turn further stimulates further production of IL-6 and BMSC-MM cell adhesion (Hideshima et al., 2007; Klein et al., 1995; Urashima et al., 1996).

Part B describes the reciprocal relationship between the suppression of osteoblastic activity and the stimulation of MM cell production. Both BMSC-MM cell adhesion and soluble factors (produced or induced by MM cells) can block the differentiation of mesenchymal progenitors into mature osteoblasts, while at the same time stimulate osteoblast apoptosis, resulting in an inhibition of osteoblast activity and bone formation (Bataille et al., 1986, 1990, 1991; Calvani et al., 2004; Roodman, 2011). Conversely, preventing the differentiation into mature osteoblasts can stimulate MM cell production, since immature osteoblasts support growth and survival of MM cells; while mature osteoblasts enhance apoptosis of myeloma cells (Matsumoto and Abe, 2011). Therefore, in the underlying mechanism, IL-6 expressed by immature osteoblasts (mesenchymal stem cells) promotes MM cell growth and resistance to apoptosis (Stewart and Shaughnessy, 2006), while small leucine-rich proteoglycans (SLRPs) (such as decorin expressed and produced by mature osteoblasts) have an anti-myeloma effect (Li et al., 2008).

Part A and Part B also have direct connections with each other, *i.e.* the blockade of differentiation into mature osteoblasts contributes to an increase in the RANKL/OPG ratio, since immature osteoblasts produce RANKL, while mature osteoclasts produce OPG (labelled as arrow 5 in Figure 5.12) (Atkins et al., 2003). In addition, TGF- β released by bone resorption inhibits later phases of osteoblast differentiation and maturation (labelled as arrow 6 in Figure 5.12) (Matsumoto and Abe, 2011).

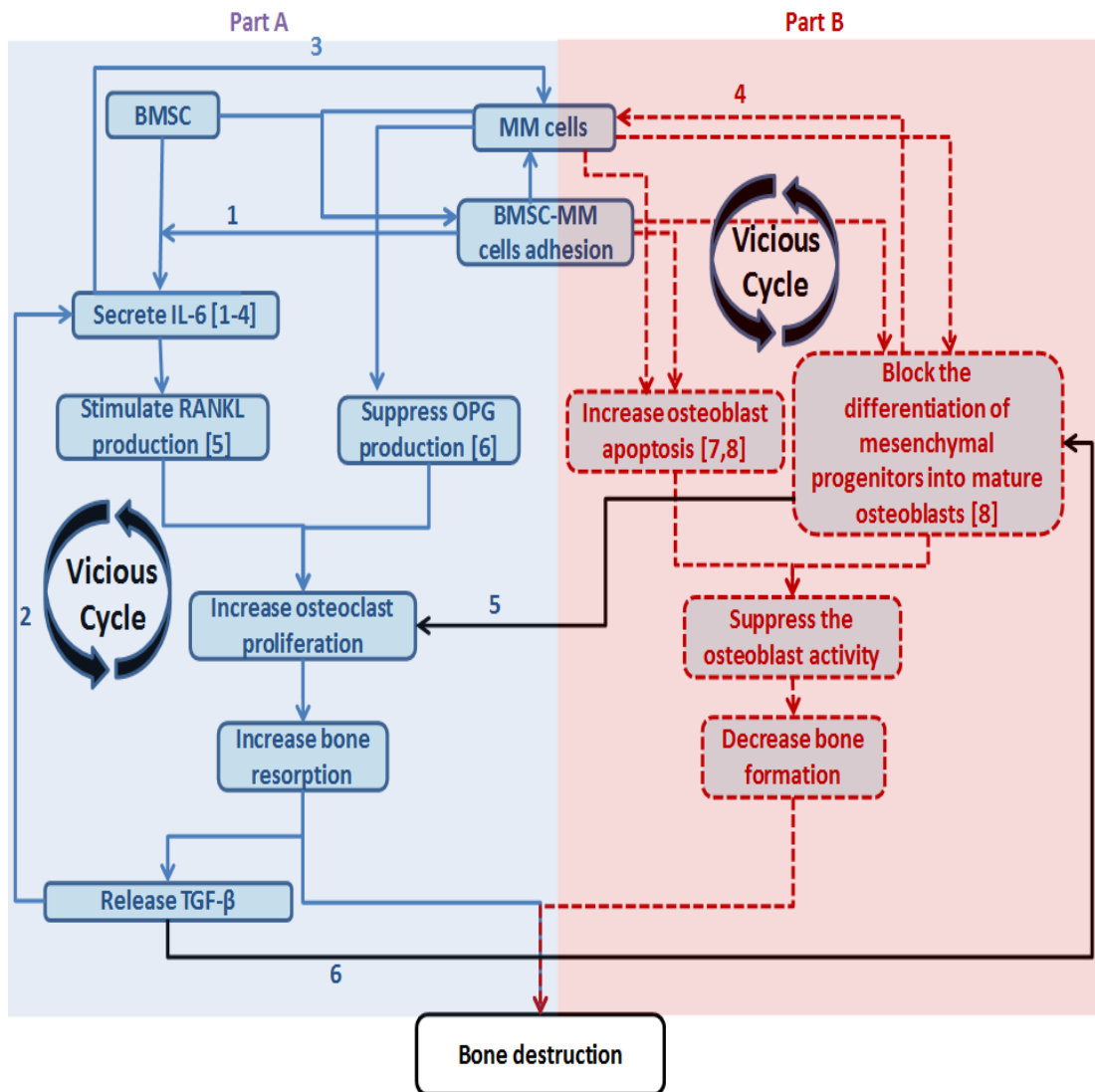


Figure 5.12: Proposed cellular interactions in MM development. (For references, see below).

1. BMSC-MM cells adhesion enhances the production of IL-6 by BMSCs (bone marrow stromal cells) [10]; 2. TGF- β stimulates the production of IL-6 [1,9]; 3. IL-6 stimulates the proliferation of MM cells [1,9,11]; 4. Immature osteoblasts support the growth and survival of MM cells, while mature osteoblasts enhance the apoptosis of MM cells; 5. the blockade of differentiation into mature osteoblasts contributes to the increase of the ratio of RANKL/OPG; and 6. TGF- β potentially inhibits later phases of osteoblast differentiation and maturation.

[1] Hideshima et al., 2007; [2] Lauterbach et al., 2001; [3] Bataille et al., 1992; [4] Chauhan et al., 1996; [5] Kwan et al., 2004; [6] Terpos and Dimopoulos, 2005; [7] Calvani et al., 2004; [8] Roodman, 2011; [9] Teoh and Anderson, 1997; [10] Urashima et al., 1996; [11] Klein et al., 1995.

5.3.2 MODEL EQUATIONS

The model equations are mathematical representations of the basic mechanisms and relationships shown in Figure 5.12. In addition to the four equations describing the normal temporal variations of bone cells and bone volume (detailed in Section 5.2), another equation was introduced to describe the temporal variation of MM cells. In the model of MM-induced bone disease, only three stages of MM cells (MM cell precursors, active MM cells and apoptotic MM cells) were considered.

The model subsequently contained four state variables: osteoblast precursors (OB_p), active osteoblasts (OB_a), active osteoclasts (OC_a) and active MM cells (MM). Using the same nomenclature as Section 5.2, the equations describing the dynamics of cell concentrations are as follows:

$$\frac{dOB_p}{dt} = D_{OB_u} \cdot \pi_{act,OB_u}^{TGF\beta} \cdot OB_u - D_{OB_p} \cdot \pi_{rep,OB_p}^{TGF\beta} \cdot \pi_{rep,OB_p}^{VCAM1} \cdot OB_p \quad (5-17)$$

$$\frac{dOB_a}{dt} = D_{OB_p} \cdot \pi_{rep,OB_p}^{TGF\beta} \cdot \pi_{rep,OB_p}^{VCAM1} \cdot OB_p - A_{OB_a} \cdot \pi_{act,OB_a}^{VCAM1} \cdot OB_a \quad (5-18)$$

$$\frac{dOC_a}{dt} = D_{OC_p} \cdot \pi_{act,OC_p}^{RANKL} \cdot OC_p - \pi_{act,OC_a}^{TGF\beta} \cdot A_{OC_a} \cdot OC_a \quad (5-19)$$

$$\frac{dMM}{dt} = D_{MM} \cdot \pi_{act,MM}^{IL6} \cdot \pi_{act,MM}^{VCAM1} \cdot MM \cdot \left(1 - \frac{MM}{MM_{max}}\right) - A_{MM} \cdot \pi_{rep,MM}^{SLRPs} \cdot MM \quad (5-20)$$

The definitions of some variables, functions and parameters have been described previously in section 5.2.2, but also:

- MM represents the concentration of MM cells;
- $\frac{dMM}{dt}$ is the variation of MM with time;
- D_{MM} represents the differentiation rates of the MM cell precursors;
- A_{MM} is the apoptosis rate of active MM cells;
- MM_{max} is the maximum concentration of MM cells;
- D_{MM} represents the proliferation of MM cells regulated by IL-6 and BMSC-MM cell adhesion; and
- π functions denote the stimulating or inhibiting functions of ligand to receptor binding.

The production of MM cells is regulated by several soluble factors, such as IL-6, insulin-like growth factor 1 (IGF-1), vascular endothelial growth factor (VEGF) and macrophage inflammatory protein-1 ($MIP-1\alpha$) (Fowler et al., 2011; Terpos and Dimopoulos, 2005; Wittrant et al., 2004).

The model of MM-induced bone disease includes four additional Hill functions: $\pi_{act,MM}^{IL6}$, $\pi_{act,MM}^{VCAM1}$, π_{rep,OB_p}^{VCAM1} and π_{act,OB_a}^{VCAM1} , where,

- $\pi_{act,MM}^{IL6}$ represents IL-6 regulation of the proliferation of MM cells. MM-bone interaction is carried out through the binding of a cell adhesion molecule (CAMs), such as VLA-4 ($\alpha4\beta1$ integrin present on the surface of MM cells), to a vascular cell adhesion molecule-1 (VCAM-1), which is expressed on BMSC (Terpos and Dimopoulos, 2005);
- $\pi_{act,MM}^{VCAM1}$ represents the effect of MM-BMSC on the proliferation of MM cells;
- π_{rep,OB_p}^{VCAM1} represents BMSC-MM cell adhesion that blocks the differentiation of mature osteoblasts from their progenitors;
- π_{act,OB_a}^{VCAM1} represents BMSC-MM cell adhesion stimulating the apoptosis of osteoblasts; and
- $\pi_{rep,MM}^{SLRPs}$ represents small leucine-rich proteoglycans (SLRPs) produced by mature osteoblasts suppressing the proliferation of MM cells (Roodman, 2011).

The definitions of these π functions are as follows:

$$\pi_{act,MM}^{IL6} = \frac{IL6}{IL6 + K_{D,IL6,MM,act}} \quad (5-21)$$

$$\pi_{act,MM}^{VCAM1} = \frac{VCAM1}{VCAM1 + K_{D,VCAM1,MM,act}} \quad (5-22)$$

$$\pi_{rep,OB_p}^{VCAM1} = \frac{1}{1 + VCAM1/K_{D,VCAM1,OB_p,rep}} \quad (5-23)$$

$$\pi_{act,OB_a}^{VCAM1} = \frac{VCAM1}{VCAM1 + K_{D,VCAM1,OB_a,act}} \quad (5-24)$$

$$\pi_{rep,MM}^{SLRPs} = \frac{1}{1 + (SLRPs/K_{D,SLRPs,MM,rep})} \quad (5-25)$$

where, $IL6$, $VCAM1$ and $SLRPs$ represent the concentrations of $IL6$, $VCAM1$ and $SLRPs$, respectively. The definitions and values of $K_{D,IL6,MM,act}$, $K_{D,VCAM1,MM,act}$, $K_{D,VCAM1,OB_p,rep}$, $K_{D,VCAM1,OB_a,act}$ and $K_{D,SLRPs,MM,rep}$ are included in Table 5.2.

Parameters	Value	Description
D_{OB_u}	3.24e+2/day (estimated)	Differentiation rate of osteoblast progenitors
D_{OB_p}	3.67e-1/day (estimated)	Differentiation rate of osteoblast precursors
A_{OB_a}	3.00e-1 /day (Pivonka et al., 2008)	Rate of elimination of active osteoblasts
D_{OC_p}	1.73e-1/day (estimated)	Differentiation rate of osteoclast precursors
A_{OC_a}	1.20 /day (Pivonka et al., 2008)	Rate of elimination of active osteoclasts
$K_{D1,TGF\beta}$	4.28e-4 pM (calculation by genetic algorithm (GA))	Activation coefficient related to growth factors binding on OB_u
$K_{D2,TGF\beta}$	2.19e-4 pM (Pivonka et al., 2008)	Repression coefficient related to growth factors binding on OB_p
$K_{D3,TGF\beta}$	4.28e-4 pM (Pivonka et al., 2008)	Activation coefficient related to growth factors binding on OC_a
$K_{D1,PTH}$	2.09e+1 pM (calculation by GA)	Activation coefficient for RANKL production related to PTH binding
$K_{D2,PTH}$	2.21e-1 pM (Pivonka et al., 2008)	Repression coefficient for OPG production related to PTH binding
$K_{D,TGF\beta,IL6,act}$	1.2e-4 pM (calculation by GA)	Half-maximal concentration of $TGF\beta$ on promoting the production of IL-6
$K_{D,IL6,RANKL,act}$	0.2 pM (calculation by GA)	Half-maximal concentration of IL6 on promoting the production of RANKL
$K_{D,RANKL}$	4.12e+1 pM (estimated)	Activation coefficient related to RANKL binding to RANK
α	1.00 pM/% (Pivonka et al., 2008)	TGF- β content stored in bone matrix

Table 5.2: Definitions and values of model parameters used in the model of MM-induced bone disease. (GA = genetic algorithm).

$\tilde{D}_{TGF\beta}$	2.00e+2 /day (Wakefield et al., 1990)	Rate of degradation of $TGF\beta$
β_{PTH}	9.74e+2 pM/day (Schmitt et al., 1998)	Rate of synthesis of systemic PTH
\tilde{D}_{PTH}	3.84e+2 /day (Schmitt et al., 1998)	Rate of degradation of PTH
β_{IL6}	1.20e+7/day (Klein et al., 1995; Wong et al., 2003)	Rate of synthesis of IL6 per cell
D_{IL6}	4.99e+1/day (van Zaanen et al., 1996)	The degradation rate of IL6
$IL6_{max}$	8.04e-1pM (Alexandrakis et al., 2003)	The maximum concentration of IL-6
β_{OPG}	5.02e+6/day (estimated)	Minimum rate of production of OPG per active osteoblast
\tilde{D}_{OPG}	4.16/day (Hideshima et al., 2007)	Rate of degradation of OPG
OPG_{max}	7.98e+2pM (Terpos et al., 2003)	Maximum possible OPG concentration
β_{RANKL}	8.25e+5/day (estimated)	Production rate of RANKL per cell
\tilde{D}_{RANKL}	4.16/day (Fan et al., 2004)	Rate of degradation of RANKL
R^{RANKL}	3.00e+6 (Pivonka et al., 2008)	Maximum number of RANKL on the surface of each osteoblastic precursor
RANK	1.28e+1pM (Pivonka et al., 2008)	Fixed concentration of RANK
$K_{A,OPG}$	5.68e-2/pM (Cheng et al., 2004)	Association rate constant for RANKL binding to OPG.
$K_{A,RANK}$	7.19e-2/pM (Cheng et al., 2004)	Association rate constant for RANKL binding to RANK.
K_{res}	2.00e+2%/(pM.day) (Kuehl and Bergsagel, 2002)	Relative rate of bone resorption (normalized with respect to normal bone resorption)

Table 5.2 (cont): Definitions and values of model parameters used in the model of MM-induced bone disease. (GA = genetic algorithm).

K_{form}	3.32e+1%/(pM.day) (calculation by GA)	Relative rate of bone formation (normalized with respect to normal bone resorption)
D_{MM}	5.50e-2/day (estimated)	MM proliferation controlled by IL-6 and BMSC-MM adhesion
A_{MM}	2.00e-3/day (Wols et al., 2002)	Rate of elimination of active MM cells
MM_{max}	1.98 pM (Salmon and Smith, 1970)	Maximum possible MM concentration
$K_{D,VCAM1,MM,act}$	1.5667e-4 /pM (calculation by GA)	Half-maximal concentration of <i>VLA</i> – 4 on promoting the MM cells production
$K_{D,VLA4,IL6,act}$	1.88e+4/pM (calculation by GA)	Half-maximal concentration of <i>VLA</i> – 4 on promoting the IL-6 production
$K_{D,IL6,MM,act}$	1.2151e-5 pM (calculation by GA)	Half-maximal concentration of <i>IL</i> – 6 on promoting the MM cells production
$K_{D,SLRPs,MM,rep}$	1.306e+9 pM (calculation by GA)	Half-maximal concentration of <i>SLRPs</i> on promoting the MM cells production
$K_{D,VCAM1,OB_p,rep}$	1.4e-1pM (calculation by GA)	Half-maximal concentration of <i>VCAM1</i> on repressing the differentiation of <i>OB_p</i>
$K_{D,VCAM1,OB_a,act}$	2.2e-1pM (calculation by GA)	Half-maximal concentration of <i>VCAM1</i> on promoting the apoptosis of <i>OB_a</i>
β_{VLA4}	2.04e+6/day (estimated)	Rate of synthesis of <i>VLA4</i> per cell
\tilde{D}_{VLA4}	1.5/day (estimated)	Rate of degradation of <i>VLA4</i>
R^{VLA4}	5.6e+4 (Zwartz et al., 2004)	Maximum number of <i>VLA4</i> expressed on the surface of MM cells

Table 5.2 (cont): Definitions and values of model parameters used in the model of MM-induced bone disease. (GA = genetic algorithm).

$VCAM1_{tot}$	1.92pM (Zwartz et al., 2004)	Total concentration of VCAM-1
$K_{A,VCAM1}$	8.3e-2/pM (Chigaev et al., 2001)	The association rate for VLA-4 binding to VCAM-1.
$D_{OPG,MM}$	4.16/(pM.day) (estimated)	The degradation rate of OPG by MM cells

Table 5.2 (cont): Definitions and values of model parameters used in the model of MM-induced bone disease. (GA = genetic algorithm).

The concentrations of $IL6$, $VCAM1$ and $SLRPs$ are proposed as follows:

$$IL6 = \frac{P_{IL6,d} + \beta_{IL6} \cdot OB_u \cdot \pi_{act,IL6}^{TGF} \cdot \pi_{act,IL6}^{VLA4}}{\frac{\beta_{IL6} \cdot OB_u \cdot \pi_{act,IL6}^{TGF} \cdot \pi_{act,IL6}^{VLA4}}{IL6_{max}} + D_{IL6}} \quad (5-26)$$

$$VCAM1 = \frac{VCAM1_{tot}}{1 + K_{A,VCAM1} \cdot VLA4} \quad (5-27)$$

$$SLRPs = \frac{\beta_{SLRPs} \cdot OB_a + P_{SLRPs,d}(t)}{\frac{\beta_{SLRPs} \cdot OB_a}{SLRPs_{max}} + \bar{D}_{SLRPs}} \quad (5-28)$$

where,

- $\pi_{act,IL6}^{TGF\beta}$ denotes that $TGF\beta$ stimulates the production of IL-6 and $\pi_{act,IL6}^{TGF\beta} = \frac{TGF\beta}{TGF\beta + K_{D,TGF\beta,IL6,act}}$;
- $\pi_{act,IL6}^{VLA4}$ denotes that BMSC-MM cells adhesion enhances the production of IL-6 by BMSCs and $\pi_{act,IL6}^{VLA4} = \frac{VLA4}{VLA4 + K_{D,VLA4,IL6,act}}$; and
- The definitions and values of the parameters in Eqs. (5-26) to (5-28) are included in Table 5.2.

Soluble factors produced by MM cells also suppress osteoblast differentiation via inhibiting Wnt signalling pathway (Matsumoto and Abe, 2011; Roodman, 2011), but were not considered in the model since the underlying mechanisms are not fully understood (Edwards et al., 2008; Yeh and Berenson, 2006). However, it is believed that the effect of these soluble factors is relatively minor compared to that of BMSC-MM cell adhesion. The MM model describes the variation of bone volume through the same method detailed in Section 5.2 as follows:

$$\frac{dBV}{dt} = -K_{res} \cdot OC_a + K_{form} \cdot OB_a \quad (5-29)$$

where, BV represents the normalized bone volume and the definitions and values of K_{res} and K_{form} in Eq. (5-29) are included in Table 5.2.

Note, in this model of MM-induced bone disease, the secretion of OPG by active osteoblasts is regulated by MM cells, while the production of RANKL by osteoblast precursors is regulated by MM-BMSC interaction. Thus, the definition of OPG and RANKL concentrations in the model of MM-induced bone disease must be updated as follows:

$$OPG = \frac{P_{OPG,d} + \beta_{OPG} \cdot OB_a \cdot \pi_{rep,OB_a}^{PTH}}{\frac{\beta_{OPG} \cdot OB_a \cdot \pi_{rep,OB_a}^{PTH}}{OPG_{max}} + D_{OPG} + D_{OPG,MM} \cdot MM} \quad (5-30)$$

$$RANKL = \frac{P_{RANKL,d} + \beta_{RANKL} \cdot OB_p}{(1 + K_{A,OPG} \cdot OPG + K_{A,RANK} \cdot RANK) \cdot \left(\frac{\beta_{RANKL}}{R_{RANKL} \cdot \pi_{act,RANKL}^{IL6} \cdot \pi_{act,RANKL}^{PTH}} + D_{RANKL} \right)} \quad (5-31)$$

where, $\pi_{act,RANKL}^{IL6}$ denotes that *IL6* stimulates the production of RANKL and $\pi_{act,RANKL}^{IL6} = \frac{IL6}{IL6 + K_{D,IL6,RANKL,act}}$. The definitions of π_{rep,OB_a}^{PTH} and π_{rep,OB_a}^{PTH} have been defined before. The definitions and values of parameters in Eqs. (5-30) and (5-31) are included in Table 5.2.

5.3.3 SIMULATION RESULTS

As in the normal condition, the bone microenvironment should remain in a dynamical steady-state, as do other biological systems under physiological conditions without external stimuli, and able to return to the steady-state after perturbations are removed (Lemaire et al., 2004; Zumsande et al., 2011). The model was first used to simulate how cell concentrations fluctuate from their steady-state due to the invasion of MM cells, but then return to the steady-state after the removal of the MM cells. The variation in bone volume with time was also calculated to demonstrate the MM-induced bone destruction. The precise reason for the bone destruction was then examined by considering the variation in the ratios of active osteoblasts to osteoclasts. Also, a sensitivity study was undertaken to investigate how the variations of model parameters (D_{OB_u} , D_{OB_p} , D_{OC_p} , A_{OB_a} , A_{OC_a} , A_{MM} , β_{OPG} , β_{RANKL} , β_{PTH} , β_{IL6} and $\tilde{D}_{TGF\beta}$) affect MM concentration and bone volume.

The initial values of the cell concentrations used in the model are listed in Table 5.3 (where the MM cells were added at day 201 in the simulation). The model parameters without biological meaning or corresponding experimental data are estimated or optimized by genetic algorithm, which is a method for solving optimization problems based on a natural selection process that mimics biological evolution and has a good performance due to its this random nature. The simulation

was carried using Matlab computational software package (v7.7.0, Mathworks, Natick, USA), where the solver of genetic algorithm is provided.

Variables	Values	Unit
OB_u	3.27e-6 [1,2]	pM
OB_p	7.67e-4 [3]	pM
OB_a	6.39e-4 [4,5]	pM
OC_p	1.28e-3 [6]	pM
OC_a	1.07e-4 [4,5]	pM
MM	3.26e-1 [7,8]	pM

Table 5.3: The initial values of cell concentrations in the model.
 [1] Caplan, 2007; [2] Cristy, 1981; [3] Wang et al., 2011; [4] Lerner, 2004; [5] Cowin, 2001; [6] Parfitt, 1994; [7] Salmon and Smith, 1970; [8] International Myeloma Working Group, 2003.
 (MM cell concentration is at day 201; other cell concentrations are at day 1)

Figure 5.13 describes the variations of MM cells and bone cells during different periods: the normal period from day 1 to day 50, the invasion of MM cells from day 51 to day 300 and the removal of MM cells from day 301. It confirms that the bone microenvironment remains in a steady-state until the invasion of the MM cells at day 50, with the cell concentrations remaining constant at their initial values (given in Table 5.2). The steady-state is disturbed due to the appearance of MM cells after the 200th day, which causes a fluctuation of cell concentrations as illustrated in Figure 5.13. MM cells undergo a rapid initial increase and then gradually reach their 5.8 fold at day 300. The concentrations of OB_p , OB_a and OC_a also increase to its 2.8, 2 and 2.5 fold respectively due to the invasion of MM cells. Figures 5.14 and 5.15 show how bone volume and $OB_a:OC_a$ ratio vary after the invasion of MM cells. Figures 5.16 to 5.18 describe the variations in the concentrations of OPG, RANKL and IL-6 during the different periods respectively.

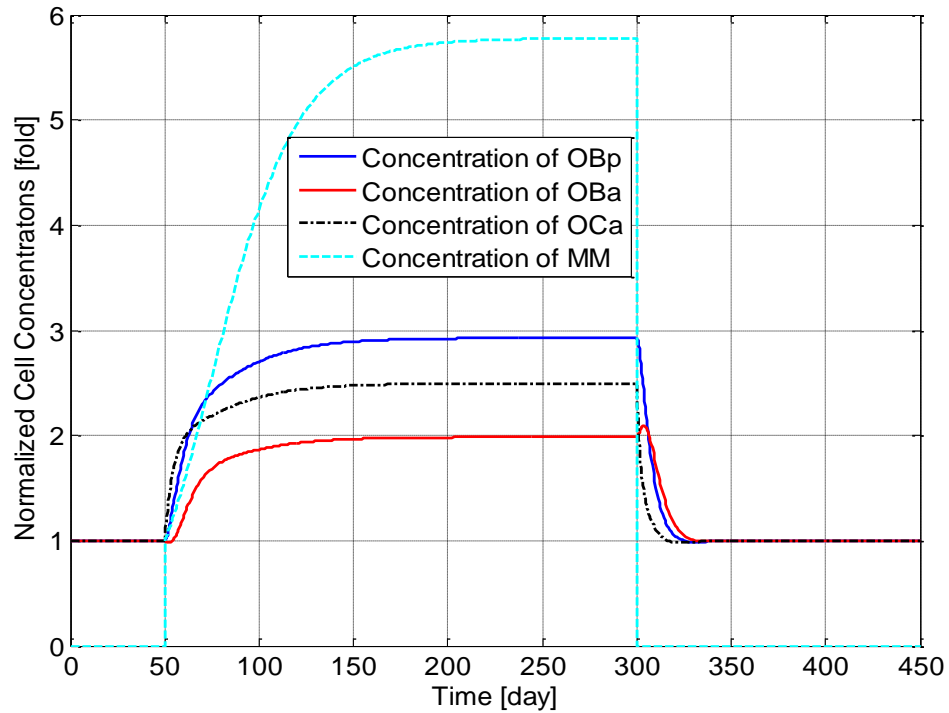


Figure 5.13: Model simulations of the variation in the normalized concentrations of osteoblast precursors, active osteoblasts, active osteoclasts and active tumour cells with respect to their initial values during different periods: the normal period from day 1 to day 50, the invasion of MM cells from day 51 to day 300 and removal of MM cells from day 301.

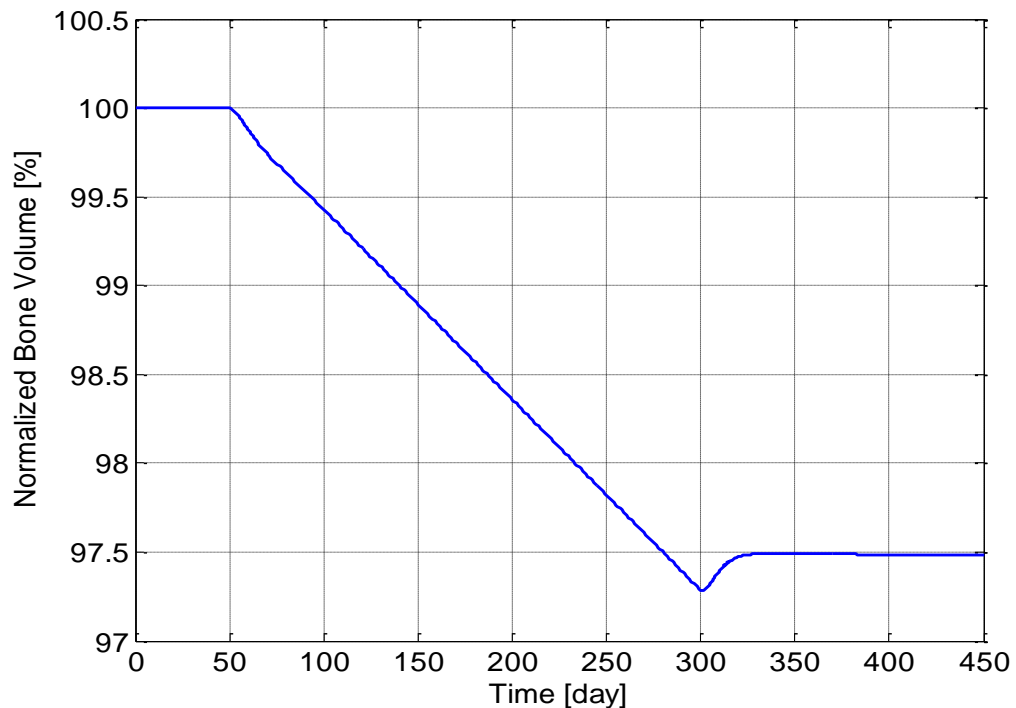


Figure 5.14: Model simulations of the variation in normalized bone volume with respect to its initial value during different periods: the normal period from day 1 to day 50, the invasion of MM cells from day 51 to day 300 and removal of MM cells from day 301.

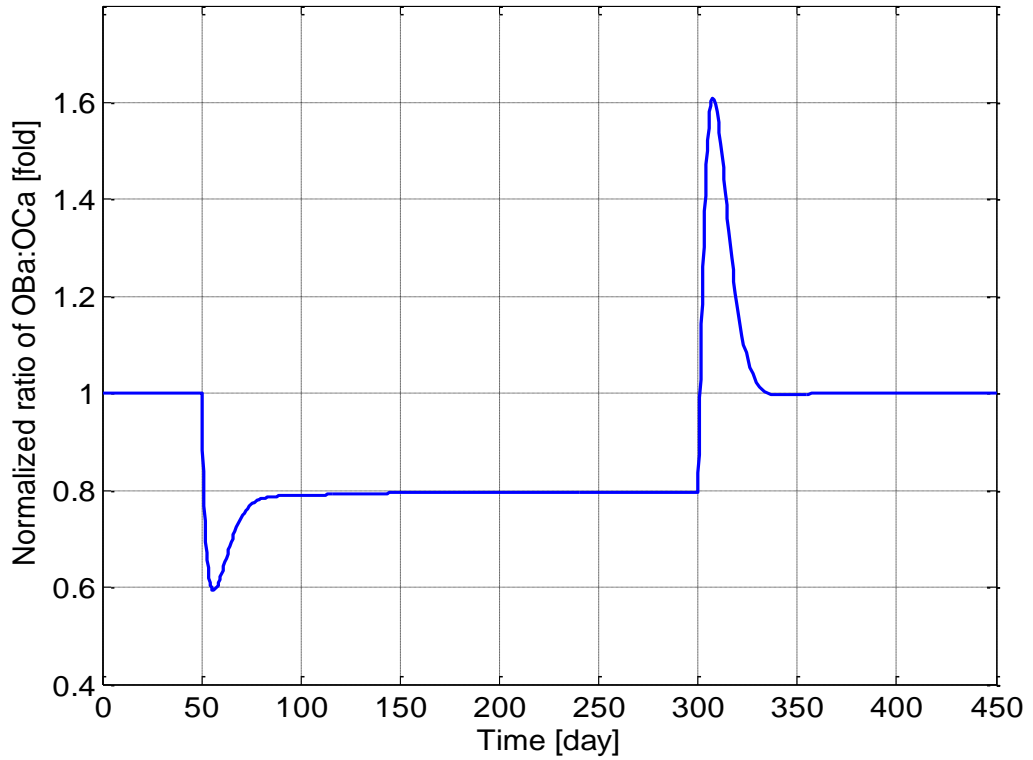


Figure 5.15: Model simulations of the variation in the normalized ratio of $OB_a:OC_a$ with respect to its initial value during different periods: the normal period from day 1 to day 50, the invasion of MM cells from day 51 to day 300 and removal of MM cells from day 301.

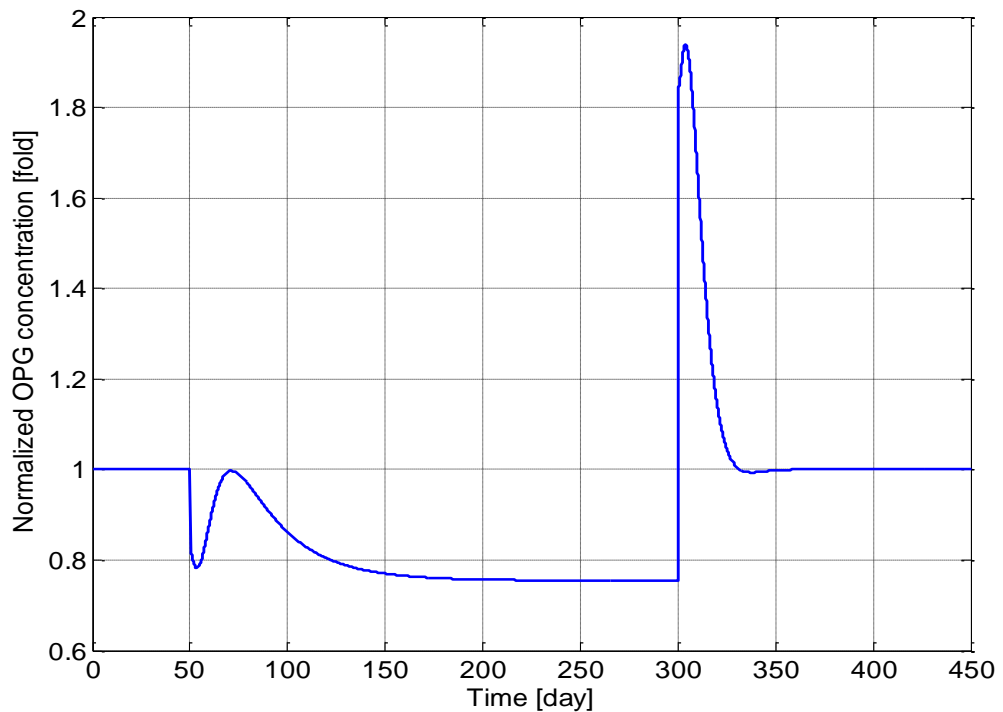


Figure 5.16: Model simulations of the variation in normalized OPG concentration with respect to its initial value during different periods: the normal period from day 1 to day 50, the invasion of MM cells from day 51 to day 300 and removal of MM cells from day 301.

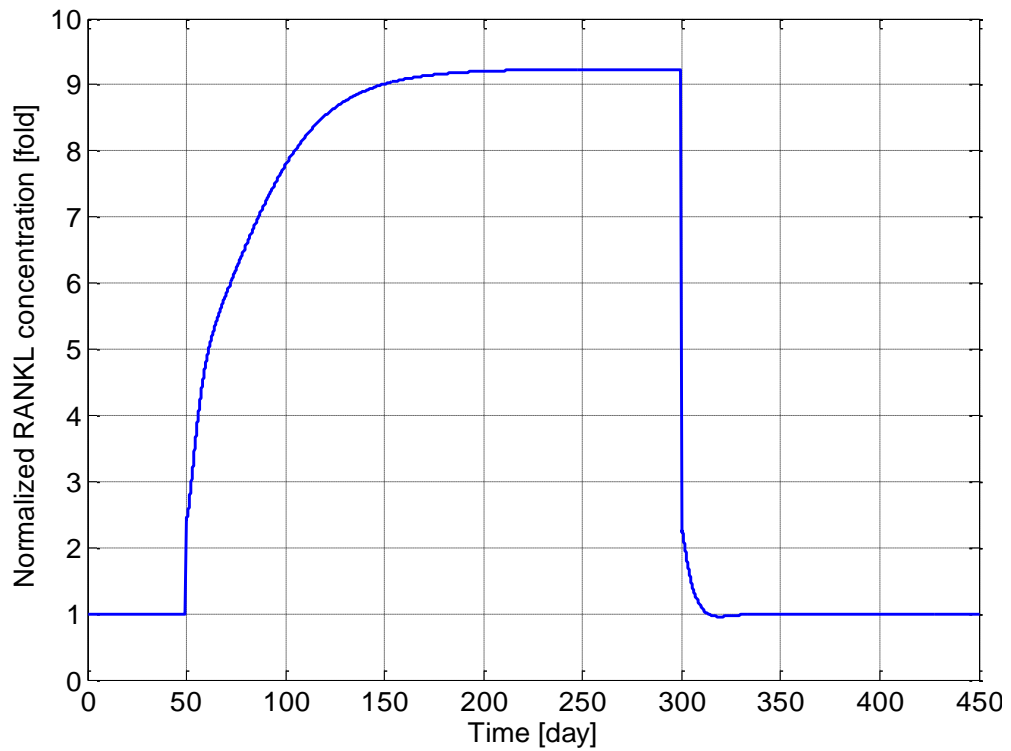


Figure 5.17: Model simulations of the variation in normalized RANKL concentration with respect to its initial value during different periods: the normal period from day 1 to day 50, the invasion of MM cells from day 51 to day 300 and removal of MM cells from day 301.

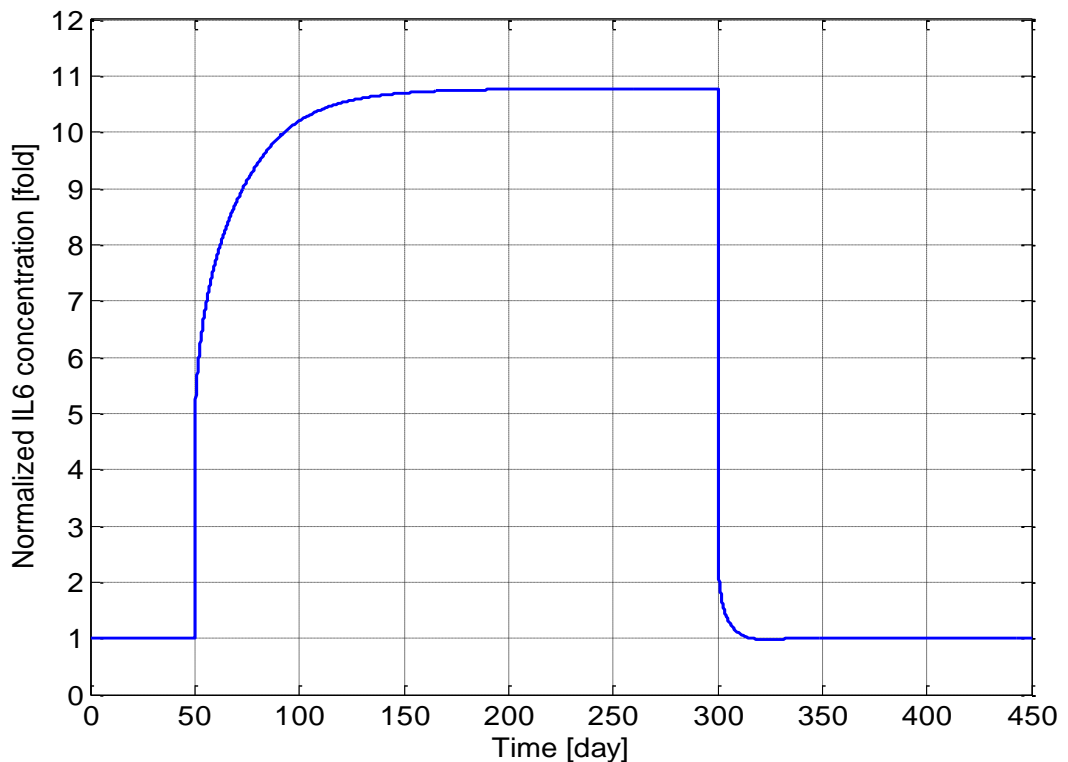


Figure 5.18: Model simulations of the variation in normalized IL-6 concentration with respect to its initial value during different periods: the normal period from day 1 to day 50, the invasion of MM cells from day 51 to day 300 and removal of MM cells from day 301.

5.3.4 SENSITIVITY STUDY

Further information on the underlying biochemical mechanisms are elucidated by the sensitivity study of eleven of the key parameters of the model (namely D_{OB_u} , D_{OB_p} , D_{OC_p} , A_{OB_a} , A_{OC_a} , A_{MM} , β_{OPG} , β_{RANKL} , β_{PTH} , β_{IL6} and $\tilde{D}_{TGF\beta}$), thereby suggesting possible strategies for management of MM. The parameters are varied individually between 50 to 150% of their initial base values (as defined in Table 5.2) and the effects on MM concentrations and bone volume are examined, normalized with respect to their (maximal) values at day 300 (in Figures 5.13 and 5.14). Thus, Figures 5.19 and 5.20 demonstrate how the variation in each parameter influences MM concentration at day 300, and Figures 5.21 and 5.22 show how bone volume is affected.

Figures 5.19 and 5.20 show that many of these eleven parameters have a significant influence on MM concentration. As some parameter values increase (between 50% and 150% of their base values) so MM concentration increases, while the opposite effect is observed with the other parameters. For example, as D_{OC_p} increases from 50% to 150% of its base value, MM concentration varies by 81% to 121%. Conversely, for the same variation in A_{OC_a} , a significant decrease in MM concentration (from 141% to 87% of its base value) is observed. Figures 5.21 and 5.22 show this variation in parameter values affects bone volume. For example, a change in A_{OB_a} and $\tilde{D}_{TGF\beta}$ (from 50% to 150% of base value) produces a variation in bone volume (between 106% to 97% and 104% to 98% respectively), while the same variation in A_{MM} has a negligible effect. The variations in D_{OC_p} and A_{OC_a} (from 50% to 150% of its base value) cause a decrease (between 101% to 99%) and an increase (between 96.5% to 100.5%) in bone volume respectively.

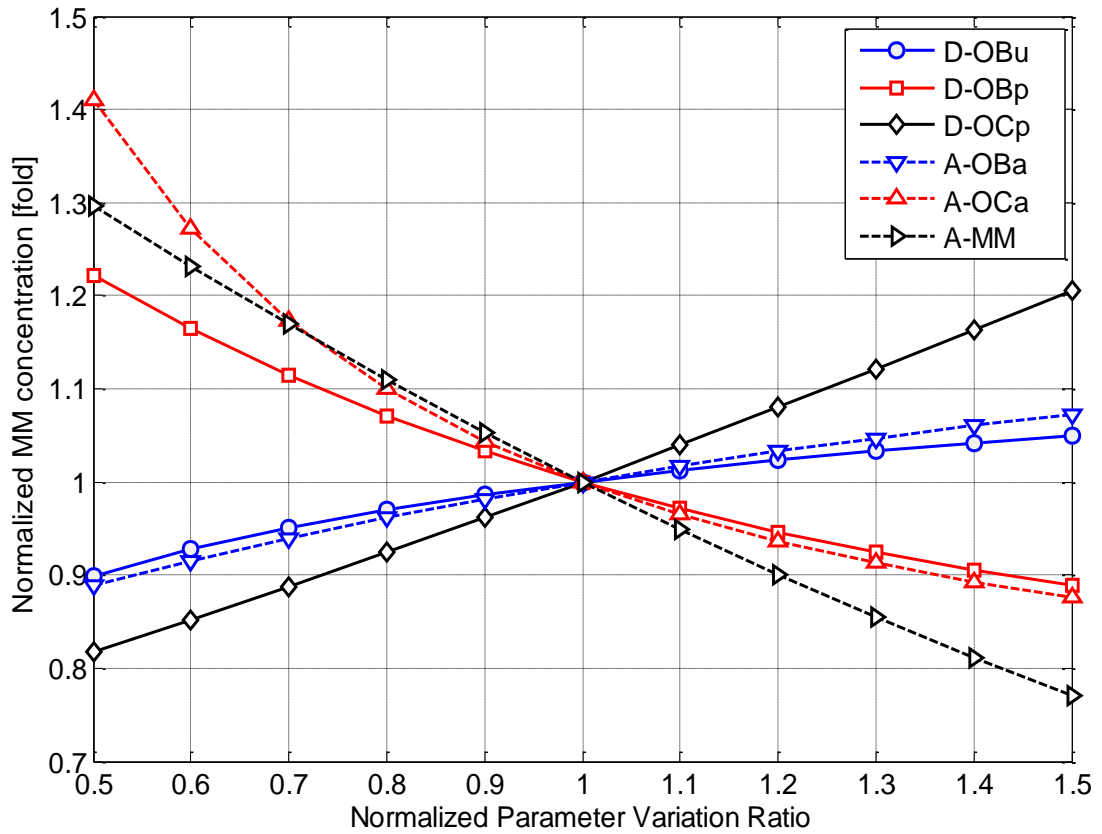


Figure 5.19: The effects of independently varying each model parameter (D_{OB_u} , D_{OB_p} , D_{OC_p} , A_{OB_a} , A_{OC_a} and A_{MM}) on MM concentration at day 300. Parameter variance and MM concentration were normalized to the values of the base case.

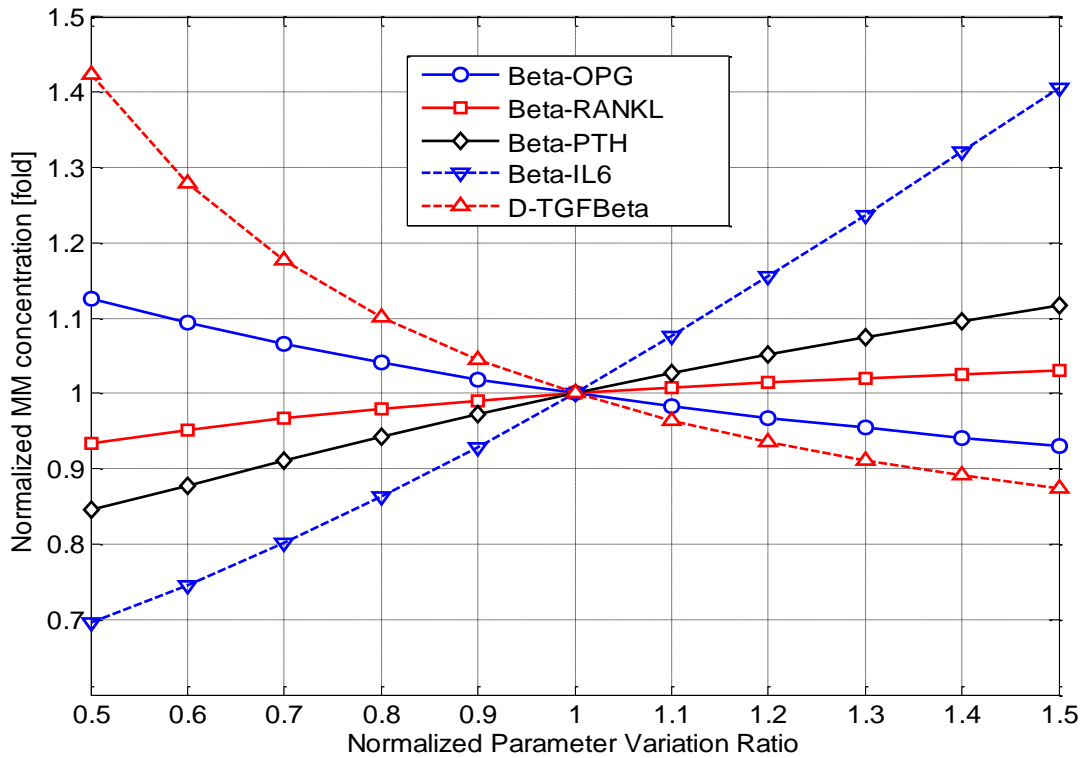


Figure 5.20: The effects of independently varying each model parameter (β_{OPG} , β_{RANKL} , β_{PTH} , β_{IL6} and $\tilde{D}_{TGFB\beta}$) on MM concentration at day 300. Parameter variance and MM concentration were normalized to the values of the base case.

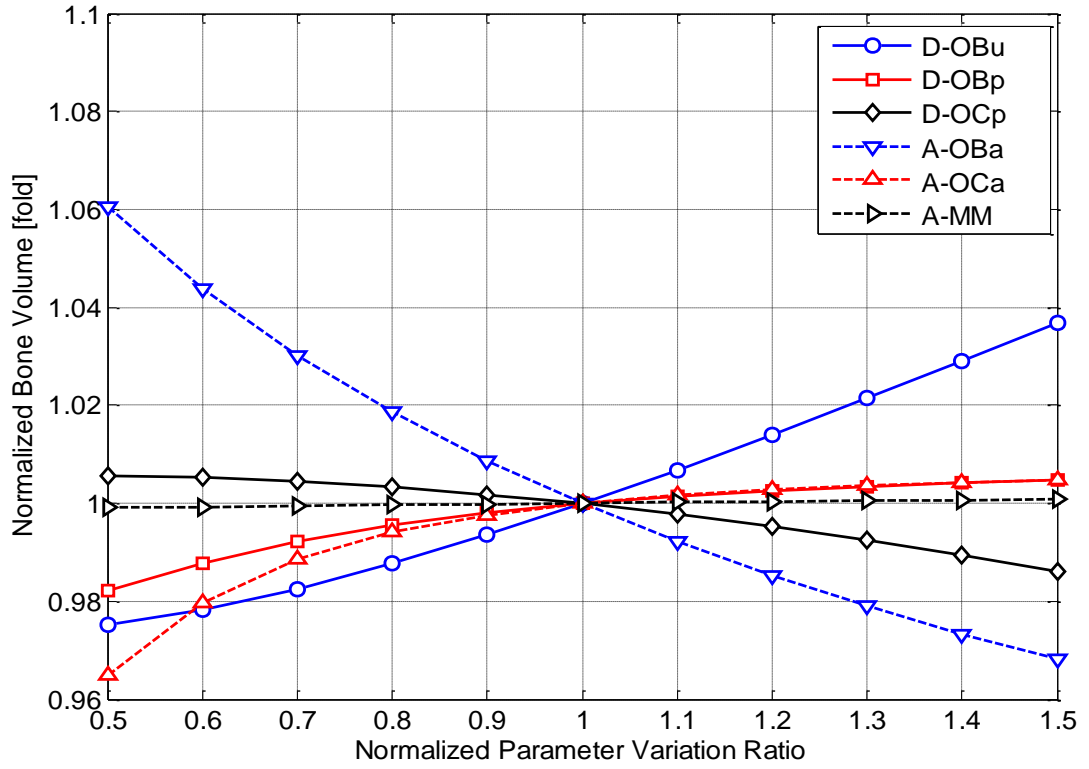


Figure 5.21: The effects of independently varying each model parameter (D_{OBu} , D_{OBp} , D_{OCp} , A_{OBa} , A_{OCa} and A_{MM}) on bone volume at day 300. Parameter variance and bone volume were normalized to the values of the base case.

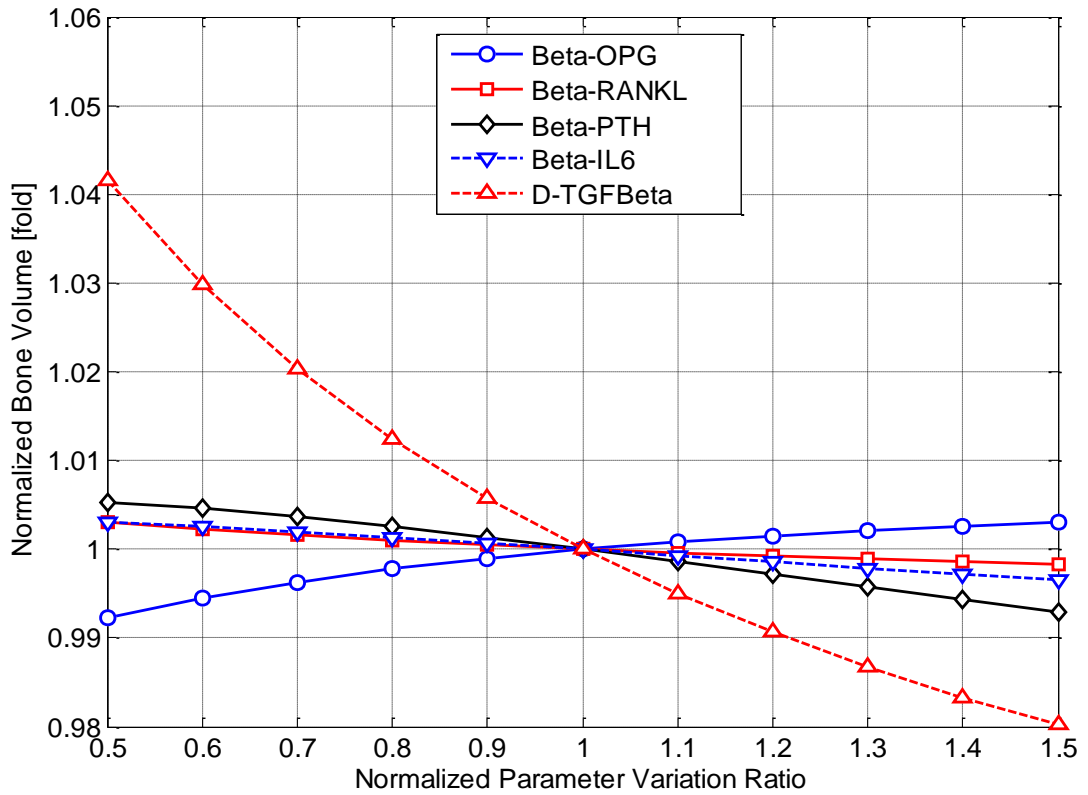


Figure 5.22: The effects of independently varying each model parameter (β_{OPG} , β_{RANKL} , β_{PTH} , β_{IL6} and $\tilde{D}_{TGFBeta}$) on bone volume at day 300. Parameter variance and bone volume were normalized to the values of the base case.

5.3.5 DISCUSSION

The increase in the concentrations of OB_a , OC_a and MM cells after the introduction of MM cells (shown in Figure 5.13) agrees with the experimental observations of Alexandrakis et al. (2002), Diamond et al. (1997) and Terpos et al. (2003). The 578% increase in MM cell concentration is similar to the 600% increase reported in the experimental work of Diamond et al. (1997). OB_p concentration is seen to increase nearly threefold due to the invasion of MM cells, which arises because the MM cells inhibit the differentiation of OB_p into OB_a (Bataille et al. 1986, 1990, 1991; Roodman 2011). Furthermore, Figure 5.14 confirms that the invasion of MM cells lead to bone destruction, which also agrees with the observation of a decline in bone volume within MM patients by Diamond et al. (1997). This can be explained by the variation in the ratio of $OB_a:OC_a$, as shown in Figure 5.15. In addition, the OPG concentration decreases to 75% of that in the healthy condition after the invasion of MM cells (shown in Figure 5.16), which again compares well with experimental data which ranges from 59 to 82% (Lipton et al., 2002; Seidel et al., 2001; Standal et al., 2002; Terpos et al., 2003). Similarly, the increase in the IL-6 concentration to 1077% (shown in Figure 5.17) is consistent with the 979% increase reported by Alexandrakis et al. (2003). RANKL concentration increased to 924% (shown in Figure 5.18), which also within observed range of experimental data: 226% (Goranova-Marinova et al., 2007) to 1567% (Terpos et al., 2006).

It can be seen that some cell concentrations and the ratio of OB_a to OC_a experience a short period of oscillation, and then returned to their initial steady-state values after the removal of tumour cells, as shown in Figure 5.13 and Figure 5.15, This agrees with the observation that the steady-state of biological systems is dynamical, and they are capable of restoring themselves to a steady-state after the removal of external perturbations (Lemaire et al., 2004; Zumsande et al., 2011). The MM-induced bone destruction also ceased after removal of the tumour cells, however the bone volume remained at a lower level compared to its initial volume (as shown in Figure 5.14). This is consistent with the observation that MM-induced bone lesions rarely heal even after the removal of MM cells (Roodman, 2011; Terpos and Dimopoulos, 2005). It is explained by the observation that the OB_a to OC_a ratio returns to its initial steady-state value, meaning that near zero bone balance is

achieved at the end of each remodelling cycle, and thus there is an opportunity for additional bone building to take place and bone lesions to be healed.

A sensitivity study is conducted to show how the variations in model parameters influence MM concentration and bone volume, thus suggesting the potential treatment for MM-induced bone disease. For example, the sensitivity study indicates that D_{OC_p} and A_{OC_a} are tightly related to MM concentration and bone volume. Thus the intervention targeting these two factors can be a potential treatment for reducing the tumour burden. This prediction is consistent with the mechanism of bisphosphonate treatment, which manages MM-induced bone disease by inhibiting the differentiation of osteoclast precursors into mature osteoclasts and promoting osteoclast apoptosis (Rogers et al. 2000; Shay and Rogers 2011).

5.4 SIMULATION OF THERAPIES FOR MM-INDUCED BONE DISEASE

Currently, several therapies are proposed to treat MM-induced bone disease including bisphosphonates, bortezomib, TGF- β inhibition, radiotherapy and surgery (Foundation, 2008; Matsumoto and Abe, 2011; Roodman, 2011; Terpos and Dimopoulos, 2005). In this thesis, bisphosphonates, bortezomib and TGF- β inhibition which work in quite different ways are examined by the model.

5.4.1 BISPHOSPHONATE TREATMENT

Bisphosphonates are able to target high turnover skeletal sites and then bind to the mineralized bone matrix within these sites, due to their special pharmacological properties (Luftner et al., 2007; Rogers et al., 2000; Shay and Rogers, 2011). After they are internalized by osteoclasts, bisphosphonates can inhibit osteoclast activity and the resultant bone resorption by suppressing the differentiation of osteoclast precursors into mature osteoclasts, promoting osteoclast apoptosis and disrupting osteoclast function (Rogers et al., 2000; Shay and Rogers, 2011). Bisphosphonates are first-line treatment for MM-induced bone disease (Luftner et al., 2007; Morgan and Lipton, 2010), although further investigation is required to determine the optimal duration of bisphosphonate therapy, and bisphosphonates may also result in some side effects (Foundation, 2008; Green et al., 2010; Sarro and Minutoli, 2012).

In addition to inhibiting osteoclast-mediated bone resorption, several preclinical and clinical data suggest that bisphosphonates may also have a direct anti-

tumour effect (*e.g.* induction of apoptosis and inhibition of tumour cell adhesion and invasion) or an indirect anti-tumour effect (*e.g.* inhibition of angiogenesis and cell migration) (Chlebowski et al., 2010; Coleman et al., 2010; Eidtmann et al., 2010; Gnant and Eidtmann, 2010; Gnant et al., 2009; Holen and Coleman, 2010; Newcomb et al., 2010; Rennert et al., 2010). However, several studies provide contradictory results and claim that bisphosphonates do not improve mortality of patients (McCloskey et al., 1998; Mhaskar et al., 2010; Musto et al., 2008).

The possible anti-tumour effects of bisphosphonates are not included in the model, since further investigations are required to confirm this point. Thus, the model only considers the role of bisphosphonates inhibiting bone resorption by suppressing the differentiation of mature osteoclasts as well as promoting the apoptosis of osteoclasts. Thus, in the simulation, a parameter 'Factor.Bisphosphonate' is used to represent the degree that the bisphosphonates inhibit bone resorption. For example, when 'Factor.Bisphosphonate' is set as 0.7, it means that the differentiation rate of active osteoclasts decreases to 70% (0.7), while the apoptosis of osteoclasts increases by 30% ($0.3 = 1 - 0.7$).

Figures 5.23 to 5.25 demonstrate how a bisphosphonates therapy would influence cell concentrations and bone volume (Factor.Bisphosphonate = 0.7). Figure 5.23 indicates that bisphosphonates therapy reduces MM concentrations by 10% (for the period considered) and helps bone cell concentrations return to their normal values (*i.e.* values before the invasion of tumour cells). It should be noted that the anti-tumour effects of bisphosphonates are not considered, therefore, the decreased tumour burden is due to the inhibited osteoclast activity by bisphosphonates, which agrees with the experimental conclusion that the decrease in osteoclast activity can inhibit the proliferation of MM cells (Lauta, 2001; Terpos and Dimopoulos, 2005). As illustrated in Figure 5.25, the $OB_a:OC_a$ ratio increases by 18% after the introduction of bisphosphonates therapy, which thus results in a significant slowdown of the bone destruction (shown in Figure 5.24). Again, this is confirmed by published data that shows bisphosphonates are beneficial to the suppression of MM-induced bone destruction (Rogers et al., 2000; Shay and Rogers, 2011).

Figures 5.26 to 5.28 show the variations of MM concentration, bone volume and $OB_a:OC_a$ ratio caused by bisphosphonates with different values of 'Factor.Bisphosphonate' (0.7, 0.5 and 0.3) for the same treatment strategy. MM concentration decreases to 86.8%, 85.2% and 84% of its value at day 300, and

OB_a:OC_a ratio increases to 120%, 130% and 140%, when ‘Factor.Bisphosphonate’ is set as 0.7, 0.5 and 0.3 (shown in Figure 5.26 and 5.28). As illustrated in Figure 5.27, when ‘Factor.Bisphosphonate’ is set as 0.7, the bone destruction continues although its rate is decreased dramatically, due to the increasing OB_a:OC_a ratio, however when ‘Factor.Bisphosphonate’ is set to 0.5 or 0.3, the bone destruction stops and bone volume begins to increase. Thus, the simulation results suggest that a smaller ‘Factor.Bisphosphonate’ produces more significant inhibition of MM concentration and bone destruction.

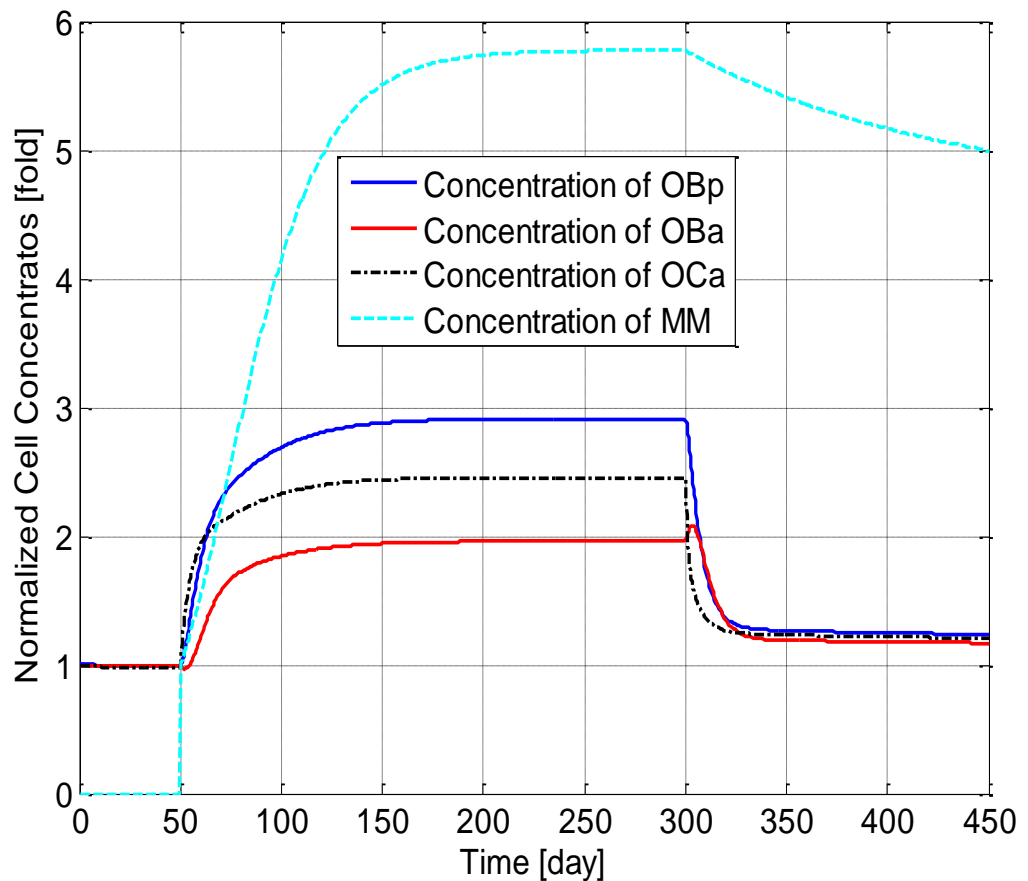


Figure 5.23: The variation of normalized cell concentrations with respect to their initial value during different periods: the normal period from day 1 to day 50, the invasion of MM cells from day 51 to day 300 and the intervention of the bisphosphonates therapy from day 301.

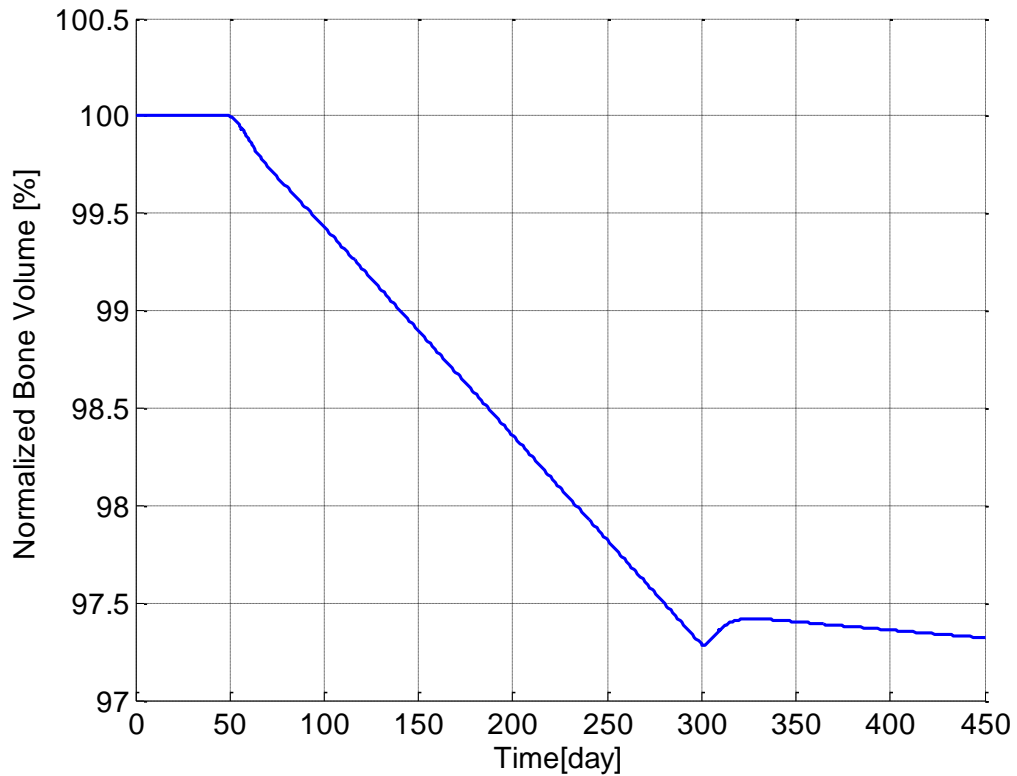


Figure 5.24: The variation of normalized bone volume with respect to its initial value during different periods: the normal period from day 1 to day 50, the invasion of MM cells from day 51 to day 300 and the intervention of the bisphosphonates therapy from day 301.

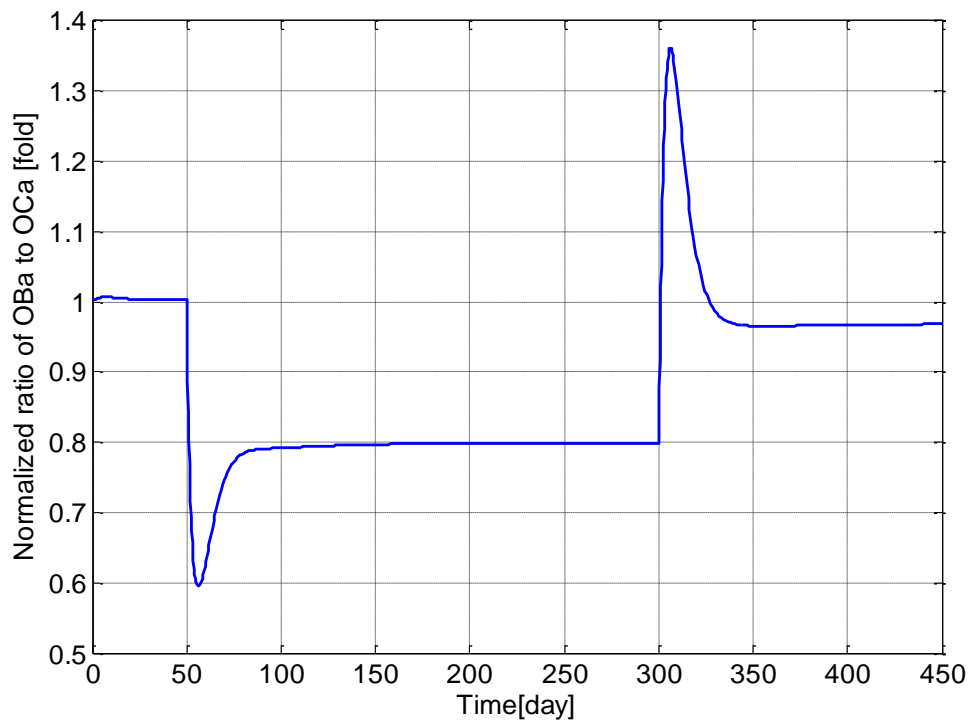


Figure 5.25: The variation of normalized ratio of OB_a:OC_a with respect to its initial value during different periods: the normal period from day 1 to day 50, the invasion of MM cells from day 51 to day 300 and the intervention of the bisphosphonates therapy from day 301.

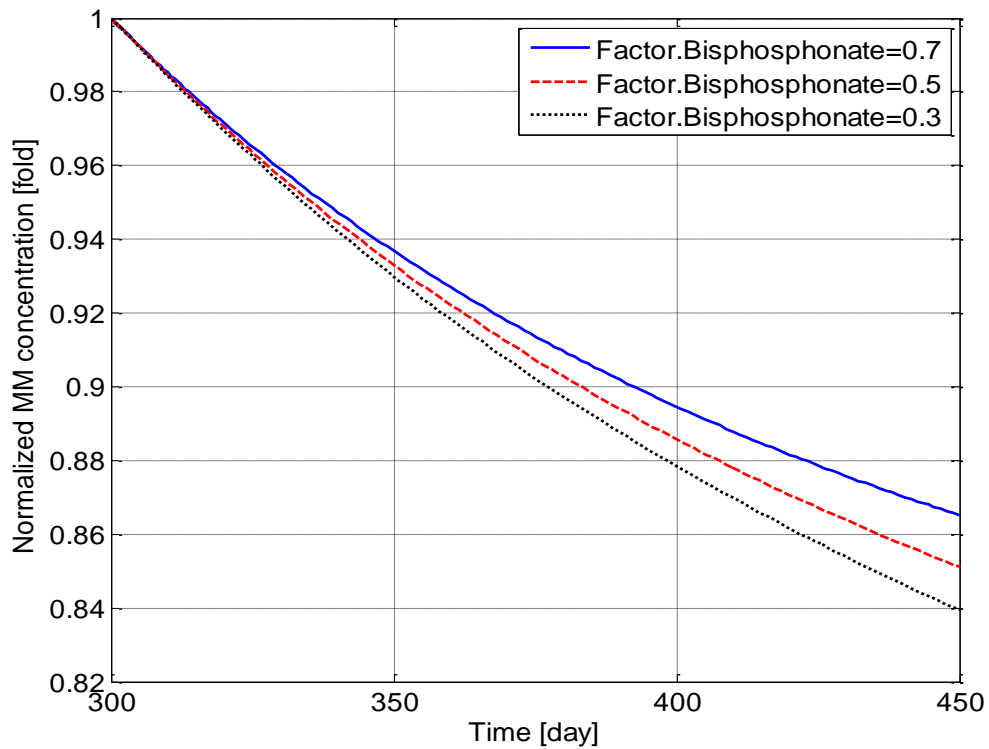


Figure 5.26: The variation of normalized MM concentration with respect to the value at day 300 after use of the bisphosphonates therapy with different values of 'Factor.Bisphosphonate'.

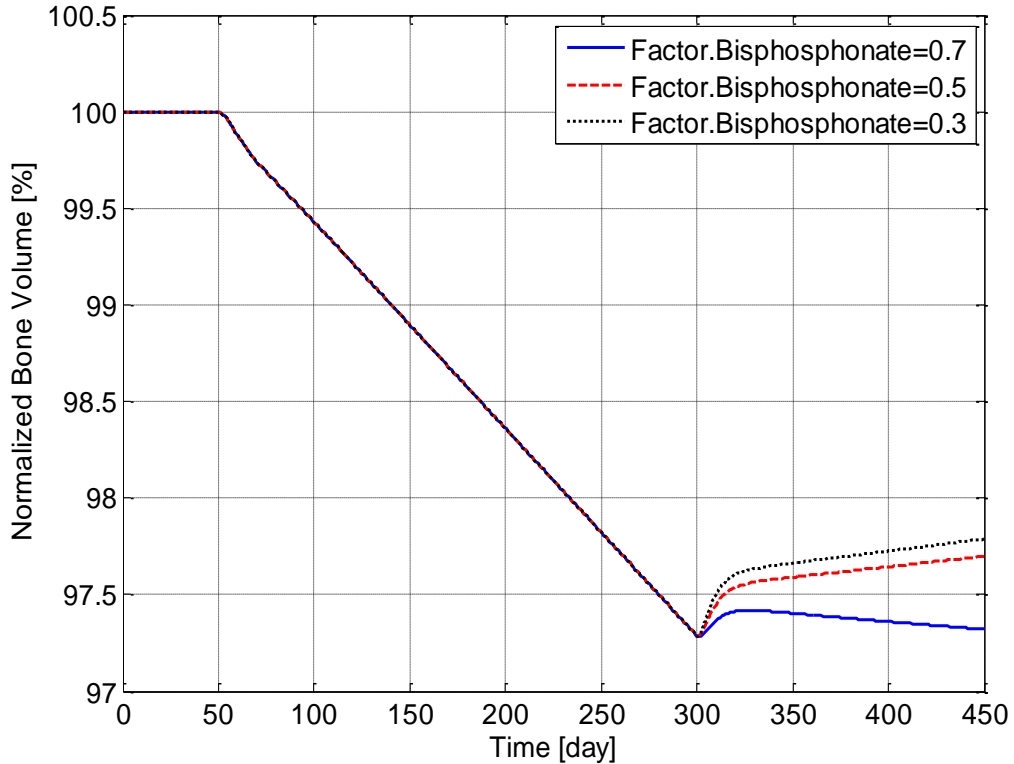


Figure 5.27: The variation of normalized bone volume with respect to its initial value after use of the bisphosphonate therapy with different values of 'Factor.Bisphosphonate'.

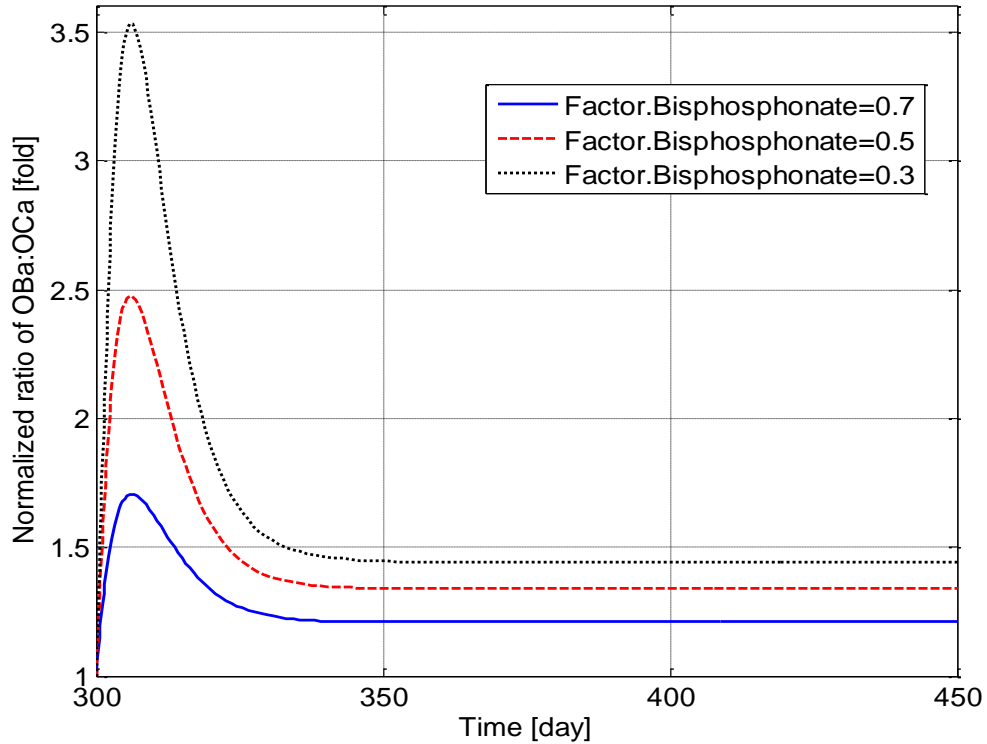


Figure 5.28: The variation of normalized ratio of $OB_a:OC_a$ with respect to the value at day 300 after use of the bisphosphonate therapy with different values of ‘Factor.Bisphosphonate’.

5.4.2 BORTEZOMIB TREATMENT

Osteoblast suppression, which mainly occurs from the blockade of osteoblast precursors differentiating into mature osteoblast, can promote the growth of tumour cells as well as bone destruction by promoting the production of anti-apoptotic factors and growth factors for MM cells (Atkins et al., 2003; Roodman, 2011). Thus, the stimulation of osteoblast differentiation is thought to be able to reduce tumour burden and bone destruction in MM patients (Roodman, 2011; Yaccoby, 2010). Bortezomib, a boron containing molecule with the potential of enhancing osteoblast proliferation and bone formation in MM patients, has been proposed as a potential target for MM-induced bone disease.

Therefore, in the simulation, a parameter ‘Factor.Bortezomib’ is used to represent the degree by which osteoblast differentiation is promoted. For example, when ‘Factor.Bortezomib’ is set to 2.0, it means that osteoblast activity is increased two fold.

Figures 5.29 to 5.31 show the variations in cell concentrations, bone volume and the ratio of $OB_a:OC_a$ after the intervention of bortezomib therapy from day 301,

when 'Factor.Bortezomib' is set as 2.2. As shown in Figure 5.29, bortezomib causes a rapid decrease in the concentration of MM cells, which agrees with the experimental finding that increased osteoblast proliferation is able to reduce tumour burden in MM patients (Edwards, 2008; Qiang et al., 2008; Yaccoby, 2010). The concentrations of OB_p , OB_a and OC_a also decrease after the introduction of Bortezomib and reach new equilibrium points around day 500, which are quite near their initial values before the invasion of MM cells. Figure 5.30 shows that MM-induced bone loss nearly stops after a short period of fluctuation due to the intervention of bortezomib, while the $OB_a:OC_a$ ratio (shown in Figure 5.31) undergoes a short period of fluctuation and then returns to a quite similar level to that without the tumour cells, which explains the termination or inhibition of MM-induced bone loss due to bortezomib.

Figures 5.32 to 5.34 show the variations in cell concentrations, bone volume and the $OB_a:OC_a$ ratio with different values of 'Factor.Bortezomib' (2.0, 2.2 and 2.4), as a result of which MM concentration decreases to 96.7%, 96.3% and 95.7%, and the $OB_a:OC_a$ ratio increases to 116%, 118% and 121%, respectively (shown in Figures 5.32 and 5.34). In Figure 5.33, when 'Factor.Bortezomib' equals 2.0, MM-induced bone loss continues although its rate is greatly reduced, due to the rising $OB_a:OC_a$ ratio; while when 'Factor.Bortezomib' is set as 2.2 or 2.4, a nearly zero or positive bone balance is achieved after the bortezomib therapy, which supports the fact that increasing osteoblast differentiation reduces bone destruction in MM patients (Yaccoby, 2010). The results suggest that the magnitudes of decreasing MM concentration and suppressing bone destruction are both positively related to the value of 'Factor.Bortezomib', and the stimulation of osteoblast activity can inhibit or even stop bone destruction as well as the tumour burden, and thus is an effective therapy for MM patients.

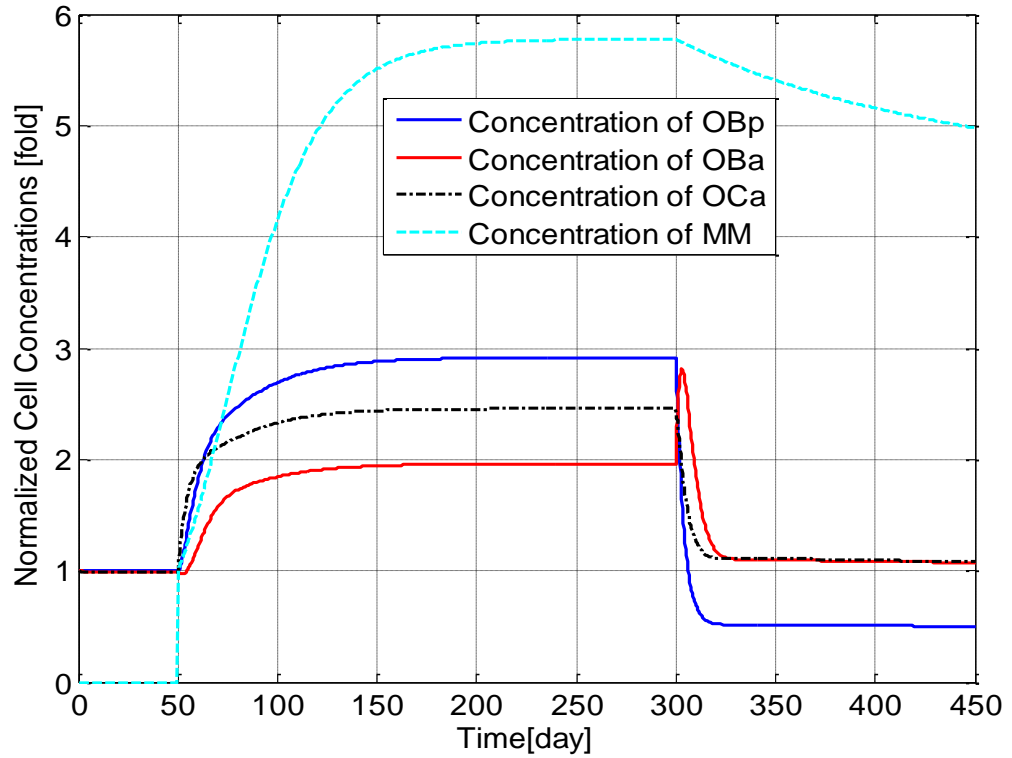


Figure 5.29: The variation of normalized cell concentrations with respect to their initial values during different periods: the normal period from day 1 to day 50, the invasion of MM cells from day 51 to day 300 and the intervention of bortezomib therapy from day 301.

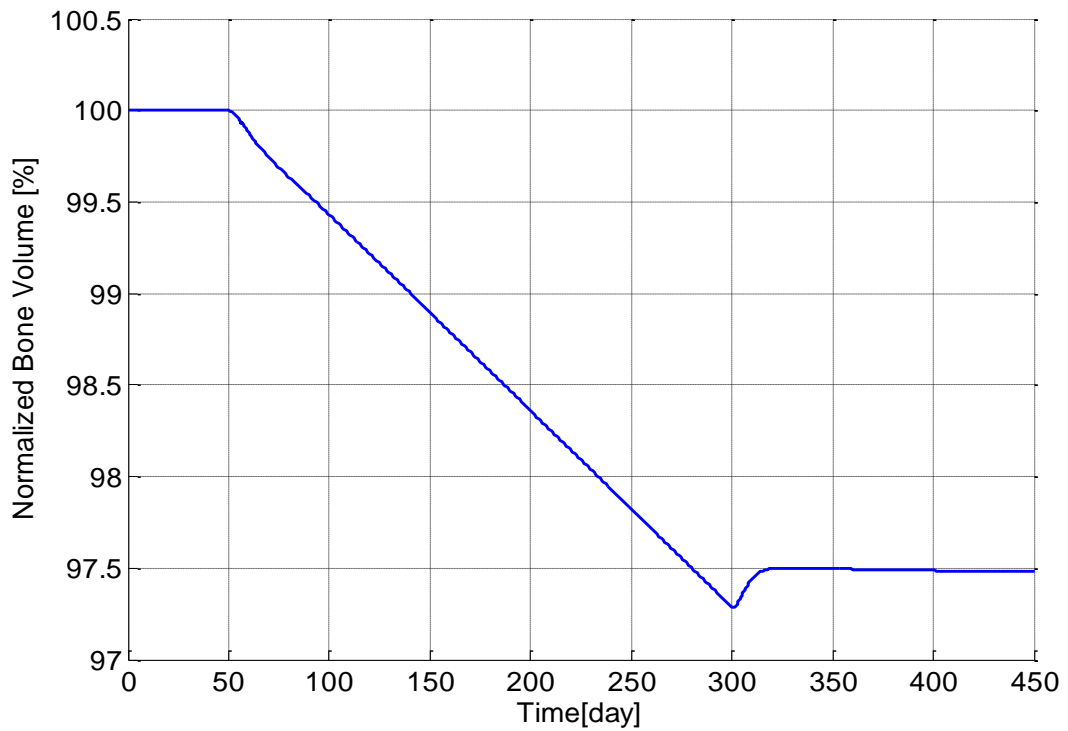


Figure 5.30: The variation of normalized bone volume with respect to its initial value during different periods: the normal period from day 1 to day 50, the invasion of MM cells from day 51 to day 300 and the intervention of bortezomib therapy from day 301.

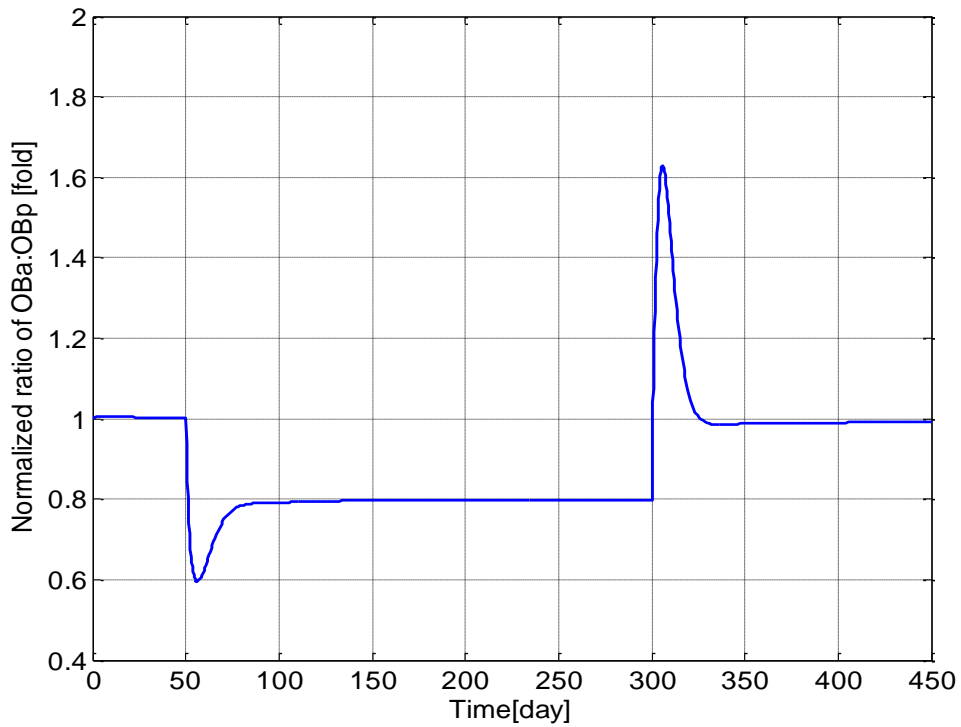


Figure 5.31: The variation of normalized ratio of $OB_a : OC_a$ with respect to its initial value during different periods: the normal period from day 1 to day 50, the invasion of MM cells from day 51 to day 300 and the intervention of bortezomib therapy from day 301.

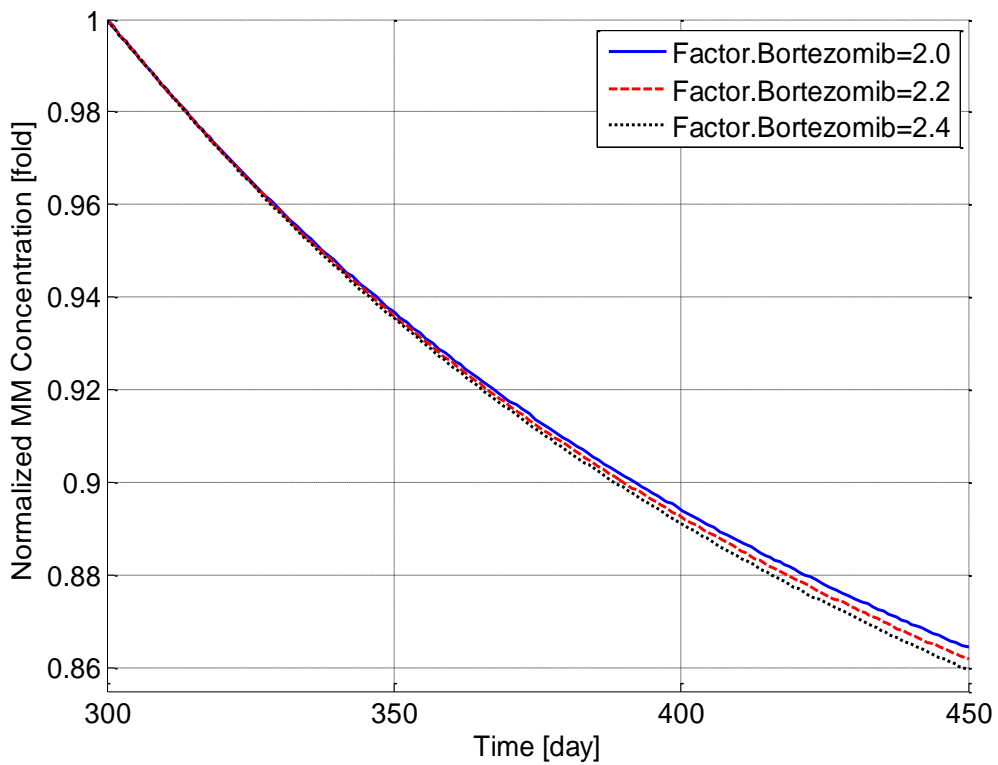


Figure 5.32: The variation of normalized MM concentration with respect to the value at day 300 after use of the bortezomib therapy with different values of 'Factor.Bortezomib'.

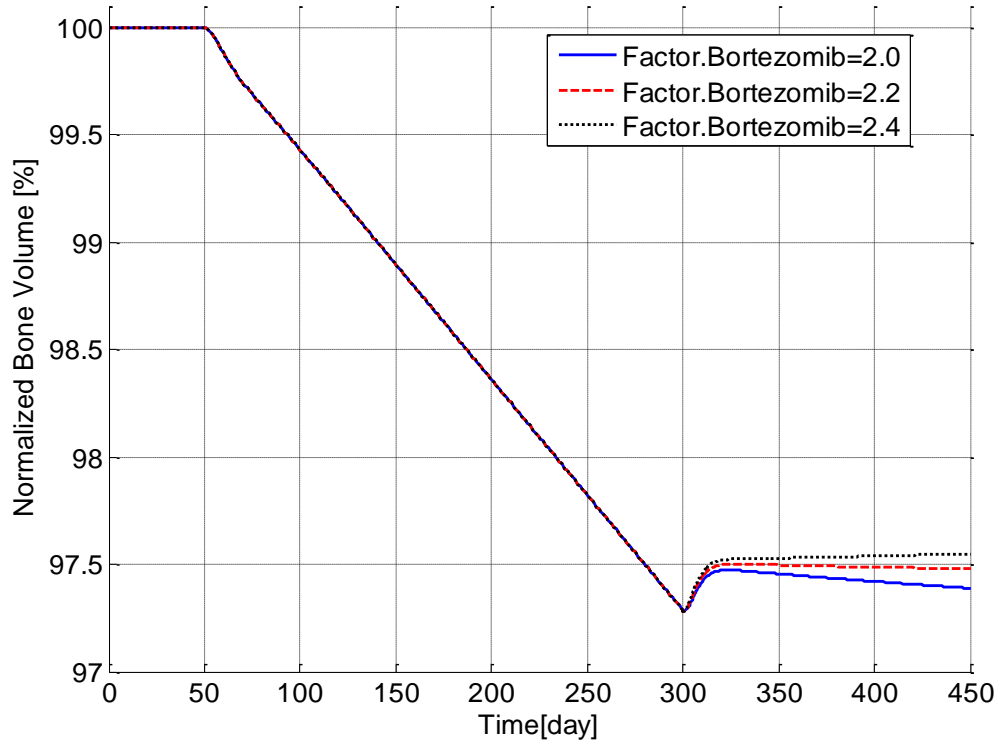


Figure 5.33: The variation of normalized bone volume with respect to its initial value after use of the bortezomib therapy with different values of ‘Factor.Bortezomib’.

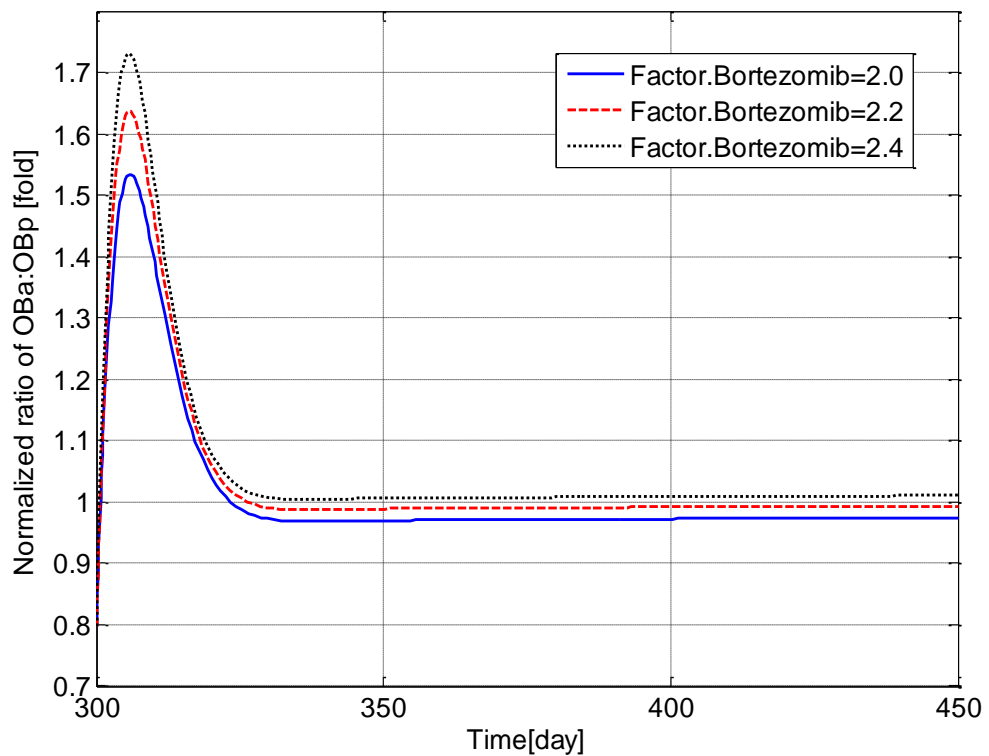


Figure 5.34: The variation of normalized ratio of OB_a:OC_a with respect to the value at day 300 after use of the bortezomib therapy with different values of ‘Factor.Bortezomib’.

5.4.3 TGF- β TREATMENT

TGF- β is reported to contribute to the progression of MM-induced bone disease (Matsumoto and Abe, 2011). It is released with bone resorption and stimulates the production of osteoblast progenitors while inhibiting the differentiation of mature osteoblasts. This then suppresses bone formation and indirectly promotes the progression of MM cells (immature osteoblast cells facilitate the growth and survival of MM cells, while mature cells enhance apoptosis of MM cells). Thus, the suppression of TGF- β is proposed as a new approach to treat MM-induced bone disease. However, some controversies still exist and further investigation is required to test the overall effect of this therapy (Matsumoto and Abe, 2011). In this section, the model is used to clarify the existing controversies and evaluate the therapy of inhibiting TGF- β in MM patients.

In the simulation, 'Factor.TGF-Beta' is used to describe the degree in which TGF- β is suppressed, where (for example) a 'Factor.TGF-Beta' value of 0.9 represents a decrease in TGF- β concentration to 90% (0.9). Thus, Figures 5.35 to 5.37 show the variations in cell concentrations, bone volume and the ratio of $OB_a:OC_a$ after the intervention of TGF- β therapy from day 301, with 'Factor.TGF-Beta' set to 0.7. The inhibition of TGF- β leads to a significant drop (13.3%) in MM cell concentration and the bone cells, which indicates that the tumour burden can be reduced through the suppression of TGF- β . However, the MM-induced bone destruction does not decrease and actually increases after the TGF- β therapy. This increasing bone loss can be explained by the decreasing $OB_a:OC_a$ ratio (24.3% decrease compared to the value at day 300) caused by the TGF- β therapy as shown in Figure 5.37. Therefore, it is concluded that the inhibition of TGF- β is not an effective therapy for MM-induced bone disease, since it cannot reduce the bone destruction, although it does reduce MM cell concentration.

Figures 5.38 to 5.40 show the variations in cell concentrations, bone volume and the $OB_a:OC_a$ ratio with different values of 'Factor.TGF-Beta' (0.7, 0.8 and 0.9). As a result, the MM concentration decreases to 86.5%, 86.7% and 86.9%, and the $OB_a:OC_a$ ratio decrease to 82.0%, 89.0% and 95.5%, respectively. As demonstrated in Figure 5.39, the smallest 'Factor.TGF-Beta' leads to the most bone loss. The simulation suggests that a larger decrease in TGF- β leads to a greater drop in MM concentration but a quicker bone loss.

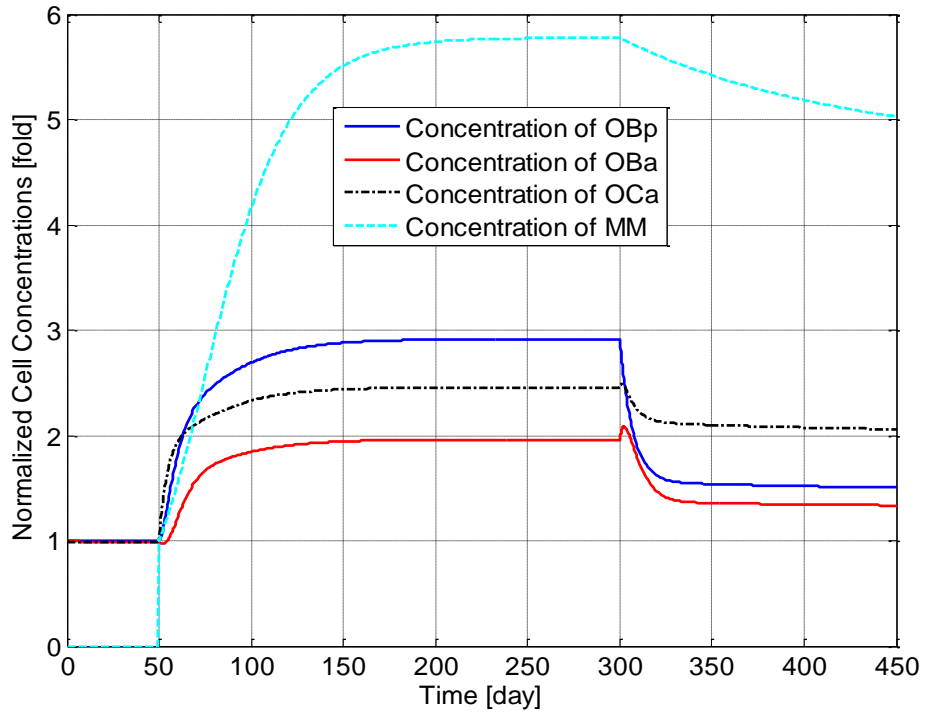


Figure 5.35: The variation of normalized cell concentrations with respect to their initial values during different periods: the normal period from day 1 to day 50, the invasion of MM cells from day 51 to day 300 and the intervention of TGF- β therapy from day 301.

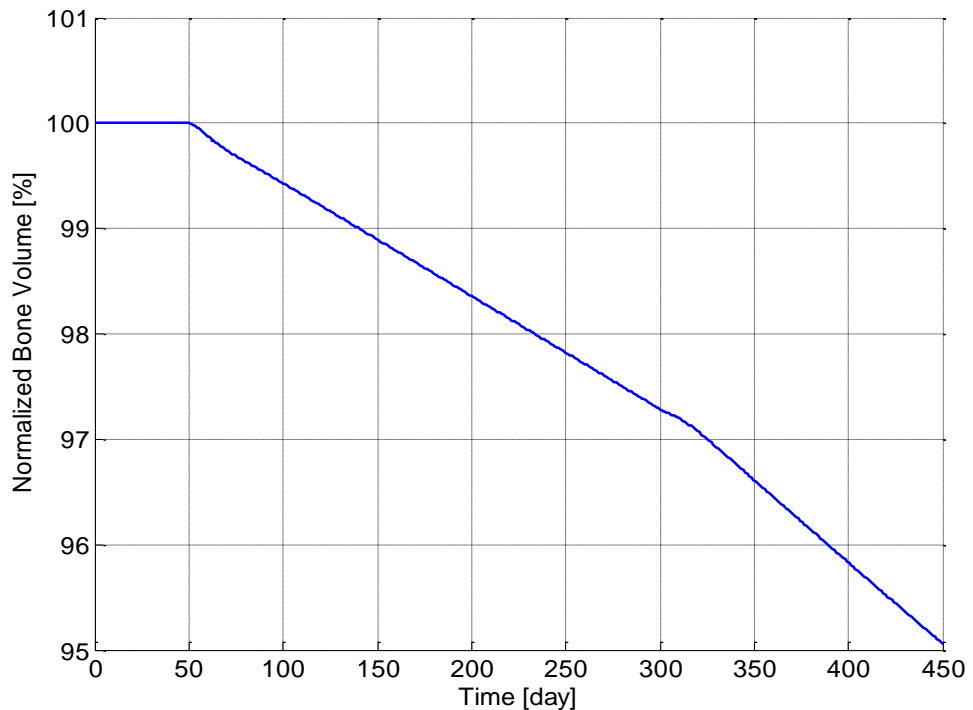


Figure 5.36: The variation of normalized bone volume with respect to its initial value during different periods: the normal period from day 1 to day 50, the invasion of MM cells from day 51 to day 300 and the intervention of the TGF- β therapy from day 301.

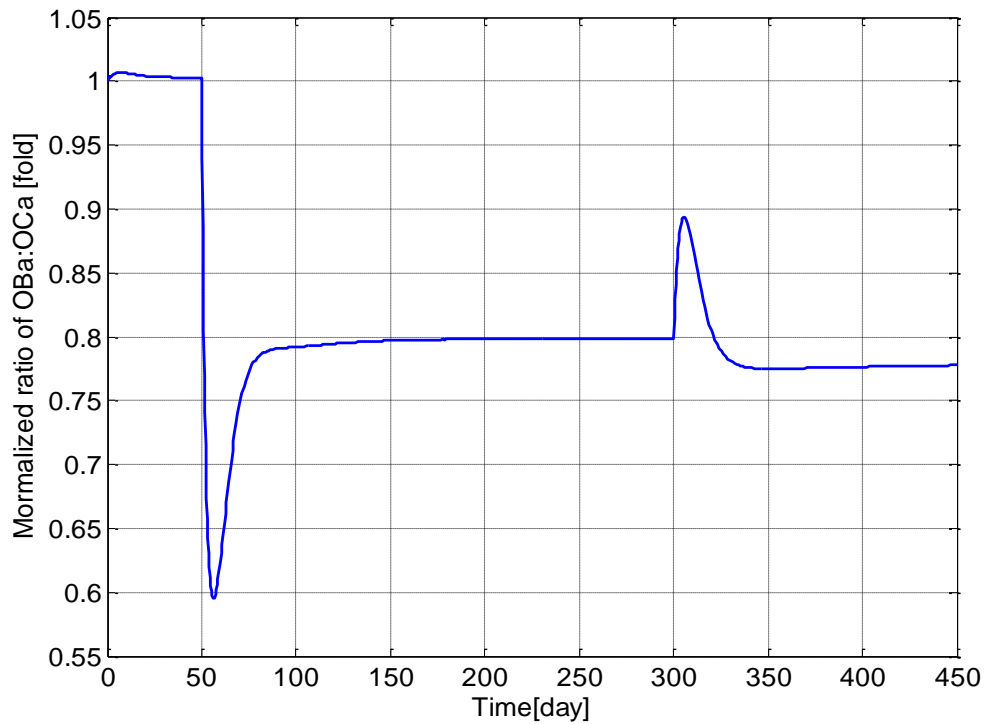


Figure 5.37: The variation of normalized ratio of OB_a :OC_a with respect to its initial value during different periods: the normal period from day 1 to day 50, the invasion of MM cells from day 51 to day 300 and the intervention of the TGF-β therapy from day 301.

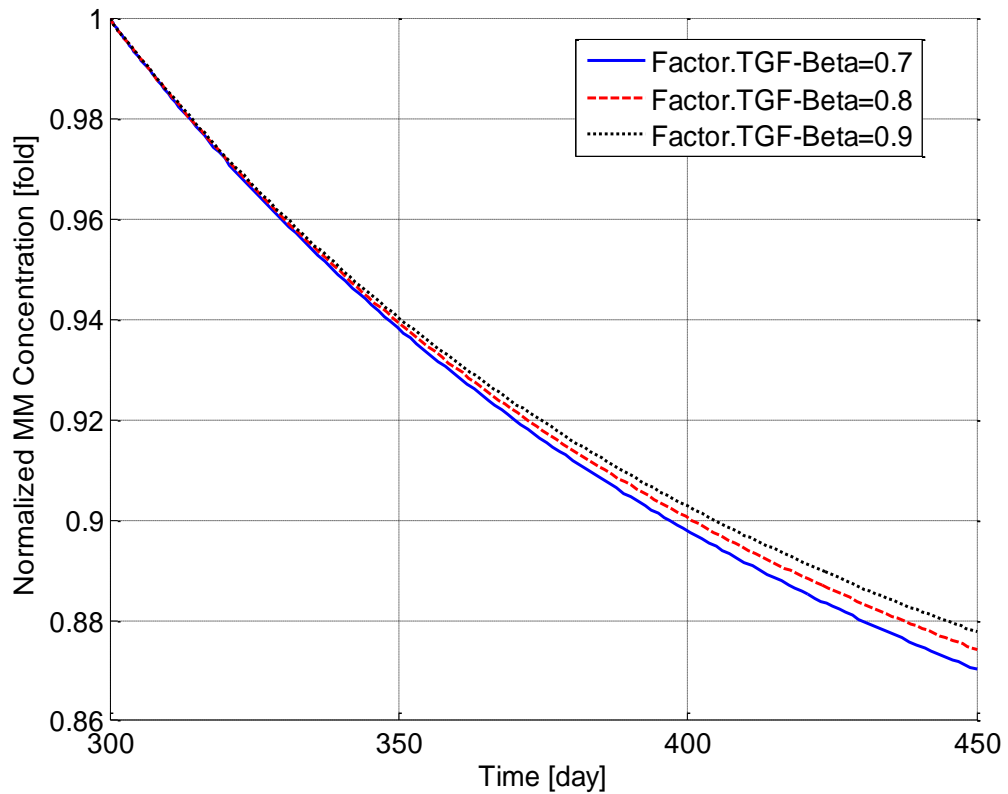


Figure 5.38: The variation of normalized MM concentration with respect to the value at day 300 after use of the TGF-β therapy with different values of 'Factor.TGF-β'.

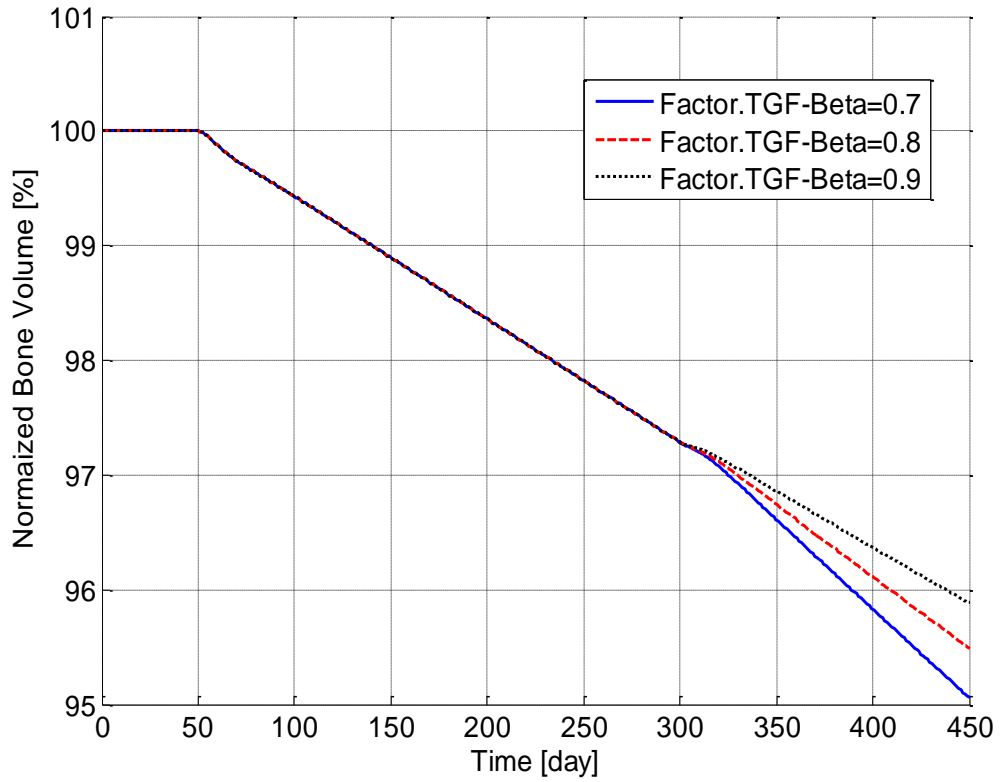


Figure 5.39: The variation of normalized bone volume with respect to its initial value after use of the TGF- β therapy with different values of ‘Factor.TGF- β ’.

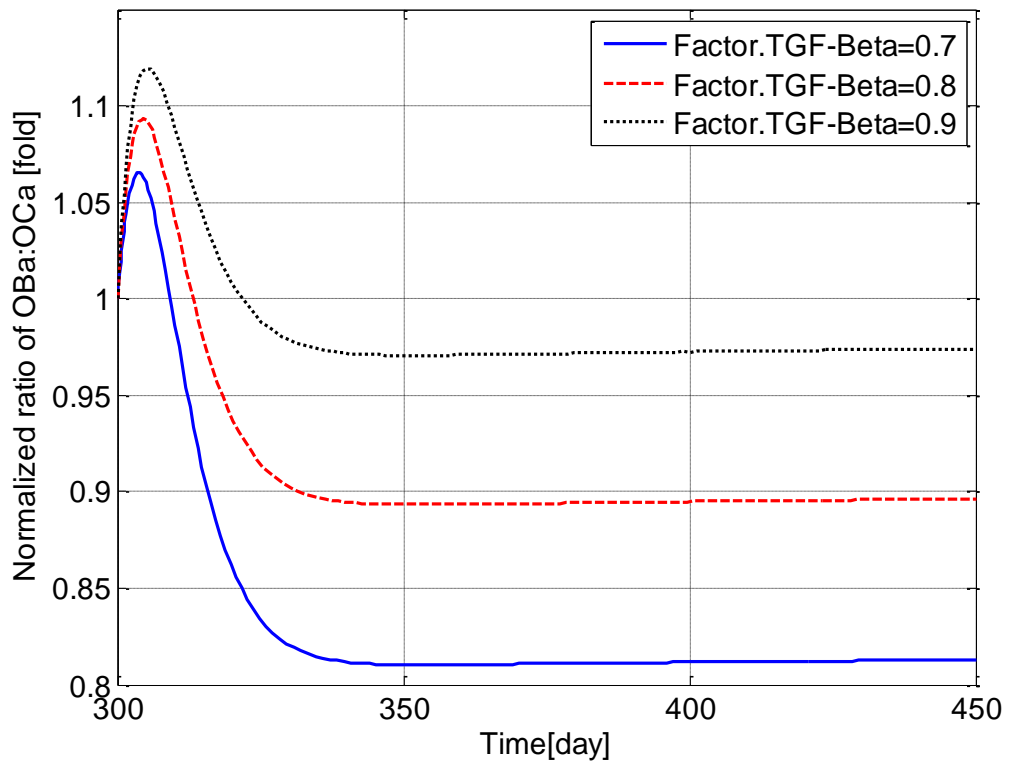


Figure 5.40: The variation of normalized ratio of OB_a:OC_a with respect to the value at day 300 after use of the TGF- β therapy with different values of ‘Factor.TGF- β ’.

5.5 CONCLUSION

The results presented in this chapter demonstrate that the model can simulate the interaction between MM cells and the bone microenvironment, and the contribution of that interaction to the progression of the MM cells and the resultant bone destruction. The sensitivity study demonstrates how the variations of parameters (D_{OB_u} , D_{OB_p} , D_{OC_u} , β_{OPG} , β_{RANKL} , β_{PTH} and β_{IL6}) influence MM concentration and bone volume and identifies those that are most critical. There therapies for treatment of MM-induced bone disease are also examined. The model simulation indicates that the bisphosphonates and bortezomib treatments are effective therapies for MM-induced bone disease by reducing the tumour burden as well as bone destruction, however the TGF- β treatment cannot inhibit MM-induced bone loss although MM concentration is suppressed.

The development of MM-induced bone disease involves many biochemical factors and mechanisms, although only a minority of these are considered in the current literature. This model integrates these partial findings and tries to analyse the progression of MM-induced bone disease. It goes much further than the recent model of Wang et al. (2011) by including the effects of osteoblast activities. However, the effects of soluble factors responsible for inhibiting osteoblast activity are still currently not considered.

The model demonstrates how bone cell concentrations fluctuate after the invasion of MM cells, and how these variations result in bone destruction. The simulation results agree with published experimental data and explain why the lesions resulting from MM-induced bone destruction rarely heal, even after the disappearance of MM cells. The model also shows how therapies bisphosphonate and bortezomib reduce tumour cells and inhibit (or stop) bone destruction (as observed in experimental investigations). However, although TGF- β treatment also suppresses MM concentration, it cannot inhibit MM-induced bone loss. The model thus serves as a solid foundation for more detailed analyses of the development of MM-induced bone disease.

A general discussion follows in Chapter 6 which highlights the background, novelties, assumptions and potential application of the proposed mathematical models.

6. DISCUSSION

In this project, two mathematical models have been developed to simulate the trabecular bone remodelling process at the cellular level and the pathology of MM-induced bone disease, respectively. The models and their predictions are discussed in detail earlier in this thesis, and their relationships to other published work are evaluated. This chapter summarises the main points of this research project and demonstrates how it develops the previous work, and contributes to the understanding of the mechanobiology of bone (*e.g.* the bone remodelling process and bone related diseases) via computational simulations.

Bone remodelling has a vital function in enabling bone to adapt to the mechanical demands exerted by the biological environment. It involves a large number of complex processes and knowledge of this natural phenomenon is still incomplete. Mathematical modelling can be used to improve our understanding of the bone remodelling process.

Probably the first mathematical model of bone remodelling was developed by Kroll (2000) to simulate the interaction between osteoclasts and osteoblasts in response to PTH. The model simulations confirmed the clinical observation that intermittent PTH administration increases bone formation, while constant PTH administration stimulates bone loss. Rattanakul et al. (2003) developed Kroll's model further by including the effect of oestrogen stimulation on the dynamics of the osteoblast and osteoclast populations. The model developed by Komarova et al. (2003) was the first attempt to include autocrine and paracrine interactions between the osteoclastic and osteoblastic lineages at a single BMU. It was developed further by Moroz et al. (2006) to include the role of osteocyte apoptosis on bone remodelling. The RANK-RANKL-OPG pathway, along with growth factors, is the underpinning control network for regulating bone remodelling and was included in mathematical modelling by Lemaire et al. (2004). This model was further refined by Pivonka et al. (2008) to investigate the functional implications of the RANKL/OPG expression profile. In addition, the same group built another mathematical model to investigate the effect of the RANK-RANKL-OPG pathway on the bone remodelling process. Buenzli et al. (2011) included both temporal and spatial properties of BMUs in their models through a group of the material-balance equations. A different type of model

was constructed by Zumsande et al. (2011), who focused on the bifurcation properties of mathematical models through a generalised model.

While these models have become increasingly complex and biologically reasonable, they reconstruct the bone remodelling cycle in a qualitative way. Therefore, in the first part of this current research we developed a novel predator-prey based mathematical model to simulate the bone remodelling process quantitatively. The motivation to adopt the predator-prey model was based on its key characteristic of enabling competitive cyclic growth between the prey and predator populations, and restricting the populations from decreasing into negative values. These properties are similar to the growth of osteoclasts, which is tightly coupled to the growth of osteoblasts during the remodelling process at a BMU (Parfitt, 2000; Udagawa et al., 2006).

Several assumptions exist in the predator-prey based mathematical model: (1) the osteoclastic and osteoblastic lineages contain several intermediate stages (*e.g.* precursors and mature cells) which were not distinguished in this model, and were represented by two terms ‘osteoclast’ and ‘osteoblast’; (2) the factors activating the bone remodelling cycle (such as biological and mechanobiological signals) were not included in the model; (3) the resorption and formation rates are determined by the resorptive and formative activities of osteoclasts and osteoblasts, as well as their populations. However, it was assumed that osteoclasts and osteoblasts both had a constant level of activity during one bone remodelling cycle, and the bone resorption and formation rates were solely related to their population; and (4) the end of the resorption period (and start of the formation period) was defined when the number of osteoclasts fell below 0.5. However, the end of the formation period (and the start of the quiescent period) was defined as the moment when the formed cavity depth reached 99.5% of its maximal value (rather than the time when the osteoblast population fell below 0.5). This inconsistency lies in the underlying predator-prey equations, in which the preys (osteoclasts) thrive again as soon as the predators (osteoblasts) have decreased (and vice versa), and not after a period where neither population is present.

There are four novelties of the proposed model: (1) the adoption of a predator-prey model to replicate the sequential dynamic interaction between osteoclasts and osteoblasts at a BMU; (2) the bone remodelling cycles were reconstructed quantitatively for the first time; (3) a feedback mechanism was used to

maintain the balance of bone thickness during a remodelling cycle; and (4) a genetic algorithm was used to optimize the values of model parameters corresponding to various biochemical conditions, including normal and pathological conditions, based on published experimental data.

The model consisted of three ordinary differential equations, which describe the variation of osteoclast and osteoblast populations, and bone volume with time. The model reconstructed trabecular bone remodelling cycles for normal and two pathological conditions (hypothyroidism and primary hyperparathyroidism). The values of model parameters were actually statistical values of a group of experimental data, and thus the reconstructed remodelling cycle did not correspond to one single bone remodelling cycle, but rather reflected the average of many remodelling cycles. A sensitivity study was conducted to show how the variation in model parameters influenced the maximum populations of osteoclasts and osteoblasts. Also, a stability analysis was performed to determine whether the numerical solution to model equations was stable. The model was partly validated through the comparison between model predictions of maximum osteoclast and osteoblast populations and experimental results. However, further data is still required to confirm model predictions regarding maximum populations of osteoclast and osteoblast under the two pathological conditions.

The bone remodelling process actually involves complex cellular interactions which the predator-prey model does not consider. However the second mathematical model does include those cellular interactions in both normal and a chronic pathological condition that of multiple myeloma (MM). MM is the second most frequent haematological malignancy and can induce a destructive bone disease characterised by bone removal, bone pain and pathological fractures. Ayati et al. (2010) built the first model to simulate MM-induced bone disease, however they did not consider specific cellular mechanisms. Another model developed by Wang et al. (2011) included some of the underlying mechanisms in the development of MM-induced bone disease, but critically did not consider the MM-induced inhibition of osteoblastic activity. In the second half of this thesis, a mathematical model is developed to simulate the pathology of MM-induced bone disease based on the published clinical observations shown in Figure 5.12. The model is based on the work of Pivonka et al. (2008) and was developed in parallel with the work of Wang et al. (2011). It includes the underlying mechanisms of osteoblast inhibition and its

role in the development of MM-induced bone disease. It consists of five ordinary differential equations, describing the temporal variation of bone cells concentrations and bone volume.

Again, there are several limitations in this model: (1) the model did not include all the stages in the lineages of osteoclasts, osteoblasts and MM cells. Only four stages of osteoblasts, three stages of osteoclasts and three stages of MM cells were considered; (2) in addition to the adhesion of bone marrow stromal cell and MM cells, soluble factors produced by MM cells also suppress osteoblast differentiation. However, these were not included in the model as the underlying mechanisms are not fully understood; and (3) it was also assumed that osteoclasts and osteoblasts have a constant level of activity during one bone remodelling cycle, and the bone resorption and formation rates were only dependent on their populations.

The model mimicked bone cell concentrations and bone volume, and investigated how the variations in the levels of OPG, RANKL and PTH influence bone cell concentrations and bone volume in the normal bone microenvironment. These simulation results are consistent with the findings of earlier work (Lemaire et al., 2004; Pivonka et al., 2008). The model was then extended by including the effect of MM cells to simulate how bone cell concentrations vary due to the appearance of tumour cells. This extended model also simulated the variation of the $OB_a:OC_a$ ratio after the invasion of MM cells, which can be used to explain MM-induced bone destruction. Therapies were subsequently simulated (such as bisphosphonates, bortezomib and the inhibition of TGF- β) to demonstrate the model's potential in modelling treatments for MM-induced disease.

Chapter 7 concludes the findings of this study and outlines potential further work that is required to develop the proposed models further.

7. CONCLUSIONS AND FUTURE WORK

Mathematical modelling has the potential to predict and help us understand the behaviour of complex biological systems. The current application of computational simulation in research of biological systems has been demonstrated through a review of existing mathematical models of bone remodelling and the detailed discussion of two new mathematical models in this project.

Bone remodelling is a complicated process and has important biological and biomechanical functions. A greater understanding of the bone remodelling process can help to explain the pathology of bone related diseases, and even propose and evaluate therapeutic treatments. MM-induced bone disease is a major cause of morbidity and remains incurable for the majority of MM patients. The interaction between MM cells and the bone microenvironment is known to form a ‘vicious cycle’ which facilitates the development of the disease. A mathematical model was developed to simulate the bone remodelling process within trabecular bone at the cellular level, while another modelled the interaction between MM cells and the bone microenvironment.

The proposed mathematical model of bone remodelling was used to simulate the dynamic interaction between osteoclasts and osteoblasts and their corresponding resorption and formation activities at a BMU during the bone remodelling process. The model initially reconstructed the variations in osteoclast and osteoblast populations and bone volume with time, during normal bone remodelling cycles. The predicted cellular activity correlated to primary histomorphometry data, plus the pattern of the whole remodelling cycles was predicted. The model was also used to investigate the bone remodelling cycle under the pathological conditions of primary hyperparathyroidism and hypothyroidism. The model predicted the osteoclast and osteoblast populations under these two pathological conditions. However, it was difficult to validate these predictions as there is currently no available data.

A sensitivity study was conducted to show how the variations in model parameters influence the maximum populations of osteoclasts and osteoblasts. Based on this the connection between model parameters and factors involved with bone remodelling is considered with the aim of increasing the physiological representation of the simulations. The model was constructed through a group of nonlinear ordinary differential equations, with a numerical method employed to solve the model

equations. A stability analysis was performed to assess the stability of the numerical method. Although future work is required to validate the model, the predicted data and remodelling cycles compared well with published experimental data. The proposed model has the potential to model a range of pathological conditions and investigate associated treatments of those conditions.

MM is a cancer of the plasma cells in bone marrow and leads to bone pain and fracture, anaemia, infections and other complications. Recent experimental findings have demonstrated the important role of the interaction between MM cells and the bone microenvironment in the development of MM bone disease. In order to integrate these experimental observations, a mathematical model is proposed to simulate how the interaction between MM cells and the bone microenvironment drives the progression of MM bone disease and induces bone destruction. The model is first developed without the MM cells to simulate the normal (healthy) bone microenvironment. Then model was subsequently extended to include the effect of MM cells, to describe the bone microenvironment after the invasion of MM cells. Based on these two mathematical models, it demonstrated how tumour cells influence the bone microenvironment, and how such changes promote the growth and survival of these cells, forming a 'vicious cycle' between the bone microenvironment and MM cells.

The model was used to simulate how cell concentrations fluctuate from the stable state due to the invasion of MM cells, but return to the stable state after the removal of the MM cells. The variation in bone volume with time was also presented to demonstrate the MM-induced bone destruction, and the reason for the bone destruction was revealed by examining the variation in the ratio of active osteoclasts to osteoblasts. The simulation results matched the published data and explained why the lesions resulting from MM-induced bone destruction rarely heal, even after the disappearance of MM cells. A sensitivity study was also performed to show how the variations in eleven model parameters MM concentration and bone volume. The model was also used to simulate three therapeutic interventions including bisphosphonates, bortezomib and TGF- β for MM-induced bone disease.

The mathematical modelling in this thesis of the bone remodelling process and MM-induced bone disease are not complete and the further work is required. The predator-prey based mathematical model has provided encouraging results in quantitatively reconstructing bone remodelling cycles for normal and two

pathological conditions. The model was validated by the consistency of the model's predictions and the experimental data. In addition, it predicted the populations of osteoclasts and osteoblasts under two pathological conditions. Further experimental studies are required to validate this work.

Osteoporosis is a disease caused by a disorder in the bone remodelling process, primarily targeting the elderly and postmenopausal women. The proposed predator-prey based mathematical model could be applied to simulate the pathology of osteoporosis to obtain a greater understanding of the underlying mechanisms of this disease, and evaluate potential treatments in the future.

Another mathematical model successfully simulated the contribution of the interaction between multiple myeloma (MM) cells and the bone microenvironment to the development of MM cells and the induced bone destruction. The simulation results agree with clinical observations well providing some validation of the model. However, the current model did not consider the role of soluble factors produced by MM cells in the inhibition of osteoblastic activity. This is because the process, which involves the Wnt signalling pathway and its underlying mechanisms, is not fully understood. Therefore, the model could be improved by including the effect of soluble factors on the inhibition of osteoblastic activity in future work. The model's potential in modelling therapies for MM-induced bone disease has been demonstrated by simulating these therapies (bisphosphonates, bortezomib and TGF- β). The model could be used to evaluate and find new therapies for MM-induced bone disease in the future.

REFERENCES

- Agerbaek, M.O., Eriksen, E.F., Kragstrup, J., Mosekilde, L., Melsen, F., 1991.** A reconstruction of the remodelling cycle in normal human cortical iliac bone. *Bone and Mineral* 12, 101-112.
- Alexandrakis, M.G., Passam, F.H., Sfiridaki, A., Kandidaki, E., Roussou, P., Kyriakou, D.S., 2003.** Elevated serum concentration of hepatocyte growth factor in patients with multiple myeloma: correlation with markers of disease activity. *American Journal of Hematology* 72, 229-233.
- Alliston, T., Choy, L., Ducy, P., Karsenty, G., Derynck, R., 2001.** TGF-beta-induced repression of CBFA1 by Smad3 decreases cbfa1 and osteocalcin expression and inhibits osteoblast differentiation. *The EMBO Journal* 20, 2254-2272.
- Allori, A.C., Sillon, A.M., Warren, S.M., 2008.** Biological basis of bone formation, remodeling, and repair-part I: biochemical signaling molecules. *Tissue Engineering. Part B, Reviews* 14, 259-273.
- Altabas, V., Berkovic, M., Becejac, B., Solter, M., 2007.** Bone remodeling and thyroid function. *Acta Clinica Croatica* 46, 41-47.
- Atkins, G.J., Kostakis, P., Pan, B.Q., Farrugia, A., Gronthos, S., Evdokiou, A., Harrison, K., Findlay, D.M., Zannettino, A.C.W., 2003.** RANKL expression is related to the differentiation state of human osteoblasts. *Journal Of Bone And Mineral Research* 18, 1088-1098.
- Aubin, J.E., 1998.** Advances in the osteoblast lineage. *Biochemistry and Cell Biology* 76, 899-910.
- Aubin, J.E., Bonnelye, E., 2000.** Osteoprotegerin and its ligand: a new paradigm for regulation of osteoclastogenesis and bone resorption. *Osteoporosis International* 11, 905-913.
- Ayati, B.P., Edwards, C.M., Webb, G.F., Wikswow, J.P., 2010.** A mathematical model of bone remodeling dynamics for normal bone cell populations and myeloma bone disease. *Biology Direct* 20, 28.
- Baron, R., 1999.** Anatomy and ultrastructure of bone, in: Favus, M.J. (Ed.), *Primer on the Metabolic Bone Disease and Disorder of Mineral Metabolism*, 4th ed. Lippincott-Raven, New York, pp. 356-364.
- Bassett, J.H.D., Williams, G.R., 2003.** The molecular actions of thyroid hormone in bone. *Trends in Endocrinology and Metabolism* 14, 356-364.
- Bataille, R., Chappard, D., Alexandre, C., Dessauw, P., Sany, J., 1986.** Importance of Quantitative Histology of Bone Changes in Monoclonal Gammopathy. *British Journal of Cancer* 53, 805-810.

- Bataille, R., Chappard, D., Marcelli, C., Dessauw, P., Baldet, P., Sany, J., Alexandre, C., 1991.** Recruitment of New Osteoblasts and Osteoclasts Is the Earliest Critical Event in the Pathogenesis of Human Multiple-Myeloma. *Journal Of Clinical Investigation* 88, 62-66.
- Bataille, R., Chappard, D., Marcelli, C., Rossi, J.F., Dessauw, P., Baldet, P., Sany, J., Alexandre, C., 1990.** Osteoblast Stimulation in Multiple-Myeloma Lacking Lytic Bone-Lesions. *British Journal of Haematology* 76, 484-487.
- Bell, N.H., 2003.** RANK ligand and the regulation of skeletal remodeling. *Journal of Clinical Investigation* 111, 1120-1122.
- Bentolila, V., Boyce, T.M., Fyhrie, D.P., Drumb, R., Skerry, T.M., Schaffler, M.B., 1998.** Intracortical remodeling in adult rat long bones after fatigue loading. *Bone* 23, 275-281.
- Bilezikian, J.P., 1990.** Hyperparathyroidism, in: Stein, J.H. (Ed.), *International Medicine*, 2nd ed. Little Brown, Boston, pp. 2372-2378.
- Bilezikian, J.P., 1993.** Primary hyperparathyroidism, in: Favus, M.J. (Ed.), *Primer on the Metabolic Bone Disease and Disorder of Mineral Metabolism*, 4th ed. Lippincott – Raven, New York, pp. 33-37.
- Bland, R., 2000.** Steroid hormone receptor expression and action in bone. *Clinical Science* 98, 217-240.
- Blum, B., Moseley, J., Miller, L., Richelsoff, K., Haggard, W., 2004.** Measurement of bone morphogenetic proteins and other growth factors in demineralized bone matrix. *Orthopedics* 27, 161-165.
- Bonewald, L.F., 2004.** Osteocyte biology: its implications for osteoporosis. *Journal of Musculoskeletal & Neuronal Interactions* 4, 101-104.
- Bonewald, L.F., Dallas, S.L., 1994a.** Role of Active and Latent Transforming Growth-Factor-Beta in Bone-Formation. *Journal of Cellular Biochemistry* 55, 350-357.
- Bonewald, L.F., Dallas, S.L., 1994b.** Role of active and latent transforming growth factor beta in bone formation. *Journal of Cellular Biochemistry* 55, 350-357.
- Boyce, B.F., Xing, L.P., 2008.** Functions of RANKL/RANK/OPG in bone modeling and remodeling. *Archives of Biochemistry and Biophysics* 473, 139-146.
- Boyle, W.J., Simonet, W.S., Lacey, D.L., 2003.** Osteoclast differentiation and activation. *Nature* 423, 337-342.
- Brauer, F., Castillo-Chávez, C., 2001.** *Mathematical models in population biology and epidemiology*. Springer.
- Bronner, F., Worrell, R.V., 1999.** *Orthopaedics: Principles of Basic and Clinical Science*. CRC Press, Boca Raton.

- Buenzli, P.R., Pivonka, P., Smith, D.W., 2011.** Spatio-temporal structure of cell distribution in cortical Bone Multicellular Units: A mathematical model. *Bone* 48, 918-926.
- Burgess, T.L., Qian, Y., Kaufman, S., Ring, B.D., Van, G., Capparelli, C., Kelley, M., Hsu, H., Boyle, W.J., Dunstan, C.R., Hu, S., Lacey, D.L., 1999.** The ligand for osteoprotegerin (OPGL) directly activates mature osteoclasts. *The Journal of Cell Biology* 145, 527-538.
- Burr, D.B., 1997.** Muscle strength, bone mass, and age-related bone loss. *Journal of Bone and Mineral Research* 12, 1547-1551.
- Burr, D.B., 2002.** Targeted and nontargeted remodeling. *Bone* 30, 2-4.
- Calvani, N., Silvestris, F., Cafforio, P., Dammacco, F., 2004.** Osteoclast-like cell formation by circulating myeloma B lymphocytes: role of RANK-L. *Leukemia & Lymphoma* 45, 377-380.
- Canalis, E., 1993.** Regulation of Bone Remodelling, in: Favus, M.J. (Ed.), *Primer on the Metabolic Bone Disease and Disorder of Mineral Metabolism*, 4th ed. Lippincott – Raven, New York, pp. 33-37.
- Canalis, E., Centrella, M., Burch, W., McCarthy, T.L., 1989.** Insulin-like growth factor I mediates selective anabolic effects of parathyroid hormone in bone cultures. *The Journal of Clinical Investigation* 83, 60-65.
- Chappard, D., Baslé M.F., Audran, M., Benhamou, C.L., Rebel, A., 1996.** Osteoclast Cytomorphometry in Patients with Femoral Neck Fracture. *Pathology - Research and Practice* 192, 573-578.
- Cheng, X., Kinosaki, M., Takami, M., Choi, Y., Zhang, H., Murali, R., 2004.** Disabling of receptor activator of nuclear factor-kappaB (RANK) receptor complex by novel osteoprotegerin-like peptidomimetics restores bone loss in vivo. *The Journal of Biological Chemistry* 279, 8269-8277.
- Chigae, A., Blenc, A.M., Braaten, J.V., Kumaraswamy, N., Kepley, C.L., Andrews, R.P., Oliver, J.M., Edwards, B.S., Prossnitz, E.R., Larson, R.S., Sklar, L.A., 2001.** Real time analysis of the affinity regulation of alpha 4-integrin. The physiologically activated receptor is intermediate in affinity between resting and Mn(2+) or antibody activation. *Journal of Biological Chemistry* 276, 48670-48678.
- Christiansen, C., 1999.** Introduction to Osteoporosis. *Medical Science Symposia Series* 13, 109-116.
- Christiansen, P., 2001.** The skeleton in primary hyperparathyroidism: A review focusing on bone remodeling, structure, mass, and fracture. *APMIS* 109, 5-52.
- Cohen, M.M., 1997.** Transforming growth factor beta s and fibroblast growth factors and their receptors: role in sutural biology and craniosynostosis. *Journal of Bone and Mineral Research* 12, 322-331.

Collin-Osdoby, P., Rothe, L., Anderson, F., Nelson, M., Maloney, W., Osdoby, P., 2001. Receptor activator of NF-kappa B and osteoprotegerin expression by human microvascular endothelial cells, regulation by inflammatory cytokines, and role in human osteoclastogenesis. *Journal of Biological Chemistry* 276, 20659-20672.

Cox, W., 1996. Ordinary Differential Equations. Arnold.

Defranoux, N.A., Stokes, C.L., Young, D.L., Kahn, A.J., 2005. In silico modeling and simulation of bone biology: a proposal. *Journal of Bone and Mineral Research* 20, 1079-1084.

Dempster, D.W., Cosman, F., Parisien, M., Shen, V., Lindsay, R., 1993. Anabolic actions of parathyroid hormone on bone. *Endocrine reviews* 14, 690-709.

Di Ventura, B., Lemerle, C., Michalodimitrakis, K., Serrano, L., 2006. From in vivo to in silico biology and back. *Nature* 443, 527-533.

Diamond, T., Levy, S., Day, P., Barbagallo, S., Manoharan, A., Kwan, Y.K., 1997. Biochemical, histomorphometric and densitometric changes in patients with multiple myeloma: effects of glucocorticoid therapy and disease activity. *British Journal Haematology* 97, 641-648.

Edwards, C.M., Zhuang, J., Mundy, G.R., 2008. The pathogenesis of the bone disease of multiple myeloma. *Bone* 42, 1007-1013.

Eijken, M., 2007. Human Osteoblast Differentiation and Bone Formation: Growth Factors, Hormones and Regulatory Networks [PhD Thesis]. [Rotterdam, The Netherlands]; Erasmus Universiteit.

Einhorn, T.A., 1996. The bone organ system: Form and Function, in: Marcus, R., Feldman, D., Kelsey, J. (Eds.), *Osteoporosis*. Academic Press, San Diego, pp. 3-21.

Eriksen, E.F., Gundersen, H.J., Melsen, F., Mosekilde, L., 1984b. Reconstruction of the formative site in iliac trabecular bone in 20 normal individuals employing a kinetic model for matrix and mineral apposition. *Metabolic Bone Disease & Related Research* 5, 243-252.

Eriksen, E.F., Kassem, M., 1992. The cellular basis of bone remodelling. Triangle; *The Sandoz Journal of Medical Science* 31, 45-57.

Eriksen, E.F., Melsen, F., Mosekilde, L., 1984a. Reconstruction of the resorptive site in iliac trabecular bone: a kinetic model for bone resorption in 20 normal individuals. *Metabolic Bone Disease & Related Research* 5, 235-242.

Eriksen, E.F., Mosekilde, L., Melsen, F., 1985. Trabecular Bone Remodeling and Bone Balance in Hyperthyroidism. *Bone* 6, 421-428.

Eriksen, E.F., Mosekilde, L., Melsen, F., 1986a. Kinetics of trabecular bone resorption and formation in hypothyroidism: evidence for a positive balance per remodeling cycle. *Bone* 7, 101-108.

Eriksen, E.F., Mosekilde, L., Melsen, F., 1986b. Trabecular bone remodeling and balance in primary hyperparathyroidism. *Bone* 7, 213-221.

Erlebacher, A., Filvaroff, E.H., Ye, J.Q., Derynck, R., 1998. Osteoblastic responses to TGF-beta during bone remodeling. *Molecular Biology of the Cell* 9, 1903-1918.

Fan, X., Roy, E., Zhu, L., Murphy, T.C., Ackert-Bicknell, C., Hart, C.M., Rosen, C., Nanes, M.S., Rubin, J., 2004. Nitric oxide regulates receptor activator of nuclear factor-kappaB ligand and osteoprotegerin expression in bone marrow stromal cells. *Endocrinology* 145, 751-759.

Filvaroff, E., Derynck, R., 1998. Bone remodelling: A signalling system for osteoclast regulation. *Current Biology* 8, 679-682.

Fowler, J.A., Edwards, C.M., Croucher, P.I., 2011. Tumor-host cell interactions in the bone disease of myeloma. *Bone* 48, 121-128.

Frost, H.M., 1979. Treatment of osteoporoses by manipulation of coherent bone cell populations. *Clinical Orthopaedics And Related Research*, 227-244.

Frost, H.M., 1986. *Intermediary Organization of the Skeleton*. CRC Press, Boca Raton.

Frost, H.M., 1987. The Mechanostat - a Proposed Pathogenic Mechanism of Osteoporoses and the Bone Mass Effects of Mechanical and Nonmechanical Agents. *Bone and Mineral* 2, 73-85.

Fuller, K., Lean, J.M., Bayley, K.E., Wani, M.R., Chambers, T.J., 2000. A role for TGFbeta(1) in osteoclast differentiation and survival. *Journal of Cell Science* 113, 2445-2453.

Gause, G.F., Smaragdova, N.P., Witt, A.A., 1936. Further Studies of Interaction between Predators and Prey. *Journal of Animal Ecology* 5, 1-18.

Gehron, R.P., Boskey, A.L., 1996. The biochemistry of bone, in: Marcus, F., D., D.F., Kelsey, J. (Eds.), *Osteoporosis*. Academic Press, San Diego, pp. 95-156.

Gilsanz, V., Gibbens, D.T., Carlson, M., Boechat, M.I., Cann, C.E., Schulz, E.E., 1988. Peak trabecular vertebral density: a comparison of adolescent and adult females. *Calcified Tissue International* 43, 260-262.

Gittoes, N.J.L., Franklyn, J.A., 1998. Hyperthyroidism - Current treatment guidelines. *Drugs* 55, 543-553.

Glowacki, J., 1996. The cellular and biochemical aspects of bone remodelling, in: Rosen, C.J. (Ed.), *Osteoporosis: Diagnostic and Therapeutic Principles*. Human Press Inc., Totowa, pp. 1-15.

Goltzman, D., 1999. Interactions of PTH and PTHrP with the PTH/PTHrP receptor and with downstream signaling pathways: Exceptions that provide the rules. *Journal of Bone and Mineral Research* 14, 173-177.

Goranova-Marinova, V., Goranov, S., Pavlov, P., Tzvetkova, T., 2007. Serum levels of OPG, RANKL and RANKL/OPG ratio in newly-diagnosed patients with multiple myeloma. *Clinical Correlations. Haematologica* 92, 1000-1001.

Gorski, J.P., 1998. Is all bone the same? Distinctive distributions and properties of non-collagenous matrix proteins in lamellar vs. woven bone imply the existence of different underlying osteogenic mechanisms. *Critical Reviews in Oral Biology and medicine* 9, 201-223.

Gray, A., Mezzino, M., Pinsky, M.A., 1997. *Introduction to ordinary differential equations with mathematica.* Wylde, New York.

Greenfield, E.M., Bi, Y., Miyauchi, A., 1999. Regulation of osteoclast activity. *Life Sciences* 65, 1087-1102.

Guisse, T.A., Chirgwin, J.M., 2003. Transforming growth factor-beta in osteolytic breast cancer bone metastases. *Clinical Orthopaedics and Related Research*, 32-38.

Gunther, T., Schinke, T., 2000. Mouse genetics have uncovered new paradigms in bone biology. *Trends in Endocrinology and Metabolism* 11, 189-193.

Halladay, D.L., Miles, R.R., Thirunavukkarasu, K., Chandrasekhar, S., Martin, T.J., Onyia, J.E., 2001. Identification of signal transduction pathways and promoter sequences that mediate parathyroid hormone 1-38 inhibition of osteoprotegerin gene expression. *Journal of Cellular Biochemistry* 84, 1-11.

Hauschka, P.V., 1989. Growth factors effects, in: Hall, B.K. (Ed.), *Bone.* CRC Press, Boca Raton.

Heider, U., Hofbauer, L.C., Zavrski, I., Kaiser, M., Jakob, C., Sezer, O., 2005. Novel aspects of osteoclast activation and osteoblast inhibition in myeloma bone disease. *Biochemical Biophysical Research Communications* 338, 687-693.

Hernandez, C.J., Beaupre, G.S., Carter, D.R., 2000. A model of mechanobiologic and metabolic influences on bone adaptation. *Journal of Rehabilitation Research and Development* 37, 235-244.

Hideshima, T., Mitsiades, C., Tonon, G., Richardson, P.G., Anderson, K.C., 2007. Understanding multiple myeloma pathogenesis in the bone marrow to identify new therapeutic targets. *Nature reviews. Cancer* 7, 585-598.

Hiorns, R.W., Cooke, D., Mathematics, I.o., Applications, I., 1981. The Mathematical theory of the dynamics of biological populations II: based on the proceedings of a conference on the mathematical theory of the dynamics of biological populations held in Oxford, 1st-3rd July, 1980. Academic Press.

- Hock, J.M., Gera, I., 1992.** Effects of continuous and intermittent administration and inhibition of resorption on the anabolic response of bone to parathyroid hormone. *Journal of Bone and Mineral Research* 7, 65-72.
- Hofbauer, L.C., Khosla, S., Dunstan, C.R., Lacey, D.L., Boyle, W.J., Riggs, B.L., 2000.** The roles of osteoprotegerin and osteoprotegerin ligand in the paracrine regulation of bone resorption. *Journal of Bone and Mineral Research* 15, 2-12.
- Hofbauer, L.C., Kuhne, C.A., Viereck, V., 2004.** The OPG/RANKL/RANK system in metabolic bone diseases. *Journal of Musculoskeletal & Neuronal Interactions* 4, 268-275.
- Hofbauer, L.C., Neubauer, A., Heufelder, A.E., 2001.** Receptor activator of nuclear factor-kappa B ligand and osteoprotegerin - Potential implications for the pathogenesis and treatment of malignant bone diseases. *Cancer* 92, 460-470.
- Hofbauer, L.C., Schoppet, M., 2004.** Clinical implications of the osteoprotegerin/RANKL/RANK system for bone and vascular diseases. *The Journal of the American Medical Association* 292, 490-495.
- Holtrop, M.E., Weinger, J.M., 1972.** Ultrastructural evidence for a transport system in bone, in: Talmage, R.V., Munson, P.L. (Eds.), *Calcium, Parathyroid Hormone and Calcitonins. Excerpta Medica*, Amsterdam.
- Hoppensteadt, F., 2006.** Predator-prey model, Scholarpedia, p. 1563.
- Horwood, N.J., Elliott, J., Martin, T.J., Gillespie, M.T., 1998a.** Osteotropic agents regulate the expression of osteoclast differentiation factor and osteoprotegerin in osteoblastic stromal cells. *Endocrinology* 139, 4743-4746.
- Ishikawa, Y., Genge, B.R., Wuthier, R.E., Wu, L.N., 1998.** Thyroid hormone inhibits growth and stimulates terminal differentiation of epiphyseal growth plate chondrocytes. *Journal of Bone and Mineral Research* 13, 1398-1411.
- Ismal, N.M., 1997.** Postmenopausal osteoporosis: epidemiology, pathophysiology and treatment. *The Malaysian Journal of Pathology* 19, 21-25.
- Itoh, K., Udagawa, N., Matsuzaki, K., Takami, M., Amano, H., Shinki, T., Ueno, Y., Takahashi, N., Suda, T., 2000.** Importance of membrane- or matrix-associated forms of M-CSF and RANKL/ODF in osteoclastogenesis supported by SaOS-4/3 cells expressing recombinant PTH/PTHrP receptors. *Journal of Bone and Mineral Research* 15, 1766-1775.
- Janssens, K., ten Dijke, P., Janssens, S., Van Hul, W., 2005.** Transforming growth factor-beta1 to the bone. *Endocrine reviews* 26, 743-774.
- Jaworski, Z.F.G., Duck, B., Sekaly, G., 1981.** Kinetics of Osteoclasts and Their Nuclei in Evolving Secondary Haversian Systems. *Journal of Anatomy* 133, 397-405.
- Jaworski, Z.F.G., Hooper, C., 1980.** Study of Cell-Kinetics within Evolving Secondary Haversian Systems. *Journal of Anatomy* 131, 91-102.

Jaworski, Z.F.G., Lok, E., Wellington, J.L., 1975. Impaired Osteoclastic Function and Linear Bone Erosion Rate in Secondary Hyperparathyroidism Associated with Chronic Renal-Failure. *Clinical Orthopaedics and Related Research*, 298-310.

Jee, W.S., 2001. Integrated bone tissue physiology: anatomy and physiology, in: S, C. (Ed.), *Bone mechanics handbook*. CRC press, London, pp. 1-68.

Jee, W.S.S., Ma, Y.F., 1997. The in vivo anabolic actions of prostaglandins in bone. *Bone* 21, 297-304.

Jemal, A., Tiwari, R.C., Murray, T., Ghafour, A., Samuels, A., Ward, E., Feuer, E.J., Thun, M.J., 2004. Cancer statistics. *A Cancer Journal for Clinicians* 54, 8-29.

Ji, B., Genever, P., Patton, R., Putra, D., Fagan, M., 2012. A novel mathematical model of bone remodelling cycles for trabecular bone at the cellular level. *Biomechanics and Modeling in Mechanobiology* 11, 973-982.

Kanatani, M., Sugimoto, T., Sowa, H., Kobayashi, T., Kanzawa, M., Chihara, K., 2004. Thyroid hormone stimulates osteoclast differentiation by a mechanism independent of RANKL-RANK interaction. *Journal of Cellular Physiology* 201, 17-25.

Kanis, J.A., 1996. Maintenance of bone mass, in: Kanis, J.A. (Ed.), *Textbook of Osteoporosis*. Blackwell Science Ltd, Oxford, pp. 1-28.

Kassem, M., Melton, L.J., Riggs, B.L., 1996. The Type I/Type II Model for Involutional Osteoporosis, in: MARCUS, R., Feldman, D., Kelsey, J. (Eds.), *Osteoporosis*. Academic Press, San Diego, pp. 691-700.

Kawaguchi, H., Pilbeam, C.C., Harrison, J.R., Raisz, L.G., 1995. The role of prostaglandins in the regulation of bone metabolism. *Clinical Orthopaedics and Related Research*, 36-46.

Kessenich, C.R., Rosen, C.J., 1996. The Pathophysiology of osteoporosis, in: Rosen, C.J. (Ed.), *Osteoporosis: Diagnostic and Therapeutic Principles*. Human Press, New Jersey, pp. 47-63.

Kleerekoper, M., Avioli, L.V., 1990. Evaluation and treatment of postmenopausal osteoporosis, in: Favus, M.J. (Ed.), *Primer on the Metabolic Bone Diseases and Disorders of Mineral Metabolism*, Second Edition ed. Lippincott-Raven, New York, pp. 223-228.

Klein, B., Zhang, X.G., Lu, Z.Y., Bataille, R., 1995. Interleukin-6 in Human Multiple-Myeloma. *Blood* 85, 863-872.

Komarova, S.V., Smith, R.J., Dixon, S.J., Sims, S.M., Wahl, L.M., 2003. Mathematical model predicts a critical role for osteoclast autocrine regulation in the control of bone remodeling. *Bone* 33, 206-215.

Kong, Y.Y., Yoshida, H., Sarosi, I., Tan, H.L., Timms, E., Capparelli, C., Morony, S., Oliveira-dos-Santos, A.J., Van, G., Itie, A., Khoo, W., Wakeham, A., Dunstan, C.R., Lacey, D.L., Mak, T.W., Boyle, W.J., Penninger, J.M., 1999. OPGL is a key regulator of osteoclastogenesis, lymphocyte development and lymph-node organogenesis. *Nature* 397, 315-323.

Kroll, M.H., 2000. Parathyroid hormone temporal effects on bone formation and resorption. *Bulletin of Mathematical Biology* 62, 163-188.

Kuang, Y., 1988. Nonuniqueness of limit cycles of Gause-type predator-prey systems. *Applicable Analysis* 29, 269-287.

Kuang, Y., 1990. Global Stability of Gause-Type Predator-Prey Systems. *Journal of Mathematical Biology* 28, 463-474.

Kuehl, W.M., Bergsagel, P.L., 2002. Multiple myeloma: evolving genetic events and host interactions. *Nature reviews. Cancer* 2, 175-187.

Kwan Tat, S., Padrines, M., Theoleyre, S., Heymann, D., Fortun, Y., 2004. IL-6, RANKL, TNF-alpha/IL-1: interrelations in bone resorption pathophysiology. *Cytokine Growth Factor Reviews* 15, 49-60.

Lanyon, L.E., 1996. Using functional loading to influence bone mass and architecture: Objectives, mechanisms, and relationship with estrogen of the mechanically adaptive process in bone. *Bone* 18, 37-43.

Lanyon, L.E., Rubin, Raisz, Marotti, Lees, 1993. Osteocytes, Strain Detection, Bone Modeling and Remodeling. *Calcified Tissue International* 53, 102-107.

Lee, S.K., Lorenzo, J.A., 1999. Parathyroid hormone stimulates TRANCE and inhibits osteoprotegerin messenger ribonucleic acid expression in murine bone marrow cultures: correlation with osteoclast-like cell formation. *Endocrinology* 140, 3552-3561.

Lemaire, V., Tobin, F.L., Greller, L.D., Cho, C.R., Suva, L.J., 2004. Modeling the interactions between osteoblast and osteoclast activities in bone remodeling. *Journal of Theoretical Biology* 229, 293-309.

Li, X., Pennisi, A., Yaccoby, S., 2008. Role of decorin in the antimyeloma effects of osteoblasts. *Blood* 112, 159-168.

Lian, J.B., Stein, G.S., Canalis, E., Gehron-Robey, P., Boskey, A.L., 1999. Bone formation: osteoblast lineage cells, growth factors, matrix proteins and the mineralization process, in: Favus, M. (Ed.), *Primer on the Metabolic Bone Diseases and Disorders of Mineral Metabolism*, 4th ed. Lippincott/Williams & Wilkins, Philadelphia.

Lipton, A., Ali, S.M., Leitzel, K., Chinchilli, V., Witters, L., Engle, L., Holloway, D., Bekker, P., Dunstan, C.R., 2002. Serum osteoprotegerin levels in healthy controls and cancer patients. *Clinical Cancer Research* 8, 2306-2310.

- Lorenzo, J.A., 1991.** The role of cytokines in the regulation of local bone resorption. *Critical Reviews in Immunology* 11, 195-213.
- Ma, Y.L., Cain, R.L., Halladay, D.L., Yang, X., Zeng, Q., Miles, R.R., Chandrasekhar, S., Martin, T.J., Onyia, J.E., 2001.** Catabolic effects of continuous human PTH (1--38) in vivo is associated with sustained stimulation of RANKL and inhibition of osteoprotegerin and gene-associated bone formation. *Endocrinology* 142, 4047-4054.
- Majeska, R.J., 2001.** Cell biology of bone, in: Cowin, S.C. (Ed.), *Bone Mechanics Handbook*, 2nd ed. CRC Press, Washington.
- Manolagas, S.C., 2000.** Birth and death of bone cells: Basic regulatory mechanisms and implications for the pathogenesis and treatment of osteoporosis. *Endocrine Reviews* 21, 115-137.
- Martin, B., 1995.** Mathematical-Model for Repair of Fatigue Damage and Stress-Fracture in Osteonal Bone. *Journal of Orthopaedic Research* 13, 309-316.
- Martin, R.B., Burr, D.B., Sharkey, N.A., 1998.** *Skeletal tissue mechanics*. Springer, New York.
- Martin, T.J., 2004.** Paracrine regulation of osteoclast formation and activity: milestones in discovery. *Journal of Musculoskeletal & Neuronal Interactions* 4, 243-253.
- Martin, T.J., Sims, N.A., 2005.** Osteoclast-derived activity in the coupling of bone formation to resorption. *Trends in Molecular Medicine* 11, 76-81.
- Mathews, J.H., Fink, K.D., 2004.** *Numerical methods using Matlab*, 4th ed. Prentice-Hall Inc, New Jersey, USA.
- MathWorks, 2011.** Global Optimization Toolbox [online].
- Matsumoto, T., Abe, M., 2011.** TGF-beta-related mechanisms of bone destruction in multiple myeloma. *Bone* 48, 129-134.
- Matsuo, K., Irie, N., 2008.** Osteoclast-osteoblast communication. *Archives of Biochemistry Biophysics* 473, 201-209.
- McLeod, K.J., Rubin, C.T., Otter, M.W., Qin, Y.X., 1998.** Skeletal cell stresses and bone adaptation. *The American Journal of the Medical Sciences* 316, 176-183.
- Melsen, F., Mosekilde, L., 1977.** Morphometric and dynamic studies of bone changes in hyperthyroidism. Acta pathologica et microbiologica Scandinavica. Section A, *Pathology* 85A, 141-150.
- Meng, X.W., Liang, X.G., Birchman, R., Wu, D.D., Dempster, D.W., Lindsay, R., Shen, V., 1996.** Temporal expression of the anabolic action of PTH in cancellous bone of ovariectomized rats. *Journal of Bone and Mineral Research* 11, 421-429.

- Miller, S.C., Bowman, B.M., Smith, J.M., Jee, W.S., 1980.** Characterization of endosteal bone-lining cells from fatty marrow bone sites in adult beagles. *The Anatomical Record* 198, 163-173.
- Miller, S.C., Jee, W.S., 1987.** The bone lining cell: a distinct phenotype? *Calcified Tissue International* 41, 1-5.
- Miramontes, P., 1992.** A cellular automaton model for the evolution of nucleic acids. UNAM.
- Miura, M., Tanaka, K., Komatsu, Y., Suda, M., Yasoda, A., Sakuma, Y., Ozasa, A., Nakao, K., 2002.** A novel interaction between thyroid hormones and 1,25(OH)(2)D-3 in osteoclast formation. *Biochemical and Biophysical Research Communications* 291, 987-994.
- Mizuno, A., Amizuka, N., Irie, K., Murakami, A., Fujise, N., Kanno, T., Sato, Y., Nakagawa, N., Yasuda, H., Mochizuki, S., Gomibuchi, T., Yano, K., Shima, N., Washida, N., Tsuda, E., Morinaga, T., Higashio, K., Ozawa, H., 1998.** Severe osteoporosis in mice lacking osteoclastogenesis inhibitory factor osteoprotegerin. *Biochemical and Biophysical Research Communications* 247, 610-615.
- Momsen, G., Schwarz, P., 1997.** A mathematical/physiological model of parathyroid hormone secretion in response to blood-ionized calcium lowering in vivo. *Scandinavian Journal of Clinical and Laboratory Investigation* 57, 381-394.
- Mori, S., Burr, D.B., 1993.** Increased Intracortical Remodeling Following Fatigue Damage. *Bone* 14, 103-109.
- Moroz, A., Crane, M.C., Smith, G., Wimpenny, D.I., 2006.** Phenomenological model of bone remodeling cycle containing osteocyte regulation loop. *Biosystems* 84, 183-190.
- Mosekilde, L., Melsen, F., 1978a.** Morphometric and dynamic studies of bone changes in hypothyroidism. *Acta pathologica et microbiologica Scandinavica*. Section A, *Pathology* 86, 56-62.
- Mosekilde, L., Melsen, F., 1978b.** A tetracycline-based histomorphometric evaluation of bone resorption and bone turnover in hyperthyroidism and hyperparathyroidism. *Acta medica Scandinavica* 204, 97-102.
- Mundy, G.R., 1999.** Cellular and molecular regulation of bone turnover. *Bone* 24, 35-38.
- Mundy, G.R., Boyce, B.F., 1996.** Cytokines and bone remodelling, in: Marcus, R., Feldman, D., Kelsey, J. (Eds.), *Osteoporosis*. Academic Press, New York, pp. 301-313.
- Mundy, G.R., Boyce, B.F., Yoneda, T., Bonewald, L.F., Roodman, G.D., 1996.** Cytokines and bone remodelling, in: Marcus, R., Feldman, D., Kelsey, J. (Eds.), *Osteoporosis*. Academic Press, New York, pp. 301-313.

Mundy, G.R., Shapiro, J.L., Bandelin, J.G., Canalis, E.M., Raisz, L.G., 1976. Direct Stimulation of Bone-Resorption by Thyroid-Hormones. *Journal Clinical Investigation* 58, 529-534.

MyPhysicsLab, 2011. Numerical and analytic solutions, online.

Nagle, R.K., Saff, E.B., Snider, A.D., 2008. *Fundamentals Of Differential Equations*. Pearson Education, Inc, Boston.

Nakchbandi, I.A., Lang, R., Kinder, B., Insogna, K.L., 2008. The role of the receptor activator of nuclear factor-kappaB ligand/osteoprotegerin cytokine system in primary hyperparathyroidism. *The Journal of Clinical Endocrinology & Metabolism* 93, 967-973.

Nau, K.C., Lewis, W.D., 2008. Multiple myeloma: diagnosis and treatment. *Americal Family Physician* 78, 853-859.

Noble, B., 2003. Bone microdamage and cell apoptosis. *European Cells & Materials* 6, 46-55.

ODE Laboratories, 2011. Numerical methods for solving differential equations, online.

Onyia, J.E., Miles, R.R., Yang, X., Halladay, D.L., Hale, J., Glasebrook, A., McClure, D., Seno, G., Churgay, L., Chandrasekhar, S., Martin, T.J., 2000. In vivo demonstration that human parathyroid hormone 1-38 inhibits the expression of osteoprotegerin in bone with the kinetics of an immediate early gene. *Journal of Bone and Mineral Research* 15, 863-871.

Parfitt, A.M., 1983. The physiologic and clinical significance of bone histomorphometric data, in: Recker, R.R. (Ed.), *Bone Histomorphometry: Techniques and Interpretation*. CRC Press, Boca Raton.

Parfitt, A.M., 1994. Osteonal and Hemi-Osteonal Remodeling - the Spatial and Temporal Framework for Signal Traffic in Adult Human Bone. *Journal of Cellular Biochemistry* 55, 273-286.

Parfitt, A.M., 2000. The mechanism of coupling: a role for the vasculature. *Bone* 26, 319-323.

Pfeilschifter, J., Mundy, G.R., 1987. Modulation of Type-Beta Transforming Growth-Factor Activity in Bone Cultures by Osteotropic Hormones. *Proceedings of the National Academy of Science of USA* 84, 2024-2028.

Pivonka, P., Zimak, J., Smith, D.W., Gardiner, B.S., Dunstan, C.R., Sims, N.A., Martin, T.J., Mundy, G.R., 2008. Model structure and control of bone remodeling: A theoretical study. *Bone* 43, 249-263.

- Pivonka, P., Zimak, J., Smith, D.W., Gardiner, B.S., Dunstan, C.R., Sims, N.A., Martin, T.J., Mundy, G.R., 2010.** Theoretical investigation of the role of the RANK-RANKL-OPG system in bone remodeling. *Journal of Theoretical Biology* 262, 306-316.
- Putra, D., Patton R.J., Genever, P., Fagan, M.J., 2009.** Mathematical Model of Remodelling Cycles with Feedback Mechanism for Maintaining the Balance between Bone Resorption and Formation, *Journal of Bone and Mineral Research* 23, 1280.
- Rabaglio, M., Sun, Z., Price, K.N., Castiglione-Gertsch, M., Hawle, H., Thurlimann, B., Mouridsen, H., Campone, M., Forbes, J.F., Paridaens, R.J., Colleoni, M., Pienkowski, T., Nogaret, J.M., Lang, I., Smith, I., Gelber, R.D., Goldhirsch, A., Coates, A.S., Breast, B.-C.I., 2009.** Bone fractures among postmenopausal patients with endocrine-responsive early breast cancer treated with 5 years of letrozole or tamoxifen in the BIG 1-98 trial. *Annals of Oncology* 20, 1489-1498.
- Raisz, L.G., 1999.** Physiology and pathophysiology of bone remodeling (vol 45, pg 1353, 1999). *Clinical Chemistry* 45, 1885-1885.
- Rajkumar, S.V., 2011.** Patient information: Multiple myeloma symptoms, diagnosis, and staging (Beyond the Basics). *UpToDate*, online.
- Rattanakul, C., Lenbury, Y., Krishnamara, N., Wollkind, D.J., 2003.** Modeling of bone formation and resorption mediated by parathyroid hormone: response to estrogen/PTH therapy. *Biosystems* 70, 55-72.
- Recker, R.R., 1983.** *Bone Histomorphometry: Techniques and Interpretation*. CRC Press, Boca Raton, FL, .
- Riggs, B.L., 1991.** Overview of osteoporosis. *The Western Journal of Medicine* 154, 63-77.
- Riggs, B.L., Melton, L.J., 3rd, 1992.** The prevention and treatment of osteoporosis. *The New England journal of medicine* 327, 620-627.
- Robling, A.G., Castillo, A.B., Turner, C.H., 2006.** Biomechanical and molecular regulation of bone remodeling. *Annual Reviews of Biomedical Engineering* 8, 455-498.
- Rodan, G.A., Martin, T.J., 2000.** Therapeutic approaches to bone diseases. *Science* 289, 1508-1514.
- Roodman, G.D., 1996.** Advances in bone biology: the osteoclast. *Endocrine reviews* 17, 308-332.
- Roodman, G.D., 1999.** Cell biology of the osteoclast. *Experimental Hematology* 27, 1229-1241.
- Roodman, G.D., 2004.** Pathogenesis of myeloma bone disease. *Blood Cells, Molecules & Diseases* 32, 290-292.

Roodman, G.D., 2006. Regulation of osteoclast differentiation. *Annals of the New York Academy of Sciences* 1068, 100-109.

Roodman, G.D., 2011. Osteoblast function in myeloma. *Bone* 48, 135-140.

Ryser, M.D., Komarova, S.V., Nigam, N., 2010. The cellular dynamics of bone remodeling: a mathematical model. *SIAM Journal on Applied Mathematics* 70, 1899-1921.

Ryser, M.D., Nigam, N., Komarova, S.V., 2007. Spatio-temporal dynamics of a single bone remodeling. *Journal of Bone and Mineral Research* 22, 68-69.

Salmon, S.E., Smith, B.A., 1970. Immunoglobulin synthesis and total body tumor cell number in IgG multiple myeloma. *Journal of Clinical Investigation* 49, 1114-1121.

Samuels, M.H., Veldhuis, J., Cawley, C., Urban, R.J., Luther, M., Bauer, R., Mundy, G., 1993. Pulsatile secretion of parathyroid hormone in normal young subjects: assessment by deconvolution analysis. *Journal of Clinical Endocrinology & Metabolism* 77, 399-403.

Schmitt, C.P., Huber, D., Mehls, O., Maiwald, J., Stein, G., Veldhuis, J.D., Ritz, E., Schaefer, F., 1998. Altered instantaneous and calcium-modulated oscillatory PTH secretion patterns in patients with secondary hyperparathyroidism. *Journal of the American society of nephrology* 9, 1832-1844.

Schulz, A., Bressel, M., Delling, G., 1976. Activity of osteoclastic bone resorption in primary hyperparathyroidism — a comparative electron microscopic and histomorphometric study. *Calcified Tissue International* 22, 307-310.

Seeman, E., 2003. Reduced bone formation and increased bone resorption: rational targets for the treatment of osteoporosis. *Osteoporosis International* 14, 2-8.

Seeman, E., Delmas, P.D., 2006. Bone quality--the material and structural basis of bone strength and fragility. *The New England journal of medicine* 354, 2250-2261.

Seidel, C., Hjertner, O., Abildgaard, N., Heickendorff, L., Hjorth, M., Westin, J., Nielsen, J.L., Hjorth-Hansen, H., Waage, A., Sundan, A., Borset, M., 2001. Serum osteoprotegerin levels are reduced in patients with multiple myeloma with lytic bone disease. *Blood* 98, 2269-2271.

Simmons, D.J., Grynopas, M.D., 1990. Mechanisms of bone formation in vivo, in: Hall, B.K. (Ed.), *Bone*. CRC Press, Boca Raton.

Simonet, W.S., Lacey, D.L., Dunstan, C.R., Kelley, M., Chang, M.S., Luthy, R., Nguyen, H.Q., Wooden, S., Bennett, L., Boone, T., Shimamoto, G., DeRose, M., Elliott, R., Colombero, A., Tan, H.L., Trail, G., Sullivan, J., Davy, E., Bucay, N., RenshawGegg, L., Hughes, T.M., Hill, D., Pattison, W., Campbell, P., Sander, S., Van, G., Tarpley, J., Derby, P., Lee, R., Boyle, W.J., 1997. Osteoprotegerin: A novel secreted protein involved in the regulation of bone density. *Cell* 89, 309-319.

Singer, F.R., Eyre, D.R., 2008. Using biochemical markers of bone turnover in clinical practice. *Cleveland Clinic Journal of Medicine* 75, 739-750.

Smith, M.R., Martin, T.J., 2011. Foreword: Skeletal Complications of Cancer. *Bone* 48, 5.

Sommerfeldt, D.W., Rubin, C.T., 2001. Biology of bone and how it orchestrates the form and function of the skeleton. *European Spine Journal* 10, 86-95.

Standal, T., Seidel, C., Hjertner, O., Plesner, T., Sanderson, R.D., Waage, A., Borset, M., Sundan, A., 2002. Osteoprotegerin is bound, internalized, and degraded by multiple myeloma cells. *Blood* 100, 3002-3007.

Stewart, J.P., Shaughnessy, J.D., 2006. Role of osteoblast suppression in multiple myeloma. *Journal of Cellular Biochemistry* 98, 1-13.

Stilgren, L.S., Hegedüs, L.M., Beck-Nielsen, H., Abrahamsen, B., 2003. Osteoprotegerin Levels in Primary Hyperparathyroidism: Effect of Parathyroidectomy and Association with Bone Metabolism. *Calcified Tissue International* 73, 210-216.

Takahashi, N., Udagawa, N., Suda, T., 1999. A new member of tumor necrosis factor ligand family, ODF/OPGL/TRANCE/RANKL, regulates osteoclast differentiation and function. *Biochemical Biophysical Research Communications* 256, 449-455.

Talmage, R.V., 1969. Calcium homeostasis--calcium transport--parathyroid action. The effects of parathyroid hormone on the movement of calcium between bone and fluid. *Clinical Orthopaedics and Related Research* 67, 211-223.

Taube, T., Beneton, M.N., McCloskey, E.V., Rogers, S., Greaves, M., Kanis, J.A., 1992. Abnormal bone remodelling in patients with myelomatosis and normal biochemical indices of bone resorption. *European Journal of Haematology* 49, 192-198.

Taylor, D., Hazenberg, J.G., Lee, T.C., 2003. The cellular transducer in damage-stimulated bone remodelling: a theoretical investigation using fracture mechanics. *Journal of Theoretical Biology* 225, 65-75.

Teitelbaum, S.L., 2000. Bone resorption by osteoclasts. *Science* 289, 1504-1508.

Teoh, G., Anderson, K.C., 1997. Interaction of tumor and host cells with adhesion and extracellular matrix molecules in the development of multiple myeloma. *Hematology/oncology Clinics of North America* 11, 27-42.

Terpos, E., Dimopoulos, M.A., 2005. Myeloma bone disease: pathophysiology and management. *Annals of Oncology* 16, 1223-1231.

Terpos, E., Heath, D.J., Rahemtulla, A., Zervas, K., Chantry, A., Anagnostopoulos, A., Pouli, A., Katodritou, E., Verrou, E., Vervessou, E.C.,

Dimopoulos, M.A., Croucher, P.I., 2006. Bortezomib reduces serum dickkopf-1 and receptor activator of nuclear factor-kappaB ligand concentrations and normalises indices of bone remodelling in patients with relapsed multiple myeloma. *British Journal of Haematology* 135, 688-692.

Terpos, E., Szydlo, R., Apperley, J.F., Hatjiharissi, E., Politou, M., Meletis, J., Viniou, N., Yataganas, X., Goldman, J.M., Rahemtulla, A., 2003. Soluble receptor activator of nuclear factor kappaB ligand-osteoprotegerin ratio predicts survival in multiple myeloma: proposal for a novel prognostic index. *Blood* 102, 1064-1069.

Torre, D.M., Lamb, G.C., Van Ruiswyk, J., 2008. *Kochar's Clinical Medicine for Students*, Fifth edition ed. Lippincott Williams & Wilkins.

Turner, C.H., 1999. Toward a mathematical description of bone biology: The principle of cellular accommodation. *Calcified Tissue International* 65, 466-471.

Udagawa, N., Nakamura, M., Sato, N., Takahashi, N., 2006. The Mechanism of Coupling between Bone Resorption and Formation. *Journal of Oral Biosciences* 48, 185-197.

Urashima, M., Ogata, A., Chauhan, D., Hatziyanni, M., Vidriales, M.B., Dederá, D.A., Schlossman, R.L., Anderson, K.C., 1996. Transforming growth factor-beta1: differential effects on multiple myeloma versus normal B cells. *Blood* 87, 1928-1938.

van Zaanen, H.C., Koopmans, R.P., Aarden, L.A., Rensink, H.J., Stouthard, J.M., Warnaar, S.O., Lokhorst, H.M., van Oers, M.H., 1996. Endogenous interleukin 6 production in multiple myeloma patients treated with chimeric monoclonal anti-IL6 antibodies indicates the existence of a positive feed-back loop. *Journal of Clinical Investigation* 98, 1441-1448.

Vera, L., Dolcino, M., Mora, M., Oddo, S., Gualco, M., Minuto, F., Giusti, M., 2011. Primary hyperparathyroidism diagnosed after surgical ablation of a costal mass mistaken for giant-cell bone tumor: a case report. *Journal of Medical Case Reports* 5, 596.

Wakefield, L.M., Winokur, T.S., Hollands, R.S., Christopherson, K., Levinson, A.D., Sporn, M.B., 1990. Recombinant latent transforming growth factor beta 1 has a longer plasma half-life in rats than active transforming growth factor beta 1, and a different tissue distribution. *Journal of Clinical Investigation* 86, 1976-1984.

Wang, Y., Pivonka, P., Buenzli, P.R., Smith, D.W., Dunstan, C.R., 2011. Computational Modeling of Interactions between Multiple Myeloma and the Bone Microenvironment. *Plos One* 11: e27494.

Washington, R.L., Bernhardt, D.T., Brenner, J.S., Gomez, J., Martin, T.J., Reed, F.E., Rice, S.G., Krein, C., LeBlanc, C., Young, J.C., Lindros, J.C., Hamill, M.B., Dankner, S.R., Diaz-Rohena, R., Garrity, J., Huaman, A., Jampel, H., Pickering, T.D., Vrabec, T., Sternberg, P., Kraus, P., Alward, G., Harris, A., C.S.M.F., 2004. Protective eyewear for young athletes. *Pediatrics* 113, 619-622.

- Watson, P.H., Fraher, L.J., Kiesel, M., DeSousa, D., Hendy, G., Hodsman, A.B., 1999.** Enhanced osteoblast development after continuous infusion of hPTH(1-84) in the rat. *Bone* 24, 89-94.
- Wittrant, Y., Theoleyre, S., Chipoy, C., Padrines, M., Blanchard, F., Heymann, D., Redini, F., 2004.** RANKL/RANK/OPG: new therapeutic targets in bone tumours and associated osteolysis. *Biochimica Biophysica Acta* 1704, 49-57.
- Wols, H.A.M., Underhill, G.H., Kansas, G.S., Witte, P.L., 2002.** The role of bone marrow-derived stromal cells in the maintenance of plasma cell longevity. *The Journal of Immunology* 169, 4213-4221.
- Wong, P.K.K., Campbell, I.K., Egan, P.J., Ernst, M., Wicks, I.P., 2003.** The role of the interleukin-6 family of cytokines in inflammatory arthritis and bone turnover. *Arthritis and Rheumatism* 48, 1177-1189.
- Wozney, J.M., Rosen, V., Celeste, A.J., Mitsock, L.M., Whitters, M.J., Kriz, R.W., Hewick, R.M., Wang, E.A., 1988.** Novel regulators of bone formation: molecular clones and activities. *Science* 242, 1528-1534.
- Yasuda, H., Shima, N., Nakagawa, N., Yamaguchi, K., Kinosaki, M., Mochizuki, S., Tomoyasu, A., Yano, K., Goto, M., Murakami, A., Tsuda, E., Morinaga, T., Higashio, K., Udagawa, N., Takahashi, N., Suda, T., 1998.** Osteoclast differentiation factor is a ligand for osteoprotegerin osteoclastogenesis-inhibitory factor and is identical to TRANCE/RANKL. *Proceedings of National Academy of Science of USA* 95, 3597-3602.
- Yeh, H.S., Berenson, J.R., 2006.** Myeloma bone disease and treatment options. *European Journal Cancer* 42, 1554-1563.
- Zaidi, M., 2007.** Skeletal remodeling in health and disease. *National Medicine* 13, 791-801.
- Zaidi, M., Davies, T.F., Zallone, A., Blair, H.C., Iqbal, J., Moonga, S.S., Mechanick, J., Sun, L., 2009.** Thyroid-stimulating hormone, thyroid hormones, and bone loss. *Current Osteoporosis Reports* 7, 47-52.
- Zill, D.G., 2005.** First order differential equations, in: Hinrichs, C., Ramin, J.P., Lahr, L., Brayton, K., Chow, L. (Eds.), *A first course in differential equations with modelling applications*. Thomson Brooks, cole, Canada.
- Zumsande, M., Stiefs, D., Siegmund, S., Gross, T., 2011.** General analysis of mathematical models for bone remodeling. *Bone* 48, 910-917.
- Zwartz, G., Chigaev, A., Foutz, T., Larson, R.S., Posner, R., Sklar, L.A., 2004.** Relationship between molecular and cellular dissociation rates for VLA-4/VCAM-1 interaction in the absence of shear stress. *Biophysical Journal* 86, 1243-1252.

APPENDIX A

Journal Papers

Ji B, Putra D, Patton R, Genever P, Fagan MJ. A novel mathematical model of bone remodelling cycles for trabecular bone at the cellular level. *Biomechanics and Modelling in Mechanobiology* 11: 973-982, 2012.

Ji B, Genever P, Patton R, Fagan MJ. Mathematical modelling of the pathology of multiple myeloma-induced bone disease. Submitted to *Journal of Computer Methods in Biomechanics and Biomedical Engineering*.

Conference Presentations

Ji B, Putra D, Patton R, Genever P, Fagan MJ. Reconstructing bone remodelling cycle at the cellular level using a predator-prey based model. *International Society of Biomechanics*, Brussels, 3-7 July, 2011.

Ji B, Putra D, Patton R, Genever P, Fagan MJ. A new 'predator-prey' based simulation of the BMU remodelling cycle. *17th Congress of the European Society of Biomechanics*, Edinburgh, 5-8 July, 2010.

Journal Abstracts

Ji B, Putra D, Patton R, Genever P, Fagan MJ. A predator-prey mathematical model of bone remodelling cycles at the cellular level. *Osteoporosis International* 21:S3, S517, 2010.

Jahani M, Ahwal F, **Ji B**, Patton R, Genever P, Fagan MJ. Simulation of osteocyte apoptosis on signalling in the osteocyte-bone lining cell network and implications for osteoporosis. *Osteoporosis International* 21:S3, S514, 2010.

Putra D, **Ji B**, Patton R, Genever P, Fagan MJ. Simulation of the BMU remodelling cycle using a new predator-prey algorithm. *Bone* 47:1, S95, 2010.